O. Richter, B. Diekkrüger, P. Nörtersheuser

# Environmental Fate Modelling of Pesticides

**VCH**

O. Richter,
B. Diekkrüger,
P. Nörtersheuser

# Environmental Fate Modelling of Pesticides

From the Laboratory to the Field Scale

**VCH**

Prof. Dr. Otto Richter
Technische Universität
Braunschweig
Institut für Geographie
und Geoökologie
Langer Kamp 19c
D-38106 Braunschweig

Dr. Bernd Diekkrüger
Geographisches Institut
der Rheinischen
Friedrich-Wilhelms-Universität
Meckenheimer Allee 166
D-53115 Bonn

Dr. Peter Nörtersheuser
Knoll AG
Biometrics and
Information Technology
P. O. Box 210805
D-67008 Ludwigshafen

# Preface

The fate of a substance in the environment is determined by physical, chemical and biological processes. These processes take place simultaneously and are closely interlocked. Environmental systems do not conform with manmade distinctions between different branches of sciences.

Therefore environmental fate modelling demands an interdisciplinary approach. This concerns not only interdisciplinarity between different disciplines such as soil physics, mathematics, soil chemistry and biology, but also interdisciplinarity within a discipline. Mathematics may serve as an example. Kinetic processes, if they are mediated by biological processes, are nonlinear. They are modelled by sets of nonlinear ordinary differential equations, which, in general, are not amenable to analytical solutions. The understanding of the dynamics of such equations is based on knowledge of dynamical systems theory and on numerical methods for obtaining approximate solutions. Coupling kinetics with transport leads to systems of partial differential equations. Furthermore, these processes are imbedded into a random environment. Soils are by no means homogeneous media. As a consequence variability itself has to be modeled by stochastic approaches based on modern geostatistical theory. All the methods mentioned above stem from different fields within the realm of mathematics.

Models cannot be derived from first principles alone. Models summarize experimental knowledge at the abstract level of mathematics. Therefore, many experimental data are necessary at various stages of model development. In the beginning experimental knowledge guides us in the conception of models and in later stages, thoroughly designed experiments serve to identify model parameters and to validate models. Parameter estimation techniques both in ordinary and in partial differential equations are therefore necessary tools to provide the link between models and experiments. These techniques combine aspects of numerical mathematics and statistics.

Model parameters such as sorption constants, degradation rates and diffusion coefficients are all closely related to soil properties. The translation of models across scales, from the laboratory scale to field and catchment scales, therefore demands first the mapping of geo-referenced soil information to model parameters. This is mediated by so-called pedotransfer functions. The link between spatial information and pesticide environmental fate models can best be achieved in the frame of a geographical information system.

If processes are only vaguely known, fuzzy-theory provides a promising new concept to deal with uncertainty. At the end of the book, a simple fuzzy-expert system is presented apt to predict decay modes and half-lives of a herbicide.

It is the objective of this book, to bring together many different aspects of environmental fate modelling of pesticides comprising such diverse subjects as

- linear compartment theory
- nonlinear biological degradation models
- biological temperature and humidity response of degradation

- herbicide dynamics, i.e. modelling toxicity
- parameter identification in ordinary and partial differential equations
- parameter estimation in sparse data situations
- coupled reaction and diffusion processes in form of coupled
  partial differential equations
- coupling of physical and biological processes
- transport processes in random environments
- pedotransfer functions
- coupling of random soil parameter fields and reactive transport models
- the translation of models across scales
- coupling of geographical information systems with models
- fuzzy approaches

This book has several origins. Part of the material is based on a course on environmental modelling for environmental science students of the new course "Geoecology" at Braunschweig University. More advanced parts and many experimental data are due to the activities of the Collaborative Research Program 179 "Water and Matter Dynamics in Agro-Ecosystems", which was established in 1986 at the Technical University of Braunschweig, Germany, sponsored by the Deutsche Forschungsgemeinschaft. Part of the research program was the development and validation of physically, chemically and biologically based transport and reaction models for pesticides in soils. The subprojects "Integrated Site and Catchment Models", "The Dynamics of Herbicides", "Investigations on Pesticide Residues and corresponding Metabolites" deserve special mention. Furthermore, the research was sponsored by BASF, where several kinetic studies were carried out by PhD students.

August 1996                                                                                        O. Richter
Braunschweig, Bonn and Ludwigshafen                                        B. Diekkrüger
                                                                                                      P. Nörtersheuser

# Contents

# 1    Introduction

### Environmental Fate of Pesticides

If one regards the environmental fate of a substance such as a pesticide one is intrigued by the number of interacting processes. Let us follow a pesticide in the plant soil system after spraying. Fig. 1.1 depicts the main processes. Before it reaches the soil, the substance may undergo decay by photodecomposition, it may be transported in the air and it may adsorb to plant leaves. Once it enters the soil, it is subject to various transformation processes. It may decay by a simple chemical process, e.g. by hydrolysis. Most important, it may be transformed by biochemical reactions mediated by microorganisms. These reactions are called metabolic if microorganisms are able to use the substance as C-source, otherwise they are called cometabolic. The latter notation expresses the fact that degradation is connected to microbial activity for instance by the release of hydrolytic enzymes. Degradation processes mostly take place in the liquid phase. In the soil the substance partitions between the liquid phase, the solid phase and the gaseous phase. Furthermore it is sorbed to binding sites with different strength of binding.
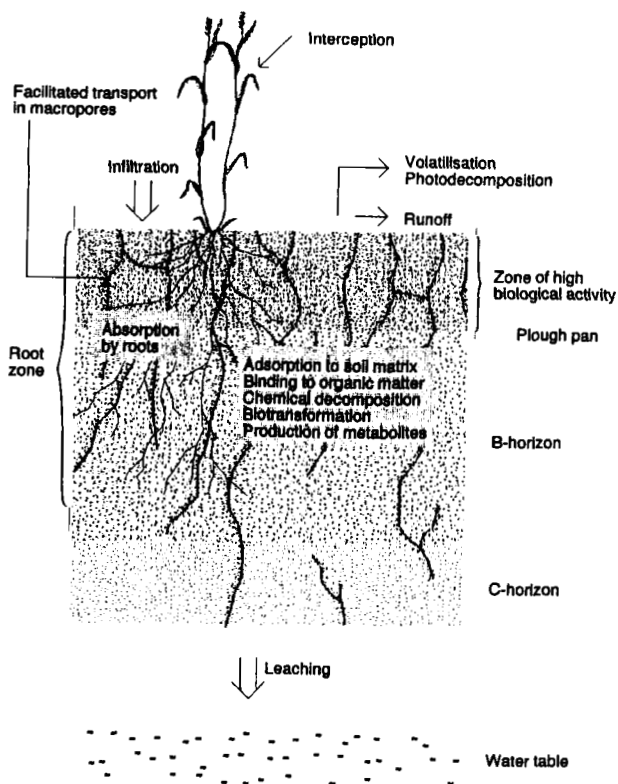


**Fig. 1.1:** Main processes in the plant soil system.

Solute transport through soil is mediated by water flow and is strongly influenced by solute sorption. To complicate matters, soil structures are heterogeneous. There are wormholes, cracks and complex soil structures caused by e.g. glacial processes (cf. Fig. 1.2) giving rise to preferential flow facilitating the transport of pollutants into the subsoil. All these processes are embedded in a spatio-temporal hierarchy (cf. Tabs. 1.1 and 1.2). If one considers all these processes in detail it does not seem feasible to devise mathematical models able to cope with this sort of complexity. However, the experience of systems at the laboratory scale - continuously stirred reactors, soil columns and lysimeters - show that in spite of this apparent complexity decay curves and breakthrough curves can well be described by mathematical models with different degree of sophistication.



**Fig. 1.2:** Preferential flow paths in a highly variable soil of a push moraine. The flow region is colored by Rhodamine applied during a tracer experiment.

## Simple Mathematical Models

Notations

$y$        : concentration [$M/L^3$]
$y_0$       : initial concentration [$M/L^3$]
$t$        : time [T]
$T$        : temperature [°C, resp. K]
$k$        : rate constant [1/T]
$R$        : gas constant = 8.314 $JK^{-1} mol^{-1}$
$\Delta E$       : activation energy [J/mol]

The simplest kinetics encountered is the mono-exponential decay with an Arrhenius law for the dependence of the rate constant on temperature. Figure 1.3 shows decay curves for several temperature values obtained in the laboratory.
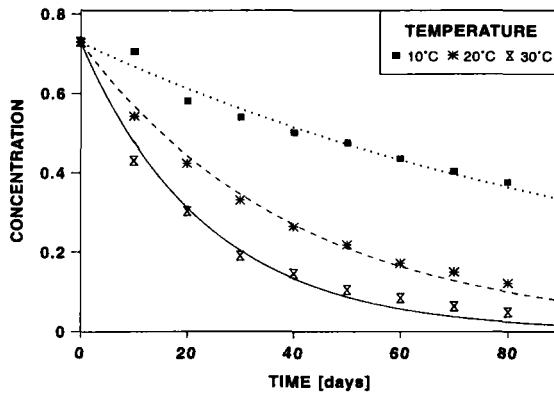


**Fig 1.3:** Decay curves for several temperature values obtained in the laboratory.

Assuming that the rate of decay is proportional to the amount of pesticide present the adequate model in differential form is

$$\frac{dy}{dt} = -ky \quad with \quad y(t=0) = y_0 \tag{1.1}$$

which is easily integrated to yield (cf. section 2.1)

$$y(t) = y_0 e^{-kt} \tag{1.2}$$

The Arrhenius law establishes the following dependence of the rate constant $k$ on temperature $T$

$$k(T) = k_0 e^{-\frac{\Delta E}{RT}} \tag{1.3}$$

This is one of the simplest models. There are no nonlinear effects such as lag times or other forms of non-mono-exponential kinetics. If one wants to apply this model to time varying temperatures $T(t)$, one has to start from the underlying differential equation Eq. (1.1) introducing a time dependent rate constant:

$$\frac{dy}{dt} = - k(T(t))y \quad with \quad y(t=0) = y_0 \tag{1.4}$$

Integration of this differential equation yields (cf. section 2.1)

$$y(t) = y_0 e^{\int_0^t -k(T(\tau))d\tau} \tag{1.5}$$

This example demonstrates, that it is possible to apply a model, which has been derived from simple experimental conditions, to a more complex situation. However, care has to be taken, if one is leaving the range of those experimental conditions which served to establish the temperature law. If degradation is mediated by microorganisms, the validity of the Arrhenius law is confined to only a small temperature range (cf. section 3.4.1).

However, simple mono-exponential models do not always apply. Frequently, one is faced with significant deviations from this simple kinetic behavior due to nonlinear effects at the microbial level. Figure 1.4 shows decay curves of 2,4-D (2,4-dichlorophenoxyacetic acid), which obviously cannot be described by a mono-exponential model, because it is not capable of simulating lag-phases. Effects like this pose a challenge to model builders and render environmental fate models interesting from the mathematical point of view.
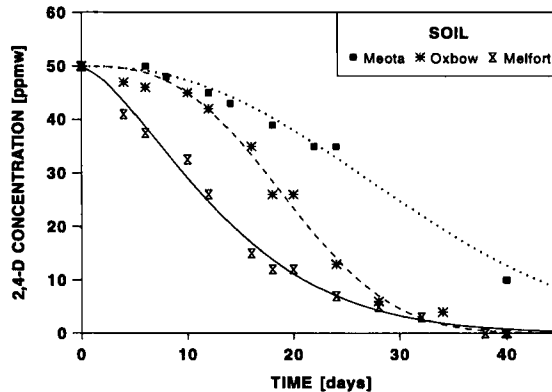


**Fig. 1.4:** Decay curves of 2,4-D. This example will be discussed in section 4.4.

## Spatial and Temporal Scales

Once released pesticides become part of agricultural ecosystems. Therefore it is important to study the scales involved in agricultural ecosystems first and then to see how pesticides fit into this scheme. Table 1.1 summarizes some basic processes in an agricultural ecosystem and their characteristic times.

**Tab. 1.1:** Processes in (agricultural) ecosystems and their characteristic times.

| Process | State variables | Characteristic time |
|---|---|---|
| enzymatic reactions, e.g. the hexo-kinase reaction | glucose (substrate) and glucose-6-phosphate (product) | minutes |
| growth of a microbial population | biomass in C units, N-content, activity | 30 minutes |
| nitrification and denitrification | $NH_4^+$, $NO_3^-$, $N_2O$, $N_2$, microbial activity | 1 day - several weeks |
| short-term population dynamics of pests and diseases | density of eggs, larvae and adults | 1 week (eggs) 2 - 7 weeks (adults) |
| long-term population dynamics of pests and diseases | density of eggs, larvae and adults | period of crop rotations, several years |
| crop growth | biomass of shoot and root, N-content, leaf area index, yield | several weeks |
| long-term population-dynamics of weeds | seedbank, density | vegetation period to years |
| water transport in the soil | water content, water potential | 1 h to several days |
| matter transport and degradation in the unsaturated zone | concentration in liquid, solid and gaseous phase | weeks to several years |
| evolutionary processes induced by agriculture: enhanced biodegradation of pesticides, emergence of resistance | biodegradation rates, response to pesticides | ~1 to 10 years |
| change in biodiversity, dying back of species, immigration of species (e.g. weeds) | number and abundance of species | ~1 to several 100 years |

In dealing with pesticides one has to consider in addition various levels of experimentation. Following Blackburn (1989) one can distinguish the continuously stirred tank reactor level,

the column reactor level, the field-scale and last the catchment or aquifer-scale. It is important to note that there are long-term processes associated with periodic applications of pesticides at the evolutionary level of microbial populations and the target populations. Enhanced biodegradation has been frequently observed, although the molecular and genetic mechanisms for this effect are still being investigated. Figure 1.5 shows enhanced degradation of EPTC as measured by Obrigawitch et al. (1983).
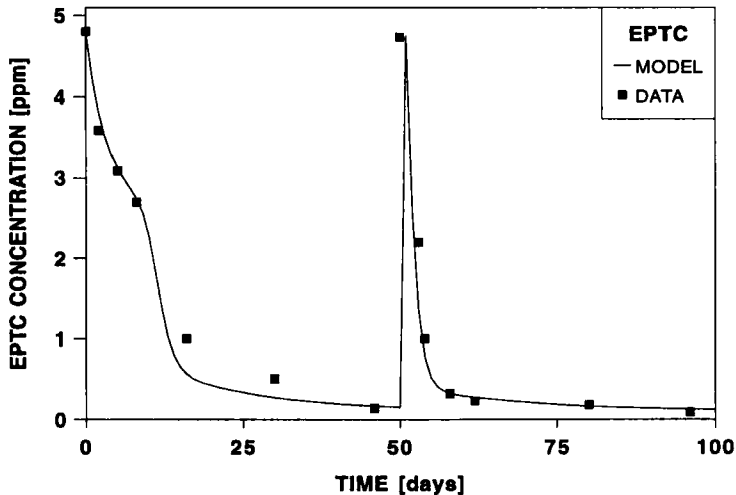


**Fig. 1.5:** Degradation of EPTC as measured by Obrigawitch et al. (1983). This example will be duscussed in section 3.3.3.

Target populations may eventually become resistant against the pesticide. These biological long-term effects pose a major problem for the conception of deterministic fate models. In chapter 3 some possible modeling approaches are presented.

**Dealing with Spatial Heterogeneity**

If one proceeds from the laboratory level to higher spatial scales one has to include the dependence of rate constants on soil properties. The spatial distribution of soil properties has both, a deterministic (soil type) and a random component. The random component has to be modeled explicitly. This implies that in addition to deterministic process models for laboratory conditions one has to devise stochastic models for the spatial distribution of parameters. In the simplest case these are probability density functions. If three-dimensional transport in a soil is considered, the models are spatial stochastic processes yielding realizations of parameter fields (cf. section 7.3). By combination of stochastic models for soil parameters and deterministic models for the kinetics one is able to tackle the problem of spatial heterogeneity. A key concept is the notion of ecotope. An ecotope is defined as the intersection of a pedological unit and the landuse pattern. At the catchment scale the landscape is composed of a large number of ecotopes each with characteristic soil properties (cf. section 7.5). Table 1.2 summarizes spatial scales and possible model approaches taking into account spatial heterogeneity.

**Tab. 1.2:** Model approaches on different scales.

| Scale | Soil Heterogeneity | Model |
|---|---|---|
| continuously stirred tank reactor | homogeneous | kinetic models in form of ordinary differential equations |
| column reactor | almost homogeneous microscale variation | kinetic models coupled with one-dimensional transport models in form of partial differential equations |
| field scale (intersection of pedological unit and landuse) | random soil properties | stochastic models for soil properties plus deterministic model |
| catchment scale | large deterministic structures (several pedological units) with random soil properties | pedotransfer functions plus stochastic model plus deterministic model |

**Tab. 1.3:** Information hierarchy associated with spatial scales.

| Scale | Information Density | Information Quality |
|---|---|---|
| continuously stirred tank reactor | high temporal resolution | interval scale level |
| column reactor level | high temporal resolution | interval scale level |
| experimental plot | high temporal and spatial resolution | detailed measurements at interval scale level, low spatial variability |
| experimental field | reduced temporal and spatial resolution | detailed measurements at interval and ordinal scale level, spatial variability |
| experimental farm | reduced temporal and spatial resolution | detailed measurements at interval scale and ordinal scale level, increasing spatial variability |
| ordinary farm, catchments and landscapes | only few measurements | qualitative information (linguistic level, fuzzy information) |

**Information Hierarchy**

The various approaches mentioned above to cope with spatial heterogeneity all demand large data bases. In order to identify the parameters of a spatial random process one has to collect data with a high spatial resolution by nesting grids of different mesh sizes. This method is referred to as "nested sampling design". Such extensive experimental efforts are only possible in the frame of a large collaborative research program. One can state that an information hierarchy is associated with the hierarchy of spatial scales. Table 1.3 illustrates the relation between spatial scales and information density and information quality. This is one of the major issues in environmental fate modelling: the translation of models across spatial and temporal scales in view of this information hierarchy. We will address this problem in chapter 7, but we admit that here many questions still remain open.

# 2 Mathematical Preliminaries

## 2.1 Ordinary Differential Equations

In this book, ordinary differential equations are applied to the dynamics of chemical reaction systems. They are modeled by systems of simultaneous first-order differential equations of the general form

$$\frac{dy_1}{dt} = f_1(y_1, \ldots, y_n)$$

$$\frac{dy_2}{dt} = f_2(y_1, \ldots, y_n)$$

$$\vdots$$

$$\frac{dy_n}{dt} = f_n(y_1, \ldots, y_n)$$

(2.1)

The $y_i$ are the state variables, which are unknown functions of time $t$. In our applications the $y_i$ will denote concentrations of chemicals in various phases, e.g. liquid phase and solid phase pesticide concentrations. The system is of first order, because only the first derivative of the $y_i$ with respect to time $t$ appears in the equations. The system behavior is specified by the initial conditions of the state variables:

$$y_1(t=0) = y_{10}, \quad y_2(t=0) = y_{20}, \ldots, \quad y_n(t=0) = y_{n0}$$

(2.2)

The mathematical problem to solve the equation system (Eq. (2.1)) together with the initial conditions (Eq. (2.2)) is referred to as an **initial value problem**. In physical applications, one is frequently lead to second order differential equations, because the basic physical laws involve second derivatives with respect to time. E.g., the differential equation for the motion of a damped mass-spring system is

$$m\frac{d^2x}{dt^2} + r\frac{dx}{dt} + kx = 0$$

(2.3)

Here, $x$ means the displacement of the mass, $m$ the mass, $r$ the coefficient of friction and $k$ the spring constant. However, it is always possible to write a higher order equation as a system of coupled first-order equations. Consider the above example. By the introduction of the auxiliary variable $v = dx/dt$, which has the meaning of a velocity, the first order equation is replaced by the system

$$\frac{dv}{dt} = -\frac{r}{m}v - \frac{k}{m}x$$

(2.4)

A system is defined to be **linear** if the functions on the right hand side (r.h.s.) of Eq. (2.1) are all linear functions of the state variables $y_i$. The number of equations is referred to as the **dimension of the system**. The constants appearing in the equations, e.g. $m$, $r$ and $k$ in Eq. (2.3) are referred to as **parameters**. They reflect the material properties of the system to be modeled. We consider now simple first order systems, which are amenable to analytical solutions, i.e. solutions in closed form, by elementary methods. The simplest model of a chemical reaction is based on the assumption, that the reaction rate is proportional to the actual mass or concentration.

$$\frac{dy}{dt} = -ky \qquad with \quad y(t=0) = y_0 \tag{2.5}$$

The negative sign of the r.h.s. means that a loss occurs because the rate of change is negative. This equation is linear. A famous example of a nonlinear equation is the differential equation of logistic growth.

$$\frac{dy}{dt} = ry\left(1 - \frac{y}{K}\right) \qquad with \quad y(t=0) = y_0 \tag{2.6}$$

Population growth is limited by the parameter $K$, which is - in the context of population dynamics - referred to as environmental capacity. Both equations are of the general form

$$\frac{dy}{dt} = ag(y) \tag{2.7}$$

where the parameter $a$ is a constant.

### Method of Separation of Variables

Equations of this type are solved by the method of separation of variables. This procedure implies the following steps.

1. Step: separation of variables

$$\frac{dy}{g(y)} = a\,dt \tag{2.8}$$

2. Step: integration

$$\int_{y_0}^{y} \frac{dy}{g(y)} = a\int_{t_0}^{t} d\tau \tag{2.9}$$

$$G(y) - G(y_0) = a(t - t_0)$$

3. Step: deriving the explicit form of the solution

$$y(t) = G^{-1}[G(y_0) + a(t - t_0)]$$  (2.10)

where $G^{-1}$ is the inverse function of $G$. In the following examples, $t_0$ is set equal to zero. For the initial value problem Eq. (2.5) these steps are:
1. step: separation of variables

$$\frac{dy}{y} = -k\,dt$$  (2.11)

2. Step: integration

$$\int_{y_0}^{y} \frac{dy}{y} = -k \int_0^t d\tau$$  (2.12)

3. Step: deriving the explicit form of the solution

$$\ln(y) - \ln(y_o) = -kt$$

$$y(t) = e^{\left(\ln(y_o) - kt\right)} = y_o e^{-kt}$$  (2.13)

In the same way the solution of the initial value problem Eq. (2.6) is obtained as

$$y(t) = \frac{Ky_0}{y_0 - \left(y_0 - K\right)e^{-rt}}$$  (2.14)

Even if an analytic expression of the integral of $1/g(y)$ is known, it is not always possible to get an explicit solution as the following example shows. Consider the enzymatic degradation of a substance according to the Michaelis-Menten kinetic law (cf. section 3.2).

$$\frac{dy}{dt} = -\frac{Vy}{y + K} \qquad with \quad y(t=0) = y_0$$  (2.15)

After separation of variables and integration one obtains

$$y - y_0 + \frac{K}{V}\left(\ln y - \ln y_0\right) = -t$$  (2.16)

This equation cannot be explicitly solved for $y$.

**Non-Autonomous Equations**

In the foregoing examples the r.h.s. does not explicitly depend on time $t$. Equations of this type are referred to as autonomous. If one considers for example the degradation of a

pesticide in the field, changing temperature conditions render the degradation "constant" time dependent.

$$\frac{dy}{dt} = - k(t)y \qquad with \quad y(t=0) = y_0 \tag{2.17}$$

This equation is a special case of the general form

$$\frac{dy}{dt} = f(t)g(y) \qquad with \quad y(t=0) = y_0 \tag{2.18}$$

Equations with explicit time dependency of the r.h.s. are called non-autonomous. Again, the solution of this initial value problem can be obtained by application of the method of separation of variables.

1. Step: separation of variables

$$\frac{dy}{g(y)} = f(t)dt \tag{2.19}$$

2. Step: integration

$$\int_{y_0}^{y} \frac{dy}{g(y)} = \int_{t_0}^{t} f(\tau)d\tau \tag{2.20}$$

$$G(y) - G(y_0) = F(t) - F(t_0)$$

3. Step: deriving the explicit form of the solution

$$y(t) = G^{-1}[G(y_0) + F(t) - F(t_0)] \tag{2.21}$$

where $G^{-1}$ is the inverse function of $G$. In the following example, $t_0$ is set equal to zero.

Consider the initial value problem Eq. (2.17) with a periodical time dependence of the degradation rate according to

$$k = k_0 + a \sin(\omega t) \tag{2.22}$$

1. Step: separation of variables

$$\frac{dy}{y} = f(t)dt \tag{2.23}$$

2. Step: integration

$$\int_{y_0}^{y} \frac{dy}{y} = -\int_{0}^{t} \left(k_0 + a\sin(\omega\tau)\right)d\tau$$

(2.24)

$$\ln(y) - \ln(y_0) = -k_0 t - a\left(-\frac{1}{\omega}\cos(\omega t) + \frac{1}{\omega}\right)$$

3. Step: deriving the explicit form of the solution

$$y(t) = y_0 e^{\left[-k_0 t - \frac{a}{\omega}\left(1 - \cos(\omega t)\right)\right]}$$

(2.25)

**Inhomogeneous equations and the trick of the integrating factor**

We consider differential equations of the general form

$$\frac{dy}{dt} + a(t)y = f(t)$$

(2.26)

Equations of this type model for example the situation that a substance, which decays with time dependent rate constant $a(t)$, is entering the system with time dependent rate $f(t)$. An equation of this type is called inhomogeneous. The first step of the solution procedure is the solution of the homogeneous equation

$$\frac{dy}{dt} + a(t)y = 0$$

(2.27)

Applying the method of separation of variables one obtains

$$y(t) = y_o e^{A(t_o)} e^{-A(t)}$$

$$A(t) - A(t_o) = \int_{t_o}^{t} a(\tau)d\tau$$

(2.28)

This solution can also be obtained by the following trick: the differential equation is multiplied by the "integrating factor" $e^{A(t)}$. One easily verifies that the l.h.s. of the differential equation can be written as the derivative

$$\frac{d}{dt}\left[e^{A(t)}y(t)\right] = e^{A(t)}\frac{d}{dt}y(t) + e^{A(t)}a(t)y(t)$$

(2.29)

so that the homogeneous equation takes the form

$$\frac{d}{dt}\left[e^{A(t)}y(t)\right] = 0 \tag{2.30}$$

Integration yields the solution of the initial value problem Eq. (2.26). In the inhomogeneous case multiplication by the integrating factor leads to

$$\frac{d}{dt}\left[e^{A(t)}y(t)\right] = e^{A(t)}f(t) \tag{2.31}$$

Integration and multiplication both sides by $e^{-A(t)}$ yields

$$y(t) = e^{-A(t)}\left[y_0 e^{A(t_0)} + \int_{t_0}^{t} e^{A(\tau)}f(\tau)d\tau\right] \tag{2.32}$$

Consider the simple case that $a(t) = const = k$ and that $f(t) = const = v$. The integrating factor is then given by $e^{kt}$ and application of the general formula Eq. (2.32) yields the solution ($t_0$ is set equal to zero)

$$y(t) = e^{-kt}\left[y_0 + \int_{0}^{t} e^{k\tau}v d\tau\right] = \frac{v}{k}\left(1 - e^{-kt}\right) + y_0 e^{-kt} \tag{2.33}$$

Further examples will be given in the next chapter.

## Remarks on Existence and Uniqueness of the Solutions

The fundamental theorem of Picard-Lindelöf ensures that the solution of the initial value problem

$$\frac{dy}{dt} = f(t,y) \qquad with \quad y(t=0) = y_0 \tag{2.34}$$

exists and is unique, if the r.h.s. of the differential equation is **Lipschitz-continuous**.

**Def.:** $f(t,y)$ is called Lipschitz-continuous with respect to $y$, if there exists a positive constant $L$ such that

$$|f(t,y) - f(t,y^*)| \leq L |y - y^*| \tag{2.35}$$

This condition is always fulfilled for the class of kinetic equations encountered in this book.

## 2.2 Partial Differential Equations

### Modelling Processes by Partial Differential Equations

Ordinary differential equations (ODEs) have only one independent variable, which is in the context of our applications, the time. They are thus lacking any spatial component. The application of ODEs to dynamic systems makes only sense, if the compartments of the system under study are spatially homogeneous. This is for instance realized for reaction systems in a "well stirred" medium in a laboratory. However, if the fate of a substance in the environment is considered, transport processes in inhomogeneous soils prevail. Therefore models are needed, which contain explicitly spatial coordinates and which yield the evolution in time of the concentration field, i.e. the concentration as function of time and space. The resulting differential equation therefore contains also derivatives of the state variables with respect to the space coordinates. Such an equation is called a partial differential equation (PDE).

### Derivation of the Continuity Equation

The basic equation for the derivation of transport models is the mass balance equation for a volume element. Although the shape of the elements is arbitrary, we consider, for ease of presentation, a rectangular box centered at $P(x,y,z)$ with dimensions $\Delta x$, $\Delta y$ and $\Delta z$ (cf. Fig. 2.1). Imagine that this box is placed into a flow field $\vec{J}$. This is also referred to as control volume or control box. Let $c$ denote the mass of a substance (or any other extensive property) in a volume element $\Delta V$. Then the rate of change of $c$ in $\Delta V$ is the excess of inflow over outflow during a time interval $\Delta t$. Summing up the flows in $x$, $y$ and $z$ direction through the surfaces of the control box yields the conservation equation

$$\frac{\Delta c}{\Delta t}\Delta V = \left[J_{in} - J_{out}\right]_x \Delta y \Delta z + \left[J_{in} - J_{out}\right]_y \Delta x \Delta z + \left[J_{in} - J_{out}\right]_z \Delta x \Delta y \qquad (2.36)$$
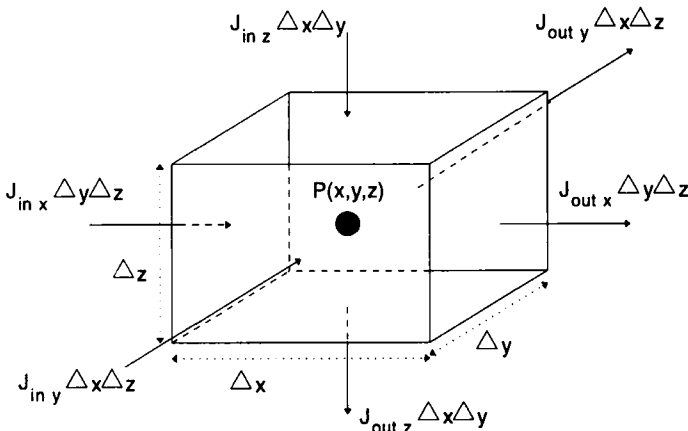


**Fig. 2.1:** Flux balance for a control volume.

Under the assumption that the flow field is continuous, the value of $\vec{J}$ at the surfaces can be derived from the flow at the center by a Taylor expansion

$$J_x\left(x - \Delta\frac{x}{2}, y, z\right) = J_x(x,y,z) - \frac{\partial J_x}{\partial x}\Big|_x \frac{\Delta x}{2} \tag{2.37}$$

$$J_x\left(x + \Delta\frac{x}{2}, y, z\right) = J_x(x,y,z) + \frac{\partial J_x}{\partial x}\Big|_x \frac{\Delta x}{2} \tag{2.38}$$

so that the excess of inflow over outflow in $x$-direction is given by

$$\left[J_{in} - J_{out}\right]_x \Delta y \Delta z = - 2\frac{\partial J_x}{\partial x}\Big|_x \frac{\Delta x}{2}\Delta y \Delta z \tag{2.39}$$

Summing up the excess in all three directions gives the expression

$$\frac{\Delta c}{\Delta t}\Delta x \Delta y \Delta z = -\left(\frac{\partial J_x}{\partial x} + \frac{\partial J_y}{\partial y} + \frac{\partial J_z}{\partial z}\right)\Delta x \Delta y \Delta z \tag{2.40}$$

In the limit $\Delta V \to 0$ and $\Delta t \to 0$ one finally obtains the fundamental conservation equation

$$\frac{\partial c}{\partial t} + \left(\frac{\partial J_x}{\partial x} + \frac{\partial J_y}{\partial y} + \frac{\partial J_z}{\partial z}\right) = 0 \tag{2.41}$$

By use of the gradient operator [1]

$$\nabla = \left(\frac{\partial}{\partial x} \frac{\partial}{\partial y} \frac{\partial}{\partial z}\right) \tag{2.42}$$

this equation is written in condensed form as

$$\frac{\partial c}{\partial t} + \nabla\cdot\vec{J} = 0 \tag{2.43}$$

The second term is the scalar product of the vectors $\nabla$ and $\vec{J}$:

---

[1]"A differential operator is something hungry to differentiate something" (The Feynman Lectures on Physics)

$$\nabla \cdot \vec{J} = \left( \frac{\partial}{\partial x} \frac{\partial}{\partial y} \frac{\partial}{\partial z} \right) \begin{pmatrix} J_x \\ J_y \\ J_z \end{pmatrix}$$

If there are any sources or sinks in the control volume, i.e. any processes creating or consuming the substance, the mass balance is completed by a sink or source term $Q$:

$$\frac{\partial c}{\partial t} + \nabla \cdot \vec{J} = Q \tag{2.44}$$

This equation can also be derived from a famous theorem of vector analysis. Let $V$ denote any volume and $\vec{n}$ the unit vector normal to the surface. For this volume the mass balance equation is

$$\int_V \frac{\partial c}{\partial t} dV = - \int_S \vec{J} \cdot \vec{n} \, da \tag{2.45}$$

stating that the rate of change of $c$ in $V$ equals the integral over the flow over the surfaces of $V$ (cf. Fig. 2.2). By application of Gauss' divergence theorem

$$\int_S \vec{J} \cdot \vec{n} \, da = \int_V \nabla \cdot \vec{J} dV \tag{2.46}$$

the mass balance equation is written as

$$\int_V \left( \frac{\partial c}{\partial t} + \nabla \vec{J} \right) dV = 0 \tag{2.47}$$

This is the fundamental mass balance equation in integral form, from which Eq. (2.44) is obtained by letting $V \rightarrow 0$.
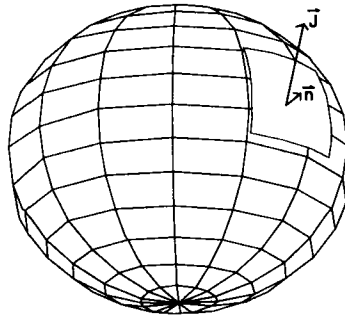


**Fig. 2.2:** The total rate of change of the quantity $c$ within the volume $V$ equals the integral over the fluxes across the surface. $\vec{n}$ is the outward normal vector to the surface element $da$, and $\vec{J}$ is the flux vector across $da$.

**Derivation of the Diffusion Equation**

To obtain a transport equation, it is necessary to express the flow $\vec{J}$ in terms of the state variable $c$. At this point, experimentally based assumptions on the transport mechanism have to be made. In the case of diffusion in an isotropic medium, Fick's law of diffusion applies, stating that a flow is generated by the gradient of a concentration.

$$\vec{J} = -D\nabla c \qquad\qquad (2.48)$$

where $\nabla c$ is the column vector

$$\nabla c = \begin{pmatrix} \dfrac{\partial c}{\partial x} \\[2mm] \dfrac{\partial c}{\partial y} \\[2mm] \dfrac{\partial c}{\partial z} \end{pmatrix} \qquad\qquad (2.49)$$

The negative sign determines the direction of the flow, which proceeds from regions of high to regions of low concentration. In an anisotropic medium, the direction of the flow is not necessarily parallel to the gradient. The transformation of the gradient vector is achieved by the multiplication of the gradient by a matrix - the so called diffusion tensor. So in isotropic media $D$ is a scalar, the diffusion constant, and in anisotropic media a tensor. Combination of Eq. (2.43) and Eq. (2.48) yields an equation, which solely depends on $c$:

$$\frac{\partial c}{\partial t} = \nabla \cdot D \nabla c \qquad\qquad (2.50)$$

The right hand side of this equation is the scalar product of the gradient operator with the gradient of $c$ yielding

$$\frac{\partial c}{\partial t} = \frac{\partial}{\partial x} D \frac{\partial c}{\partial x} + \frac{\partial}{\partial y} D \frac{\partial c}{\partial y} + \frac{\partial}{\partial z} D \frac{\partial c}{\partial z} \qquad\qquad (2.51)$$

This is a partial differential equation (PDE), which defines relationships between partial derivatives of the state variable $c$. The mathematical problem to find a solution of the above PDE has to be specified by **initial and boundary conditions**. The latter occur, because the state variable depends on time $t$ and spatial coordinates $x$, $y$, $z$. Let $G$ denote a region in $\mathbb{R}^3$ with boundary $\partial G$. Possible boundary conditions, which are motivated by the nature of the physical problem under study, are

i) prescribed concentration on the boundary (Dirichlet boundary condition)

$$c(x,y,z,t) = \phi(x,y,z,t)\,\big|_{(x,y,z)\,\in\,\partial G} \qquad\qquad (2.52)$$

ii) prescribed flow on the boundary (Neumann boundary condition)

$$\frac{\partial c}{\partial n} = \vec{n}\,\nabla c = \psi(x,y,z,t)\,|_{(x,y,z)\,\in\,\partial G} \tag{2.53}$$

where

$$\frac{\partial c}{\partial n} = \vec{n}\,\nabla c \tag{2.54}$$

is the partial derivative of $c$ in direction of the outward normal vector $\vec{n}$ (cf Fig. 2.2).

iii) prescribed loss on the boundary (Cauchy boundary condition)

$$\frac{\partial c}{\partial n} + \alpha c = \beta\,|_{(x,y,z)\,\in\,\partial G} \tag{2.55}$$

Let $c_s$ and $c_e$ denote the concentration at the surface of a medium and in the surrounding air respectively. Then the rate of volatilization at the surface is given by

$$D\frac{\partial c}{\partial n} + \kappa\!\left(c_s - c_e\right) = 0 \tag{2.56}$$

where $\kappa$ denotes the resistance of the boundary layer. Note that all three boundary conditions may occur in one problem at different regions of the boundary. Specification of the problem is completed by prescribing the initial concentration field:

$$c(x,y,z,t=0) = f(x,y,z)\,|_{(x,y,z)\,\in\,G} \tag{2.57}$$

The mathematical problem to solve a partial differential equation subject to given initial and boundary conditions is denoted as an **initial boundary value problem.**

**Analytical Solutions**

In the following some analytical solutions for the one-dimensional version of the diffusion equation with constant diffusion coefficient will be derived for simple boundary conditions. A solution of the one-dimensional version of the diffusion equation

$$\frac{\partial c}{\partial t} = D\frac{\partial^2 c}{\partial x^2} \tag{2.58}$$

is given by

$$c(x,t) = \frac{const}{\sqrt{t}}\,e^{-\frac{x^2}{4Dt}} \tag{2.59}$$

This solution corresponds to the experimental situation that a substance concentrated at time $t = 0$ at the origin diffuses in a cylinder of infinite length. Let $M$ denote the total mass initially present at $x = 0$. Mass conservation demands that at any time $t$

$$M = \int_{-\infty}^{\infty} c(x,t)\,dx \qquad (2.60)$$

From this integral the constant is determined as

$$const = \frac{M}{2\sqrt{D\pi}} \qquad (2.61)$$

so that the final solution is given by

$$c(x,t) = \frac{M}{2\sqrt{\pi Dt}} e^{-\frac{x^2}{4Dt}} \qquad (2.62)$$

Because of the singularity encountered at $t = 0$ this function is called "singularity function". Figure 2.3 shows concentration curves obtained at different times.
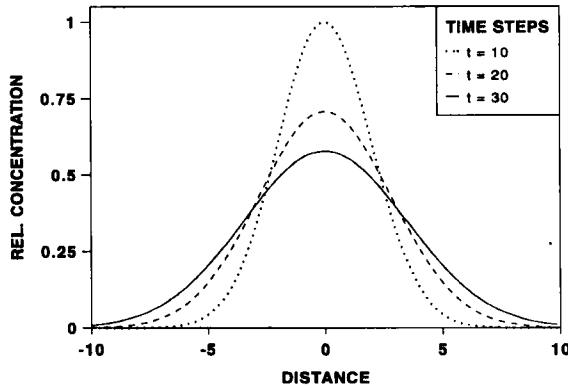


**Fig. 2.3:** Evolution in time of the singularity function (Eq. (2.62)).

The singularity function can be used to construct solutions for arbitrary initial distributions. The underlying principle is the superposition of line elements, each of which is described by the singularity function. As example we treat the case of a finite rectangular initial distribution.

$$c(x,0) = \begin{cases} 0 & x < -h \\ c_0 & -h \le x \le +h \\ 0 & x > +h \end{cases} \qquad (2.63)$$

At time $t$ the concentration at point $x^*$ is given as the superposition of the contributions of all line elements. The contribution of the line element at distance $\xi$ from point $x$ and width $d\xi$ (cf. Fig. 2.4) is

$$\frac{c_0 d\xi}{\sqrt{\pi D t}} e^{-\frac{\xi^2}{4Dt}} \tag{2.64}$$
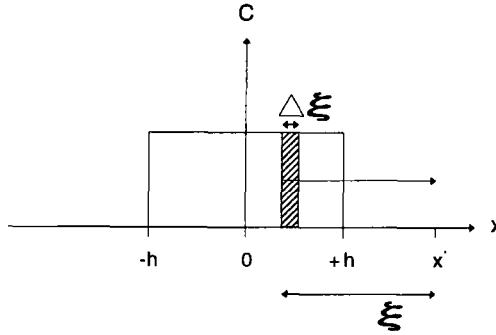


**Fig. 2.4:** Illustration of the principle of superposition. The concentration at point $x^*$ is obtained by integration over all line elements.

Hence, the concentration at any point $x$ is obtained by the integral over all line elements:

$$c(x,t) = \frac{c_0}{2\sqrt{\pi D t}} \int_{x-h}^{x+h} e^{-\frac{\xi^2}{4Dt}} d\xi \tag{2.65}$$

By the substitution

$$\eta = \frac{\xi}{2\sqrt{Dt}}$$

one obtains

$$\int_{x-h}^{x+h} \dots = \frac{c_0}{\sqrt{\pi}} \int_a^b e^{-\eta^2} d\eta \qquad with \quad a = \frac{x-h}{2\sqrt{Dt}} \quad and \quad b = \frac{x+h}{2\sqrt{Dt}} \tag{2.66}$$

It is convenient to express this integral in terms of the error function, which is defined as

$$erf(z) = \frac{2}{\sqrt{\pi}} \int_0^z e^{-\eta^2} d\eta \tag{2.67}$$

Because the error function is widely used, efficient numerical routines are available for its evaluation. Analytical solutions of boundary value problems involving the convection

dispersion equation are obtained as superposition of error functions as shall be dealt with in some detail in chapter 5. In terms of the error function the solution of the above boundary value problem is given by

$$c(x,t) = \frac{1}{2}c_0\left[erf\left(\frac{x+h}{2\sqrt{Dt}}\right) - erf\left(\frac{x-h}{2\sqrt{Dt}}\right)\right]$$

(2.68)

Figure 2.5 shows a series of concentration profiles obtained from Eq. (2.68).
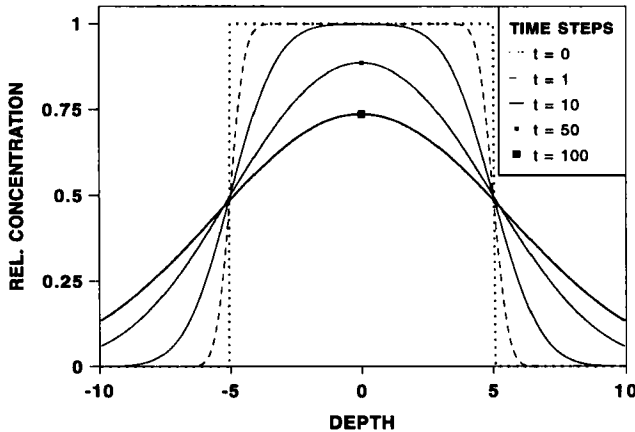


**Fig. 2.5:** Evolution in time of a rectangular initial distribution.

A powerful tool for obtaining analytical solutions of partial differential equations is the method of Laplace transformation. This method will be introduced in section 3.1.4.

**The Model Character of the Diffusion Equation**

At first sight the derivation of the diffusion equation appears straightforward and sound. So one would expect a reasonable physical behavior of the solution. However, if one closely examines Eq. (2.62) or Eq. (2.65), one notices, that they imply an infinite velocity of propagation. At any time $t > 0$ the concentration curve extends to infinity. From a physical point of view this behavior is unreasonable. However, in practical application this effect is not important, because the concentration becomes negligibly small for large $x$. This underlines the model character of the diffusion equation.

## 2.3   Geostatistics

**Measures of Spatial Continuity**

The basic idea of geostatistics is the assumption, that geo-referenced variables such as soil properties are spatially correlated. This assumption is also referred to as spatial continuity. It is intuitively clear that in a field soil properties of neighboring locations tend to be more

similar than those of more distant locations. To analyze the spatial continuity by explorative methods one can construct scatterplots for pairs of data which are separated by a certain distance. Let $Z(\vec{x_i})$ denote a variable measured at location $\vec{x_i}$. The distance vector between two points is $\vec{h}_{ij} = \vec{x_i} - \vec{x_j}$. The plot of $Z(\vec{x}+|\vec{h}|)$ versus $Z(\vec{x})$ characterizes the spatial correlation between all those locations with distance vector $\vec{h}$. If the spatial correlation does only depend on $|\vec{h}|$, the soil is isotropic with respect to this variable and one can simply construct the scatterplot of $Z(\vec{x}+|\vec{h}|)$ versus $Z(\vec{x})$. Figures 2.6 a,b show as example scatterplots of the $K_d$-value of Simazine for two different separation distances. The $K_d$-value is the equilibrium constant for adsorption and desorption of a substance on the soil matrix (cf. chapter 3).
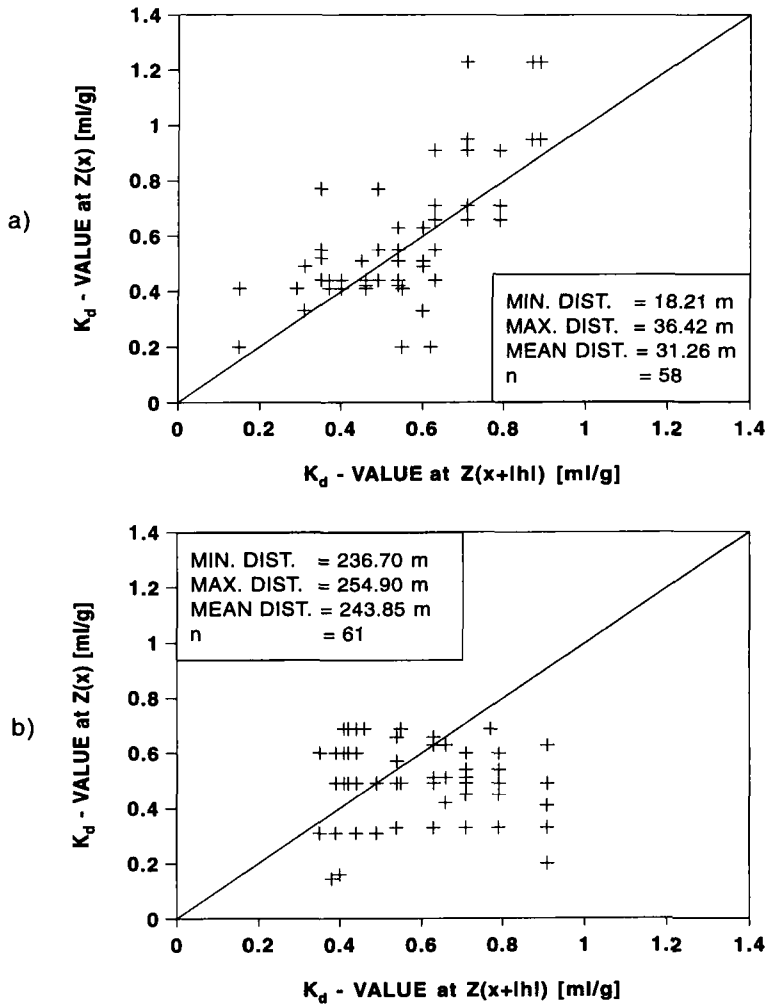


**Fig. 2.6:** Scatterplots of the $K_d$-value of Simazine for two different separation distances (data obtained by Bunte, 1991): a) at a separation distance of about 30 m the spatial correlation is obvious, b) at a separation distance of about 245 m the spatial correlation has failed.

There are several ways to characterize mathematically the spatial dependence. If one regards $Z(\vec{x})$ as a predictor for $Z$ at location $(\vec{x}+|\vec{h}|)$ it is most natural to take the prediction variance as criterion for spatial continuity

$$2\gamma(\vec{h}) = \frac{1}{n(\vec{h})} \sum_{(i,j)|\vec{x}_i-\vec{x}_j = \vec{h}} \left[Z(\vec{x}_i) - Z(\vec{x}_j)\right]^2 \tag{2.69}$$

where $n(\vec{h})$ is the sum of all pairs that are separated by $\vec{h}$. The function $\gamma(\vec{h})$ is traditionally called the semivariogram. Another measure of spatial continuity is the covariance, which is defined by

$$C(\vec{h}) = \frac{1}{n(\vec{h})} \sum_{(i,j)|\vec{x}_i-\vec{x}_j = \vec{h}} \left(Z(\vec{x}_i) - m_{-\vec{h}}\right)\left(Z(\vec{x}_j) - m_{+\vec{h}}\right) \tag{2.70}$$

$m_{-\vec{h}}$ and $m_{+\vec{h}}$ are the means of all those measurements whose locations are $-\vec{h}$ or $+\vec{h}$ respectively away from other locations. For a finite sample size, both means are in general not identical.

The covariance function is related to the correlation function by

$$\rho(\vec{h}) = \frac{C(\vec{h})}{s_{-\vec{h}} \cdot s_{+\vec{h}}} \tag{2.71}$$

$s_{-\vec{h}}$ and $s_{+\vec{h}}$ are the standard deviations of all those measurements whose locations are $-\vec{h}$ or $+\vec{h}$ respectively away from other locations. The most important tool for the analysis of spatial continuity is the semivariogram. This is due to theoretical reasons. The existence of a variogram is the weakest assumption of the underlying spatial stochastic process.

**The Spatial Law**

The three statistics to characterize spatial continuity make only sense if they are related to a stochastic model. A set of measurements taken at $n$ locations is regarded as set of realizations of the vectorial random variable

$$\left\{Z(\vec{x}_1), Z(\vec{x}_2), ..., Z(\vec{x}_n)\right\}$$

In theory, one can assign a multivariate distribution function $F(z_1, z_2, ... , z_n)$ to each random vector

$$F(z_1, z_2, ..., z_n) := P\left\{Z(\vec{x}_1) < z_1, Z(\vec{x}_2) < z_2, ..., Z(\vec{x}_n) < z_n\right\} \tag{2.72}$$

The collection of all distribution functions is referred to as the spatial law of the spatial random variable $Z$ (for a brief description of some frequently used distribution functions cf. appendix A.2).

**First and Second Order Moments**

In geostatistics it is sufficient to know only the first and second order moments, which are related to the measure of continuity given above. The first order moment is the mathematical expectation

$$E\left[Z(\vec{x})\right] = \int_0^\infty z f(z)\, dz := \mu(\vec{x}) \tag{2.73}$$

here $f(z)$ is the probability density function of the random variable $Z(\vec{x})$. Second order moments are the variance, the covariance and the semivariogram. They are defined by

$$V\left[Z(\vec{x})\right] := E\left[(Z(\vec{x}) - \mu(\vec{x}))^2\right] \tag{2.74}$$

$$C(\vec{x}_1, \vec{x}_2) := E\left[(Z(\vec{x}_1) - \mu(\vec{x}_1))(Z(\vec{x}_2) - \mu(\vec{x}_2))\right] \tag{2.75}$$

$$\gamma(\vec{x}_1, \vec{x}_2) := \frac{1}{2} V\left[Z(\vec{x}_1) - Z(\vec{x}_2)\right] \tag{2.76}$$

**Hypotheses of Stationarity**

Since there is no possibility to obtain replications at one and the same position, assumptions have to be made on the degree of spatial homogeneity. Simply speaking one has to assume that the process repeats itself in space. There are three degrees of stationarity.

1. Strict stationarity

This implies that the spatial law is known. A spatial random variable is defined to be strict stationary if the underlying distribution functions are invariant under translation.

2. Stationarity of order 2

As mentioned above, in (linear) geostatistics only the first and second moments are used. So it is sufficient to restrict stationarity assumptions on these moments. The assumptions are only valid for a limited region $G$. A spatial random variable is called second order stationary if

i) the expectation exists and does not depend on the space coordinate, i.e.:

$$E\left[Z(\vec{x})\right] = \mu = const \qquad \text{for all } \vec{x} \in G$$

ii) for each pair of random variables the covariance function exists and depends only on the distance between the space coordinates, i.e.:

$$C(\vec{x}_1, \vec{x}_2) = C(\vec{x}_1 - \vec{x}_2) = E\big[(Z(\vec{x}) - \mu)(Z(\vec{x} + \vec{h}) - \mu)\big] \qquad \textit{for all } \vec{x} \in G$$

$$\vec{h} = \vec{x}_1 - \vec{x}_2$$

It can be shown that the stationarity of the covariance function implies the stationarity of the other second order moments (cf. Journel and Huijbregts, 1989). The covariance function, the variance and the semivariogram are related by

$$V\big[Z(\vec{x})\big] = C(0)$$

(2.77)

$$\gamma(\vec{h}) = C(0) - C(\vec{h})$$

By means of the covariance function, the correlogram is defined as

$$\rho(\vec{h}) = \frac{C(\vec{h})}{C(0)} = 1 - \frac{\gamma(\vec{h})}{C(0)}$$

(2.78)

Figure 2.7 shows the relation between the variogram and the covariogram function.
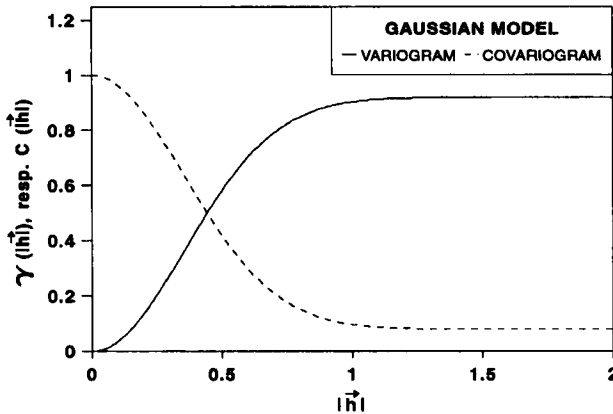


**Fig. 2.7:** Relation between the variogram and the covariogram function.

3. Intrinsic hypothesis

In practice, one frequently meets situations where the variogram is not bounded, i.e. the variance and the covariance do not exist. In this case one only assumes that

i) the expectation exists and does not depend on the space coordinate

$$E\big[Z(\vec{x})\big] = \mu = \textit{const} \qquad \textit{for all } \vec{x} \in G$$

ii) that the variogram exists, i.e. that $[Z(\vec{x}+|\vec{h}|) - Z(\vec{x})]$ has a finite variance which does not depend on the space coordinate, but only on $\vec{h}$.

## Variogram Models

The variogram can be estimated by the formula for the empirical variogram (Eq. (2.69)), which is the so called **method of moments estimator** of the variogram. For further use of the variogram function for spatial prediction it is desirable to fit the points of the empirical variogram to a model. In order to ensure positiveness of the variance, the class of admissible variogram models is subjected to the condition

$$\sum_{i=1}^{n} \sum_{j=1}^{m} \alpha_i \alpha_j \gamma(\vec{x}_i - \vec{x}_j) \leq 0 \tag{2.79}$$

for any real numbers $\alpha_i$ and $\alpha_j$ satisfying

$$\sum_{i=1}^{n} \alpha_i = \sum_{j=1}^{m} \alpha_j = 0$$

This property is called conditionally negative definite. In the following, some often used isotropic variogram models are described which possess this property. It is frequently found that the spatial correlation between variables is fading with distance and finally disappears. From Eq. (2.77) it follows that the semivariogram reaches the asymptotic value $C(0)$ for $|\vec{h}| \to \infty$. This value is called the sill. The following models are normalized to a sill value of 1.

Spherical model:

$$\gamma(|\vec{h}|) = \begin{cases} \dfrac{3}{2}\dfrac{|\vec{h}|}{a} - \dfrac{1}{2}\dfrac{|\vec{h}|^3}{a^3} & |\vec{h}| \in [0,a] \\ \\ 1 & |\vec{h}| > a \end{cases} \tag{2.80}$$

Exponential model:

$$\gamma(|\vec{h}|) = 1 - e^{-\frac{|\vec{h}|}{a}} \tag{2.81}$$

Gaussian model:

$$\gamma(|\vec{h}|) = 1 - e^{-\frac{|\vec{h}|^2}{a^2}} \tag{2.82}$$

The parameter $a$ is called the range. Figure 7.10 (cf. section 7.3) shows plots of these variogram functions. A theoretical variogram model must take the value of zero in the origin. In practice, one frequently finds a value at or near the origin greater than zero. This may be

due to the size of the spatial grid. Obviously, it is not possible to resolve spatial processes with a range smaller than the grid size. This is referred to as nugget effect and the value at the origin is called the nugget constant. Figure 2.8 shows the variogram of the $K_d$-value of the herbicide Simazine (obtained from Bunte, 1991).
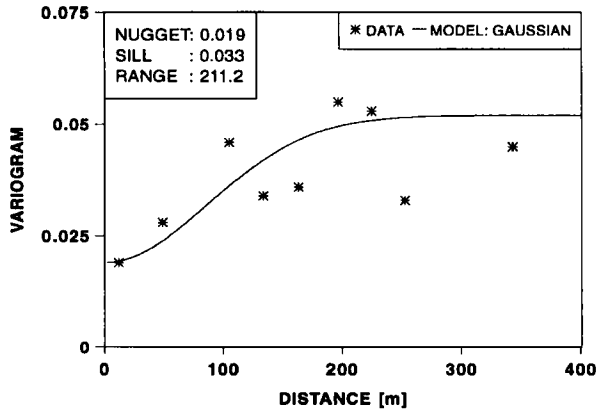


**Fig. 2.8:** Variogram of the $K_d$-value of the herbicide Simazine (Bunte, 1991). The data are fitted to a Gaussian variogram model with a nugget value.

## Spatial Prediction

In the following it is assumed that the underlying spatial process is at least intrinsic stationary. It is the most important task of geostatistics to provide methods of spatial prediction. The problem may be stated as follows:

Given are measurements of a spatial random variable $Z$ at locations $\vec{x}_1, \dots, \vec{x}_n$ in a region $G$, where the stationary hypothesis is valid. The problem is then to predict the value of $Z$ at a location $\vec{x}_0$ in $G$. Let $p(Z(\vec{x}_0))$ denote a predictor. What statistical properties should a predictor have? The first property we could ask for is its unbiasedness:

$$E\left[p\left(Z(\vec{x}_o)\right) - Z(\vec{x}_o)\right] = 0 \tag{2.83}$$

It is obvious to demand that a predictor should have a great precision. Since the predictor is a random variable itself we should ask for a predictor with minimum variance. The arithmetic mean is certainly an unbiased estimator, since

$$E\left[\frac{1}{n}\sum_{i=1}^{n} z(\vec{x}_i)\right] = \frac{1}{n}\sum_{i=1}^{n} \mu = \mu \tag{2.84}$$

However, in the arithmetic mean, each measurement is equally weighted regardless of its position with respect to $\vec{x}_0$. The information contained in the variogram or covariogram function on spatial structure is not used in this simple predictor. It is obvious that the spatial configuration of the sample points and the position of $\vec{x}_0$ with respect to the sample points

influence the information on $Z(\vec{x}_0)$. This information is contained in the variogram or the covariogram function. Variogram models are therefore essential to improve the precision of spatial prediction.

The simplest way to construct a predictor is to take the weighted sum of the $Z(\vec{x}_i)$:

$$p\big(Z(\vec{x}_o)\big) = \sum_{i=1}^{n} \lambda_i Z(\vec{x}_i) \tag{2.85}$$

Predictors of this class are called linear predictors. The mathematical problem posed is to determine the weights $\lambda_i$ such that the variance of the predictor is minimized. A linear unbiased predictor with these properties is called best linear unbiased predictor. Unbiasedness is guaranteed by imposing the constraint

$$\sum_{i=1}^{n} \lambda_i = 1 \tag{2.86}$$

on the weights. The variance of the predictor is given by

$$\sigma^2\big(Z(\vec{x}_o)\big) = E\left[\left(Z(\vec{x}_o) - \sum_{i=1}^{n} \lambda_i Z(\vec{x}_i)\right)^2\right] \tag{2.87}$$

The mathematical problem posed is to minimize Eq. (2.87) subject to the constraint Eq. (2.86). It is at this stage, that the spatial information contained in the variogram or covariogram function is used to determine the weights $\lambda_i$.

$$\left(Z(\vec{x}_o) - \sum_{i=1}^{n} \lambda_i Z(\vec{x}_i)\right)^2$$
$$= -\frac{1}{2}\sum_{i=1}^{n}\sum_{j=1}^{n}\big(Z(\vec{x}_i) - Z(\vec{x}_j)\big)^2 + \sum_{i=1}^{n}\lambda_i\big(Z(\vec{x}_o) - Z(\vec{x}_i)\big)^2 \tag{2.88}$$

From the definition of the variogram Eq. (2.76) it follows that the expectation of the above equation can be expressed in terms of the variogram as

$$E[\ldots] = -\sum_{i=1}^{n}\sum_{j=1}^{n}\lambda_i\lambda_j\gamma\big(\vec{x}_i - \vec{x}_j\big) + 2\sum_{i=1}^{n}\lambda_i\gamma\big(\vec{x}_o - \vec{x}_i\big) \tag{2.89}$$

We shall not pursue the mathematical development further. The constrained minimization problem is solved in a straightforward manner by employing Lagrange multiplier techniques. The weights $\lambda_i$ are then obtained as solution of a linear equation system. This geostatistical

procedure is referred to as "kriging" since it goes back to the work of the South African mining engineer D. G. Krige. Figure 2.9 shows as an example the contour map of $K_d$-values of Simazine obtained by kriging using the variogram model as shown in Fig. 2.8.
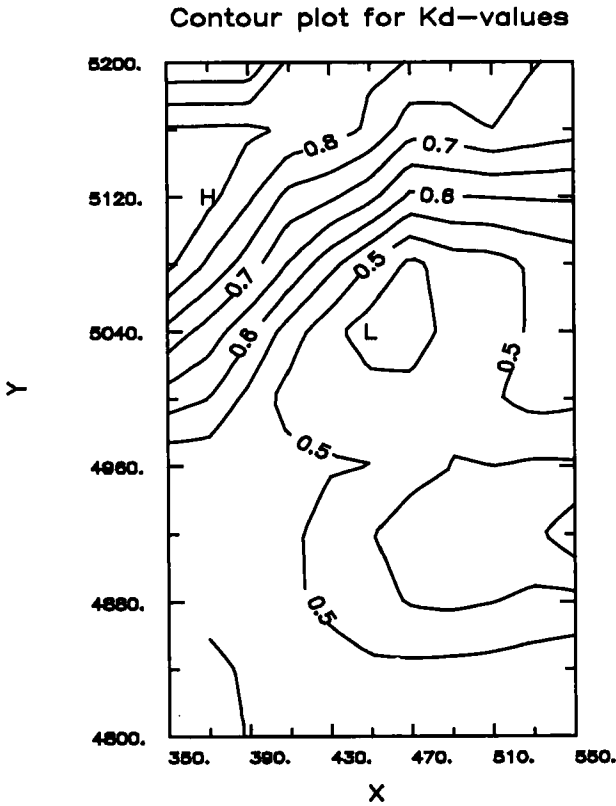


**Fig. 2.9:** Contour map of $K_d$-values of Simazine [ml/g] obtained by kriging using the variogram model as shown in Fig. 2.8. The following notation holds:
L: $K_d$-value lower than 0.5 ml/g;
H: $K_d$-value higher than 0.8 ml/g.

**Spatial Simulation**

The spatial variability of the $K_d$-value of Simazine exerts a great influence on the persistence of Simazine. The $K_d$-value is an important parameter of transport and kinetic models. However, the contour maps obtained by kriging are only one possible realization of the underlying spatial random process. If one wants to study the statistical properties of kinetic or transport models, which are treated in detail in later chapters (cf. chapters 5 to 7), one has to generate many replications of the spatial process. There are methods to simulate the spatial stochastic process for a given covariance function. A frequently used method is the so-called turning bands method, which is described in detail in the textbook of Journel and Huijbregts (1989). Chapter 7 of our book contains some examples of the application of this methods to generate three-dimensional random parameter fields for water and matter transport in soils.

# 3    Kinetics

## 3.1    Linear Models

### 3.1.1    The Compartment Concept

This section is concerned with procedures involved in constructing mathematical models of dynamic processes. It is an old philosophical question why it is possible to describe natural processes in the language of mathematics. We shall not dwell on this important philosophical background but rather try to give some practical guidelines how to proceed when translating processes into the language of mathematics. The viewpoint taken is a personal one, although shared by other scientists. In the first place, mathematical modelling is based on a detailed knowledge of the underlying processes and on the mastery of the mathematical tools. It should be kept in mind that a mathematical model is not a one to one mapping of reality into a system of equations. A mathematical model is always an abstraction of reality.

### Compartment Schemes

The starting point of mathematical modelling is the design of a **conceptual model**. The conceptual model comprises our knowledge of the system and a careful (subjective) selection of components and processes judged essential for the processes under study. At this stage, it is helpful, to represent the conceptual model graphically in form of a **compartment system.**
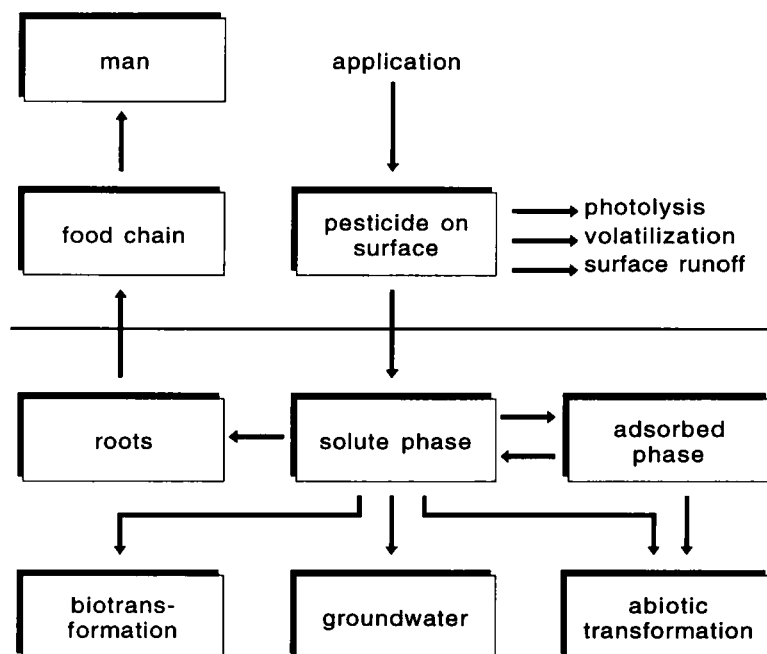


**Fig. 3.1:** Conceptual model for the fate of a substance in the soil in form of a compartment scheme. The arrows denote fluxes.

Compartments are defined with respect to morphology and to physical and chemical states. Consider the environmental fate of a chemical. Morphologically, one may roughly distinguish the compartments atmosphere, soil and water, which may be further subdivided into atmospheric and soil layers. The substance may be adsorbed to the soil matrix and be transformed chemically. Bound states and metabolites are also presented as compartments (cf. Fig. 3.1). Fluxes between compartments due to transport or chemical transformations are presented by arrows.

The design of a conceptual model already implies a choice of spatial and temporal scales. Consider for instance the metabolic transformation of a pesticide mediated by enzymatic action within microorganisms. The characteristic times involved at the macroscopic level are in the order of magnitudes of weeks or months. At the microscopic level, reactions proceed much faster e.g. the characteristic times of the formation of the enzyme-substrate complex are in the order of magnitude of $10^{-6}$ s. By omitting the compartment "enzyme-substrate complex" in the conceptual model, the macroscopic level of temporal resolution is implicitly chosen. One also speaks of aggregation with respect to time. Similar conventions hold for the spatial resolution. Unless otherwise stated, a compartment is regarded as spatially homogeneous. It is considered as a "well stirred" reaction tube, where no spatial inhomogeneities can persist. This is equivalent to the notion of a system with "concentrated" parameters in contrast to systems with "distributed" parameters.

**Physical Principles**

Although most models of biological processes cannot be derived from "first principles", the law of conservation of mass applies to all systems. Therefore, the first step in modelling is the setup of the basic mass balance equations. This is easily done as shown in the following example.
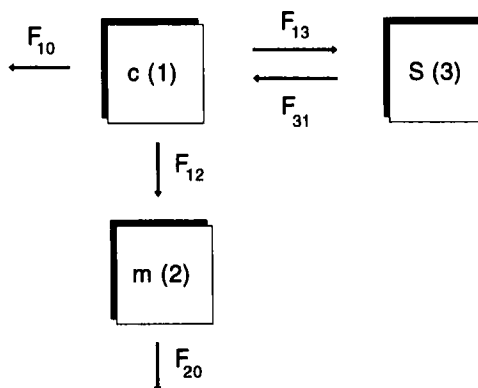


**Fig. 3.2:** Mass flows in a compartment system describing the fate of a substance and its metabolite ($m$) in soil. The substance is degraded in the solute phase ($c$), it is reversibly bound to the soil matrix ($S$) and it may leave the system by leaching (further explanations see text).

Consider the compartment system as given in Fig. 3.2 which describes the fate of a pesticide and its metabolite. The pesticide is degraded in the solute phase, it is reversibly bound to the soil matrix and it may leave the system by leaching. Let us first invent a convenient notation.

Frequently, $c$ is used for pesticide concentration in the solute phase, $S$ in the sorbed phase and $m$ for metabolites. If the compartments are numbered, it is suitable to define the fluxes between two adjacent compartments numbered $i$ and $j$ by $F_{ij}$. The index 0 denotes the environment of the system. Thus, the flux $F_{10}$ denotes the flux from compartment 1 to the environment. The set of mass balance equations is set up according to the following sign convention: losses are endowed with a negative and gains with a positive sign. The rate of change of the substance in a compartment is then given by the sum of all fluxes.

$$\frac{dc}{dt} = -F_{12} - F_{13} - F_{10} + F_{31} \tag{3.1a}$$

$$\frac{dS}{dt} = F_{13} - F_{31} \tag{3.1b}$$

$$\frac{dm}{dt} = F_{12} - F_{20} \tag{3.1c}$$

This set of ordinary differential equations has to be specified by the mathematical form of the fluxes and by the initial values.

Whereas the mass balance equations are easily set up following the principle of mass conservation, the appropriate form of the fluxes can only be derived by experiments. Let us consider the rate of degradation $F_{12}$. The pesticide may decay abiotically, for instance by hydrolysis. In this case, the degradation rate will be found to be proportional to $c$:

$$F_{12} = kc \tag{3.2a}$$

This is the most simple approach possible. A reaction of this type is referred to as first order reaction or linear reaction. If the substance is degraded by microorganisms it is most probably transformed in an enzymatic reaction. For the simplest mechanism of enzyme catalytic action, the rate law is given by the Michaelis-Menten form

$$F_{12} = \frac{V_{max} c}{K_M + c} \tag{3.2b}$$

The flux or reaction rate depends in a **nonlinear** manner on concentration $c$. As we shall see in subsequent chapters, the system behavior is drastically changed, when nonlinear rate laws hold. For concentrations much lower than the Michaelis constant $K_M$, the Michaelis-Menten law becomes approximately linear:

$$V \approx \frac{V_{max}}{K_M} c = kc \qquad for \quad c << K_M \tag{3.3}$$

For concentrations far above the Michaelis constant, the reaction rate approaches the maximum velocity $V_{max}$. In this range, the reaction is of apparent zero order. Nonlinearities

of this type are difficult to detect from single experiments. Only if initial concentrations are far above the $K_M$-value, deviations from first order kinetics become apparent. Due to measurement errors the parameter estimation problem is not "well posed" and $V_{max}$ and $K_M$ are highly correlated. They can be estimated only from a series of experiments with varying initial concentrations. Problems of this kind are dealt with in detail in chapter 4.

### 3.1.2  Simple Linear Systems

**Introduction**

If all fluxes can be assumed to be linear functions of the state variables, e.g. concentrations, the differential equations are linear. This facilitates the mathematical treatment considerably:

i)      Linear systems possess analytical solutions, i.e. solutions in form of known functions like exponential functions or sine functions.
ii)     The system behavior can be easily studied for arbitrary input functions by means of the mathematically well founded linear systems analysis.
iii)    Parameter estimation is easily carried out for small systems.
iv)     Linear systems may serve as approximations to nonlinear systems.

However, some remarks on the range of applications of linear models are in order. In nature, especially in biology, most processes exhibit nonlinear rate laws, which are approximately linear at low concentrations as pointed out above. Nonlinearities may lead to a complex dynamic behavior comprising multiple steady states, bifurcations and extreme sensitivity with respect to initial conditions. Therefore, in most applications, the design of linear models should be regarded as a first approximation only.

**Some simple examples**

In this section we shall deal with simple systems, which are amenable to analytical solutions by elementary techniques. As first example, a **one compartment system** is considered. Such a simple model may apply to substances, which are degraded by first order kinetics and do not show any interaction with the soil matrix. The corresponding initial value problem is

$$\frac{dc}{dt} = -kc \qquad with \quad c(t=0) = c_0 \tag{3.4}$$

which is solved by the method of separation of variables (cf. section 2.1) to yield

$$c(t) = c_0\, e^{-kt} \tag{3.5}$$

Consider next the case of a constant influx $v_0$. The differential equation balances the influx (positive sign) and the efflux by degradation (negative sign). Both processes occur simultaneously.

$$\frac{dc}{dt} = v_0 - kc \qquad with \quad c(t=0) = c_0 \tag{3.6}$$

Again, this initial value problem may be solved by elementary methods (cf. chapter 2) to yield

$$c(t) = c_0 \, e^{-kt} + \frac{v_0}{k}(1 - e^{-kt}) \tag{3.7}$$

It is interesting to study the asymptotic behavior of the solution. For $t \to \infty$ the equilibrium value $c_s = v_0/k$ is attained. This is an important result: **in a system with linear degradation rates, no accumulation ad infinitum can occur!** For comparison, consider the case of capacity limited degradation as modeled by the Michaelis-Menten rate law. The differential equation

$$\frac{dc}{dt} = v_0 - \frac{V_{max}\,c}{c + K_M} \tag{3.8}$$

has no analytical solution. However, it is easy to compute steady state concentrations by simply setting the left hand side of the differential equation equal to zero. This means, that the net rate of change is zero by a detailed balancing of influx and efflux. In the case of the linear degradation law this leads to the asymptotic value derived above. In the case of the nonlinear law, one is lead to

$$c_s = \frac{v_0 K_M}{V_{max} - v_0} \tag{3.9}$$

A stationary concentration exists only for $v_0 < V_{max}$. Therefore accumulation ad infinitum will occur, once this threshold is surpassed.

As next example the **two compartment system** consisting of a parent compound and one metabolite ($m$) is considered (cf. Fig. 3.3).
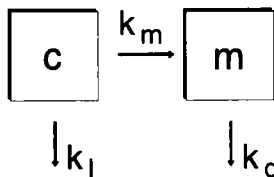


**Fig. 3.3:** Compartment scheme for a parent compound and its metabolite. The $k_j$ denote first order reaction constants.

The parent compound is either transformed to the metabolite or leaves the compartment by transport. Both processes are assumed to be linear. The dynamics is modeled by the two **coupled differential equations**

$$\frac{dc}{dt} = -(k_l + k_m)c \qquad with \quad c(t=0) = c_0 \tag{3.10a}$$

$$\frac{dm}{dt} = k_m c - k_d m \qquad with \quad m(t=0) = 0 \tag{3.10b}$$

The solution is obtained in a straightforward manner. The first equation is independent from the second and is integrated to

$$c(t) = c_0 e^{-(k_l + k_m)t} \tag{3.11}$$

Equation (3.11) is inserted into Eq. (3.10b) yielding

$$\frac{dm}{dt} = k_m c_0 e^{-(k_l + k_m)t} - k_d m \tag{3.12}$$

This equation is solved by the "trick" of the integrating factor. Multiplying Eq. (3.12) by the factor $exp\ (k_d t)$ and rearranging leads to the form

$$\frac{d}{dt}\left[e^{k_d t}\right] = k_m c_0 e^{-(k_l + k_m - k_d)t} \tag{3.13}$$

This equation can be directly integrated. For the initial condition $m(t=0) = 0$, the solution is obtained as

$$m(t) = \frac{c_0 k_m}{k - k_d}\left[e^{-k_d t} - e^{-kt}\right] \qquad with \quad k = k_l + k_m \tag{3.14}$$

Figure 3.4 shows an application of this model to the kinetics of Methazole and its metabolite DCPM as measured by Walker (1978). The model parameters were estimated by the nonlinear regression techniques described in chapter 4.
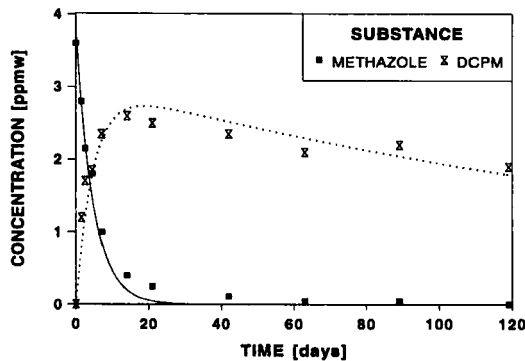


**Fig. 3.4:** Kinetics of Methazole and its main metabolite DCPM. The fit is based on Eqs. (3.11) and (3.14) (experimental data from Walker, 1978).

## 3.1.3 Solution by Matrix Methods

Notations

$D$    : total amount of a substance [M]
$c_t$    : total concentration [M/L$^3$]
$c$    : liquid phase concentration [M/L$^3$]
$g$    : gaseous phase concentration [M/L$^3$]
$S$    : solid phase concentration [M/M]
$\theta$    : volumetric water content [L$^3$/L$^3$]
$\rho$    : bulk density [M/L$^3$]
$\varepsilon$    : volumetric air content [L$^3$/L$^3$]
$K_d$    : sorption coefficient [L$^3$/M]
$\alpha$    : velocity constant for sorption and desorption [1/T]

The last example could be solved by elementary methods, because the reaction is assumed to be irreversible. This is why the first equation is independent of the second one. Let us consider now the case of a reversible reaction. When setting up the mass balance equation, one has to take into account the partition of the volume of distribution into solute, solid and gaseous phases (cf. Fig. 3.5). Let $c$ denote solute, $S$ solid and $g$ gaseous phase concentrations.
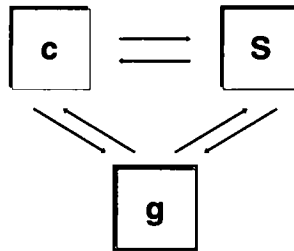


**Fig. 3.5:** Compartment scheme model for the partition of a substance into liquid ($c$), solid ($S$) and gaseous ($g$) phases of soil.

These concentrations refer to the volumes and weights of the respective phases within one unit of soil. However, mass balance equations refer to unit volumes of soil comprising all three phases. Therefore, the concentration of a substance with respect to a unit volume of soil is given by

$$c_t = \theta c + \rho S + \varepsilon g$$

In the following model, the gaseous phase is neglected. If degradation, sorption and desorption to the soil matrix obey linear kinetics the adequate mass balance equations are

$$\frac{d}{dt}(\theta c) = -\alpha\rho(K_d c - S) - \theta k_l c \qquad (3.15a)$$

$$\frac{d}{dt}(\rho S) = \alpha\rho(K_d c - S) \tag{3.15b}$$

The equations describe one site kinetic adsorption. That means, that adsorption-desorption are so slow that they can be kinetically distinguished. If these processes are fast with respect to degradation, concentrations in liquid and solute phase are in a quasi equilibrium. In the equilibrium state, the time derivative of Eq. (3.15b) is equal to zero and one obtains the relationship $S = K_d c$. Thus, $K_d$ has the meaning of an equilibrium constant. The parameter $\alpha$ determines the velocity of the adsorption-desorption process. It is assumed that degradation occurs only in the liquid phase with rate constant $k_l$.

The above equations cannot be solved by the elementary methods used previously. Equation (3.15a) is linked to Eq. (3.15b) via the adsorption-desorption term and cannot be integrated independently. The problem is amenable to a solution in a straightforward manner, if it is presented in matrix form:

$$\frac{d}{dt}\begin{pmatrix} c \\ \\ S \end{pmatrix} = \begin{pmatrix} -\dfrac{\rho}{\theta}\alpha K_d - k_l & \dfrac{\rho}{\theta}\alpha \\ \\ \alpha K_d & -\alpha \end{pmatrix}\begin{pmatrix} c \\ \\ S \end{pmatrix} \tag{3.16a}$$

For ease of presentation the notations $y_1, ..., y_n$ will be used for the state variables and $a_{ij}$ for the elements of the system matrix, which is denoted by $A$. Equation (3.16a) thus takes the simple form

$$\frac{d}{dt}\begin{pmatrix} y_1 \\ \\ y_2 \end{pmatrix} = \begin{pmatrix} a_{11} & a_{12} \\ \\ a_{21} & a_{22} \end{pmatrix}\begin{pmatrix} y_1 \\ \\ y_2 \end{pmatrix} \tag{3.16b}$$

with

$$a_{11} = -\frac{\rho}{\theta}\alpha K_d - k_l \qquad a_{12} = \frac{\rho}{\theta}\alpha$$

$$a_{21} = \alpha K_d \qquad\qquad a_{22} = -\alpha$$

In the general case, a linear differential equation system is written as

$$\frac{d\vec{y}}{dt} = A\vec{y} \tag{3.17}$$

The one-dimensional equation, where $a$ is a scalar,

$$\frac{dy}{dt} = ay$$

is solved by the ansatz $y(t) = e^{\lambda t}$:

$$\frac{d(e^{\lambda t})}{dt} = \lambda e^{\lambda t} = a e^{\lambda t}$$

It is reasonable to try an analogous approach for the multidimensional system.

Inserting

$$\vec{y} = \begin{pmatrix} y_1 \\ y_2 \\ \cdot \\ \cdot \\ \cdot \\ y_n \end{pmatrix} = \begin{pmatrix} v_1 \\ v_2 \\ \cdot \\ \cdot \\ \cdot \\ v_n \end{pmatrix} e^{\lambda t} = \vec{v} e^{\lambda t} \qquad (3.18)$$

into Eq. (3.17) yields

$$\frac{d}{dt}(\vec{v} e^{\lambda t}) = \vec{v} \lambda e^{\lambda t} = A \vec{v} e^{\lambda t} \qquad (3.19)$$

By division by the factor $e^{\lambda t}$ and rearranging one obtains the following homogeneous linear equation system.

$$(A - \lambda I)\vec{v} = 0 \qquad (3.20)$$

where $I$ denotes the unit matrix. This equation system possesses nontrivial solutions, i.e. solutions $\neq 0$, only, if the matrix $B = (A - \lambda I)$ is singular. This is the case, if the determinant of the matrix is zero. The condition

$$\det(A - \lambda I) = 0 \qquad (3.21)$$

leads to a polynomial of degree n for $\lambda$. This polynomial is denoted as the characteristic polynomial. A polynomial of degree n possesses n roots. The roots of the characteristic polynomial are denoted as the eigenvalues (latent roots) of $B$. For each eigenvalue $\lambda_i$ there exists an eigenvector $\vec{v}^{(i)}$ (components of a vector are denoted by subscripts, vectors are indexed by a superscript). Let us consider the case, that all eigenvalues are distinct. Then the general solution of the differential equation system Eq. (3.17) is the superposition of all special solutions:

$$\vec{y} = \begin{pmatrix} y_1 \\ y_2 \\ \cdot \\ \cdot \\ \cdot \\ y_n \end{pmatrix} = \sum_{i=1}^{n} c_i \begin{pmatrix} v_1 \\ v_2 \\ \cdot \\ \cdot \\ \cdot \\ v_n \end{pmatrix}_i e^{\lambda_i t} = \sum_{i=1}^{n} c_i \vec{v}^{(i)} e^{\lambda_i t} \qquad (3.22)$$

The constants $c_1, c_2, \dots, c_n$ are determined by the choice of the $n$ initial conditions. Let us return now to the sorption-desorption model as presented in Eq. (3.16a,b). To avoid the use of too many indices the matrix elements are denoted by $a$, $b$, $c$ and $d$. The characteristic polynomial is derived as

$$\det(A - \lambda I) = \det \begin{pmatrix} a - \lambda & b \\ c & d - \lambda \end{pmatrix} = (a - \lambda)(d - \lambda) - bc = 0 \qquad (3.23)$$

Its two roots are

$$\lambda_{1/2} = \frac{1}{2}(a + d) \pm \sqrt{\frac{1}{4}(a + d)^2 - ad + bc} =$$

$$= -\frac{1}{2}\left(\frac{\rho}{\theta}\alpha K_d + k_l + \alpha\right) \pm \sqrt{\frac{1}{4}\left(\frac{\rho}{\theta}\alpha K_d + k_l + \alpha\right)^2 - \alpha k_l} \qquad (3.24)$$

Note that both roots have a negative sign, because all parameters are positive constants. It is also obvious, that the absolute values of the two roots differ. The differences are determined by the value of $\alpha$. Remember that the general solution of the linear differential equation system is a sum of exponential functions with the roots of the characteristic polynomial as parameters. Without proceeding further, we can already conclude, that the system exhibits a biphasic kinetic, i.e. a kinetic with two different characteristic times.

The next task is the **computation of the eigenvectors**. To this end, the homogeneous linear equations system (Eq. (3.20)) is solved for each eigenvalue. For the first eigenvalue, the equation system is

$$\begin{pmatrix} a - \lambda_1 & b \\ c & d - \lambda_1 \end{pmatrix} \begin{pmatrix} v_1 \\ v_2 \end{pmatrix} = 0 \qquad (3.25)$$

These two linear equations are linearly dependent. This is ensured by inserting for $\lambda$ the eigenvalue $\lambda_1$, which renders the matrix of the system singular. From the first equation, one obtains the following relationship between $v_1$ and $v_2$:

$$v_1 = -\frac{bv_2}{a - \lambda_1}$$                                                                                                    (3.26a)

The second equation yields:

$$v_1 = -\frac{d - \lambda_1}{c}v_2$$                                                                                                   (3.26b)

Both relationships are identical because $\lambda_1$ is an eigenvalue of the system matrix. Thus, either $v_1$ or $v_2$ may be arbitrarily chosen. $v_2$ is set equal to 1. Note, that this degree of freedom is removed once the initial values are specified as will be shown soon. Employing Eq. (3.26b) the first eigenvector is then given by

$$\vec{v}_1 = \begin{pmatrix} -\dfrac{d - \lambda_1}{c} \\ 1 \end{pmatrix}$$                                                            (3.27)

For the second eigenvector, the same procedure is performed just changing $\lambda_1$ into $\lambda_2$. Inserting these results into Eq. (3.22) leads to the general solution

$$\begin{pmatrix} y_1 \\ y_2 \end{pmatrix} = c_1 \begin{pmatrix} \dfrac{\lambda_1 - d}{c} \\ 1 \end{pmatrix} e^{\lambda_1 t} + c_2 \begin{pmatrix} \dfrac{\lambda_2 - d}{c} \\ 1 \end{pmatrix} e^{\lambda_2 t}$$                                                      (3.28)

In the next step, the constants $c_1$ and $c_2$ are determined by the initial conditions. For the situation of a first application of the chemical, initial conditions are $y_1(t=0) = y_{10}$ and $y_2(t=0) = 0$. Inserting these values into Eq. (3.28) yields the relations

$$y_{10} = c_1 \frac{\lambda_1 - d}{c} + c_2 \frac{\lambda_2 - d}{c}$$                                                                    (3.29)

$$c_1 = -c_2$$

from which $c_1$ is determined as

$$c_1 = y_{10} \frac{c}{\lambda_1 - \lambda_2}$$                                                                                         (3.30)

One finally arrives at the solution

$$y_1(t) = y_{10}\left(A e^{\lambda_1 t} + B e^{\lambda_2 t}\right)$$                                                                     (3.31a)

$$y_2(t) = c_1\left(e^{\lambda_1 t} - e^{\lambda_2 t}\right)$$                    (3.31b)

with

$$A = \frac{\lambda_1 - d}{\lambda_1 - \lambda_2} , \qquad B = -\frac{\lambda_2 - d}{\lambda_1 - \lambda_2}$$

Due to sorption and desorption, the time course of the concentration in the solute phase, $y_1(t)$, is described by the sum of two exponentials. This is denoted as bi-exponential decay. Figure 3.6 shows a plot of a bi-exponential decay curve derived from 2,4-D data published by McCall et al. (1981).
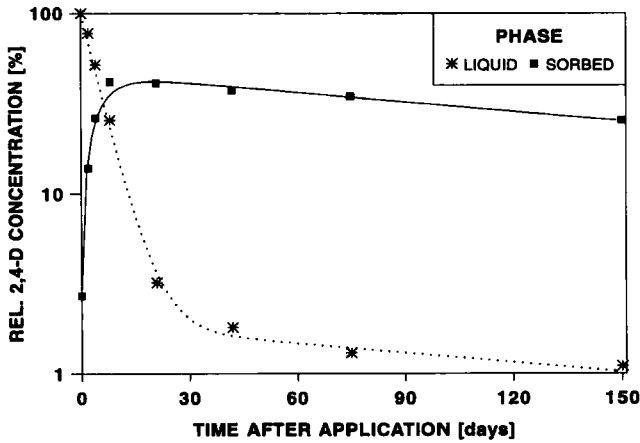


**Fig. 3.6:** Sorption-desorption processes lead to a bi-exponential decay curve of 2,4-D (experimental data from McCall et al., 1981). The fit is based on Eq. (3.31a,b), assuming the acetic acid ethylether extractable fraction of 2,4-D is available for degradation processes. The semilogarithmic plot reveals the biphasic decay.

One clearly distinguishes a fast and a slow phase. The fast phase is mainly determined by sorption, whereas the slow phase is mainly determined by degradation. If sorption and desorption are fast compared to degradation, the duration of the first phase is very short and quasi equilibrium prevails. Frequently, in practice, the fast phase is not observed, because its characteristic time is shorter than the time until the first measurement. In this case, only the slow phase is observable. In a semilogarithmic plot $y_1(t)$ approaches a straight line both for short and for large times.

**Equilibrium Approach**

Often the characteristic times of absorption and desorption processes are orders of magnitude faster than the degradation times. Therefore, a quasi equilibrium prevails. Mathematically, the equilibrium solution is obtained in the limit $\alpha \to \infty$. For $\lambda_1$ the limit is obtained in the following way. In the first step, $\lambda_1$ is written as

$$\lambda_1 = -\frac{1}{2}\left(\frac{\rho}{\theta}\alpha K_d + k_l + \alpha\right)\left[1 - \sqrt{1 - \frac{\alpha k_l}{\frac{1}{4}\left(\frac{\rho}{\theta}\alpha K_d + k_l + \alpha\right)^2}}\right] \quad (3.32)$$

By employing the inequality

$$(1 + \varepsilon)^m \le (1 + m\varepsilon) \qquad m < 1$$

with

$$\varepsilon = \frac{\alpha k_l}{\frac{1}{4}\left(\frac{\rho}{\theta}\alpha K_d + k_l + \alpha\right)^2}$$

one obtains the limit

$$\lambda_1 = -\frac{k_l}{1 + \frac{\rho}{\theta}K_d}$$

For $\lambda_2$ the limit is obtained by simply neglecting $k_l$ in those terms, which contain the sum of all rate constants. One finally arrives at

$$y_1(t) = \frac{y_{10}}{1 + \frac{\rho}{\theta}K_d}\left[e^{-k_{eff}t} + \frac{\rho}{\theta}K_d e^{-\left(\frac{\rho}{\theta}\alpha K_d + \alpha\right)t}\right] \quad (3.33)$$

where the effective degradation rate, $k_{eff}$, is defined by

$$k_{eff} = \frac{k_l}{1 + \frac{\rho}{\theta}K_d}$$

This equation shows that in the limit of very fast sorption-desorption processes the degradation curve becomes quasi mono-exponential, since the second term of Eq. (3.33) goes to zero for $\alpha \rightarrow \infty$. This is illustrated in Figs. 3.7 a,b. However, and this is an important result, the effective degradation rate is now dependent on the $K_d$-value and on the partitioning of the solid and liquid phase. **Degradation is retarded by sorption.** This is due to the assumption, that degradation only occurs in the liquid phase. The $K_d$-value in turn depends on soil properties like silt or $C_{org}$-content and on the physico-chemical properties of the substance.
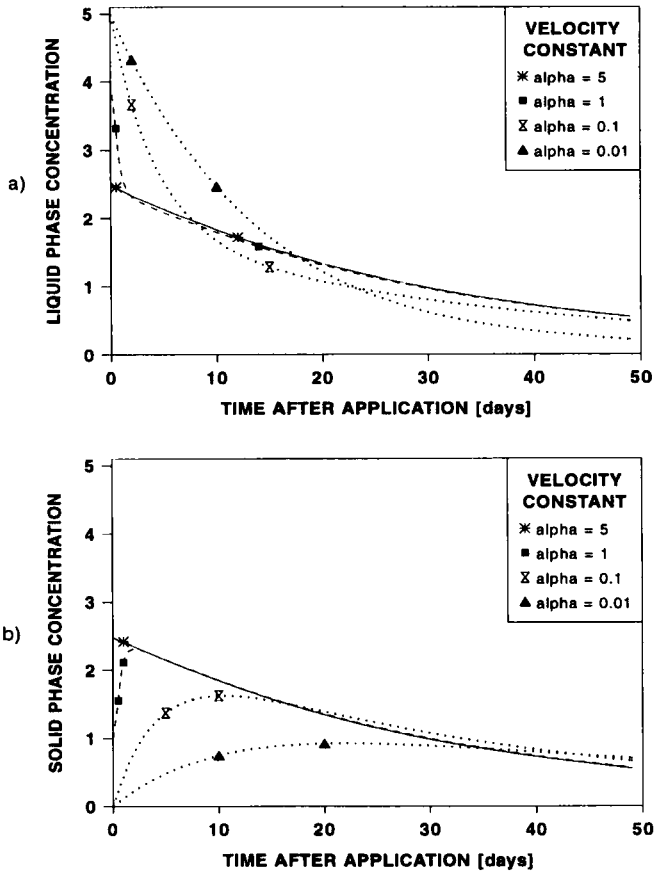
**Fig. 3.7:** In the limit of very fast sorption-desorption processes the degradation curve becomes quasi mono-exponential. This transition is demonstrated in the figure by a series of decay curves for increasing velocity constant $\alpha$ [1/day]: a) liquid phase concentrations and b) solid phase concentrations.

This result can also be derived by a direct equilibrium approach using the mass balance equation in integral form. At each time point $t$ the mass balance is expressed by

$$\theta y_1(t) + \rho y_2(t) + \theta \int_0^t k_l y_1(\tau) d\tau = D \tag{3.34}$$

At equilibrium, $y_2 = K_d\, y_1$. Inserting this relation into Eq. (3.34) one obtains after differentiation and rearrangement the differential equation

$$\frac{dy_1}{dt} = - \frac{k_l}{1 + \frac{\rho}{\theta} K_d} y_1 = -k_{eff} y_1 \tag{3.35}$$

Since equilibrium is attained instantaneously, the initial value of the differential equation has to be modified according to

$$(y_{10})_{eq} = \frac{y_{10}}{1 + \frac{\rho}{\theta}K_d}$$

Thus the solution of Eq. (3.35) is identical to the limit of Eq. (3.33).

### Two Binding Sites

It is frequently observed that $K_d$-values change with time. Sorption apparently becomes stronger with time. This behavior is shown in Fig. 3.8, where the time courses of the $K_d$-values of Simazine (cf. Fig. 3.8 a) and Quinmerac (cf. Fig. 3.8 b) are plotted vs. time. Obviously, the "equilibrium constant" increases with time. This effect is denoted as "aging of the binding".
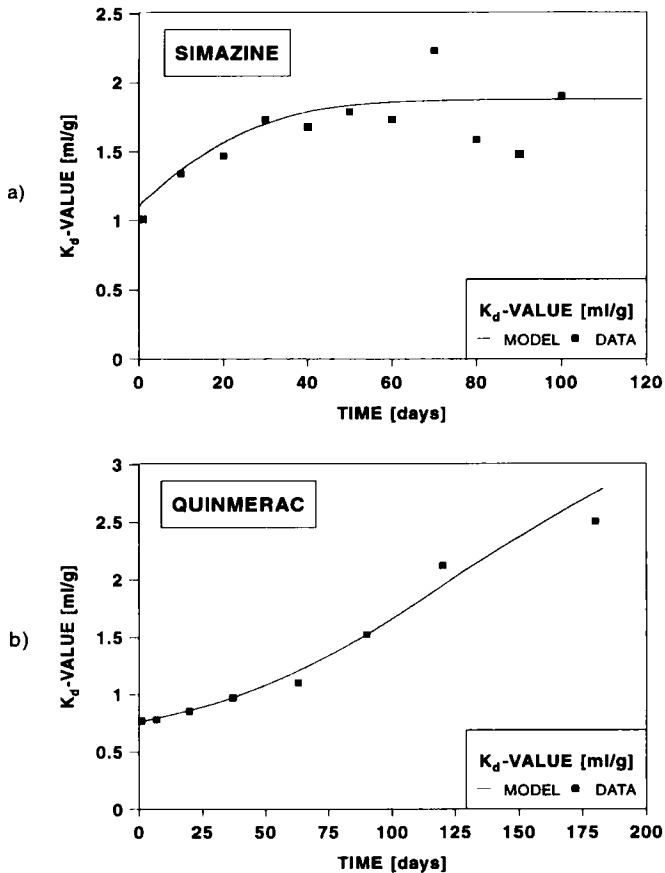


Fig. 3.8: $K_d$-value of a) Simazine and b) Quinmerac vs. time. The binding "constant" increases with time. This effect is modeled by Eq. (3.40).

A possible explanation is that two binding sites are involved, one with a weak binding and one with a strong binding. Whereas weak binding is a very fast reversible reaction, strong binding is postulated to be slow and nearly irreversible. This is modeled by coupling an equilibrium model with a kinetic model. First the case of an irreversible strong binding is treated. The compartment scheme is presented in Fig. 3.9. It is assumed that the substance may undergo degradation in the liquid phase and in the strong binding state.

The following notations hold:

$c$        : liquid phase concentration [$M/L^3$]
$S_1$     : solid phase concentration (weak binding site) [$M/L^3$]
$S_2$     : solid phase concentration (strong binding site) [$M/L^3$]
$k_l$      : degradation rate in liquid phase [$1/T$]
$k_e$     : degradation rate in solid phase (only slow binding site) [$1/T$]
$k_b$     : rate constant for the transition weak to strong binding site [$1/T$]
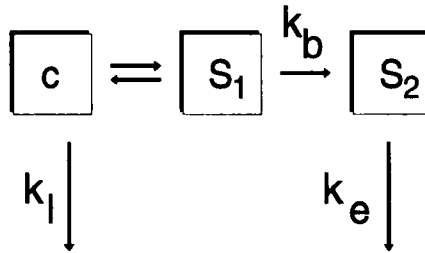


**Fig. 3.9:** Compartment scheme for two binding sites. Note that the binding to site 2 is irreversible.

At any time $t$, the mass balance in integral form is given by

$$\theta c(t) + \rho S_1(t) + \rho S_2(t) + \theta \int_0^t k_l c(\tau) d\tau + \rho \int_0^t k_e S_2(\tau) d\tau = \theta c(t=0) = D \qquad (3.36a)$$

The first binding site is assumed to be in quasi equilibrium with the liquid phase:

$$S_1 = K_d c \qquad (3.36b)$$

The transition between the weak and strong binding state is assumed to proceed slow with respect to sorption:

$$\frac{d}{dt}\left(\rho S_2\right) = \rho k_b S_1 - \rho k_e S_2 \qquad (3.36c)$$

Note that in this scheme the substance may also decay from the strong binding state with rate $k_e$. By differentiating Eqs. (3.36a,b) with respect to time one obtains after rearrangement the differential equations

$$\frac{dc}{dt} = - \frac{k_l + k_b \frac{\rho}{\theta} K_d}{1 + \frac{\rho}{\theta} K_d} c = - k_{eff} c \tag{3.37a}$$

$$\frac{dS_2}{dt} = k_b K_d c - k_e S_2 \tag{3.37b}$$

Note that these equations are equivalent to Eq. (3.10a,b). With the initial conditions

$$c(t=0) = \frac{c_0}{1 + \frac{\rho}{\theta} K_d} := c_{0 eff}$$

$$S_2(t=0) = 0$$

the above equations have the solution

$$c(t) = c_{0 eff}\, e^{-k_{eff} t} \tag{3.38a}$$

$$S_2(t) = \frac{k_b K_d c_{0\, eff}}{k_e - k_{eff}} \left( e^{-k_{eff} t} - e^{-k_e t} \right) \tag{3.38b}$$

with

$$k_{eff} = \frac{k_l + k_b \frac{\rho}{\theta} K_d}{1 + \frac{\rho}{\theta} K_d}$$

The apparent $K_d$-value as obtained by measurements is

$$K_{d\, app} = \frac{S}{c} = \frac{S_1 + S_2}{c} \tag{3.39}$$

Inserting Eqs. (3.36b), (3.38a) and (3.38b) into Eq. (3.39) a **time dependent expression** for the apparent $K_d$-value is derived

$$K_{d\, app}(t) = K_d \left[ 1 + \frac{k_b}{k_e - k_{eff}} \left( 1 - e^{-(k_e - k_{eff})t} \right) \right] \tag{3.40}$$

If $k_e > k_{eff}$ the apparent $K_d$-value reaches the limit

$$\lim_{t \to \infty} K_{d\ app}(t) = K_d \left( 1 + \frac{k_b}{k_e - k_{eff}} \right) \tag{3.41}$$

If $k_e < k_{eff}$ the apparent $K_d$-value increases ad infinitum.

A further interesting case is the situation of two reversible binding sites with degradation in both bound states. The reaction scheme is depicted in Fig. 3.10. The following model goes back to van Genuchten (1981) and Parker and van Genuchten (1984).

Additional notations

$f$       : fraction of type 1 binding sites  [1]
$k_{S1}$  : degradation rate in binding state 1 [1/T]
$k_{S2}$  : degradation rate in binding state 2 [1/T]
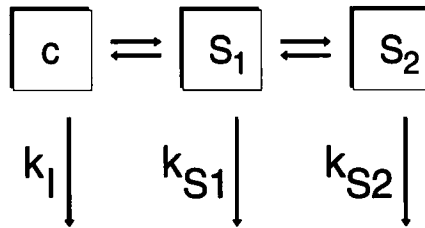


**Fig. 3.10:** Compartment scheme for two reversible binding sites and degradation occurring in both bound sites.

The $K_d$-value data are shown in Figs. 3.8 a,b and 3.11 a,b. The starting point for the derivation of the model is again the mass balance equation in integral representation. At any time $t$ the law of mass conservation requires that

$$\theta c(t) + \rho S_1(t) + \rho S_2(t) + \theta \int_0^t k_l c(\tau) d\tau + \rho \int_0^t k_{S1} S_1(\tau) d\tau + \rho \int_0^t k_{S2} S_2(\tau) d\tau = D \tag{3.42}$$

holds. It is assumed that quasi equilibrium prevails with respect to binding site 1. The fraction of this binding site is denoted by $f$. Thus, at any time, the concentration of occupied sites of type 1 is related to the liquid phase concentration via

$$S_1 = f K_d c \tag{3.43}$$

For type 2 binding sites, kinetic adsorption-desorption is assumed.

$$\frac{dS_2}{dt} = \alpha\left[(1 - f)K_d c - S_2\right] - k_{S2}S_2 \tag{3.44}$$

A differential equation for the liquid phase concentration $c$ is derived by differentiating Eq. (3.42) with respect to time and replacing the time derivatives of $S_1$ and $S_2$ by the time derivative of Eq. (3.43) and by Eq. (3.44) respectively.

$$\frac{dc}{dt} = \frac{-\alpha\rho\left[(1 - f)K_d c - S_2\right] - \theta k_l c - fK_d\rho k_{S1} c}{\theta + \rho f K_d} \tag{3.45}$$

Equations (3.44) and (3.45) are equivalent to Eq. (3.16b). The apparent $K_d$-value constructed from the solution of the above system is

$$K_{d\,app}(t) = \frac{S_1 + S_2}{c} = \frac{fK_d c + S_2}{c} = K_d\left[f + (1 - f)\frac{1 - e^{(\lambda_2 - \lambda_1)t}}{A + Be^{(\lambda_2 - \lambda_1)t}}\right] \tag{3.46}$$

with

$$A = \frac{\lambda_1}{\alpha} + 1 + \frac{k_{S2}}{\alpha} \quad and \quad B = -\left(\frac{\lambda_2}{\alpha} + 1 + \frac{k_{S2}}{\alpha}\right)$$

In the limit $\alpha \to \infty$ equilibrium is attained also with respect to site 2 and $K_{d\,app}$ approaches the constant value $K_d$. Figures 3.11 a,b show the application of this model to data of Simazine and Quinmerac.
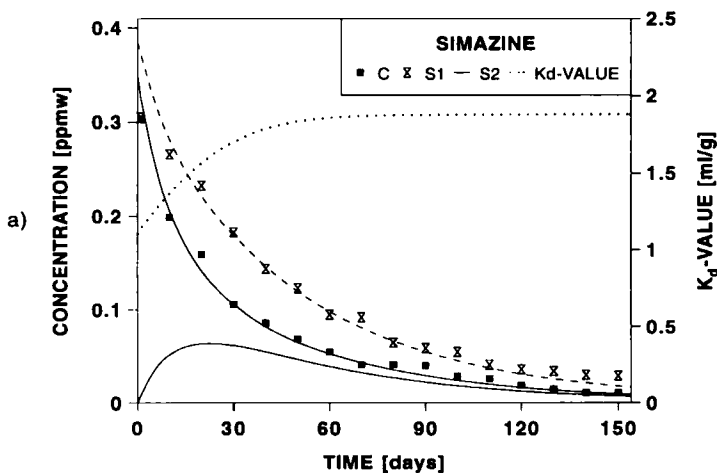


Fig. 3.11 a: Simulated and measured time courses of Simazine in water- and methanole-extractable phase. The underlying model is given by Eqs. (3.44) - (3.46).
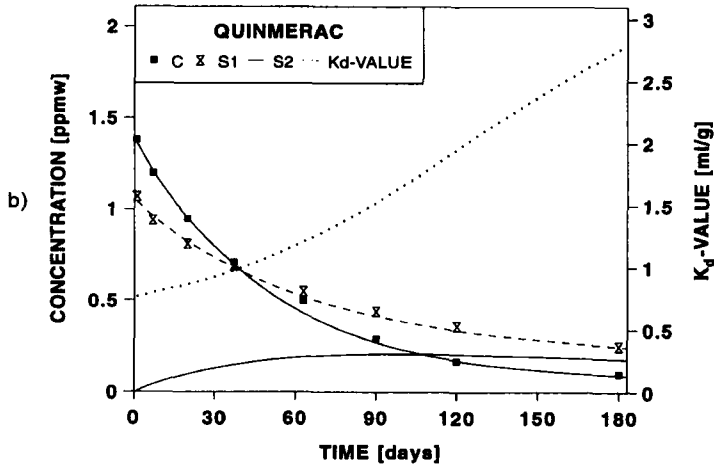
**Fig. 3.11 b:** Simulated and measured time courses of Quinmerac in water- and methanole-extractable phase. The underlying model is given by Eqs. (3.44) - (3.46).

### 3.1.4   Solution by Laplace Transformation

The solution of linear differential equations is considerably facilitated by use of the Laplace transformation. Let $f(t)$ denote a function with domain $[0, \infty)$ and $s$ a complex variable with $\mathrm{Re}(s) > 0$. Then the Laplace transform of $f(t)$ is defined by

$$L[f(t)] := \int_0^\infty e^{-st} f(t)\, dt := F(s) \tag{3.47}$$

Examples:

The Laplace transform of $f(t) = 1$ is

$$L[1] = \lim_{A \to \infty} \int_0^A e^{-st}\, dt = \lim_{A \to \infty} \frac{1}{s}\left[1 - e^{-sA}\right] = \frac{1}{s} \tag{3.48}$$

The Laplace transform of $f(t) = e^{at}$ is

$$L[e^{at}] = \lim_{A \to \infty} \int_0^A e^{-(s-a)t}\, dt = \frac{1}{s-a} \tag{3.49}$$

The Laplace transform of the derivative of $f(t)$ with respect to $t$ is

$$L\left[\frac{df}{dt}\right] = \lim_{A \to \infty} \int_0^A \frac{df}{dt} e^{-st} dt$$

$$= \lim_{A \to \infty} [f(t)e^{-st}]_0^A - \int_0^A -sf(t)e^{-st} dt = -f(0) + sF(s) \tag{3.50}$$

Differential equations are solved in three steps. In the first step, the differential equation system is Laplace transformed. **Linear differential equations transform into linear algebraic equations in Laplace space.** In the second step the linear equation system is solved, and in the third step, the solution in the time domain is obtained by the inverse transformation. More technical details on Laplace transformations are given in Appendix A.1.

This method shall be employed to derive solutions for linear compartment models in a general form. The following example shows how the three steps are performed. Consider again the two compartment model given by Eq. (3.16). For ease of presentation the model is now written in the form

$$\frac{dy_1}{dt} = ay_1 + by_2$$

$$\frac{dy_2}{dt} = cy_1 + dy_2 \tag{3.51}$$

where $a$, $b$, $c$ and $d$ are defined in terms of reaction constants as before (cf. Eqs. (3.16b) and (3.23)).

**In the first step**, the differential equation system is Laplace transformed.

$$L\left[\frac{dy_1}{dt}\right] = sY_1(s) - y_1(0) = aY_1(s) + bY_2(s)$$

$$L\left[\frac{dy_2}{dt}\right] = sY_2(s) - y_2(0) = cY_1(s) + dY_2(s) \tag{3.52}$$

Note that the initial values enter already in the first step.

**In the second step**, the linear equation system

$$\begin{pmatrix} a-s & b \\ c & d-s \end{pmatrix} \begin{pmatrix} Y_1(s) \\ Y_2(s) \end{pmatrix} = - \begin{pmatrix} y_1(0) \\ y_2(0) \end{pmatrix} \tag{3.53}$$

is solved in the Laplace domain yielding

$$
\begin{pmatrix} Y_1(s) \\ Y_2(s) \end{pmatrix} = \frac{-1}{(a - s)(d - s) - bc} \begin{pmatrix} (d - s)y_1(0) - by_2(0) \\ -cy_1(0) + (a - s)y_2(0) \end{pmatrix}
\tag{3.54}
$$

In the following, the initial value $y_2(0)$ is set equal to zero.

**In the last step**, the solutions are transformed again into the time domain. This is achieved by employing the inverse transforms of known functions, for example

$$
L^{-1}\left[\frac{1}{s + k}\right] = e^{-kt}
\tag{3.55}
$$

The inverse transform of the following expression plays an important role in many applications. Let

$$
F(s) = \frac{G(s)}{H(s)} = \frac{G(s)}{(\beta_1 + s)(\beta_2 + s) \dots (\beta_n + s)}
\tag{3.56}
$$

where $G(s)$ and $H(s)$ are polynomials with the degree of $G(s)$ less or equal the degree of $H(s)$. The $\beta_i$ are the negative roots of the polynomial $H(s)$. Then, by decomposition into partial fractions, one obtains terms, which are easily transformed back by use of Eq. (3.55). The inverse transform of $F(s)$ is thus derived as

$$
L^{-1}[F(s)] = \sum_{i=1}^{n} A_i e^{-\beta_i t}
\tag{3.57}
$$

with

$$
A_i = \lim_{s \to -\beta_i} \frac{G(s)(\beta_i + s)}{(\beta_1 + s)(\beta_2 + s) \dots (\beta_n + s)}
\tag{3.58}
$$

Let us return now to the problem to find the inverse transform of

$$
Y_1(s) = -\frac{(d - s)y_1(0)}{(a - s)(d - s) - bc} = -\frac{(d - s)y_1(0)}{(\beta_1 + s)(\beta_2 + s)}
$$

$$
Y_2(s) = \frac{cy_1(0)}{(a - s)(d - s) - bc} = \frac{cy_1(0)}{(\beta_1 + s)(\beta_2 + s)}
$$

with

$$\beta_{1/2} = -\frac{(a + d)}{2} \pm \sqrt{\frac{(a + d)^2}{4} - ad + bc}$$

By application of Eq. (3.57) with $G(s) = (d - s)$ one finally obtains the solution

$$y_1(t) = \frac{y_1(0)}{\beta_1 - \beta_2} \left[(d + \beta_1)e^{-\beta_1 t} - (d + \beta_2)e^{-\beta_2 t}\right]$$

$$y_2(t) = \frac{c y_1(0)}{\beta_1 - \beta_2} \left[e^{-\beta_2 t} - e^{-\beta_1 t}\right]$$

(3.59)

which is identical to the solution previously obtained by the eigenvector method (Eqs. (3.31a,b)).

**The general case**

Let us consider now a linear compartment model in general form with n compartments.

$$\frac{d\vec{y}}{dt} + D\vec{y} = \vec{f}(t) \qquad with \quad \vec{y}(0) = \vec{y}_0$$

(3.60)

The matrix $D$ is completely determined by the structure of the compartment system. If the equation system represents the mass balance equations, then $D$ has the general form

$$D = \begin{pmatrix} k_1 & -k_{21} & -k_{31} & \cdots & -k_{n1} \\ -k_{12} & k_2 & -k_{32} & \cdots & -k_{n2} \\ & & \cdots\cdots & & \\ -k_{1n} & -k_{2n} & -k_{3n} & \cdots & k_n \end{pmatrix}$$

(3.61)

The diagonal elements of $D$

$$D_{ii} = \sum_{j=1, j \neq i}^{n} k_{ij} := k_i$$

summarize the rate constants of the fluxes leaving compartment $i$. The rate constants $k_{ij}$ govern the flux from compartment $i$ to compartment $j$. The Laplace transform of Eq. (3.60) yields the linear equation system

$$(D + sI)\vec{Y}(s) = \vec{y}(0) + \vec{F}(s)$$

(3.62)

in the Laplace domain, where $I$ denotes the unit matrix. Under the assumption that the matrix

$(D + sI)$ is regular the inverse exists and the solution is given by

$$\vec{Y}(s) = [D + sI]^{-1}(\vec{y}(0) + \vec{F}(s)) \tag{3.63}$$

Employing Cramer's rule the solution for compartment $k$ is obtained as

$$Y_k(s) = \sum_{m=1}^{n} (-1)^{k+m} y_m(0) \frac{|D_{ij,mk}(s)|}{|D_{ij}(s)|} + \sum_{m=1}^{n} (-1)^{k+m} F_m(s) \frac{|D_{ij,mk}(s)|}{|D_{ij}(s)|} \tag{3.64}$$

$|D_{ij}(s)|$ denotes the determinant of the matrix $(D + sI)$. $|D_{ij,mk}(s)|$ denotes the sub-determinant of $(D + sI)$ obtained by canceling the $m$th row and $k$th column. First, the homogeneous case $f_m = 0$ is treated. To this end, the determinant $|D_{ij}(s)|$ is written in the form

$$|D_{ij}(s)| = (s + \beta_1)(s + \beta_2)\ldots(s + \beta_n) = \prod_{i=1}^{n} (s + \beta_i) \tag{3.65}$$

It is assumed that all roots of the characteristic polynomial of the matrix $D$ are distinct. In this case, the inverse transform of Eq. (3.64) is easily obtained by use of Eq. (3.57):

$$y_k(t) = \sum_{m=1}^{n} (-1)^{k+m} y_m(0) \sum_{l=1}^{p} e^{-\beta_l t} \lim_{s \to -\beta_l} \frac{|D_{ij,mk}(s)|(s + \beta_l)}{|D_{ij}(s)|} \tag{3.66}$$

where $p$ denotes the number of roots of the polynomial Eq. (3.65). In the inhomogeneous case the inverse transformation is obtained by use of the convolution theorem:

$$L^{-1}[F(s)G(s)] = f(t) * g(t) = \int_0^t f(\tau)g(t - \tau)d\tau = \int_0^t f(t - \tau)g(\tau)d\tau \tag{3.67}$$

The solution of the initial value problem Eq. (3.60) is then

$$y_k(t) = \tag{3.68}$$

$$\sum_{m=1}^{n} \sum_{l=1}^{p} (-1)^{k+m} \lim_{s \to -\beta_l} \frac{|D_{ij,mk}(s)|(s + \beta_l)}{|D_{ij}(s)|} \left( y_m(0)e^{-\beta_l t} + \int_0^t f_m(\tau)e^{-\beta_l(t - \tau)}d\tau \right)$$

This derivation is taken from Bozler et al. (1977).

## The Environmental Soil Pathway of 2,4,5-Trichlorophenoxyacetic Acid (2,4,5-T)

The degradation pathway of 2,4,5-trichlorophenoxyacetic acid was investigated by Mc Call et al. (1981) in several soil types. The proposed pathway is shown in Fig. 3.12. The parent substance is subsequently transformed to the two major metabolites 2,4,5-trichlorophenole and 2,4,5-trichloroanisole. The reaction between the two metabolites is reversible. Residues of both metabolites are incorporated into the humus fraction of the soil. $CO_2$ is released in all transformations. The second metabolite is also volatilized.
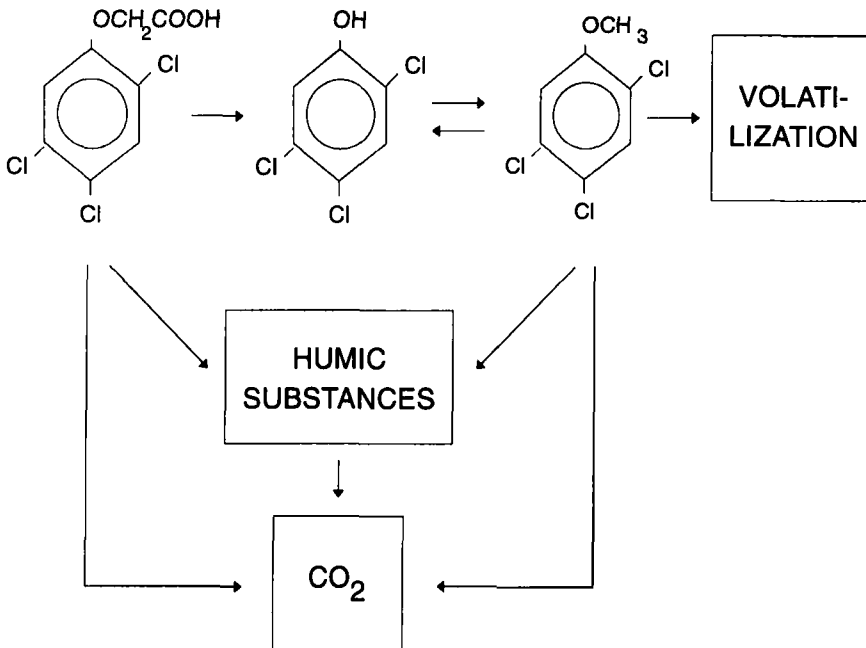


**Fig. 3.12:** Proposed pathway of 2,4,5-T according to McCall et al. (1981).

The following notations hold:

$y_1$     : concentration of parent compound $[M/L^3]$
$y_2$     : concentration of first metabolite $[M/L^3]$
$y_3$     : concentration of second metabolite $[M/L^3]$
$y_4$     : concentration of carbon dioxide $[M/L^3]$
$y_5$     : residues bound to the humus fraction of the soil $[M/L^3]$
$k_{ij}$     : reaction constants, e.g. $k_{12}$ is the constant for the transformation of the parent compound to the first metabolite $[1/T]$

Assuming that all reaction rates are linear functions of the concentrations, the system is modeled by

$$\frac{d}{dt}\begin{pmatrix} y_1 \\ y_2 \\ y_3 \\ y_4 \\ y_5 \end{pmatrix} = \begin{pmatrix} -k_{12} & 0 & 0 & 0 & 0 \\ k_{12} & -(k_{23}+k_{24}+k_{25}) & k_{32} & 0 & 0 \\ 0 & k_{23} & -(k_{34}+k_{35}+k_{32}+k_{30}) & 0 & 0 \\ 0 & k_{24} & k_{34} & -k_{40} & k_{54} \\ 0 & k_{25} & k_{35} & 0 & -k_{54} \end{pmatrix}\begin{pmatrix} y_1 \\ y_2 \\ y_3 \\ y_4 \\ y_5 \end{pmatrix} \tag{3.69}$$

To conform with the notations of the general scheme, the system is written in the following form

$$\frac{d\vec{y}}{dt} + D\vec{y} = 0 \tag{3.70}$$

with

$$D = \begin{pmatrix} a & 0 & 0 & 0 & 0 \\ b & c & d & 0 & 0 \\ 0 & e & f & 0 & 0 \\ 0 & g & h & \bar{i} & \bar{k} \\ 0 & \bar{l} & \bar{m} & 0 & \bar{n} \end{pmatrix}$$

and

$$a = k_{12} \qquad b = -k_{12} \qquad c = k_{23} + k_{25} + k_{24}$$

$$d = -k_{32} \qquad e = -k_{23} \qquad f = k_{32} + k_{34} + k_{35} + k_{30}$$

$$g = -k_{24} \qquad h = -k_{34} \qquad \bar{i} = k_{40}$$

$$\bar{k} = -k_{54} \qquad \bar{l} = -k_{25} \qquad \bar{m} = -k_{35} \qquad \bar{n} = k_{54}$$

To avoid confusing with indices the matrix elements $i$, $k$, $l$, $m$ and $n$ are written with a bar. Because of the simple structure of $D$, the determinant of $(D + sI)$ is easily represented as the product:

$$|D + sI| = (a + s)(\bar{i} + s)(\bar{n} + s)[(f + s)(c + s) - de] \tag{3.71}$$

$$= (s + \beta_1)(s + \beta_2)(s + \beta_3)(s + \beta_4)(s + \beta_5)$$

with

$$\beta_1 = a$$

$$\beta_2 = \frac{1}{2}(c + f) + \sqrt{\frac{(c + f)^2}{4} + de - cf}$$

$$\beta_3 = \frac{1}{2}(c + f) - \sqrt{\frac{(c + f)^2}{4} + de - cf}$$

$$\beta_4 = \bar{i}$$

$$\beta_5 = \bar{n}$$

Employing now the general formula (Eq. (3.66)) the solutions of the above initial value problem are now obtained in a straightforward manner.

$y_1$:

The solution is given by

$$y_1(t) = y_1(0)e^{-\beta_1 t} \tag{3.72}$$

$y_2$:

The subdeterminant $|D_{ij,12}(s)|$ is obtained from $D(s)$ by omitting the first row and the second column:

$$|D_{ij,12}(s)| = \begin{vmatrix} b & d & 0 & 0 \\ 0 & f+s & 0 & 0 \\ 0 & h & \bar{i}+s & k \\ 0 & m & 0 & \bar{n}+s \end{vmatrix} = b(f+s)(\bar{i}+s)(\bar{n}+s)$$

Inserting this subdeterminant into Eq. (3.66) yields the expression

$$y_2(t) = y_1(0) \sum_{i=1}^{5} e^{-\beta_i t} \frac{-b(f - \beta_i)(\bar{i} - \beta_i)(\bar{n} - \beta_i)}{\prod\limits_{j=1, j \neq i}^{5} (\beta_j - \beta_i)} \tag{3.73}$$

For $i = 4$ and $i = 5$ the corresponding terms in the sum are zero because $\beta_4 = \bar{i}$ and $\beta_5 = \bar{n}$.

$y_3$:

The subdeterminant $|D_{ij,13}(s)|$ is obtained from $D(s)$ by omitting the first row and the third column:

$$|D_{ij,13}(s)| = \begin{vmatrix} b & c+s & 0 & 0 \\ 0 & e & 0 & 0 \\ 0 & g & \bar{i}+s & \bar{k} \\ 0 & \bar{l} & 0 & \bar{n}+s \end{vmatrix} = b\,e\,(\bar{i}+s)\,(\bar{n}+s)$$

Inserting this subdeterminant into Eq. (3.66) yields the expression

$$y_3(t) = y_1(0) \sum_{i=1}^{5} e^{-\beta_i t}\, \frac{be(\bar{i}-\beta_i)(\bar{n}-\beta_i)}{\prod_{j=1,j\neq i}^{5} (\beta_j - \beta_i)} \tag{3.74}$$

Again, the terms for $i = 4$ and $i = 5$ disappear.

$y_4$:

The subdeterminant $|D_{ij,14}(s)|$ is obtained from $D(s)$ by omitting the first row and the fourth column:

$$|D_{ij,14}(s)| = \begin{vmatrix} b & c+s & d & 0 \\ 0 & e & f+s & 0 \\ 0 & g & h & \bar{k} \\ 0 & \bar{l} & \bar{m} & \bar{n}+s \end{vmatrix}$$

$$= b\left[e(h(\bar{n}+s) - \bar{k}\bar{m}) - (f+s)(g(\bar{n}+s) - \bar{l}\bar{k})\right]$$

Inserting this subdeterminant into Eq. (3.66) yields the expression

$$y_4(t) =$$

$$y_1(0) \sum_{i=1}^{5} e^{-\beta_i t}\, \frac{-b\left[e(h(\bar{n}-\beta_i) - \bar{k}\bar{m}) - (f-\beta_i)(g(\bar{n}-\beta_i) - \bar{l}\bar{k})\right]}{\prod_{j=1,j\neq i}^{5} (\beta_j - \beta_i)} \tag{3.75}$$

$y_5$:

The subdeterminant $|D_{ij,15}(s)|$ is obtained from $D(s)$ by omitting the first row and the fourth column:

$$|D_{ij,15}(s)| = \begin{vmatrix} b & c+s & d & 0 \\ 0 & e & f+s & 0 \\ 0 & g & h & \bar{i}+s \\ 0 & \bar{l} & \bar{m} & 0 \end{vmatrix} = b\left[-e\bar{m}(\bar{i}+s) + (f+s)\bar{l}(\bar{i}+s)\right]$$

Inserting this subdeterminant into Eq. (3.66) yields the expression

$$y_5(t) = y_1(0) \sum_{i=1}^{5} e^{-\beta_i t} \frac{b(\bar{i}-\beta_i)\left[\bar{l}(f-\beta_i) - e\bar{m}\right]}{\prod_{j=1, j \neq i}^{5} (\beta_j - \beta_i)} \tag{3.76}$$

Figure 3.13 shows a plot of these functions together with the data published by Mc Call et al. (1981). Model parameters were estimated by nonlinear regression techniques, which are treated in detail in chapter 4.
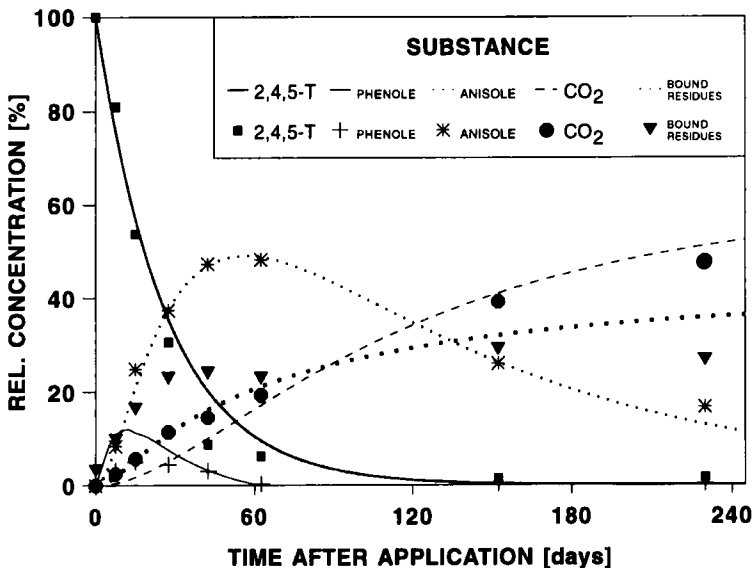


**Fig. 3.13 :** Experimental data of elimination kinetics of 2,4,5-T, observed by McCall et al. (1981) and resulting fit of Eq. (3.69). Note that not all components fit equally well to the model. This may be due to nonlinear effects.

## 3.2   Nonlinear Models

### 3.2.1   The Limits of Linear Models

Nonlinear degradation kinetics in pesticides are frequently observed. The term refers to the mathematical form of dependence of the degradation rate upon the concentration in a linear or nonlinear way. The resulting differential equations are thus either linear or nonlinear. The manifestation of nonlinearity involves effects such as time lags and concentration dependent half-lives. However, in many cases it is impossible to detect nonlinearities from **single experiments** at low concentrations. In most practical cases experimental errors prevent a distinction from simple exponential decay unless the experiment is performed at high initial concentrations.

This is drastically demonstrated in Figs. 3.14 a,b for the case of 1,3-dichloropropene (1,3-D) (Vink et al., 1994). A series of degradation curves was obtained for initial concentrations ranging from 15 mg/kg to 0.03 mg/kg thus covering several orders of magnitude (cf. Fig. 5.17 in section 5.3.2).
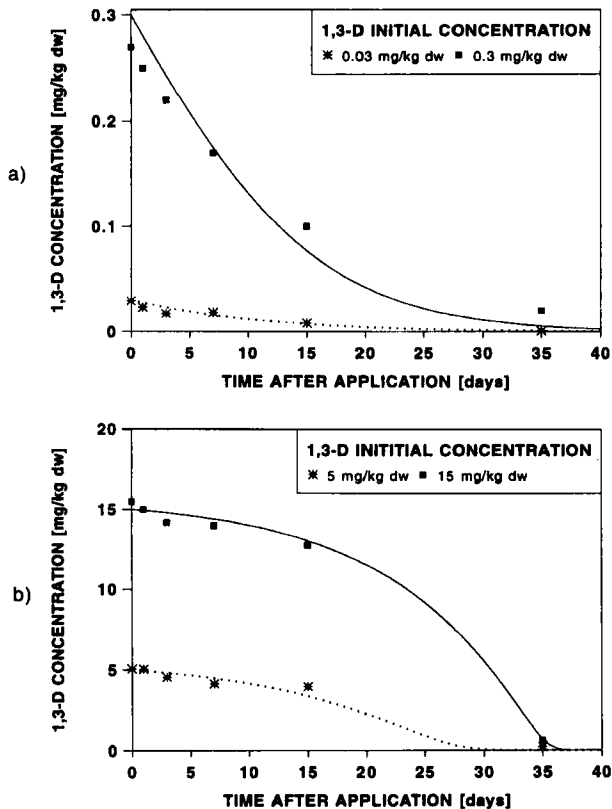


**Fig. 3.14:** Time courses of 1,3-dichloropropene degradation with different initial concentrations (experimental data from Vink et al., 1994; cf. Fig. 5.17 in section 5.3.2): a) initial concentrations of 0.03 and 0.3 mg 1,3-D/kg dw and b) initial concentrations of 5 and 15 mg 1,3-D/kg dw. The fit is based on Eqs. (3.107 - 3.108).

At low concentrations, it seems that the data do not contradict linear first order decay kinetics. However, at high concentrations, the nonlinear character of the decay curves becomes obviously.

It is therefore dangerous, to extend the linearity assumption beyond those concentration ranges for which the validity of this assumption was originally assessed. This is extremely important if one wishes to predict the behavior under a long-term application scheme. In the course of the applications concentrations may eventually surpass the range where the linearity assumption is approximately valid, and the model predicts far too low concentration levels. As pointed out earlier, **linear models should be regarded only as first approximations with a limited application range.**

The nonlinearities occurring in pesticide kinetics are either due to physico-chemical processes like binding to the soil matrix or to biological processes connected with the mode of degradation. In the case of metabolic or cometabolic degradation, the momentary degradation rate reflects both microbial activity and microbial population density. The main types of nonlinearities are listed in Tab. 3.1 below.

**Tab. 3.1:** Typical nonlinearities in pesticide degradation kinetics.

| Type | Effect | Examples | Reference |
|---|---|---|---|
| nonlinear adsorption | degradation rate depends on applied concentration | Di-allate; Tri-allate | Anderson and Domsch (1980) |
| capacity limited biotransformation | degradation rate depends on applied concentration | Bentazone; Di-allate; Tri-allate | BASF (unpublished); Anderson and Domsch (1980) |
| microbial adaption | time-lag, enhanced degradation by multiple application | 2,4-D; EPTC; Iprodione | Hurle (1982); Obrigawitch et al. (1983); Walker and Welch (1990) |
| inhibition at high concentrations | prolonged time-lag | 2,4-D; DNOC; IPC | Fournier et al. (1981); Hurle (1982); Moe (1970) |
| interaction between pesticides | inhibited degradation, enhanced degradation | Simazine-Captan; 2,4-D - Dinoseb; Simazine-Paraquat; Butylate - EPTC | Kibler (1979); Repiquet and Fournier (1977); Kibler (1979); Obrigawitch et al. (1983) |

In general, the nonlinear differential equations resulting from nonlinear degradation laws cannot be solved analytically, that means the solutions cannot be written in form of known functions like exponential functions. However, approximate numerical solutions of high accuracy can be easily obtained by standard methods.

The distinction between kinetic models, which are amenable to analytical solutions and those, which can only be solved by numerical techniques, has had a large impact on parameter estimation and model application. Because the parameter identification problem is easily solved by standard methods in the case of explicit solutions, implicit models in form of nonlinear differential equations have in most cases only been used for simulation. Evident nonlinearities are often dealt with by empirical kinetic laws with fractal order of reaction (Timme et al., 1986). It is therefore necessary to establish a link between models in form of nonlinear differential equations and parameter identification techniques. This link is provided in chapter 4.

### 3.2.2    Nonlinear Kinetics due to Adsorption

#### 3.2.2.1  Equilibrium Approach

Sorption may either be considered as to be instantaneous (equilibrium approach) or as time dependent (kinetic approach). In equilibrium, the relation between $c$ and $S$ is given by empirical relationships, which are denoted as adsorption isotherms. For many pesticides, these isotherms are nonlinear. Some often used relationships are the adsorption isotherms of Freundlich

$$S = K_F \, c^{\,n} \tag{3.77}$$

and Langmuir

$$S = \frac{\beta c}{c + K} \tag{3.78}$$

Figure 3.15 shows adsorption isotherms of Quinmerac in different soils, which fit well to Freundlich's equation, Eq. (3.77).

The starting point of the equilibrium approach is the mass balance equation Eq. (3.34) derived for the case of a single application of dose $D$ at time $t_0$

$$\theta c(t) + \rho S(c(t)) + \theta \int_0^t k_l(c(\tau)) c(\tau) d\tau = D \tag{3.79}$$

where $S$ and $k_l$ are allowed to depend on $c$. Differentiation with respect to time yields

$$\theta \frac{dc}{dt} + \rho \frac{\partial S}{\partial c} \frac{dc}{dt} + \theta k_l c = 0 \tag{3.80}$$

After rearrangement, one obtains the following differential equation for $c$:

$$\frac{dc}{dt} = -k_l \frac{c}{1 + \frac{\rho}{\theta} \frac{\partial S}{\partial c}} = -k_{eff}(c) c \tag{3.81}$$
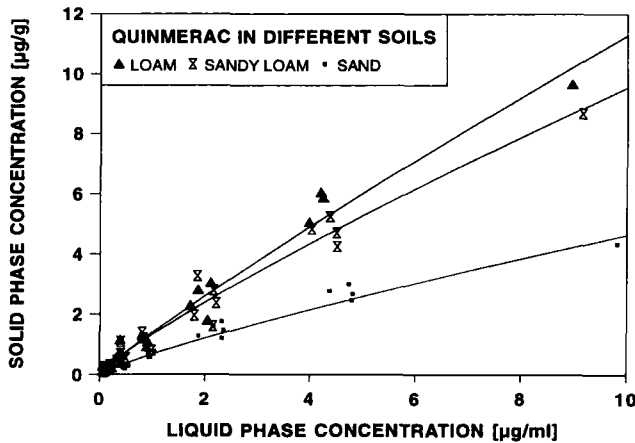
**Fig. 3.15:** Fit of Freundlich isotherm (Eq. (3.77)) to observed equilibrium sorption of Quinmerac in different soils (soil/water ratio in the batch study was 1/3).

Even if the liquid phase degradation rate $k_l$ is independent on $c$, the apparent rate constant $k_{eff}$ is concentration dependent, if the isotherm is a nonlinear function of $c$. For the Freundlich law one obtains

$$k_{eff\,Freundlich} = \frac{k_l}{1 + \frac{\rho}{\theta} K_F \, n c^{n-1}} \tag{3.82}$$

and for the Langmuir isotherm

$$k_{eff\,Langmuir} = \frac{k_l}{1 + \frac{\rho}{\theta} \frac{\beta K}{(c + K)^2}} \tag{3.83}$$

Thus, the resulting differential equations turn out to be nonlinear for nonlinear binding isotherms. If the effective rate constant $k_{eff}$ is concentration dependent, the reaction is no more of first order. Deviations from first order kinetics are often not obvious from single decay curves. They become apparent only in a series of experiments with varying initial

concentrations. Figure 3.16 demonstrates this effect. It shows three different decay curves obtained for a fictive pesticide with a Freundlich isotherm. The initial values are normalized to 100 %. The differences between the resultant decay curves are obvious.
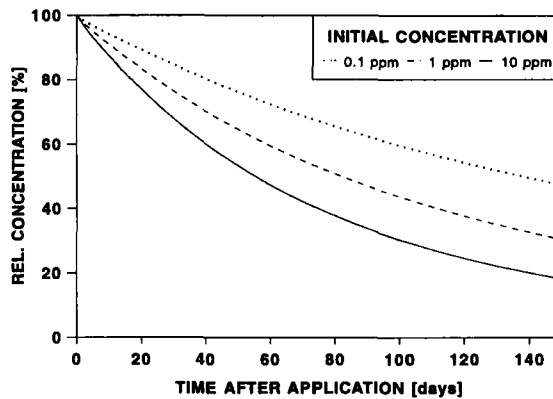


**Fig. 3.16:** Nonlinear binding isotherms render the kinetics nonlinear as is demonstrated in these simulations for a Freundlich isotherm. Although the degradation is linear the kinetic behavior depends on initial concentrations. The decay curves shown here are normalized to 100 % with respect to initial concentration.

### 3.2.2.2  Kinetic Approach

The Langmuir isotherm can be derived from a receptor binding model assuming a limited number of binding places. The species in the solute phase react with a free receptor $R$ forming the receptor-substrate complex $[R\,S]$. Let $r_0$, $r_1$ and $r_t$ denote the concentrations of free, occupied and total receptor sites. Then the elementary chemical reaction equations of the scheme

$$C + R \quad \overset{k_1}{\underset{k_{-1}}{\rightleftharpoons}} \quad [RC]$$
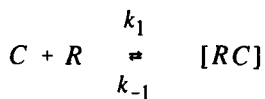
can be written down as

$$\frac{dr_1}{dt} = k_1 r_0 c - k_{-1} r_1 \tag{3.84}$$

The conservation of the sum of all receptor species demands that

$$r_t = r_0 + r_1 = const \tag{3.85}$$

combining the last two equations and identifying $r_1$ with $S$ yields

$$\frac{dS}{dt} = k_1 (r_t - S) c - k_{-1} S \tag{3.86}$$

Under equilibrium assumptions, i.e. for $dS/dt = 0$, one obtains

$$S = \frac{r_t\,c}{c + \dfrac{k_{-1}}{k_1}} \tag{3.87}$$

which is identical to Eq. (3.78) with

$$K = \frac{k_{-1}}{k_1} \quad and \quad \beta = r_t$$

The parameter $r_t$ is also referred to as strong adsorption capacity (SAC).

Nonlinearities have a strong influence on the kinetic behavior, which may turn out to be drastic under long-term applications, which shall be demonstrated by the following scenario.
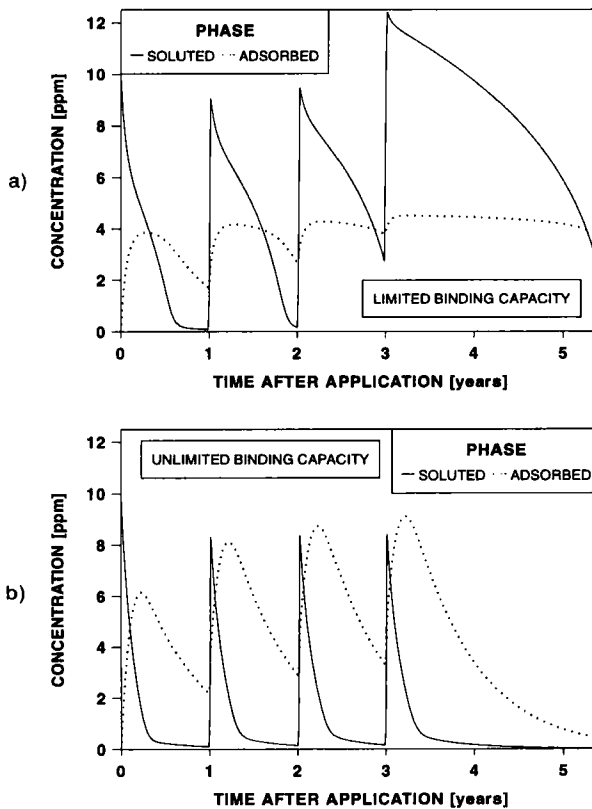


**Fig. 3.17:** a) Simulated time course of a fictive pesticide in solid matter and soil solution under multiple applications assuming a strong adsorption capacity of soil colloids. The limited binding capacity causes a dramatic rise in liquid phase concentrations if the soil is saturated. b) If the binding is linear and not capacity limited no accumulation can occur.

A substance with a limited adsorption capacity is considered. In this case, the model of Langmuir applies. It is assumed that the binding is strong, i.e. that $k_{-1} \ll k_1$. This substance is now applied to a noncontaminated soil once a year over a period of 10 years. Figure 3.17 a shows the time courses of $c$ and $S$. In the first years, $S$ is far below the adsorption capacity, which is, however, steadily approached. After the third application, the effect of the limited binding capacity becomes obviously. A further application leads now to high concentrations of the substance in the bioavailable solute phase. As a consequence, phytotoxicity is much longer maintained as at the beginning of the application. For comparison, the long-term behavior of a linear system with unlimited binding capacity is demonstrated in Fig. 3.17 b.

### 3.2.3   Nonlinearities due to Spatial Heterogeneity

Up to now, the models describe reactions in an environment, which might be characterized as "well stirred". Consider now a soil sample, which is heterogeneous at a scale much smaller than the characteristic scale of a test volume. Let us assume, that the sample is made up of a large number of small homogeneous subsamples and that in each subsample a linear kinetic law is valid. Then, due to the varying soil properties, each model has different kinetic parameters. Consider for instance the influence of organic soil content on the $K_d$-value. Even if degradation rates are constant over the whole test volume, the effective degradation rate depends on the $K_d$-value via Eq. (3.35). What is measured then, is a mean value over a large number of first order reactions exhibiting a large range of effective degradation rates. The weighting factors $w_i$ are introduced to account for different sizes of the subsamples.

$$\bar{c} = \frac{1}{n} c_0 \sum_{i=1}^{n} w_i e^{-k_i t} \tag{3.88}$$

Since the local distribution of soil properties can be regarded as random, the parameters $k_i$ are realizations of a random variable $K$. We shall not consider the concept of spatial random processes here, which are treated in chapter 7. Let us assume, that the random variable $K$ is characterized by a probability density function $f(k)$ with the following properties:

i)      The counterdomain of $f(k)$ is $[0,\infty)$.
ii)     The expectation $E[e^{-Kt}]$ is finite.

Since the concentration is a function of the random variable $K$, it is also a random variable, which is denoted by $C$. Then, in the limit $n \to \infty$ the expectation of the concentration at time $t$, $E[C(t)]$, is given by the integral

$$E[C(t)] = \int_{0}^{\infty} c_0 e^{-kt} f(k) dk \tag{3.89}$$

Gustavson and Holden (1990) evaluated this integral for the Gamma density function

$$f(k) = \lambda^{\alpha} k^{\alpha-1} \frac{e^{-\lambda k}}{\Gamma(\alpha)} \qquad for \quad \alpha, \lambda, k > 0 \tag{3.90}$$

with

$$\Gamma(\alpha) = \int_{0}^{\infty} e^{-t} t^{\alpha-1} dt \qquad for \quad \alpha > 0 \tag{3.91}$$

The expectation of a Gamma distributed random variable $K$ is

$$E[K] = \int_{0}^{\infty} k f(k) dk = \frac{\alpha}{\lambda} \tag{3.92}$$

and its variance is given by

$$V[K] = \int_{0}^{\infty} \left(k - \frac{\alpha}{\lambda}\right)^{2} f(k) dk = \frac{\alpha}{\lambda^{2}} \tag{3.93}$$

Figure 3.18 shows plots of Gamma densities for different sets of parameters exhibiting a variety of shapes from exponential to approximately Gaussian. The use of a Gamma density was motivated by the fact that frequently soil properties such as $K_d$-values or water conductivities follow positively skewed distributions, which can be modeled by a Gamma density function.
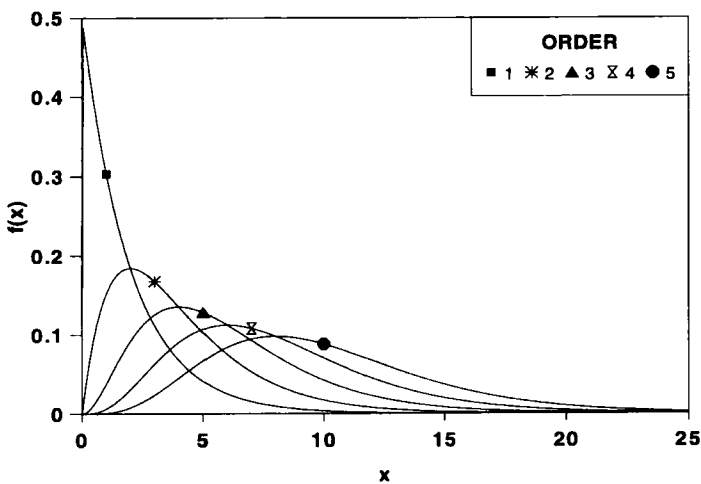


**Fig. 3.18:** Gamma density functions of order 1, 2, 3, 4 and 5.

Employing the Gamma density the integral (Eq. (3.89)) yields the simple formula

$$E[C(t)] = c_0 \int_0^\infty \lambda^\alpha k^{\alpha-1} \frac{e^{-\lambda k}}{\Gamma(\alpha)} e^{-kt} dk = \frac{c_0}{\left(1 + \frac{t}{\lambda}\right)^\alpha} \qquad (3.94)$$

This kinetic expression differs markedly from the mono-exponential decay law. Figure 3.19 shows a series of plots of Eq. (3.94) dependent upon the parameter $\alpha$. The deviations from linearity are obvious. Note that for growing $\alpha$ the exponential decay curve is apparently approached. If one varies the parameter $\lambda$ with $\alpha$ fixed, shapes very similar to double exponential decay curves are obtained.
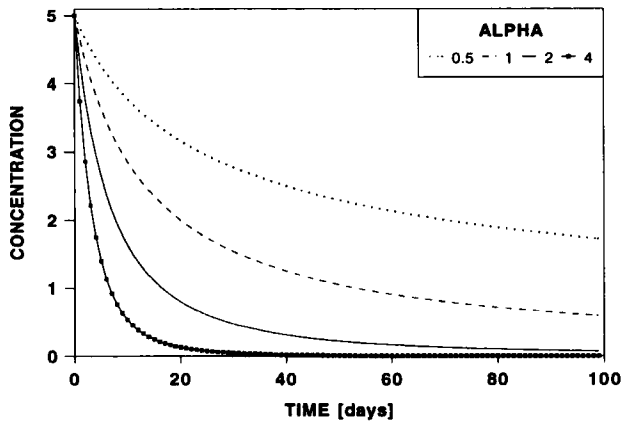


**Fig. 3.19:** Plots of Eq. (3.94) dependent upon the parameter $\alpha$. For growing $\alpha$ the shape of a mono-exponential decay curve is approached.

A fit of Eq. (3.94) to decay data of Terbufos (Felsot, 1982) demonstrates the applicability of this model (cf. Fig. 3.20). Gustavson and Holden (1990) reported a fairly large number of examples, where this model was applicable.

However, care should be taken as to the interpretation of the results. The type of curve described by Eq. (3.94) can also be derived from linear kinetic models including sorption and desorption. Figure 3.21 shows a fit of the Terbufos data to a model with a slow linear sorption and desorption, which was derived in section 3.1.2 (Eq. (3.31)). The model contains three parameters, the liquid phase degradation rate $k_l$ and the parameters $\alpha$ and $K_d$ for sorption and desorption. The fit was obtained for the total soil concentration, which has the mathematical form

$$c_t = \theta c + \rho S = c_0 \left( A e^{-\lambda_1 t} + B e^{-\lambda_2 t} \right) \qquad (3.95)$$

$$A + B = 1$$

The macroscopic parameters $A$, $B$, $\lambda_1$ and $\lambda_2$ are functions of the kinetic parameters (cf. section 3.1.2).

**Fig. 3.20:** Fit of Eq. (3.94) to decay data of Terbufos observed by Felsot (1982).
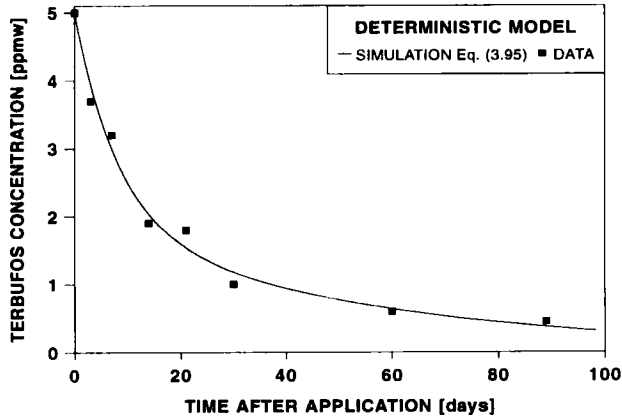


**Fig. 3.21:** Fit of kinetic model with slow linear sorption and desorption (Eq. (3.95)) to the same Terbufos data (Felsot, 1982) as shown in the previous figure, Fig. 3.20.
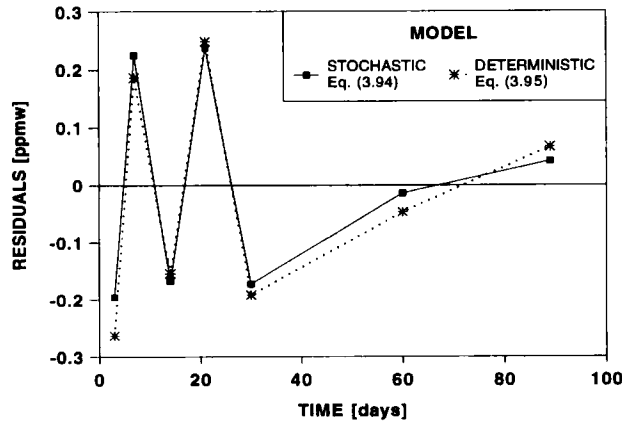


**Fig. 3.22:** Plot of residuals of both models (stochastic: Eq. (3.94)) and deterministic: Eq. (3.95) and vs. time.

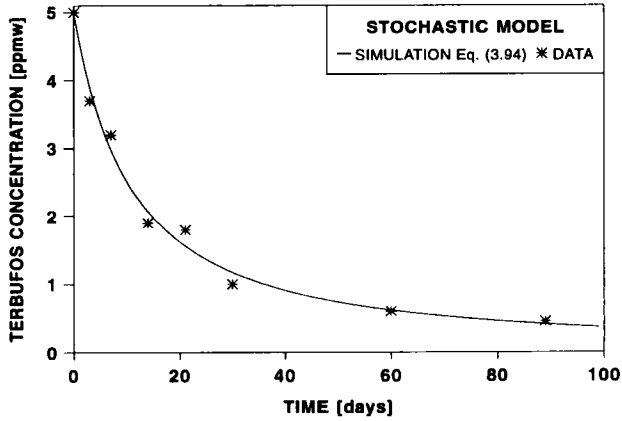Table 3.2 summarizes the results of parameter estimation for both models (for methods cf. chapter 4) including the mean square error as a measure for the goodness of the fit. The residuals of both fits are plotted in Fig. 3.22. The mean square errors of both models differ only slightly. Admittedly, the stochastic model yields the best fit and is in addition most parsimonious concerning the number of parameters. It should be emphasized, however, that model discrimination is not feasible by statistical analyses of concentration measurements of one component alone (total or solute phase concentrations). Only additional information on the time course of bound residues would allow to discriminate between the two models.

**Tab. 3.2:** Results of the statistical analysis of a stochastic (Eq. (3.94)) and a deterministic model (Eq. (3.95)) applied to degradation data of Terbufos (Felsot, 1982), standard deviations in brackets.

| Parameter | Estimate (st. dev.) |
|---|---|
| stochastic model (Eq. (3.94))<br>$\alpha$<br>$\lambda$<br>$R^2$<br>MSQ | 1.230 (0.3)<br>13.330 (4.9)<br>0.998<br>0.041 |
| deterministic model (Eq. (3.95))<br>$\lambda_1$<br>$\lambda_2$<br>$A$<br>$R^2$<br>MSQ | 0.018 ($0.9 * 10^{-2}$)<br>0.120 ($0.4 * 10^{-2}$)<br>0.380 (0.17)<br>0.997<br>0.046 |

A further important conclusion from this model concerns the concept of effective parameters. According to this concept, there exist so-called effective parameters which transform the deterministic equation into the equation obtained for the expectation.

$$E[C(t)] = c_0 e^{-k_{eff}t} \qquad\qquad (3.96)$$

As we have seen, the mathematical form of the expectation of the concentration profile is not of the form of a single profile. Therefore, it is not possible to find a value of the kinetic parameter $k$ such that Eq. (3.96) holds. However, in the limit of $Var[K] \to 0$ Eq. (3.94) approaches the mono-exponential decay law as can be seen from the following.

$$\lim_{\alpha \to \infty, \lambda \to \infty} \frac{1}{\left(1 + \dfrac{t}{\lambda}\right)^\alpha} = e^{-kt} \qquad with\ \lambda = \frac{\alpha}{k} \qquad\qquad (3.97)$$

## 3.2.4 Nonlinearities Encountered in Biological Degradation

In this section the following additional notations are used:

$V_{max}$ : maximum velocity of an enzyme catalyzed reaction [$M/L^3/T$]
$K_M$ : Michaelis constant [$M/L^3$]
$m$ : microbial population density [$M/L^3$]
$d$ : microbial mortality rate [$1/T$]
$\beta$ : coefficient of nonlinear mortality [$L^3/M$]
$\gamma$ : gain factor for biomass production [1]
$K_I$ : inhibition constant [$M/L^3$]
$\mu$ : maximum microbial growth rate [$1/T$]
$e_t$ : total enzyme concentration [$M/L^3$]
$e_0$ : concentration of free enzyme [$M/L^3$]
$e_1$ : concentration of enzyme-substrate complex [$M/L^3$]
$s$ : substrate concentration [$M/L^3$]
$p$ : product concentration [$M/L^3$]

### 3.2.4.1 Capacity Limited Degradation

Many organic substances are degraded or biotransformed by microorganisms. Most biological reactions are mediated by enzymes, which act as specific catalysators. The simplest reaction scheme (Michaelis and Menten, 1913) is

$$E + S \quad \underset{k_1}{\overset{k_{-1}}{\rightleftharpoons}} \quad [ES] \quad \overset{k_2}{\rightarrow} \quad E + P$$

The substrate $S$ binds to a free enzyme $E$ forming the enzyme-substrate complex $[ES]$, which decays into the product $P$ and the free enzyme $E$. With the notations $e_0$, $s$, $e_1$, $e_t$ and $p$ for the concentrations of free enzyme, substrate, enzyme-substrate complex, total enzyme concentration and product concentration the differential equations for the elementary chemical reactions are written as

$$\frac{de_0}{dt} = -k_1 e_0 s + k_{-1} e_1 + k_2 e_1 \tag{3.98}$$

$$\frac{de_1}{dt} = k_1 e_0 s - k_{-1} e_1 - k_2 e_1 \tag{3.99}$$

$$\frac{dp}{dt} = k_2 e_1 \tag{3.100}$$

Conservation of enzymatic forms is expressed by

$$e_1 + e_0 = e_t = const \tag{3.101}$$

Assuming quasi steady state for the formation and decay of the enzyme-substrate complex stationary concentrations of the enzymatic forms are obtained by setting $de_1/dt = 0$ and employing the conservation equation Eq. (3.101):

$$e_1 = \frac{e_t s}{s + \dfrac{k_2 + k_{-1}}{k_1}} \tag{3.102}$$

Inserting this expression into equation (3.100) yields finally

$$\frac{ds}{dt} = -\frac{dp}{dt} = -\frac{k_2 e_t s}{\dfrac{k_2 + k_{-1}}{k_1} + s} = -\frac{V_{max} s}{s + K_M} \tag{3.103}$$

with

$$V_{max} = k_2 e_t$$

and

$$K_M = \frac{k_2 + k_{-1}}{k_1}$$

This simple nonlinear differential equation is not amenable to an explicit analytical solution. Asymptotically, the equation becomes

$$\frac{ds}{dt} = -V_{max} \qquad for\ s \gg K_M \tag{3.104}$$

and

$$\frac{ds}{dt} = -\frac{V_{max}}{K_M} s \qquad for\ s \ll K_M \tag{3.105}$$

yielding pseudo first order for low and pseudo zero order kinetics for high concentrations.

Figure 3.23 shows simulated decay curves of Di-allate obtained for three different initial concentrations normalized to 100 %. The dependence of the kinetics on the initial concentration is obvious. A further example is given in chapter 4.
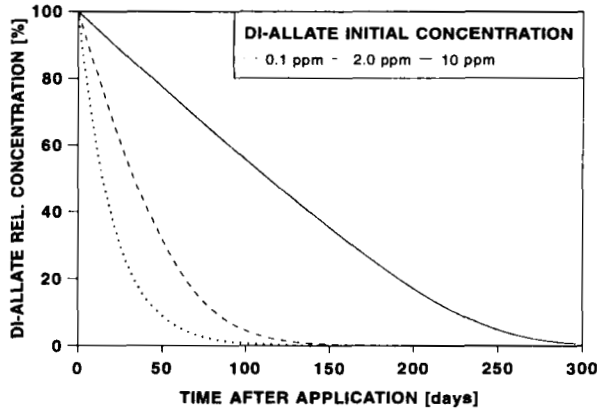
**Fig. 3.23:** Simulated decay curves of Di-allate based on a Michaelis-Menten degradation kinetics, obtained for three different initial concentrations normalized to 100 %.


### 3.2.4.2  Substrate Inhibition

At high concentrations, inihibition of microbial activity frequently occurs (Fournier et al., 1981; Hurle, 1982). A simple mechanism is an enzymatic reaction with substrate inhibition:

$$\frac{dc}{dt} = - \frac{1}{1 + \left(\dfrac{c}{K_I}\right)^n} \frac{V_{max} c}{c + K_M} \tag{3.106}$$

$K_I$ denotes the inhibitor constant and $n$ defines the steepness of the inhibition threshold.

Figure 3.24 shows a *dc/dt* vs. *c* plot of 2,4-D data, which fit well to the above model.
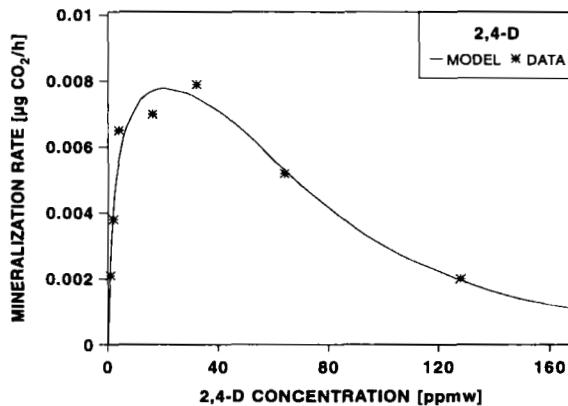


**Fig. 3.24:** Fit of the substrate inhibition model (Eq. (3.106)) to 2,4-D degradation rates as a function of initial concentrations (data from Parker and Doxtader, 1982).

This simple kinetic model is a possible mechanism for the concentration dependent time lags as observed for instance in experiments with Di-allate and 2,4-D. Figure 3.25 shows simulated decay curves obtained for a large range of initial concentrations. The curves are all normalized to 100 % to allow a better comparison. At low concentrations, the decay curve is approximately mono-exponential. With increasing initial concentrations, the nonlinear effects become apparent. The decay is delayed and lag times increase with initial concentrations.
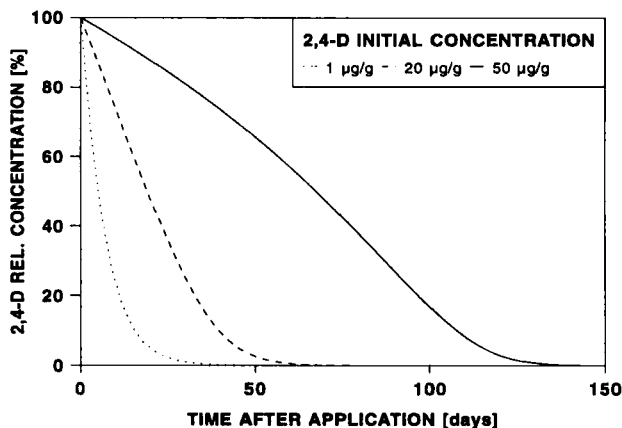


**Fig. 3.25:** Simulated decay curves based on the substrate inhibition model (Eq. (106)). High initial concentrations cause time lags.

### 3.2.4.3  Population Dynamic Effects

If a microbial population is able to grow on a pesticide as substrate, microbial population dynamics has to be modeled explicitly. Note that in the foregoing enzyme kinetic models the microbial density is implicitly contained in the parameter $V_{max}$, which is, however, assumed to remain constant in time. The following model, which goes back to Monod, couples microbial population dynamics with degradation.

$$\frac{dm}{dt} = \mu \frac{c}{c + K_M} m - dm(1 + \beta m) \tag{3.107}$$

$$\frac{dc}{dt} = -\frac{1}{\gamma} \frac{\mu c}{c + K_M} m \tag{3.108}$$

Equation (3.107) is the mass balance equation of microbial growth. The first term is the growth rate, which depends on nutrient concentration $c$ by a Michaelis-Menten type response function. The growth rate equals the consumption rate (Eq. (1.108)) corrected by the gain factor $1/\gamma$. The second term of Eq. (3.107) describes loss by mortality. The mortality rate is formulated density dependent in order to limit the population size. The coefficient $\beta$ measures the deviation of mortality rate from linearity. Only for $\beta > 0$ microbial growth is limited in the case of a constant level of $c$. If $\beta = 0$ the population either increases to infinity or dies

back, if the decay rate exceeds the growth rate. The introduction of a mortality rate as a function of microbial density prevents the population to grow beyond limits at surplus nutrient supply. Note that for the special case of a linear dependence of the mortality rate on density as is assumed in Eq. (3.107) the differential equation is equivalent to logistic growth if $c$ is kept constant, which can be seen from

$$\frac{dm}{dt} = r(c)m\left(1 - \frac{m}{K(c)}\right) \tag{3.109}$$

with

$$r(c) = \frac{\mu c}{c + K_M} - d \quad and \quad K(c) = \frac{r(c)}{d\beta}$$

$K(c)$ is denoted as environmental capacity of the population. In terms of the theory of dynamic systems, $K(c)$ is a stable attractor of the differential equation Eq. (3.109), i.e. the population density approaches this value asymptotically the region of attraction being the interval $0 < m < \infty$. Due to the density dependent mortality rate the capacity at surplus supply is limited by

$$\lim_{c \to \infty} K(c) = \frac{\mu - d}{d\beta}$$

This model may be generalized to $n$ nutrient components and $l$ biomass fractions the microorganism is able to grow on. Let $\mu_i$ denote maximum growth rate on biomass fraction $i$ and $N_{ij}$ nutrient component $j$ in biomass fraction $i$. The simplest way to model the dependence of growth rate on several essential nutrient components is to take the product of Michaelis-Menten type response functions and summing up over the biomass fractions. One thus arrives at the general model

$$\frac{dm}{dt} = m \sum_{i=1}^{n} \mu_i \left( \prod_{j=1}^{l} \frac{N_{ij}}{N_{ij} + K_{ij}} \right) - dm(1 + \beta m) \tag{3.110}$$

The consumption rate of the nutrients are coupled to microbial growth. If microbial biomass is expressed in C-units, the consumption of nutrient component $j$ depends on the $C/N_j$ - ratio of the nutrient with respect to the microorganism. Let this ratio be denoted as $\alpha_j$ and let $\gamma_i$ denote the gain factor pertaining to biomass fraction $i$. The differential equations for the nutrients are then

$$\frac{dN_{ij}}{dt} = -\frac{1}{\gamma_i}\frac{1}{\alpha_j}\mu_i \prod_{j=1}^{l} \frac{N_{ij}}{N_{ij} + K_{ij}} m \tag{3.111}$$

An alternative formulation is based on Liebig's minimum principle stating that the rate of any biological process is determined by the concentration of that nutrient, which is minimal.

$$\frac{dm}{dt} = m \sum_{i=1}^{n} \mu_i \left[ \min_{j=1\ldots l} \left( \frac{N_{ij}}{N_{ij} + K_{ij}} \right) \right] - dm(1 + \beta m) \tag{3.112}$$

Let us now consider the case of two C-sources, one naturally occurring and the other being the pesticide. All other nutrients are assumed to be present in surplus, i.e. with levels high above the respective $K_{ij}$-values. In this case, the general formula Eq. (3.110) leads to

$$\frac{dm}{dt} = \frac{\mu_0 c_0}{c_0 + K_0} m + \frac{\mu_1 c}{c + K_m} m - dm(1 + \beta m) \tag{3.113}$$

which is equivalent to

$$\frac{dm}{dt} = (r_0 + r(c))m \left( 1 - \frac{m}{K_0 + K(c)} \right) \tag{3.114}$$

It is important to consider at least one additional C-source. Otherwise, the population will totally disappear in the absence of the pesticide. According to Eq. (3.114) microbial density and hence microbial activity have two limiting states. In the presence of the pesticide as carbon source, population levels will rise from $K_0$ to a maximum value $K_{max}$ which is asymptotically reached at concentrations larger than the $K_M$-value:

$$K_{max} = K_0 + \frac{\mu_1}{d\beta}$$
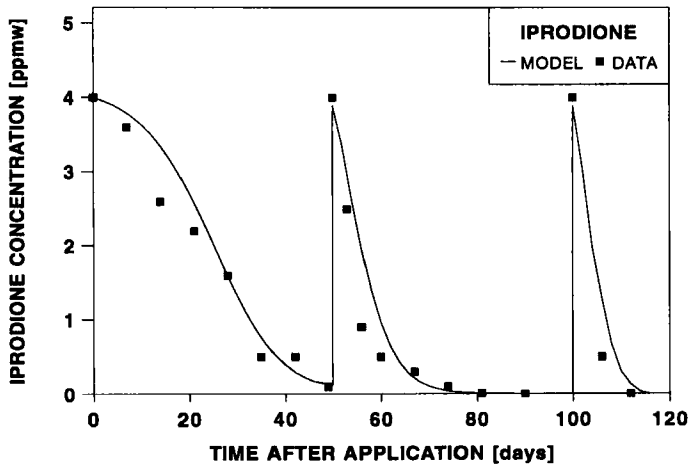


**Fig. 3.26:** Time course of the fungicide Iprodione obtained under three subsequent applications of the same dose in a soil not previously treated with the pesticide (experimental data from Walker and Welch, 1990). Note that a time lag occurs only after the first application.

The model explains the frequently observed effect of acceleration of degradation under multiple applications. Figure 3.26 shows the time course of the fungicide Iprodione, obtained under three subsequent applications of the same dose in a soil not previously treated with the pesticide. Only after the first application, a time lag occurs.

### 3.2.4.4 Long Term Persistence of Activity

The models treated so far suffer a major drawback concerning the long term persistence of activity. Once the available C-source in form of the pesticide is consumed, population levels begin to decline. The lifetime of the activity is determined by the in general short lifetime of the microorganisms. Experience shows, however, that the potential for degradation may persist for periods much longer than the average lifetimes.

This can be modeled by introducing an active state and a dormant state of the microorganisms. If conditions are favorable as concerns humidity and substrate, the organisms are in an active state which is characterized by rapid population growth and high mortality rates. Under unfavorable conditions, the organisms change into a dormant state characterized by low activity levels and low mortality rates. This behavior is typical for the so-called zymogenous microorganisms.

One possibility for modelling is the introduction of a dormant state and of transition rates which depend upon the environmental conditions and nutrient levels. Let $m_a$ and $m_d$ denote population levels in the active and dormant state respectively and $k_{ad}$ and $k_{da}$ the transition rates from active to dormant state and vice versa. The model takes the form

$$\frac{dm_a}{dt} = \mu_{max}\Phi(\theta,T,C,N)m_a - d_a m_a\left(1 + \beta_a m_a\right) - k_{ad}m_a + k_{da}m_d \qquad (3.115)$$

$$\frac{dm_d}{dt} = k_{ad}m_a - k_{da}m_d - d_d m_d\left(1 + \beta_d m_d\right) \qquad (3.116)$$

For each state, a different set of mortality parameters is defined. The function $\Phi$ is a response function normalized to 1, which depends on nutrient levels $C$ and $N$, temperature $T$ and humidity $\theta$. The dynamic behavior of the system is determined by the mathematical form of the transition rates. Let

$$\mu = \mu_{max}\Phi(\theta,T,C,N)$$

Then the population of the active state (no dormant states) will die back, if $\mu$ becomes less than $d_a$. In terms of dynamical systems theory, the state $m_a = 0$ then becomes a stable attractor. It is thus reasonable to let the transition rates depend on $\mu$ in a nonlinear way with a threshold parameter $\mu_s > d_a$. A suitable mathematical form is

$$k_{ad} = k_{max} e^{-\left(\frac{\mu}{\mu_s}\right)^\gamma} \qquad (3.117)$$

and

$$k_{da} = k_{max}\left[1 - e^{-\left(\frac{\mu}{\mu_s}\right)^\gamma}\right] \qquad (3.118)$$

Figure 3.27 shows the graph of these functions. The parameter $\mu_s$ determines the location of the threshold and the parameter $\gamma$ determines its steepness.
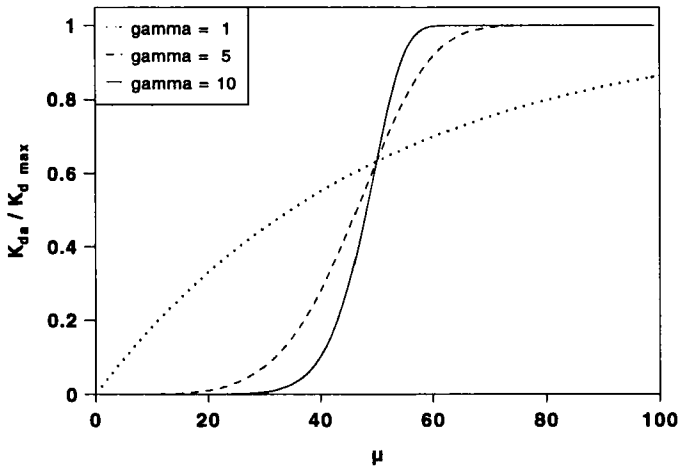


**Fig. 3.27:** Transition rate from dormant to active state as a function of actual growth rate $\mu$ according to Eq. (3.118).

In contrast to the models presented in the foregoing section the dormant state model allows the modelling of the persistence of the activity for long time periods. In other words, the model is capable of taking into account the long term treatment history of a soil. This is demonstrated in the following example. Hurle and Pfefferkorn (1972) investigated the degradation of DNOC under various pretreatment "histories". They found that the kinetic behavior both with respect to the characteristic times and the shape of decay curves is determined by the pretreatment level. Figure 3.28 shows the decay data of DNOC obtained by Hurle and Pfefferkorn (1972), 31 days after a pretreatment with 0 to 1.25 mg/kg soil.

Note that with increasing pretreatment level the lag phase becomes shorter and finally disappears. This dynamic pattern is matched by the model as is shown in Fig. 3.28. To allow for the initial decline of concentrations, the model is completed by a linear kinetic binding component. Parameters were identified for all experiments simultaneously with the methods described in chapter 4.
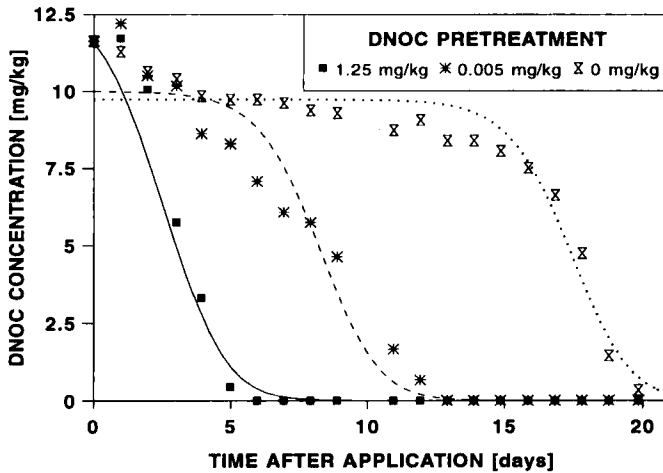
**Fig. 3.28:** Decay curves of DNOC obtained by Hurle and Pfefferkorn (1972), 31 days after pretreatment with 0 to 1.25 mg/kg soil. Increasing pretreatment levels cause a shortening of lag phases. This experiment is simulated by the model described by Eqs. (3.115) to (3.118). The systematic deviations are possibly due to nonlinear binding, which is not included in the model.

In the experiment of Hurle and Pfefferkorn (1972), both effects, the direct influence of the substrate on growth and the transition from dormant to active state are superimposed. In case of a long time lag between subsequent treatments the active component totally disappears and the degradation potential is solely preserved in the dormant component. Figure 3.29 shows the long-term behavior of the system for a fictitious treatment scenario.
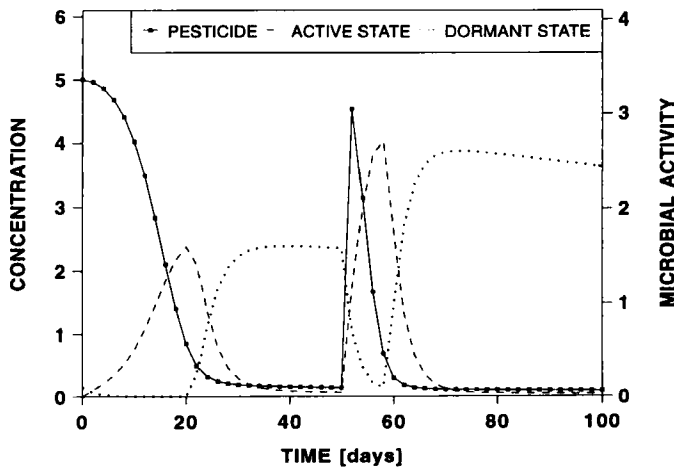


**Fig. 3.29:** Long-term behavior of the active-dormant state model. Long time lags between treatments cause the transition from active to dormant states.

Another concept, which goes back to Panikov (1992), introduces the notion of an activity state function, $R(t)$, which depends on the nutritional situation. Both, growth and mortality

rates are modulated by this function. In its simplest form, this concept is modeled by a system with the three components microbial density, nutrient concentration and activity state.

$$\frac{dm}{dt} = \frac{\mu c}{c + K_M} mR - dmR \qquad (3.119)$$

$$\frac{dc}{dt} = -\frac{1}{\gamma} \frac{\mu c}{s + K_M} mR \qquad (3.120)$$

$$\frac{dR}{dt} = \alpha \left( \frac{c}{c + K_M} - R \right) \qquad (3.121)$$

If the initial value of the activity state lies in the interval [0,1], $R(t)$ can only assume values within this interval. This is seen from the differential equation Eq. (3.121) for $R$. The argument goes as follows. For fixed levels of $c$ the equilibrium value of $R$ equals the first term in the bracket of the l.h.s. of the equation. However, this term can take on only values between 0 and 1. In the case of low nutrient levels, the activity is reduced and the population is kept alive at a low activity level. Figure 3.30 shows the behavior of this model under a long term treatment scheme.
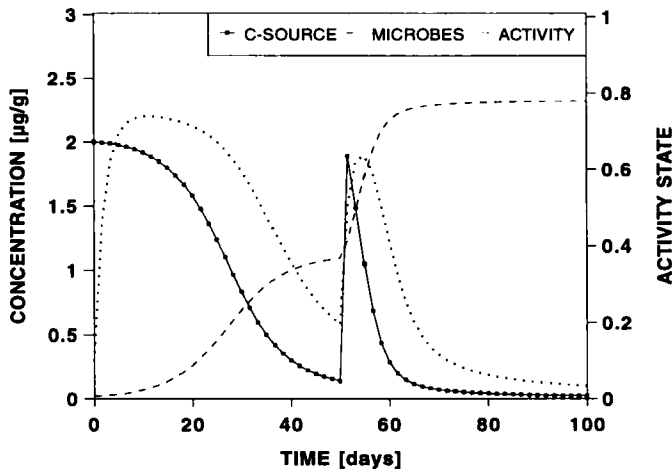


**Fig. 3.30:** Behavior of the Panikov model (Eqs. (3.119) - (3.121)) under subsequent applications. The activity function $R$ decreases with substrate and thus causes a slow down of all metabolic processes.

## 3.2.4.5  Stochastic Approach for Activity Life Times

If a pesticide has been applied over a long period, persistence of activity is likely to persist for some time after the offset of the application. This effect was modeled in the previous section by the introduction of dormant states. Although this concept is appealing from a

conceptual point of view, in practice, it is difficult to obtain measurements of microbial densities in different states. In a routine situation usually merely the time course of concentrations in the soil often even not differentiated with respect to liquid and solid phase is measured.

Therefore, for practical purposes, a simple model is needed whose parameters are estimable from routine data. From concentration measurements, lag times can be derived easily. A lag time can be considered as a random variable which is modeled by its probability density function. The probability density function is related to the kinetic parameters via the distribution function. Let $T$ denote the random variable lag time, $f(t)$ its density function and $F(t)$ its distribution function.

The distribution function is defined as $F(t) = Prob(T < t)$, i.e. as the probability that the realization of the random variable $T$ is less then $t$, or in other words as that part of the (statistical) population with lag times less then $t$. From this definition the relation between the reaction rate of a first order reaction and the distribution function of $T$ becomes quite obvious

$$k(t) = k_{max} F(t) \qquad (3.122)$$

The statistical interpretation can be applied to the microbial population. In this context, $F(t)$ is that part of the microbial population with capability of biodegradation of the pesticide under study. A suitable life time distribution is the Weibull distribution

$$F(t) = 1 - e^{-\left(\frac{t}{\tau}\right)^{\gamma}} \qquad (3.123)$$

with density function

$$f(t) = \gamma \frac{t^{\gamma-1}}{\tau^{\gamma}} e^{-\left(\frac{t}{\tau}\right)^{\gamma}} \qquad (3.124)$$

Its expectation and variance are given by

$$E[T] = \Gamma\left(\frac{1}{\gamma} + 1\right) \qquad (3.125)$$

$$V[T] = \tau^2 \left[\Gamma\left(\frac{2}{\gamma} + 1\right) - \Gamma\left(\frac{1}{\gamma} + 1\right)\right]^2 \qquad (3.126)$$

where $\Gamma$ denotes the Gamma function.

Figure 3.31 shows plots of a Weibull distribution and a Weibull density function.
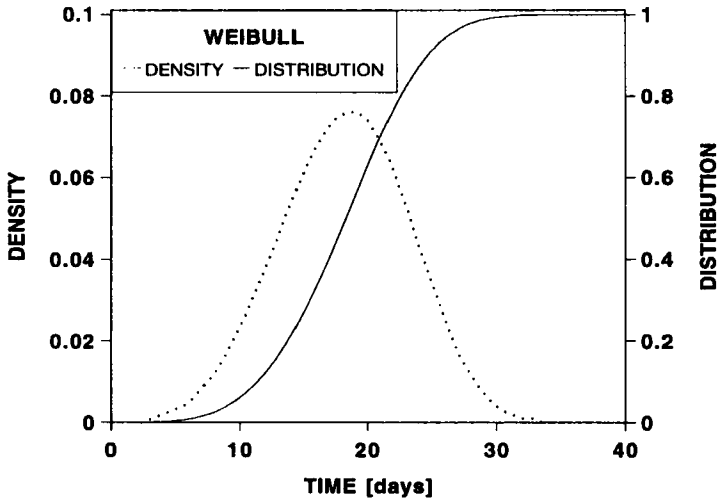


**Fig. 3.31:** Weibull distribution function and density function for activity life times.

The decay of activity can be modeled in a similar way by employing a survival function. Let $F_d$ ($t^*$) denote the distribution function of activity lifetimes after the termination of applications. Then the survival function $S(t^*) = 1 - F_d$ ($t^*$), which denotes that part of the population which is still active at time $t^*$, is used to describe the decay of activity. To trigger the onset of induction or of decay of activity, threshold concentrations $c_s$ are introduced. For a first order decay reaction, the model then takes the form:

$$\frac{dc}{dt} = \begin{cases} - k_{max} F(t)c & for \quad c > c_s \\ \\ - k_{max} S(t^*)c & for \quad c \le c_s \end{cases} \qquad (3.127)$$

where it is assumed, that concentrations are above threshold $c_s$ the first time at time $t = 0$ and below threshold for $t > t_s$ where $t^* = t - t_s$. The model is specified by the five parameters $k_{max}$, $\tau_1$, $\gamma_1$, $\tau_2$ and $\gamma_2$.

The model is capable of simulating typical long term treatment effects: enhanced degradation at the beginning of an application period and the decay of activity at the end.

Figures 3.32 a,b show time courses of concentrations and activities for a long term treatment scenario. First, the activity builds up and persists as long as the treatment is continued. After the end of the treatment, activity decays and builds up again only if the treatment is resumed.
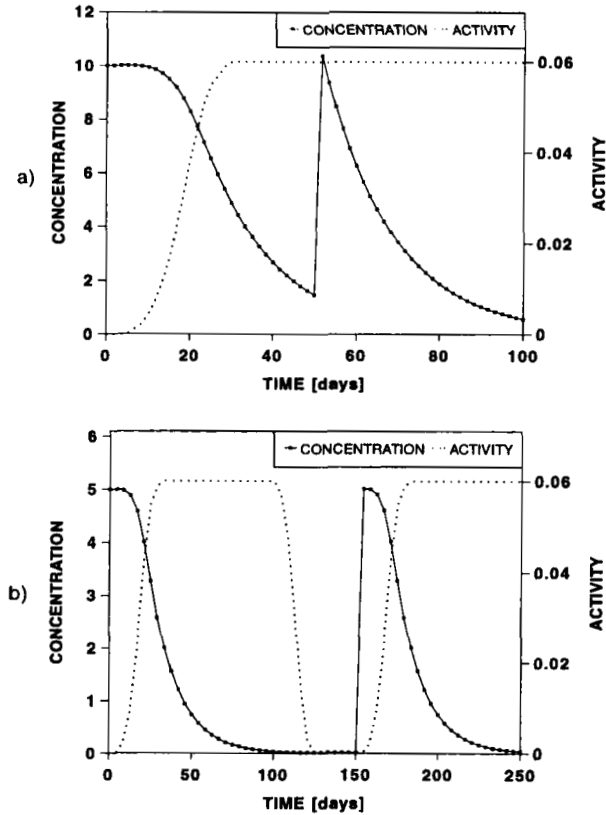
**Fig. 3.32:** Multiple applications simulated by the stochastic activity life time model (Eq. (3.127)): a) If the second application is given prior to the decay of activity, enhanced degradation occurs. b) About 100 days after the first application the activity state has decayed. Degradation occurs only after the renewed built up of the activity state.

### 3.2.4.6  Shift of Population Composition

The application of an organic chemical may also influence the ecological (quasi) equilibrium at the microbial level. To study this effect the classical Lotka-Volterra (Lotka, 1925; Volterra, 1926) competition model is combined with a degradation kinetic model. Let us assume, for simplicity, that two logistic populations exist in stable coexistence:

$$\frac{dm_1}{dt} = r_1 m_1 \left( 1 - \frac{m_1 + \alpha m_2}{K_1} \right) \tag{3.128}$$

$$\frac{dm_2}{dt} = r_2 m_2 \left( 1 - \frac{m_2 + \beta m_1}{K_2} \right) \tag{3.129}$$

The coefficients $\alpha$ and $\beta$ are a measure of the mutual competition between the species and $K_1$ and $K_2$ denote the environmental capacity of each species in the absence of the other. The stationary solutions of this system are

$$\vec{m}_{01} = \begin{pmatrix} K_1 \\ 0 \end{pmatrix} \tag{3.130}$$

$$\vec{m}_{02} = \begin{pmatrix} 0 \\ K_2 \end{pmatrix} \tag{3.131}$$

$$\vec{m}_{03} = \frac{1}{1 - \alpha\beta} \begin{pmatrix} K_1 - \alpha K_2 \\ K_2 - \beta K_1 \end{pmatrix} \tag{3.132}$$

From local stability analysis the following stability conditions are derived:

i)      State (1) is stable, if $K_1 > \alpha K_2$  and $K_2 < \beta K_1$.
ii)     State (2) is stable, if $K_1 < \alpha K_2$  and $K_2 > \beta K_1$.
iii)    State (3) is stable, if $K_1 > \alpha K_2$  and $K_2 > \beta K_1$.

Let us now assume, that a pesticide increases the mortality rate of population 2 and is cometabolically degraded by population 1. Let us further assume, that population 2 is dominant if no herbicide is present, i.e. its densities are much higher than those of population 1. The model equations for these processes are

$$\frac{dm_1}{dt} = r_1 m_1 \left( 1 - \frac{m_1 + \alpha m_2}{K_1} \right) \tag{3.133}$$

$$\frac{dm_2}{dt} = r_2 m_2 \left( 1 - \frac{m_2 + \beta m_1}{K_2} \right) - d_h m_2 c \tag{3.134}$$

The second term in the last equation models the pesticide induced mortality in analogy to a bimolecular reaction with rate $d_h$.

$$\frac{dc}{dt} = - m_1 \frac{V_{max} c}{c + K_c} \tag{3.135}$$

To analyze the qualitative behavior of this system, let us start from a constant herbicide level $c^*$. In this case, Eqs. (3.133) and (3.134) are identical in form with Eqs. (3.128) and (3.129),

if one replaces $r_2$ and $K_2$ by

$$r'_2 = r_2 \left( 1 - \frac{d_h c^*}{r_2} \right)$$

$$\text{(3.136)}$$

$$K'_2 = K_2 \left( 1 - \frac{d_h c^*}{r_2} \right)$$

An increase of equilibrium level $c^*$ shifts equilibrium population densities in favor to population 1. From the stability conditions it is obvious, that above a threshold value even the coexistence conditions are no more fulfilled which causes the eventual extinction of population 2.

The dynamics of the system under multiple applications is shown in Fig. 3.33. If the time lag between subsequent applications is short, enhanced degradation occurs. After the degradation of the herbicide, the system assumes its prior state losing its "memory" of the pretreatment and degradation occurs only after a further shift in population densities.
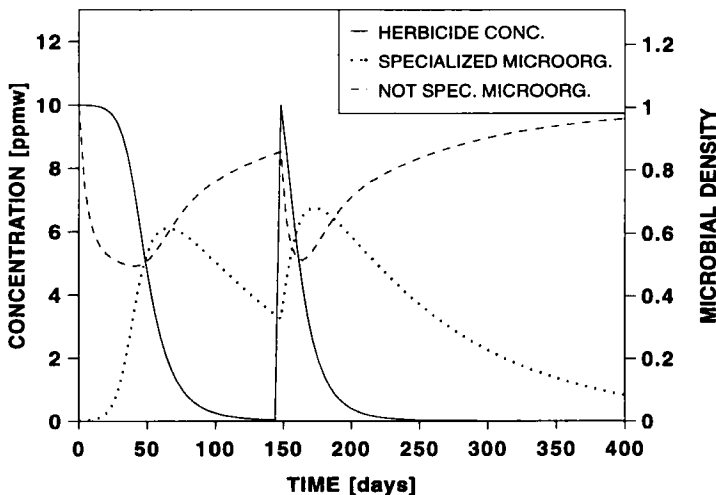


**Fig. 3.33:** Simulated time course of a fictive metabolic degraded pesticide following repeated applications and consequences on composition of microbial community. The simulation is based on Eqs. (3.133) to (3.135). For short time lags enhanced degradation occurs. After the degradation of the herbicide the microbial composition is shifted to the prior state.

In practice, it is extremely difficult to monitor the population dynamics of different microbial species. Only few data are available in the current literature. Kunc and Rybarova (1983) measured the time courses of the densities of microbial species following the application of 2,4-D. Their data can be described by the time courses produced by the above model.

Figure 3.34 shows a comparison between model and data. The estimated model parameters are presented in Tab. 3.3. Note that part of the parameters had to be fixed due to the overparameterization of the model (cf. chapter 4 for details of the estimation procedure).
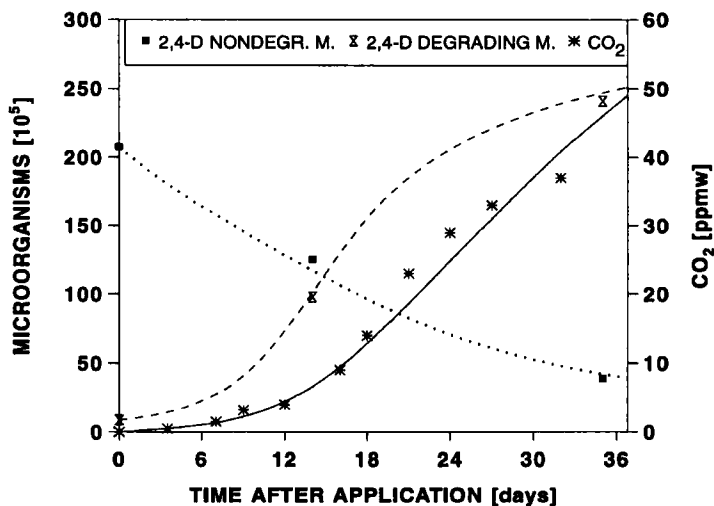


**Fig. 3.34:** Change in soil microbial composition after application of 50 mg 2,4-D per kg soil, observed by Kunc and Rybarova (1983). The fit is based on Eqs. (3.133) to (3.135).

**Tab. 3.3:** Result of fitting Eqs. (3.133) to (3.135) to observed time courses of 2,4-D concentration and microbial densities (standard deviations in brackets). The resulting fit is shown in Fig. 3.34.

| Parameter | Estimate (st. dev.) |
|---|---|
| $\alpha$ | 1.1510 (0.5689) |
| $\beta$ | 1.9987 (0.3374) |
| $r_1$ | 0.6362 (0,0153) |
| $r_2$ | 0.0269 (0.2245) |
| $d_h$ | 0.0009 (0.0001) |
| $k := V_{max}/K_c$ | 0.0001 (<0.00001) |
| **fixed** | |
| $K_1$ | 300.0 |
| $K_2$ | 300.0 |
| $m_{01}$ | 8.8 |
| $m_{02}$ | 207.8 |
| $c_0$ | 50.0 |
| $R^2$ | 0.997 |

### 3.2.4.7 Interactions

Similar to the interactions of drugs in an organism the simultaneous application of several pesticides may provoke synergistic or antagonistic effects (Poschenrieder, 1978; Hurle and Walker, 1980; Nash, 1981; Auspurg, 1985).

Consider the case that a fungicide and a biodegradable herbicide are simultaneously applied. Then it is most likely that the biodegradation of the herbicide is inhibited by the fungicide, if fungi play an important role in the breakdown of the herbicide.

However, synergistic effects have also been reported. Hurle et al. (1982) found that degradation of Chlorotoluron was enhanced in the presence of the fungicide "Cercobin Super" and inhibited by the insecticide "Metasystox R". The following model describes the interactions of two pesticides assuming that the degradation of the first is inhibited by the second.

The following notations hold:

$c_1$ : concentration of a herbicide, e.g. Simazine $[M/L^3]$
$c_2$ : concentration of a fungicide, e.g. Captan $[M/L^3]$
$k_h, k_f$ : first order degradation constants for the herbicide and fungicide respectively $[1/T]$
$K_I$ : inhibition constant $[M/L^3]$
$n$ : shape parameter $[1]$

The inhibition is modeled by a term analogous to noncompetitive inhibition of an enzymatic reaction.

$$\frac{dc_1}{dt} = -k_h c_1 \frac{1}{1 + \left(\dfrac{c_2}{K_I}\right)^n} \tag{3.137}$$

$$\frac{dc_2}{dt} = -k_f c_2 \tag{3.138}$$

These equations are amenable to an analytic solution, because the interaction is not mutual. The solution of Eq. (3.137) for the initial condition $c_2(t{=}0) = c_{20}$ is inserted into Eq. (3.138) yielding

$$\frac{dc_1}{dt} = -\frac{k_h c_1}{1 + \left(\dfrac{c_{20}}{K_I}\right)^n e^{-nk_f t}} \tag{3.139}$$

For a single application with initial concentration $c_{10}$ the solution of Eq. (3.139) is obtained by the method of separation of variables:

$$c_1(t) \quad = c_{10} e^{-k_h t} \frac{(1 + a)^\kappa}{\left(1 + a e^{-n k_f t}\right)^\kappa}$$

(3.140)

$$with \quad \kappa = \frac{k_h}{n k_f} \quad and \quad a = \left(\frac{c_{20}}{K_I}\right)^n$$

This model is applied to the interaction between Simazine and Captan as investigated by Kibler (1979). Figure 3.35 shows decay curves obtained for each substance separately and for Simazine in the presence of Captan.
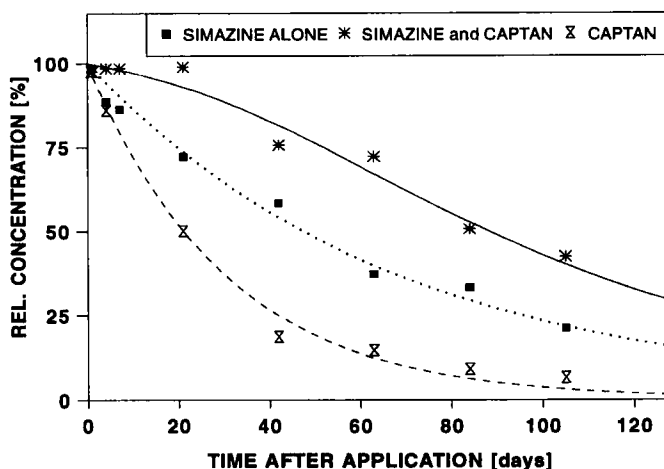


**Fig. 3.35:** Inhibition of Simazine degradation due to simultaneous application of the fungicide Captan, observed by Kibler (1979). Degradation rate of Simazine is decreased in the presence of Captan. Simazine degradation is modeled by Eq. (3.140).

As a further example, the interaction between Prometryn and Thiram as measured by Wagenbreth et al. (1970) is simulated. Figure 3.36 shows the comparison between model and data. The interaction is quite strong causing a considerable time lag of the degradation of Prometryn. The parameter sets of these two simulations are presented in Tab. 3.4.

**Tab. 3.4:** Results of fitting Eqs. (3.138) and (3.140) to Simazine/Captan and Prometryn/Thiram inhibition data (Kibler, 1979; Wagenbreth, 1970).

| Parameter | Simazine / Captan | Prometryn / Thiram |
|:---:|:---:|:---:|
| $k_h$ | 0.014 | 0.019 |
| $k_f$ | 0.033 | 0.061 |
| $K_I$ | 16.433 | 0.009 |
| $n$ | 1.249 | 1.392 |
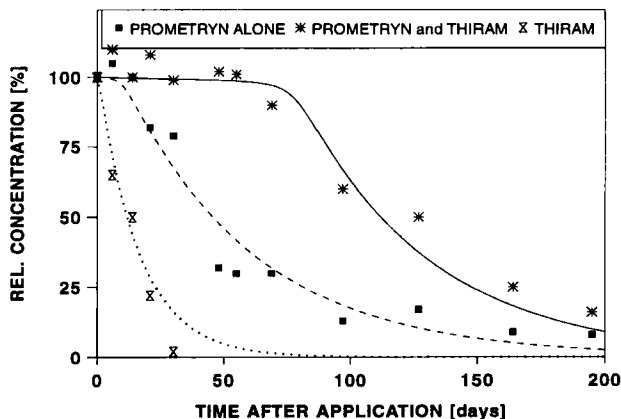
**Fig. 3.36:** Inhibition of Prometryn degradation due to simultaneous application of the fungicide Thiram (experimental data of Wagenbreth, 1970). Prometryn degradation is modeled by Eq. (3.140).

## 3.3 Kinetics of Dose-Response

### 3.3.1 Linking Concentration and Effect

The assessment of optimal application schemes for herbicides necessitates the modelling of the potential response in dependence on herbicide concentrations and hence as a function of time. Whereas there exist many kinetic models, there are only few publications concerned with linking kinetics and dynamic response.

It is sometimes helpful to look around into other disciplines. One finds that there is a striking similarity between kinetics of pharmacons and herbicides. As far as only the kinetics are concerned the mathematical approaches are identical in structure. Adsorption and desorption have their counterpart in tissue and protein binding, the elimination rates of some drugs are capacity limited and follow an enzyme kinetic expression and even time lags may occur caused by induction. In both fields, it does not suffice to be able to simulate the time course of concentrations. The goal is rather the prediction of the wanted effect and of side effects which are correlated with concentration levels. In pharmacology, the link is established by modelling drug receptor interactions and relating the number of occupied receptor binding sites directly to the effect.

Other approaches establish a statistical relationship between concentration levels and effect in form of a response function. This approach is also applicable to the analogous problem in herbicide dynamics.

Under the assumption that the characteristic times of herbicide action are much shorter than the characteristic times of degradation, time courses of concentrations are directly coupled to dose response functions. By this simple transformation of concentrations, time courses of the response are obtained. Since typical response functions are characterized by sharp thresholds and saturation levels, this transformation yields time courses characterized by abrupt changes

in the neighborhood of threshold concentrations. If there is a pronounced time lag between concentration and effect, this could be taken care of by the introduction of an additional component, the so-called "effect component". This is common practice in pharmakokinetics.

Such models provide information about the optimal application of a herbicide to ensure sufficient weed control over a critical period of time. Relating herbicide concentration profiles to its biological efficacy provides a means to fulfil both the needs of the farmers, which require an optimal weed control and the environmental protection in using the lowest herbicide application dose for a given soil. By introducing crop-specific thresholds, it is possible to simulate carryover effects for crop rotations.

The residual concentration of a soil applied herbicide in the upper soil horizon is only one of the factors critical for its efficacy. The amount of herbicide required to control a given weed in a given soil depends furthermore on physico-chemical properties as covariates and on the phenological state of the weed. If weed emergence occurs over a long period of time, the optimal timing depends both on the emergence pattern of the weed and the developmental stage of the crop.

### 3.3.2   Mathematical Form of Dose-Response-Curves

Additional notations:

$\beta$, $a_1$, $a_2$ : fitting parameters of response functions [1]
$R$        : plant response function (e.g. reduction of dry weight of weeds) [% of biomass]
$W$        : integral over the response function: performance criterion of an application schedule
$L$        : weed production without control [$M/L^2$]
$U$        : weed production under high application rates [$M/L^2$]
$D$        : dose, amount of herbicide per unit of soil [$M/L^3$]
$D_{eff}$  : effective dose [$M/L^3$]
$c_{eff}$  : effective concentration [$M/L^3$]
$c_{crit}$ : concentration threshold [$M/L^3$]
$\alpha$   : rate constant of decay of microbial activity [$1/T$]

Herbicide activity is a function of both bioavailability and metabolic efficacy. For each combination of herbicide and organism there exists a bioactive threshold level necessary to produce a significant metabolic effect (Bailey and White, 1964). A large number of bioassays under controlled conditions have been analyzed to determine the range of herbicide concentrations required for weed injury in different soils. Plant response to a chemical is frequently described by a logistic equation (Streibig, 1988):

$$R = \frac{U - L}{1 + e^{-2\left(a_1 + a_2 \ln(D)\right)}} + L \qquad\qquad (3.141)$$

The asymptotic limits of this function are the parameters $U$ (in the limit $D \to \infty$) and $L$ (in the limit $D \to 0$). The parameters $a_1$ and $a_2$ determine the horizontal position and the slope

of the curve half way between these limits. If one transforms Eq. (3.141) according to

$$y = 0.5 \ln\left(\frac{U - R}{R - L}\right) \tag{3.142}$$

the transformed response variable is a linear function in $\ln(D)$. This transformation is denoted as logit transformation and is frequently used in dose response experiments.

$$y = -\left(a_1 + a_2 \log(D)\right) \tag{3.143}$$

The $ED_{50}$-value, defined as the dose that causes 50 % of the total achievable growth reduction of the plant is given by

$$ED_{50} = e^{-\frac{a_1}{a_2}} \tag{3.144}$$

The shape of the curve is shown in Fig. 3.37. However, this curve decreases monotonically and has no peak for any values of the parameters. So this model is not capable to describe stimulation of growth at low doses, which has been observed in weeds such as *Alopecurus myosuroides* (Brain and Cousens, 1989).
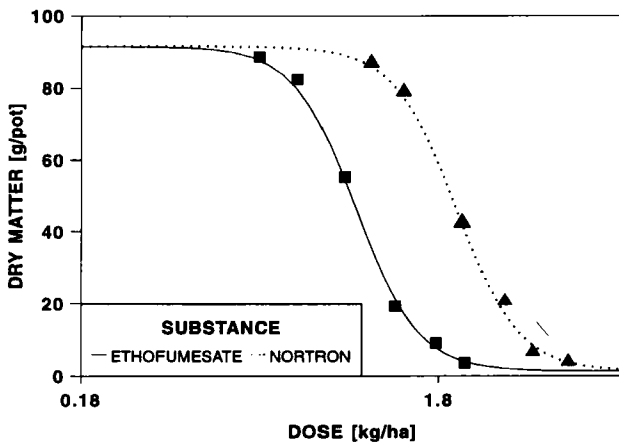


**Fig. 3.37:** Dose response curve of oat dry weight for Ethofumesate and Nortron in loamy sand (data from Streibig, 1984). The fit is obtained by the logistic regression model Eq. (3.141).

Brain and Cousens (1989) therefore suggest to modify the logistic doses response curve in the following way allowing for the occurrence of a peak a low doses:

$$R = \frac{U - L + fD e^{-2\left(a_1 + a_2 \ln(D)\right)}}{1 + e^{-2\left(a_1 + a_2 \ln(D)\right)}} + L \tag{3.145}$$

Parameter $f$ measures the initial rate of increase in plant yield at low herbicide dose, i.e. the degree of stimulation by the chemical.

Figure 3.38 shows the herbicide response curve obtained for sugar beet treated with Chlorsulfuron.
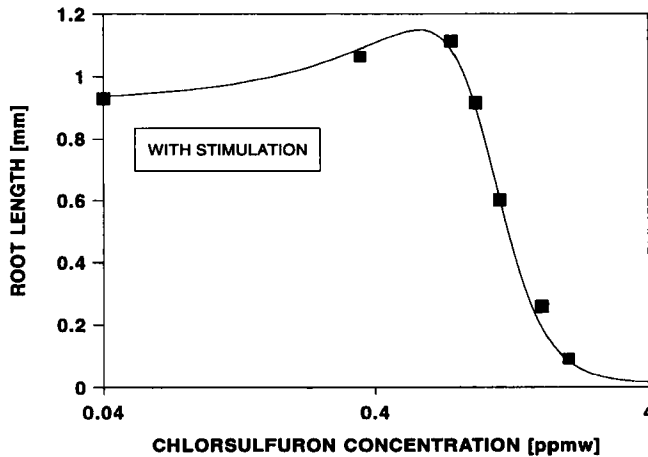


**Fig. 3.38:** Dose response curve of root length for sugar beet treated with Chlorsulfuron allowing for growth stimulation at low doses (data and model from Brain and Cousens, 1989). The fit is obtained by the modified logistic regression model Eq. (3.145).

A further suitable response function is the Weibull distribution function, which is used in statistics to model life time distributions (cf. section 3.2.4.5). Written in the following form, the meaning of its parameters becomes quite clear: the parameter $c_{crit}$ characterizes a threshold and the parameter $\beta$ determines its steepness.

$$R = e^{-\left(\dfrac{D}{C_{crit}}\right)^{\beta}} \tag{3.146}$$

If the response is expressed as toxicity rather than in dry biomass of the weed, the dose response curves take the form

$$\bar{R} = 1 - R$$

Figure 3.39 shows the application of the Weibull function to dose response experiments of the herbicides Quinmerac and Quinchlorac with carrot (*Daucus carota*) as the sensitive indicator plant (Schmider, 1990). The response variable in this experiment is the reduction in dry weight.
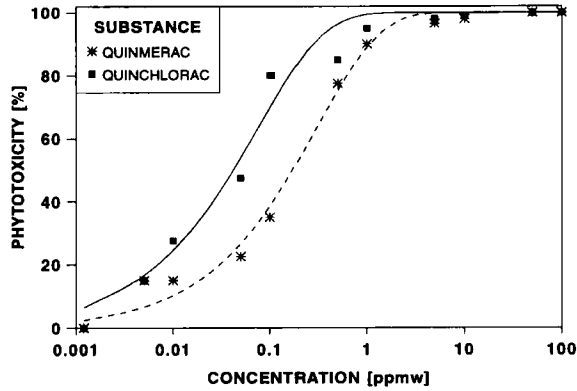
**Fig. 3.39:** Dose response curve (phytotoxicity) of Quinmerac and Quinchlorac with *Daucus carota* as indicator plant (data from Schmider, 1990). The fit is obtained by the Weibull response function Eq. (3.146).

The critical concentration $c_{crit}$ depends both on soil factors and weed species. If one assumes that only solute phase concentrations are directly related to the response, $D$ has to be modified accordingly. In the case of linear adsorption and desorption $D$ is replaced by the effective concentration (cf. section 3.1.3)

$$D_{eff} = \frac{D}{1 + \frac{\rho}{\theta} K_d}$$ 

(3.147)

Thus sorption results in a shift of the response curve to the right. Figure 3.40 shows a fit of Eq. (3.146) to data of Quinmerac activity in three different soils, where $c_{crit}$ and ß are obtained from dose response relations in water. The fit permits the direct comparison of sorption strengths of different soils.
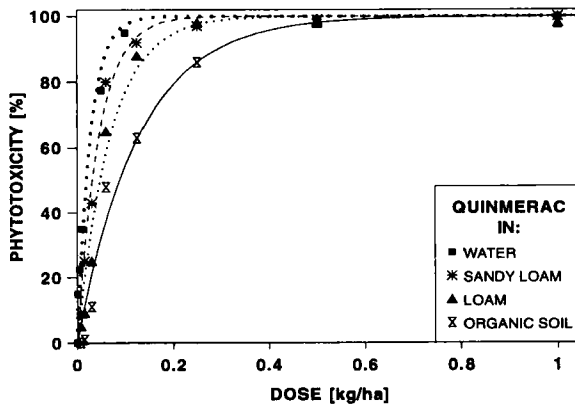


**Fig. 3.40:** Dose response curves of Quinmerac in different soils and water with *Daucus carota* as indicator plant (data from Schmider, 1990). The fit is obtained by the Weibull response function Eq. (3.146).

### 3.3.3   Time Courses of the Response

Under the assumptions, that (i) the response is directly related to solute phase concentrations and that (ii) the time delay between the response and the current concentration is negligible, time courses of the responses are simply obtained by inserting the time dependent solute concentrations into the dose response functions. I.e. the time courses of the response functions are simply nonlinear transformations of solute concentration curves.

**Linear Kinetics**

Inserting a mono-exponential decay function into the Weibull response function yields the time dependent response function

$$R(t) = 1 - \exp\left[ - \left( \frac{D_{eff} e^{-k_{eff} t}}{c_{crit}} \right)^{\beta} \right] \qquad (3.148)$$

with

$$k_{eff} = \frac{k}{1 + \frac{\rho}{\theta} K_d}$$

Note, that sorption influences $R(t)$ in two opposite ways: on the one hand, the solute concentrations are lowered resulting in a shift of the response curve, on the other hand degradation is retarded resulting in a prolonged response.

Figure 3.41 shows a fit of Eq. (3.148) to bioassay studies of Schmider (1990) with Quinmerac in three different soils.
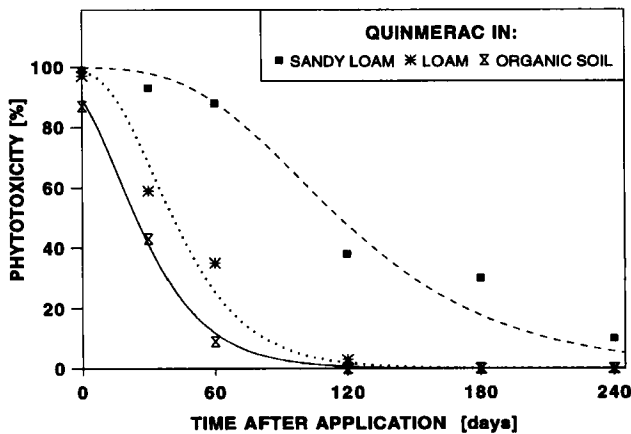


**Fig. 3.41:** Time courses of phytotoxicity of Quinmerac in different soils (data from Schmider, 1990). The fit is obtained by Eq. (3.148).

The effective degradation rate is highest in the organic soil. This is probably due to higher microbial density which is correlated to the organic matter content. In addition, the high pH-value in this soil also prohibits strong adsorption of Quinmerac.

To illustrate the effect of the degree of adsorption and hence of the soil properties on the response, an experiment performed by Loux et al. (1989) is analyzed. The results are shown in Figs. 3.42 a,b. Imazaquin kinetics and response (inhibition of root growth of wheat) were measured in two soil types. Degradation of Imazaquin in the upper 7.5 cm of Cisne and Drummer soil was found to be biphasic. A fast degradation phase of about 60 days after application is followed by a phase of slow degradation. In this soil, Imazaquin concentrations above the toxicity threshold are maintained over a long period due to desorption (cf. Fig. 3.42 b). This might explain the carryover effects of Imazaquin and resulting corn injury reported by Renner et al. (1988). The fit was obtained by inserting the biphasic kinetics (Eq. (3.31)) into a Weilbull response function.
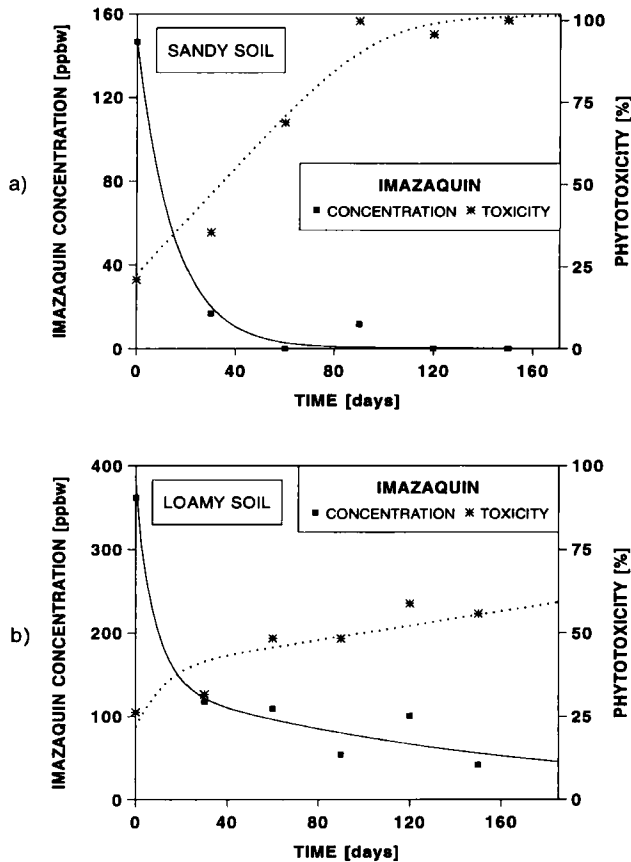


**Fig. 3.42:** Time courses of Imazaquin concentrations and toxicity on wheat (indicator variable root biomass with respect to a control) in two different soils: a) in a sandy soil (Cisne), where sorption is weak, toxicity levels are fading 90 days after application and b) in a loamy soil (Drummer) with strong sorption toxicity levels are maintained for a long time period. The fit was obtained by inserting the biphasic kinetics (Eq. (3.31)) into a Weilbull response function (Eq. (3.146)).

## Nonlinear Kinetics

The rate constants of Quinmerac degradation in a clay soil depend on initial concentrations, indicating deviations from first order kinetics. For each initial concentration the fit to a first order model is very close. The rate constants and half-lives, however, differ considerably. This may lead to drastic effects on the shape of the response curves in the neighborhood of the threshold. Due to the nonlinear decay mode (longer half-lives at higher concentrations) unexpected carryover effects may occur when concentrations are increased. Figure 3.43 shows time courses of the response of *Daucus carota* under three different concentrations.
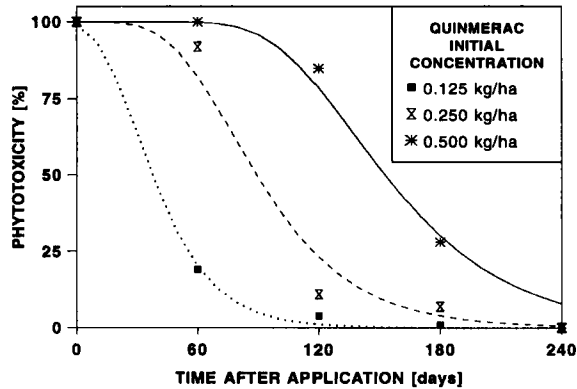


**Fig. 3.43:** Time course of the response of Quinmerac on *Daucus carota* for three different initial concentrations.

Enhanced microbial degradation of EPTC in previously treated soils causes problems in control of weeds (Rahman and James, 1983). For effective control of early flushes of wild proso millet, EPTC is applied preplant incorporated at 2.2 to 6.7 kg ha$^{-1}$ and must persist in significant quantities for approximately 15 to 30 days (Harvey, 1987). The data of EPTC degradation after repeated application, obtained by Obrigawitch et al. (1983), indicate a microbial adaptation to EPTC.

Because of lack of explicit data about the dynamics of degrading microorganisms a simplified version of model Eqs. (3.107) and (3.108) combined with a linear adsorption kinetic is fitted to experimental data, assuming first order degradation kinetics and replacing microbial density $m$ by activity $a$.

$$\frac{da}{dt} = kca - \alpha a \tag{3.149}$$

$$\frac{dc}{dt} = -kca - k_{12}c + k_{21}S \tag{3.150}$$

$$\frac{dS}{dt} = k_{12}c - k_{21}S \tag{3.151}$$

Figure 3.44 shows the fit of this model to decay data of EPTC (Obrigawitch et al., 1983). The time course of the potential efficacy of EPTC with respect to *Echinochloa crus galli* is simulated by use of the Weibull response function fitted to dose effect data published by Subba-Rao et al. (1987). In contrast to the effects shown previously, carryover effects are not to be expected but a fading of response following multiple applications.
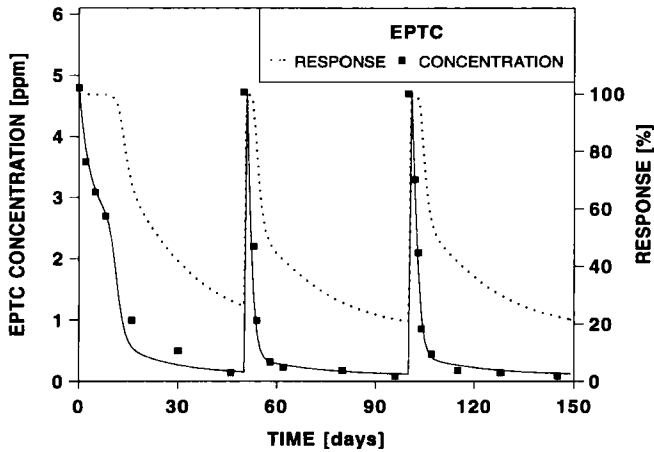


**Fig. 3.44:** Time course of EPTC and consequences for weed control under multiple applications. The fit is based on Eqs. (3.149), (3.150) and (3.151). The response is modeled by Eq. (3.146). The simulation shows that the response of EPTC on *Echinochloa crus galli* is fading under multiple applications. (Decay data from Obrigawitch et al., 1983; dose effect data for fitting the response function obtained by Subba-Rao et al., 1987).

### 3.3.4 Optimal Application Schedules

Once the link between kinetics and potential effect has been established, the potential effect can be evaluated in dependence of the mode of application and the application scheme. A convenient performance criterion is the area under the response curve.

$$W = \int_0^{t_e} R(\tau)\,d\tau \tag{3.152}$$

Let us regard as example the influence of the release kinetics of a sustained release form on the performance criterion $W$. In this example it is assumed, that both the release kinetics and the degradation follow first order reactions. Let $D$ denote the concentration of herbicide in the depot phase with initial value $D_0$ and $c$, as usual, the liquid phase concentration. The kinetic equations are then

$$\frac{dD}{dt} = -k_r D \tag{3.153}$$

$$\frac{dc}{dt} = v_r - k_e c \tag{3.154}$$

with

$$v_r = k_r D_0 e^{-k_r t}$$

The solution for the initial concentration $c(t=0) = 0$ yields

$$c(t) = \frac{D_0 k_r}{k_r - k_e} \left( e^{-k_e t} - e^{-k_r t} \right) \tag{3.155}$$

For a Weibull type response function the performance criterion is then given by

$$W(k_r, k_e) = \int_0^{t_e} \left[ 1 - e^{-\left( \frac{C(\tau)}{C_{crit}} \right)^{\gamma}} \right] d\tau \tag{3.156}$$

For a single application, the decisive parameter is the release rate constant $k_r$.

Figures 3.45 a,b show series of concentration profiles and the corresponding response profiles obtained by variation of the parameter $k_r$.
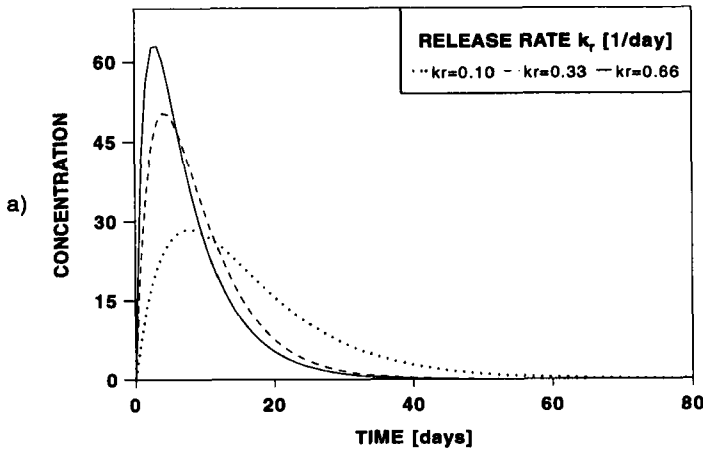


**Fig. 3.45 a:** a) Effect of release rate $k_r$ of a sustained release form on the time course of the concentration.
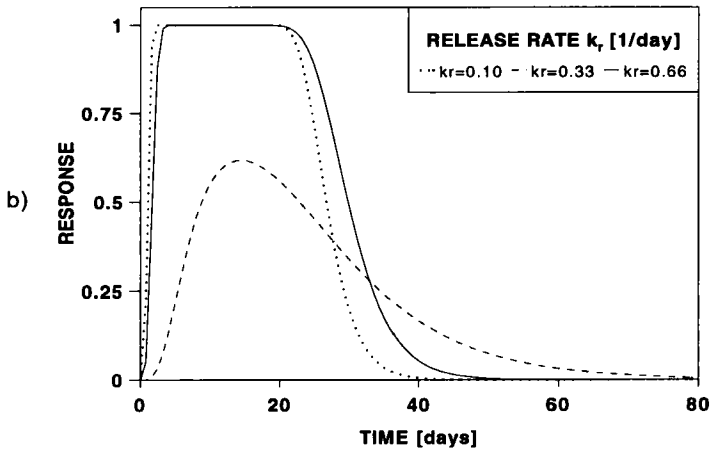
**Fig. 3.45 b:** b) Effect of release rate $k_r$ of a sustained release form on the time course of the response.

The plot of the performance criterion $W$ vs. $k_r$ (Fig. 3.46) shows that there exists an optimal value of $k_r$ for given $D_{eff}$ and $k_e$. If the release rate is too slow the concentration levels move below the response threshold $c_{crit}$. If, on the contrary, the release form is designed such that the release is fast, high concentration levels above threshold are reached, which are maintained only for a short time.
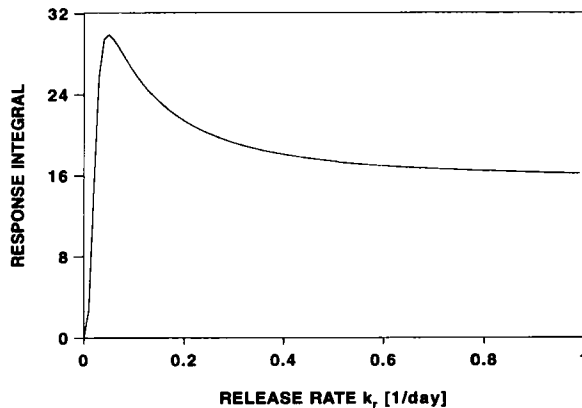


**Fig. 3.46:** Plot of the response function Eq. (3.156) as a function of the release rate $k_r$.

Of course, real situations are much more complicated involving multiple applications and population dynamics of the weed. The next example shows how the optimal timing is related to the emergence pattern of a weed.

Figure 3.47 shows cumulative emergence of wild oat in summer barley and winter wheat obtained by Rauber (1978) and the resulting fit of a emergence function (Weibull function)
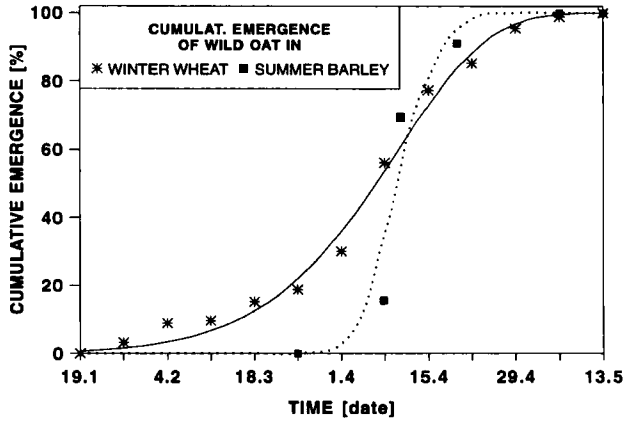
**Fig. 3.47:** Cumulative emergence of wild oat in summer barley and winter wheat (Rauber, 1978). The emergence is described well by a Weilbull function.
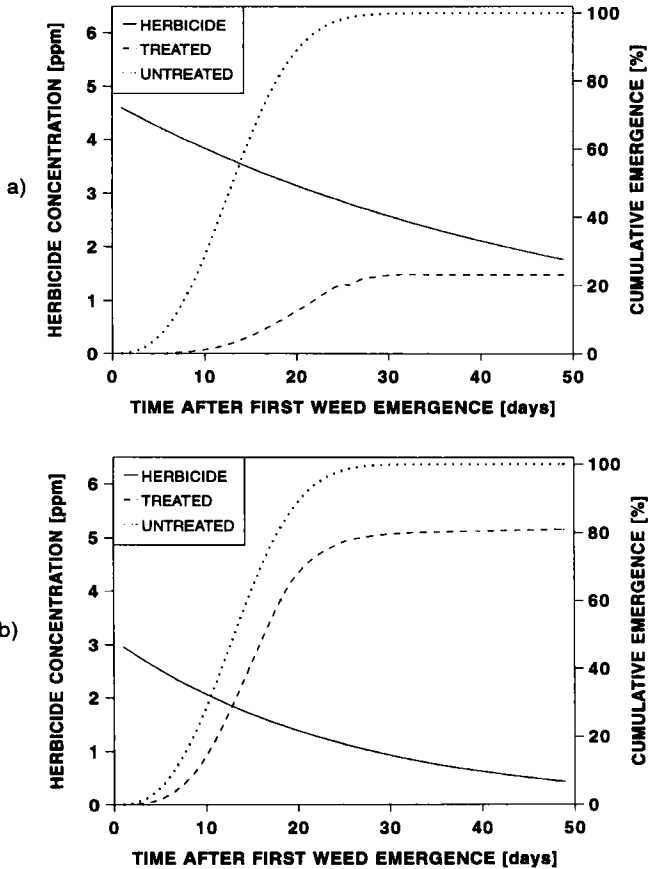


**Fig. 3.48:** Simulation of the effect of two different doses of herbicide on weed emergence. a) A significant reduction of wild oat emergence is only achieved in case of the higher dose. b) The lower dose causes just a small reduction.

Wild oat density manifests itself after three weeks in summer barley and after about ten weeks in winter wheat because of slow wheat growth. After this time wild oat is suppressed by the cereals and the emergence rate of the weed sharply decreases. The consequence for agricultural practice is to provide a sufficient effective herbicide concentration over this critical period of time. Figures 3.48 a,b show simulated time courses of degradation of a herbicide and of weed emergence and development in a treated and in an untreated field.

Figure 3.49 shows the required dose of Quinmerac for obtaining a phytotoxic effect of more than 90 % against *Daucus carota* over a period of 30 days in dependence on sorption and degradation capacity of the soil.
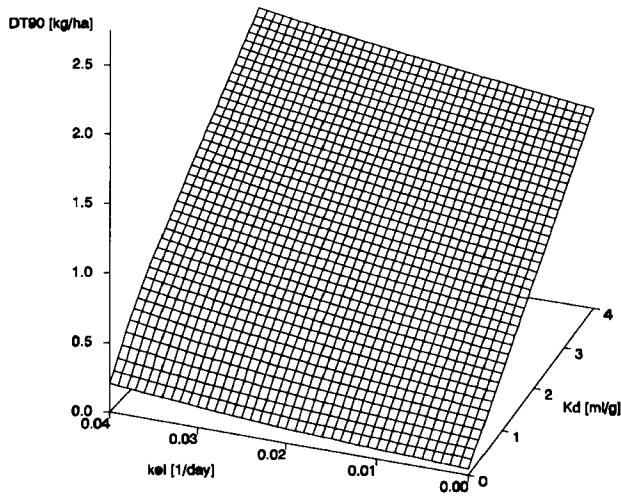


**Fig. 3.49:** Required dose of Quinmerac for maintainig a phytotoxic effect of more than 90 % on *Daucus carota* over a period of 30 days as a function of degradation rate and $K_d$-value.

## 3.4 Environmental Covariates

Notations:

$\Delta E$ : activation energy [J/mol]

$T$ : temperature [°C (O'Neill function), resp. K (Arrhenius function)]

$R$ : gas constant = 8.314 $JK^{-1}$ $mol^{-1}$

$k(T)$ : reaction rate as a function of temperature [1/T]

$k_0$ : reaction rate at reference temperature $T_0$ [1/T]

$T_{opt}$ : optimal temperature [°C]

$T_{max}$ : maximum temperature [°C]

$T_s$ : threshold temperature [°C]

$k_{max}$ : maximum reaction rate [1/T]

$Q_{10}$ : factor by which reaction velocity is increased at a temperature rise of 10 degrees [1]

$C_{org}$ : organic matter content [%]

### 3.4.1   Temperature and Humidity

#### 3.4.1.1   Chemical and Biological Temperature Response-Functions

**Arrhenius Law**

The reaction rate of a chemical reaction depends upon temperature according to the classical "law" of Arrhenius, which was first formulated in 1889:

$$k(T) = k_0 e^{-\frac{\Delta E}{RT}} \tag{3.157}$$

This equation is valid to a good approximation for elementary chemical reactions.

**O'Neill Function**

When a substance is primarily degraded by microorganisms, the pure physico-chemical form of temperature dependence is no more valid. Biological activity depends upon temperature in a specific way: below a threshold temperature $T_S$ no activity occurs. Above threshold, activity is increased with increasing temperature until a maximum rate is reached. At still higher temperatures, activity decreases again until an upper sometimes lethal temperature is reached.

Temperature influences basic life processes at the level of biochemistry in two ways: elementary reaction rates increase with temperature according to pure physico-chemical laws. Because biochemical reactions are mediated by enzymes which function only if a complex secondary structure is maintained, a rise in temperature leads to an enhanced decay rate of secondary structure: the enzymes are denatured. Both effects are superimposed. Thus, the reaction rate of a biological reaction depends on temperature in a typical way as shown in Fig. 3.50. A suitable empirical equation was derived by O'Neill (1968) and O'Neill et al. (1972), which depends on parameters, which are easily derived from empirical data:

$$k(T) = h(T - T_s) k_{max} \left[ \frac{T_{max} - T}{T_{max} - T_{opt}} \right]^x e^{\frac{x(T - T_{opt})}{T_{max} - T_{opt}}} \tag{3.158}$$

with

$$x = \frac{1}{400} W^2 \left[ 1 + \sqrt{1 + \frac{40}{W}} \right]^2 \quad and \quad W = \left( Q_{10} - 1 \right)\left( T_{max} - T_{opt} \right)$$

$h(T - T_s)$ denotes the step function, which takes the value of 1 for $T_{max} > T \geq T_s$ and is zero otherwise. The four parameters are the maximum reaction rate $k_{max}$, the optimum and lethal temperatures $T_{opt}$ and $T_{max}$ and the $Q_{10}$-value.

Figure 3.50 shows the degradation rate of 2,4-D as a function of temperature with $T_{opt}$ = 23.1°C, $T_{max}$ = 50°C and $x$ = 3.064 (data from Nash, 1989).
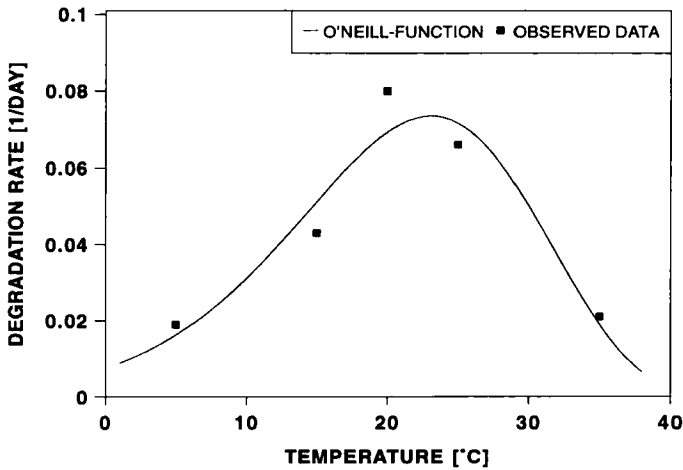


**Fig. 3.50:** Degradation rate of 2,4-D as a function of temperature with $T_{opt}$ = 23.1°C, $T_{max}$ = 50°C and $x$ = 3.064 (data from Nash, 1989). The data are modeled by the O'Neill temperature response function Eq. (3.158).

The O'Neill function is apt to describe typical temperature responses occurring in biology. It also applies well to the development rate of whole organisms.

Figures 3.51 a-d show the development rates of eggs, larvae, pupae and adults of the cabbage root fly as obtained from laboratory experiments by Müller-Pietralla (Söndgerath and Müller-Pietralla, 1996). Although the shape of the response is different for each developmental stage, each curve is matched fairly well by the O'Neill function.



a)
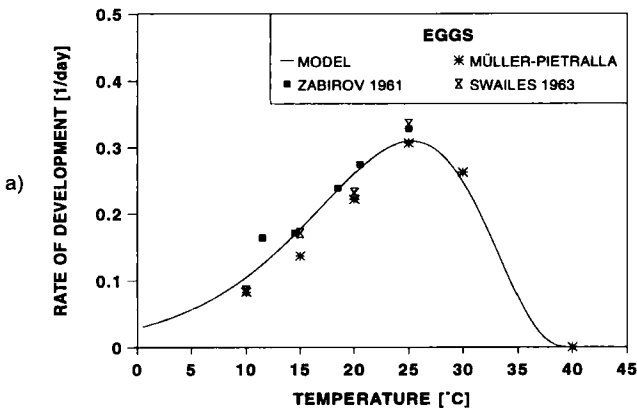
**Fig. 3.51 a:** Application of the O'Neill function to the development rate of developmental stages of the cabbage root fly (data from Söndgerath and Müller-Pietralla, 1996): a) eggs.
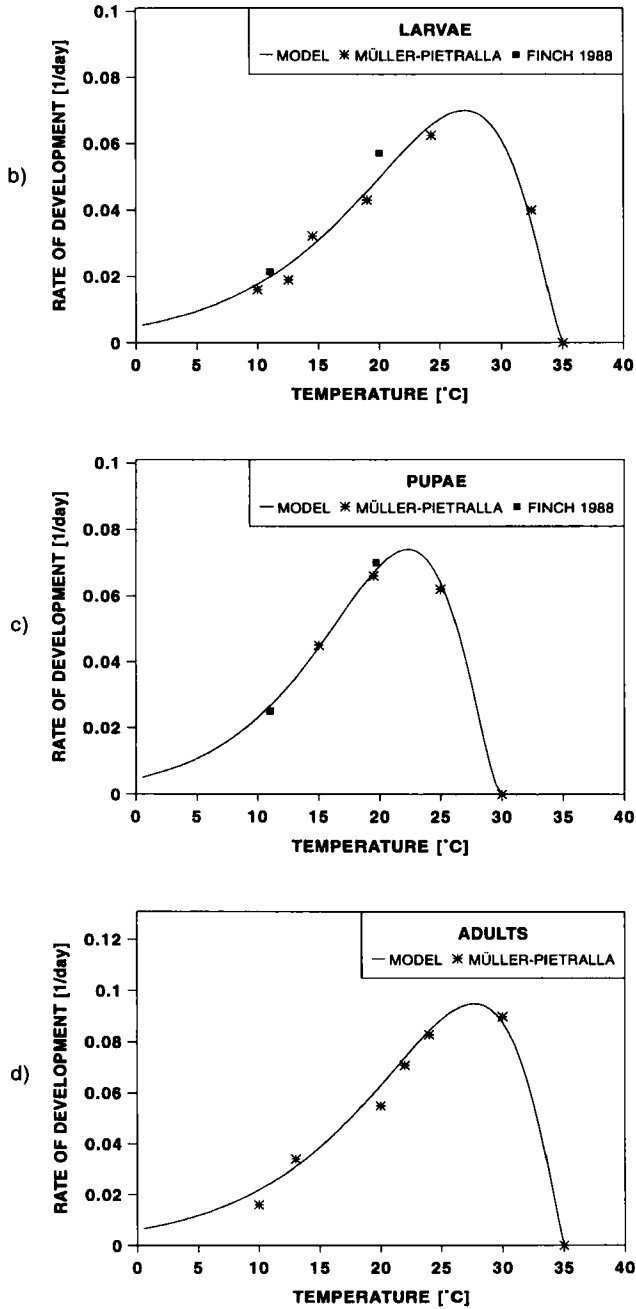
**Fig. 3.51 b-d:** Application of the O'Neill function to the development rate of developmental stages of the cabbage root fly (data from Söndgerath and Müller-Pietralla, 1996): b) larvae, c) pupae and d) adults.

## 3.4.1.2 Influence of the Time Resolution of Temperature Pattern on the Kinetics

For practical applications of pesticide degradation models it is important to know the influence of the time resolution of temperature on the long term kinetic behavior. Temperature is usually logged into degradation models as daily mean temperature or as a moving average over some time interval e.g. a week. Higher temperature resolutions are usually not considered in practice. As was demonstrated in the foregoing section, temperature response may be strongly nonlinear in certain temperature intervals. It is to be expected that the kinetic behavior is most sensitive to the temporal resolution if the temperature is strongly varying within these intervals. For a temperature and hence time dependent reaction rate the initial value problem

$$\frac{dc}{dt} = - k[T(t)]c \qquad with \quad c(t_0) = c_0 \tag{3.159}$$

has the solution

$$c(t) = c_0 e^{-\int_{t_0}^{t} k[T(\tau)]d\tau} \tag{3.160}$$

To examine the influence of temporal resolution on the kinetics, an ideal annual temperature course is assumed taking into account daily variations and a seasonal variation of temperature extremes. The following function was developed by Webb et al. (1975) for the air temperature of an Oregon forest. It serves as standard temperature variation curve in the following analysis:

$$T(t) = \mu(t) + R(t)E(t)$$

$$\mu(t) = \mu_0 + \mu_{max}\sin\left(2\pi\frac{d - 107}{365}\right)$$

$$R(t) = R_0 + R_{max}\sin\left(2\pi\frac{d - 107}{365}\right) \tag{3.161}$$

$$E(t) = \sin\left(2\pi\frac{h - 10}{24}\right)$$

Maximum temperature is reached at day 198, minimum temperature is reached at day 16. Daily minimum and maximum temperatures are assumed at 04:00 and at 16:00. Figures 3.52 a,b show the annual time course and the daily variation over an interval of 10 days.

If $k$ is a nonlinear function of $T$, the integral of $k[T(t)]$ over a 24 hour period using variable temperature differs from the value obtained by using the mean temperature. For an Arrhenius law, these differences are negligibly small as is demonstrated for a realistic parameter set in

Fig. 3.53. The differences encountered lie within the measurement errors.
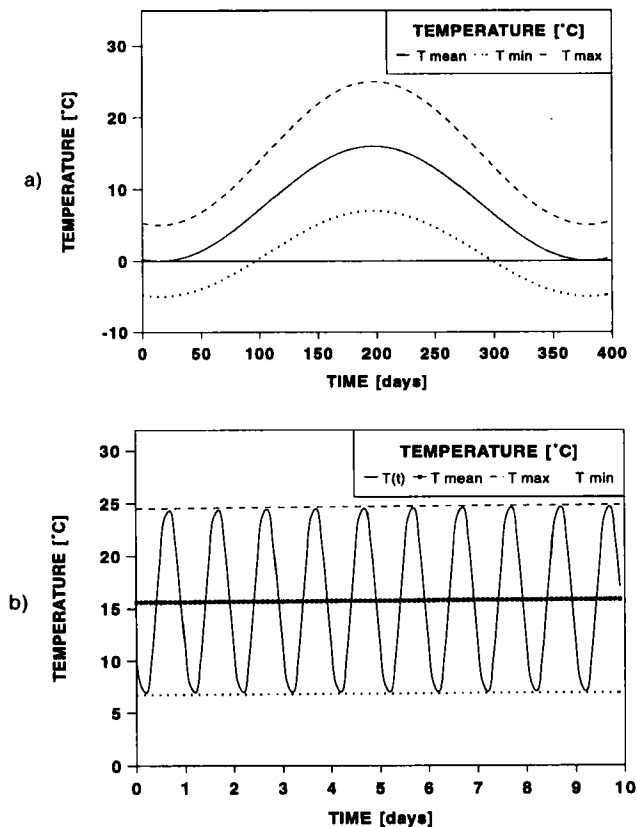


**Fig. 3.52:** Time course of temperature according to the model of Webb et al. (1975), Eq. (3.161):
a) Annual time course of temperature and b) daily temperature variation over an interval of 10 days.
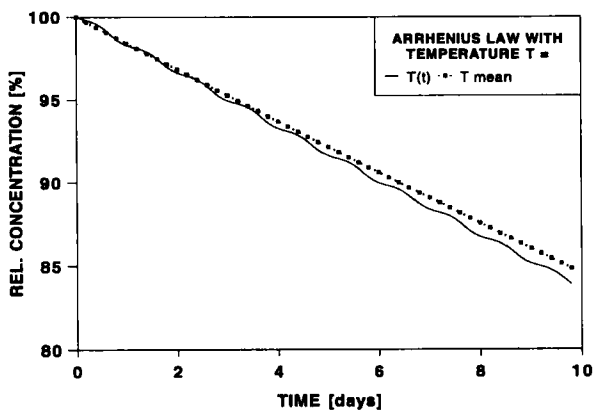


**Fig. 3.53:** Influence of the time resolution of the time course of temperature on degradation. In the case of an Arrhenius temperature dependence, the curves obtained by using the daily mean temperature $T_{mean}$ and by the daily varying temperature $T(t)$ differ only slightly.

The O'Neill function yields considerable differences, when temperatures are moving in the neighborhood of threshold or optimum temperatures. Figure 3.54 a shows degradation curves obtained with mean daily temperatures (cf. Fig. 3.54 b) and with daily varying temperatures. The differences are largest in those intervals, where mean temperatures are below threshold with daily excursions above threshold.
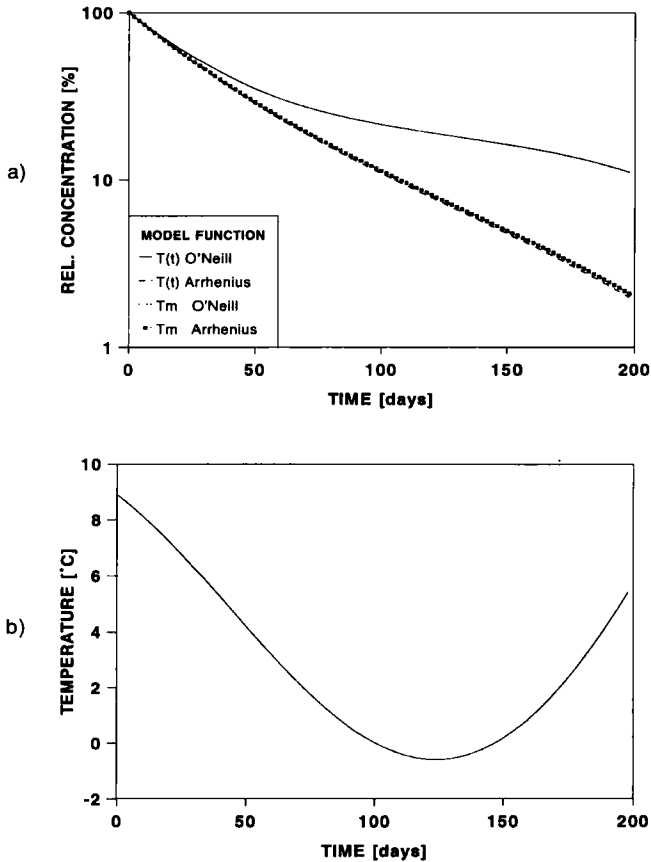


**Fig. 3.54:** a) Sensitivity of temperature response function on temperature resolution. For an O'Neill temperature response function the differences between degradation curves obtained for daily mean and for daily varying temperature are larger than is the case for an Arrhenius response function. b) Time course of temperature underlying the simulations shown in Fig. 3.54 a.

### 3.4.1.3   Influence of the Response-Function on Degradation

The form of the response curve exerts the greatest influence on the kinetics. Frequently in practice an Arrhenius response function is employed, derived from experiments in a limited temperature range, where the accordance with data is fairly well. Temperature response-functions are usually derived on the basis of degradation studies at 10, 20 and 30°C. In this range the Arrhenius and O'Neill response-functions are often quite similar in form. For temperatures outside this range the Arrhenius approach always predicts too low

concentrations. Figure 3.55 shows several fits of response-functions to degradation data of 2,4-D. If one considers only the 2,4-D degradation rates at 5, 15 and 20°C in the fitting procedure, no significant differences between the Arrhenius and O'Neill-function occurs.
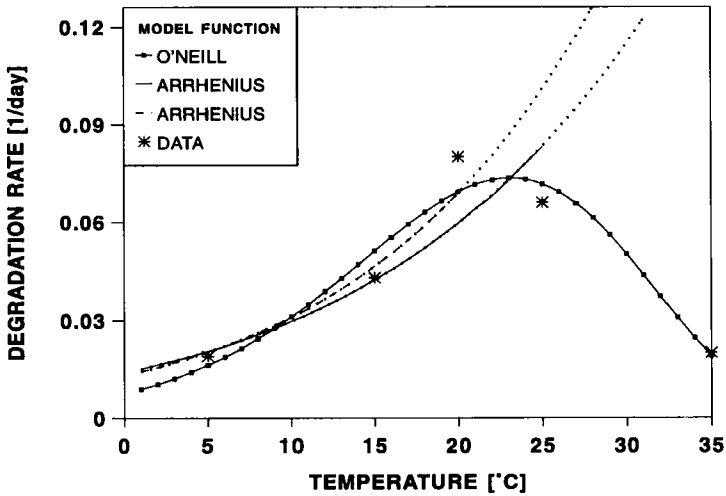


**Fig. 3.55:** Response of degradation of 2,4-D on temperature. If one only considers the temperature range from 5 to 20°C, the Arrhenius and O'Neill functions differ slightly. Differences are most pronounced at high temperatures. Dotted lines show extrapolations obtained by using the first three and the first four data points in the Arrhenius model.

Taking into account degradation data at 25 and 35°C reveals drastic differences between the two response curves and hence to drastic differences of the degradation kinetics as shown in Fig. 3.56.
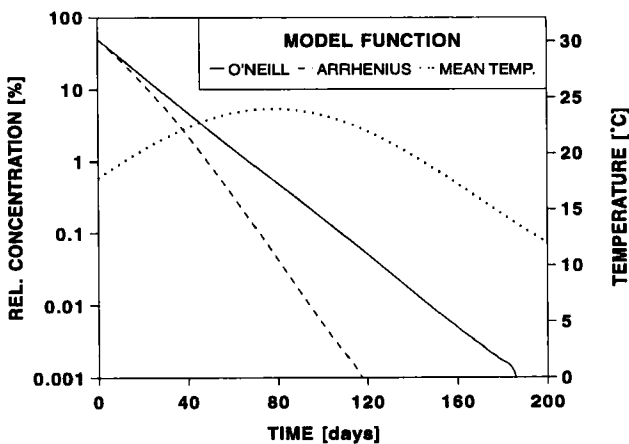


**Fig. 3.56:** The form of the temperature response curve has a large influence on the degradation rate. Simulations were performed for 2,4-D with the temperature response curves shown in Fig. 3.55. In addition to the semilogplot of concentration the underlying temperature is contained in the figure.

## 3.4.1.4 Humidity

The humidity response of the degradation rate is similar to the temperature response. The degradation rate increases with water content of the soil. This is described by the empirical formula of Walker (1984).

$$k(\theta) = A\,\theta^{\alpha} \tag{3.162}$$

For many pesticides the degradation rate decreases at water content near saturation. This is taken into account by the following response function.

$$k(\theta) = A\left[\frac{\theta}{\theta_{crit}}\right]^{b} \exp\left[1 - \left(\frac{\theta}{\theta_{crit}}\right)^{b}\right] \tag{3.163}$$

Figure 3.57 shows as example the dependence of Metribuzin and Methabenzthiazuron (MBT) on humidity and the resulting fits.
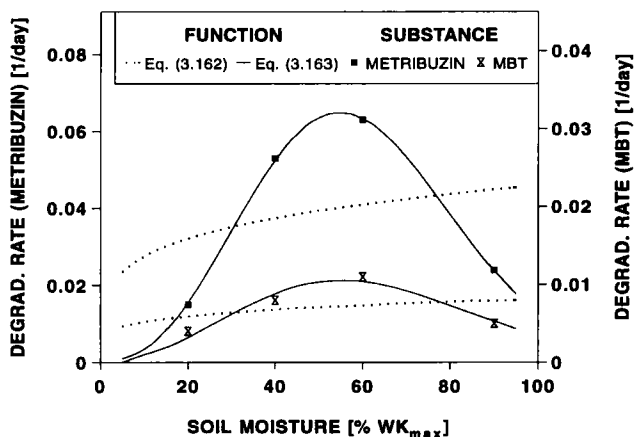


**Fig. 3.57:** Resulting fits of Eqs. (3.162) and (3.163) to observed degradation rates of Metribuzin and Methabenzthiazuron (MBT) (experimental data from Pestemer and Auspurg, 1986).

## 3.4.1.5 Combined Effect of Temperature and Humidity

Under field conditions both factors act simultaneously, i.e. the kinetic parameter $k$ is a function of $T$ and $\theta$. A reasonable approach is to formulate $k$ as the product of both response functions:

$$k(T,\theta) = k(T)\,k(\theta) \tag{3.164}$$

where the parameter $A$ of the humidity response function is set equal to 1. Equation (3.164) determines a **response surface.** The response surface for degradation rate of Chlorotoluron based on the product of Arrhenius function and the humidity function (3.162) is shown in

Figure 3.58 a. For the combination of the O'Neill function Eq. (3.158) with Eq. (3.163) the response surface is shown in Fig. 3.58 b.
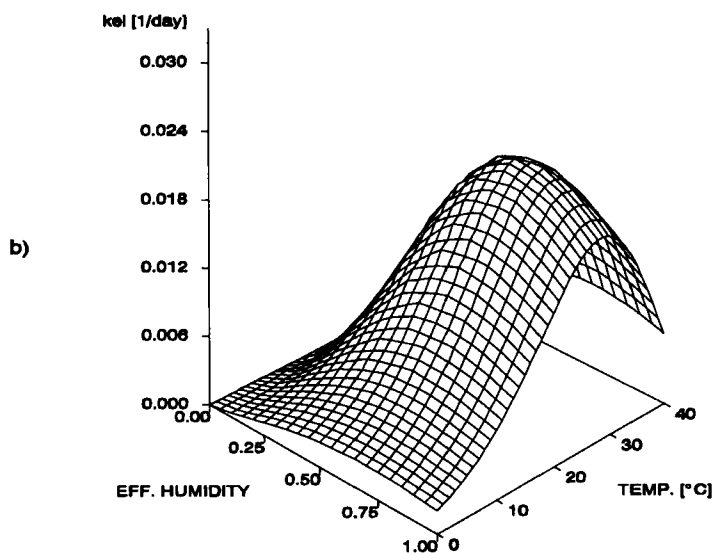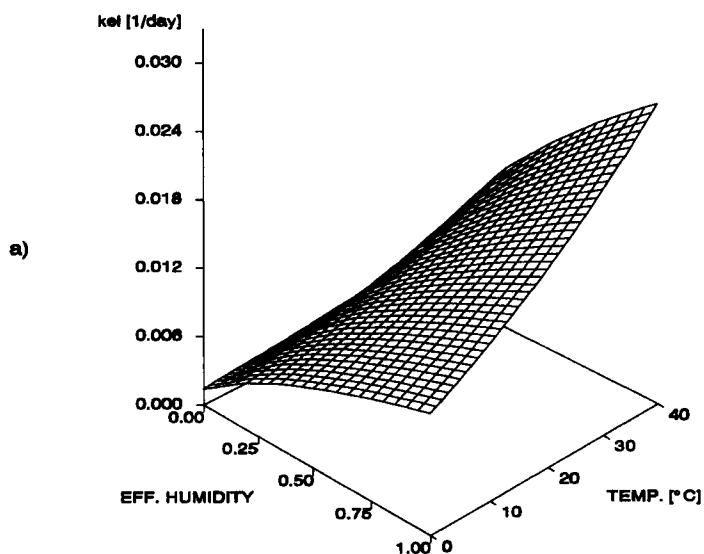


**Fig. 3.58:** Response surface of the degradation rate of Chlorotoluron with respect to temperature and humidity: a) combination of the Arrhenius function with the humidity response function Eq. (3.162) and b) combination of the O'Neill function Eq. (3.158) with the humidity response function Eq. (3.163).

Under time varying temperature and humidity conditions the degradation curve of a first order reaction is then given by

$$c(t) = c_0 e^{\displaystyle -\int_0^t k\left[T(\tau),\theta(\tau)\right]d\tau} \qquad (3.165)$$

The combination of the O'Neill response function with humidity response function Eq. (3.163) was used to simulate the degradation of Chlorotoluron. In a first step the parameters of the response surface were estimated from laboratory experiments. The model was then applied to simulate the degradation of Chlorotoluron under field conditions.

Figure 3.59 a shows the time courses of temperature and humidity. In Figure 3.59 b the resulting degradation curve is plotted together with data observed by Kibler (1979). Note that the data from which the response surface was derived and the field data were obtained from different experimental groups.
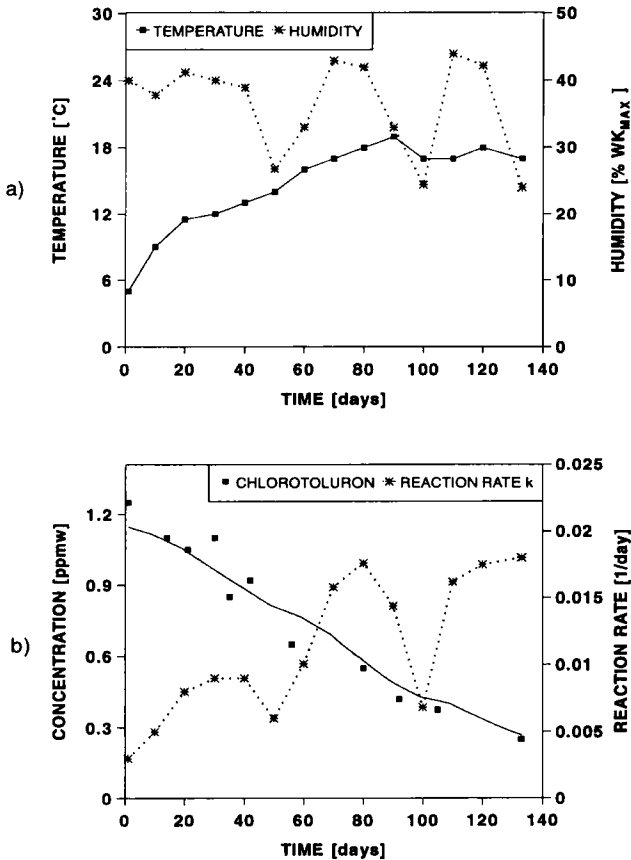


**Fig. 3.59:** a) Time courses of humidity and temperature during a Chlorotoluron degradation study performed by Kibler (1979). b) Simulated degradation curve obtained by using the combined temperature humidity response function Eq. (3.164) based on the O'Neill temperature response function and on the humidity response function $k(T, \theta)$ Eq. (3.163). The figure also shows the time course of the reaction rate.

### 3.4.2  Soil Parameters

Soil parameters such as the pH-value or the organic matter content act both on the degradation rate and the parameters pertaining to sorption and desorption. Therefore it is difficult to separate both effects for substances with a strong binding. For linear degradation kinetics and linear equilibrium sorption Eq. (3.35) is formally written as

$$\frac{dc}{dt} = -k(T,\theta,pH,C_{org})\frac{c}{1 + \frac{\rho}{\theta}K_d(T,\theta,pH,C_{org})} = -k_{eff}c \qquad (3.166)$$

The effective degradation rate $k_{eff}$ depends on all environmental covariates.

The quantification of the influence of soil properties on degradation and sorption is the necessary step for transferring the models from the laboratory scale to the field scales and higher scales (cf. chapter 7). It should be clear, that such an undertaking demands a large body of experimental data and that the mathematical relationships are solely empirical.

### 3.4.2.1  Organic Matter Content

Microbial activity is related to the organic matter content of a soil. Therefore it is to be expected that biological transformation is also positively correlated to the organic matter content. In the case of the herbicide Bentazone sorption is only weak and it is possible to measure the degradation rate as a function of the $C_{org}$-content. Figure 3.60 shows a plot of Bentazone degradation rates versus $C_{org}$-content (von Götz, 1996). The relation is slightly nonlinear and can best be described by a second order polynomial.
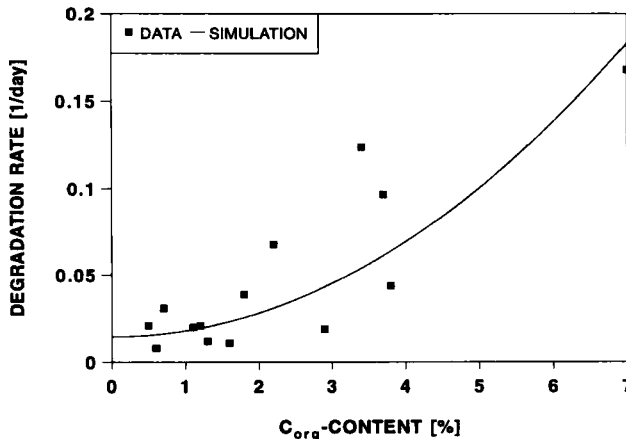


**Fig. 3.60:** Dependence of the degradation rate of Bentazone on the $C_{org}$-content. The relationship is nonlinear (data courtesy von Götz, 1996).

Humified organic soil substances are the most important adsorbents for most pesticides in soil, because of the great sorptive surface area and the great number of functional groups.

Sorption of **unpolar** pesticides is mainly due to hydrophobic interactions with organic soil substances so that sorption intensity of these pesticides is a **linear** function of the humus content of a soil. Sorption intensity of **polar** pesticides can better be described by the **nonlinear** hyperbolic equation:

$$K_d(C_{org}) = \frac{a\,C_{org}}{b + C_{org}} \qquad (3.167)$$

where $a$ and $b$ are shape parameters of the curve. Figure 3.61 shows the dependence of sorption intensity of the polar herbicide CIPC on organic matter content. Hamaker and Thompson (1972) account this nonlinear sorption behavior of polar chemicals to the **Piling-Up** effect. In soils with low organic matter content, surrounding layers of organic soil colloids are relatively thin, so that the adsorbents can reach sorption places unhindered. With increasing organic matter content, a part of sorption places cannot be reached directly, so that the sorption capacity is limited by the accessibility of protected sorption places (Müller-Wegener, 1982).
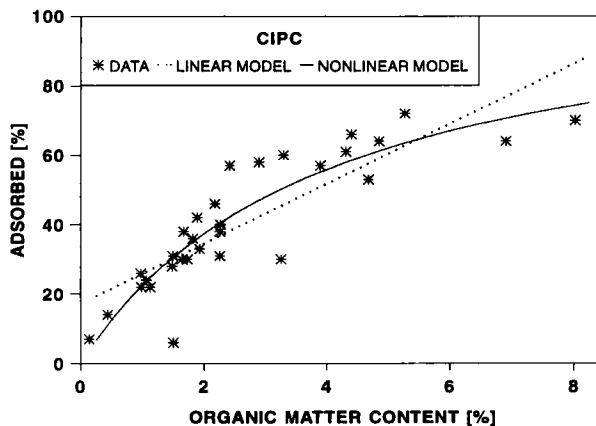


**Fig. 3.61:** Dependence of sorption intensity of the herbicide CIPC (data from Harris and Sheets, 1965) on soil content of organic matter. The fit is based on the nonlinear Eq. (3.167). For comparison the fit to a linear model is also shown.

### 3.4.2.2 pH-Value

Sorption of **polar** chemicals is influenced by the pH-value of soil, because the pH-value determines the degree of dissociation. Walker (1989) describes the dependence of the sorption coefficient of pesticides on the pH-value by the equation:

$$K_d = e^{\,a - b\,pH} \qquad (3.168)$$

where $a$ and $b$ denote shape parameters. In Eq. (3.169) the $K_d$-value is written as the sum of a pH-independent constant, $K_0$, and a pH-dependent term, which contains a threshold pH-value $pH_S$ corresponding to the $pK_A$-value (dissociation constant) of the chemical.

$$K_d = K_0 + (K_{dmax} - K_0)e^{-\left(\frac{pH}{pH_S}\right)^b} \qquad (3.169)$$

where $K_{dmax}$ denotes the maximum value of the sorption coefficient.

Figure 3.62 shows the fit of Eq. (3.169) to sorption coefficients of 2,4-D and 4-Nitrophenole measured at different pH-values of the adsorbent. At pH-values greater than 5.0, 2,4-D exists completely in anionic form and is sorbed independently of the pH-value, corresponding to the anion desorption capacity of soil.
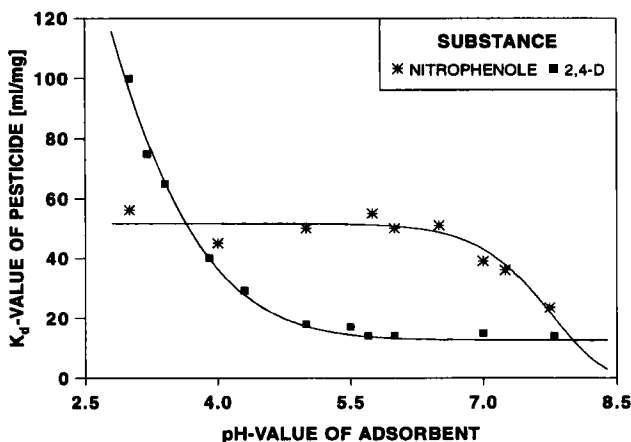


**Fig. 3.62:** Dependence of sorption intensity of 2,4-D ($pK_A$ = 2.7) and 4-Nitrophenole ($pK_A$ = 7.2) on pH-value of peat (data from Kukowsky and Brümmer, 1987). Both chemicals possess a pH-dependent and a pH-independent sorption range. Fit of Eq. (3.169) to sorption coefficients of 2,4-D and 4-Nitrophenole measured at different pH-values of the adsorbent.

Because soil colloid surfaces exhibit, in general, lower pH-values than the total solid phase (Goring and Hamaker, 1972), sorption of 2,4-D increases with decreasing pH-values lower than 5.0, although 2,4-D exists in soil solution mainly in anionic form. At pH-values greater than about 6.5, Nitrophenole exists mainly in cationic form and is sorbed in accordance to cation adsorption capacity of soil.

### 3.4.2.3  Combined Effect of Organic Matter Content and pH-Value

Under field conditions both factors, the organic matter content and pH-value, influence simultaneously the sorption coefficient. The most simple approach is a multiple linear regression model of the form

$$K_d(C_{org}, pH) = a_0 + a_1 C_{org} + a_2 pH + a_3 pH C_{org} \qquad (3.170)$$

A further possibility is to formulate $K_d$ as the product of the response functions for $C_{org}$-content (Eq. (3.167)) and pH-value (Eq. (3.169)):

$$K_d(C_{org}, pH) = \frac{a_1 C_{org}}{a_2 + C_{org}} \left[ a_3 + e^{-\left(\frac{pH}{pH_s}\right)^{a_4}} \right] \tag{3.171}$$

Figure 3.63 shows this response surface for the $K_d$-value of Quinmerac.
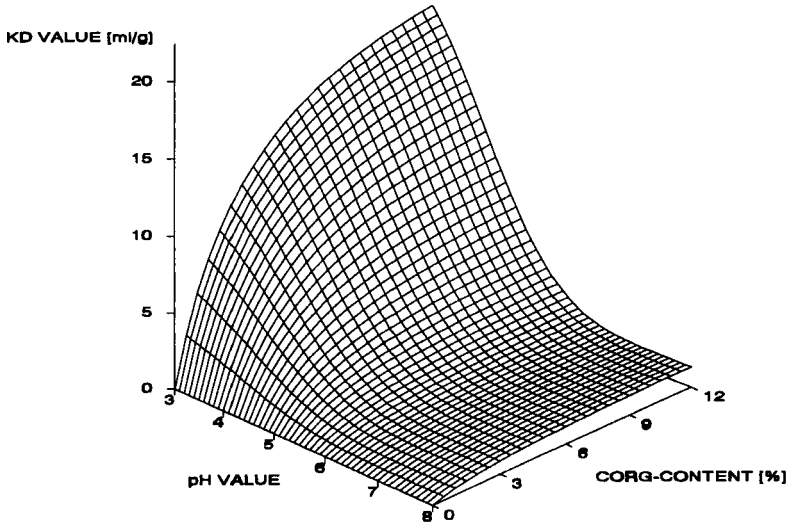


**Fig. 3.63:** Dependence of sorption intensity of the herbicide Quinmerac on soil content of organic matter and pH-value. The fit is based on Eq. (3.171).

This function is applied to data obtained for the distribution coefficient of 2,4,5-T, determined in batch studies with 0.01 molar $CaCl_2$-solution and a soil/solution relationship of 5/1.

Figure 3.64 shows the resulting fit of Eqs. (3.170) and (3.171). For alkaline soils with low $C_{org}$-values negative $K_d$-values are obtained by use of the linear regression model.

Figure 3.65 shows the application of both models to a profile in a loamy soil obtained by Hamaker and Thompson (1972). The multiple linear regression model Eq. (3.170) leads to unrealistic predictions. In the topsoil sorption intensity of 2,4,5-T is drastically overestimated, whereas negative sorption coefficients are predicted in soil depths greater than 180 cm.

**Concluding Remarks**

The examples clearly demonstrate the superiority of biological response functions over pure physico-chemical response functions for the prediction of persistence of pesticides in soil. The use of appropriate response functions improves the quality of simulation models without great mathematical efforts.
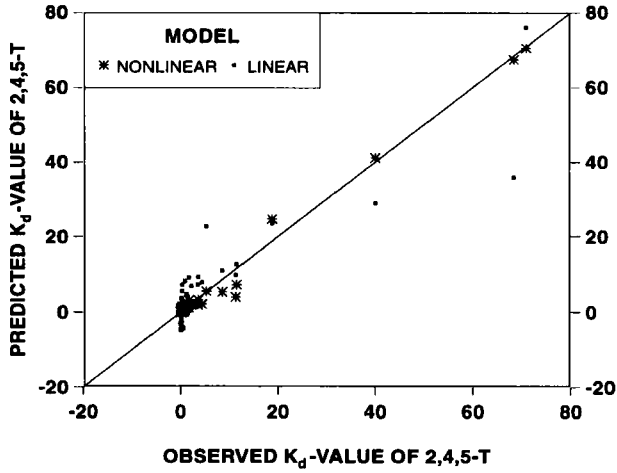
**Fig. 3.64:** Observed and predicted sorption coefficients of 2,4,5-T in soils with different content of organic matter and different pH-values. Application of the linear function Eq. (3.170) leads to negative values for soils with low content of organic matter and high pH-values. Only the nonlinear model Eq. (3.171) yields reasonable $K_d$-values for the whole range of $C_{org}$-contents and pH-values.
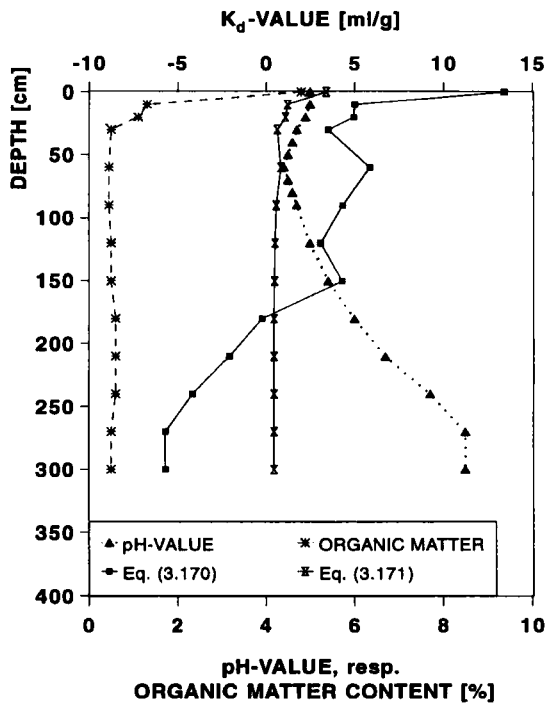


**Fig. 3.65:** Application of both models to a profile in a loamy soil obtained by Hamaker and Thompson (1972).

# 4 Parameter Estimation in Kinetic Models

This is an important chapter for practical model applications. It outlines methods of parameter estimation for models in any form. The case, where the models are only implicitly defined as the solution of nonlinear ordinary differential equations, is devoted special attention. As was pointed out in the previous chapter, most models in explicit form are based on simple linear kinetics both as concerns the mode of degradation, sorption and desorption. In the past, most statistical tools were not apt to solve problems involving regression functions defined by differential equations. This has lead to the situation that, in practice, very simple models are applied in order to obtain a proper statistical treatment. Most models in form of nonlinear differential equations are therefore classified as "simulation models" or "scientific models" in contrast to "management models". This distinction is, to the authors' opinion, simply wrong. If nonlinear kinetic effects are characteristic for a substance, oversimplified models lead to false predictions. **Therefore it is necessary to provide a link between models and data by the application of advanced statistical and numerical methods to regression problems involving systems of differential equations.** The basics of nonlinear regression are summarized in the following section. It is assumed that the reader is familiar with linear regression.

## 4.1 Problem Statement

### 4.1.1 The Estimation Problem

Given are:

i)    A dynamical (kinetic) model in form of ordinary differential equations with parameter vector $\Phi = (\phi_1, \dots, \phi_p)$,
ii)    time courses of measured state variables $y_{ij}$, e.g. concentrations or microbial biomass,
iii)    a performance criterion such as the residual sum of squares and
iv)    an error structure.

The mathematical problem then is to find a parameter vector $\Phi$ which minimizes the performance criterion chosen. Let $y(t,\Phi)$ denote the solution of the initial value problem

$$\frac{dy_i}{dt} = f_i(y_1,\dots,y_n;\theta_1,\dots,\theta_p) \qquad i = 1,\dots,n$$

$$y_i(t=0) = y_{i0}$$

(4.1)

The least squares criterion is

$$L(\Phi) = \sum_{i=1}^{n} \sum_{j=1}^{l} \left[ y_i(t_j,\Phi) - y_{ij} \right]^2$$

(4.2)

and the least squares estimator is defined by

$$L(\hat{\Phi}) = \min[L(\Phi)] \qquad \Phi \in U \tag{4.3}$$

where $U$ denotes the space of admissible parameters. If the initial value problem possesses an analytical solution, i.e. a solution in form of known functions, the regression problem is called explicit. If solutions can only be attained approximately by numerical methods, the regression problem is called implicit.

## 4.1.2  Performance Criteria of the Estimates and Experimental Design

The estimates thus obtained are subject to error. The error structure of the data, the experimental design and the model structure influence the statistical properties of the estimates. In a statistical sense, the estimates are random variables possessing a distribution function and a covariance matrix.

Important information on the statistical properties is contained in the covariance matrix, which is computed along with the estimates:

$$COV(\hat{\Phi}) = \begin{pmatrix} s_{11} & s_{12} & s_{13} & \cdots & s_{1p} \\ s_{21} & s_{22} & s_{23} & \cdots & s_{2p} \\ & & \cdots\cdots\cdots \\ s_{p1} & s_{p2} & s_{p3} & \cdots & s_{pp} \end{pmatrix} \tag{4.4}$$

The elements on the main diagonal are the variances of single estimates, e.g. $s_{11}$ is the variance of $\Phi_1$. They can be used for the construction of confidence intervals.

The covariance matrix is related to the correlation matrix of the estimates by

$$r_{ij} = \frac{s_{ij}}{\sqrt{s_{ii}s_{jj}}} \qquad -1 \leq r_{ij} \leq 1 \tag{4.5}$$

The elements of the covariance matrix are an important criterion for the "well posedness" of the estimation problem. In the limit of $|r_{ij}| = 1$ the parameters $\Phi_i$ and $\Phi_j$ cannot be estimated independently. The model is overparameterized with respect to the given experimental design. The following example clarifies this.

**Example 4.1: Degradation of Quinmerac**

Consider the simultaneous biodegradation and abiotic decay of a substance. The model parameters are the decay constants $\lambda_a$ and $\lambda_b$. Let $x$ denote the concentration of the substance and $y$ the concentration of the metabolite of the biological degradation. For first order reactions, the kinetic model is easily derived (cf. section 3.1):

$$x(t) = x_0 e^{-(\lambda_a + \lambda_b)t} \qquad (4.6a)$$

$$y(t) = \frac{x_0 \lambda_b}{\lambda_a + \lambda_b} \left[ 1 - e^{-(\lambda_a + \lambda_b)t} \right] \qquad (4.6b)$$

If only data of the time course of the parent substance are available, both parameters are perfectly correlated, and the model is overparameterized. Both parameters can be distinguished only, if additional data on the metabolite are available.

It is interesting, that in this case only one data point of the metabolite is sufficient to remove the degeneracy. Fig. 4.1 shows the correlation coefficient dependent upon the time point of the additional measurement. Table 4.1 contains further statistics. This example is resumed again in the next section.

**Tab. 4.1:** Parameter estimates, their standard deviations (in brackets) and correlation coefficients between the estimates for the model equations (Eqs. (4.6a,b)) in dependence of the allocation of a single data point of the second component. Note that the coefficient of determination $R^2$, which is a measure for the goodness of the fit, is nearly independent of the experimental design. The correlation coefficient r, which measures the dependence between the parameters, decreases with increasing measuring time.

| Days after Application | $\lambda_a$ | $\lambda_b$ | r | $R^2$ |
|:---:|:---:|:---:|:---:|:---:|
| 0 | 0.0048 (0.0009) | 0.0040 (0.0009) | -0.95 | 0.996 |
| 31 | 0.0046 (0.0005) | 0.0043 (0.0005) | -0.85 | 0.996 |
| 60 | 0.0053 (0.0004) | 0.0036 (0.0037) | -0.78 | 0.996 |
| 90 | 0.0050 (0.0004) | 0.0040 (0.0003) | -0.60 | 0.995 |
| 120 | 0.0047 (0.0003) | 0.0042 (0.0003) | -0.51 | 0.995 |
| 210 | 0.0053 (0.0003) | 0.0036 (0.0002) | -0.48 | 0.995 |
| 270 | 0.0049 (0.0003) | 0.0040 (0.0002) | -0.42 | 0.995 |
| 365 | 0.0051 (0.0003) | 0.0038 (0.0002) | -0.38 | 0.998 |
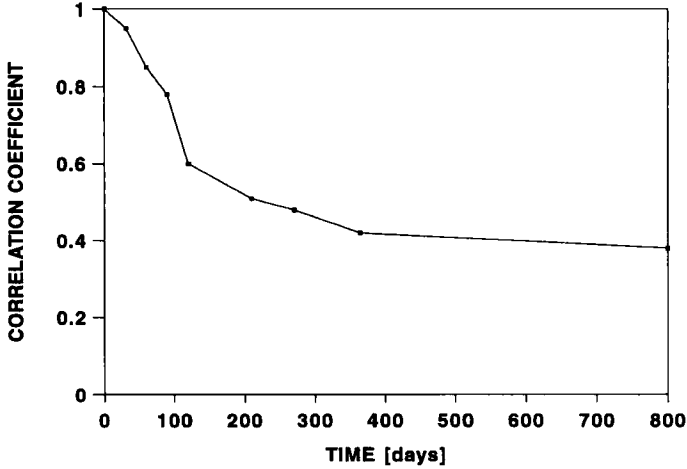
**Fig. 4.1:** Influence of the experimental design on the correlation coefficient between parameter estimates of parameters $\lambda_a$ and $\lambda_b$ of Eq. (4.6a). The plot shows the effect of the allocation of a single measurement of the metabolite.


### 4.1.3   Multi-Experiment Problems

The kinetic properties of a substance can only be assessed on the basis of decay data obtained for a wide range of initial concentrations and experimental conditions such as temperature and humidity. As was pointed out in chapter 3, deviations from linear kinetics are difficult to detect from a single experiment alone. Consider the case of a Michaelis-Menten decay mode. The estimation of the parameters $V_{max}$ and $K_M$ necessitates the analysis of a series of experiments run under different initial concentrations. This means that the parameters have to be estimated from a least squares criterion built up of all experiments.

Let $e_k$ denote the experimental condition pertaining to experiment $k$ and $y_{ijk}$ the measurement taken on component $i$ at time $t_j$ under experimental condition $e_k$. The least squares criterion is then given by

$$L(\Phi) = \sum_{i=1}^{n} \sum_{j=1}^{l} \sum_{k=1}^{m} \left[ y_i(t_j, e_k, \Phi) - y_{ijk} \right]^2 \qquad (4.7)$$

Worked examples are given in the next sections of this chapter.


## 4.2   Models in Explicit Form

If the underlying dynamic model is linear, analytical solutions are obtained (cf. section 3.1) as sums of exponential functions. In this section three case studies are presented, which are chosen to represent typical problems frequently occurring in practice.

### 4.2.1   A Multicompartment System

Consider again biodegradation of a substance, which decays into two identified metabolites, $CO_2$ and the rest. Under the assumptions that the decay of the metabolites is slow compared to the decay of the mother substance and that the decay reaction is of first order, the kinetic model is given by

$$\frac{dx}{dt} = -(\lambda_1 + \lambda_2 + \lambda_3 + \lambda_4)x \tag{4.8a}$$

$$\frac{dy_i}{dt} = \lambda_i x \qquad i = 1,...,4 \tag{4.8b}$$

The following notations hold:

$x$     : concentration of parent substance $[M/L^3]$
$y_i$    : concentration of 1st and 2nd metabolite, $CO_2$ and a rest $[M/L^3]$
$\lambda_i$    : kinetic constants $[1/T]$

With the initial values $x(t=0) = x_0$ and $y_i(t=0) = 0$ for $i = 1, ... , 4$ the differential equations have the solution

$$x(t) = x_0 e^{-\lambda t} \tag{4.9a}$$

$$y_i(t) = \frac{x_0 \lambda_i}{\lambda}\left[1 - e^{-\lambda t}\right] \qquad \textit{with } \lambda = \sum_{i=1}^{4} \lambda_i \tag{4.9b}$$

The least squares criterion is made up of the sum of squares of each component:

$$L(\lambda_1,\lambda_2,\lambda_3,\lambda_4) = \sum_{j=1}^{n} \left[x_0 e^{-\lambda t_j} - x_j\right]^2 + \sum_{i=1}^{4} \sum_{j=1}^{n} \left[\frac{\lambda_i}{\lambda}(1 - e^{-\lambda t_j}) - y_{ij}\right]^2 \tag{4.10}$$

There are many codes available for nonlinear parameter estimation. Meanwhile classical statistical program packages like SAS or BMDP offer the opportunity to solve nonlinear regression problems with user defined functions. For this example we employed BMDP as a representative out of this class. The handling of BMDP will be explained in some detail in example 4.6.

Table 4.2 summarizes a part of the output of a BMDP run. Convergence is achieved after 14 iterations. Analysis of the correlation matrix shows that no close correlations occur.

Figure 4.2 shows a plot of the estimated time courses of concentrations together with the data. Figure 4.3 shows in addition the 99% confidence bands for the parent substance and the

first metabolite. Notice that the last two values of the parent substance (low concentrations) lie outside the confidence band. This may be a hint, that systematic deviations occur at low concentrations probably due to sorption, which is not included in this model.

**Tab. 4.2:** Part of BMDP output (handling of BMDP see section 4.3.1, example 4.6):

a) Sequence of parameter estimates and residual sum of squares (RSQ) encountered during the iteration.

| Iteration No. | RSQ | $\lambda_1$ | $\lambda_2$ | $\lambda_3$ | $\lambda_4$ |
|---|---|---|---|---|---|
| 0 | 9894.57208 | 0.00500 | 0.01430 | 0.00100 | 0.00200 |
| 1 | 1321.26321 | 0.00105 | 0.00543 | 0.00154 | 0.00070 |
| 2 | 342.66981 | 0.00252 | 0.00477 | 0.00185 | 0.00064 |
| . | . | . | . | . | . |
| . | . | . | . | . | . |
| . | . | . | . | . | . |
| 12 | 103.28692 | 0.002361 | 0.00391 | 0.00207 | 0.0003 |
| 13 | 103.24831 | 0.002361 | 0.00391 | 0.00207 | 0.00053 |
| 14 | 103.24831 | 0.002355 | 0.00391 | 0.00207 | 0.00053 |

b) Final parameter estimates

| Parameter | Estimate | Standard Deviation | Coefficient of Variation |
|---|---|---|---|
| $\lambda_1$ | 0.0024 | 0.00020 | 0.0839 |
| $\lambda_2$ | 0.0039 | 0.00011 | 0.0287 |
| $\lambda_3$ | 0.0021 | 0.00010 | 0.0478 |
| $\lambda_4$ | 0.0005 | 0.00009 | 0.1755 |

c) Correlation matrix of parameter estimates. The absolute values of the correlation coefficients are far less than 1 indicating that all parameters of the model are estimable.

| | $\lambda_1$ | $\lambda_2$ | $\lambda_3$ | $\lambda_4$ |
|---|---|---|---|---|
| $\lambda_1$ | 1.000 | | | |
| $\lambda_2$ | -0.047 | 1.000 | | |
| $\lambda_3$ | -0.244 | 0.191 | 1.000 | |
| $\lambda_4$ | -0.407 | 0.053 | 0.030 | 1.000 |

The over all $R^2$ is 0.994.
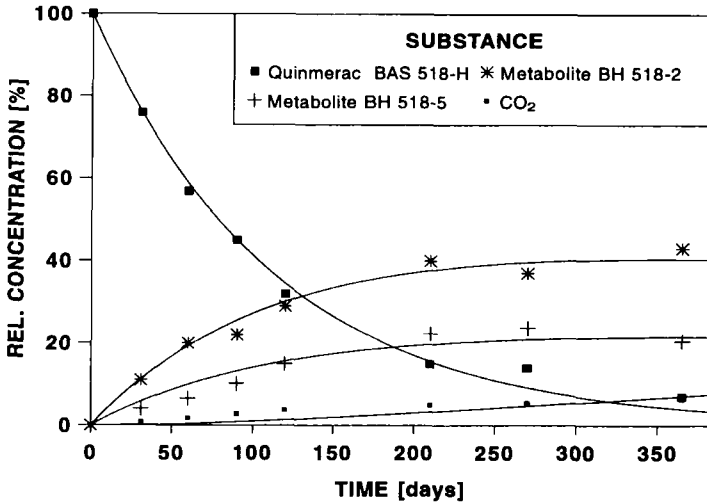
**Fig. 4.2:** Time courses of Quinmerac and its main metabolites in a sandy loam at initial concentration of 10 ppmw Quinmerac. Solid lines represent the fit of the model equations (Eqs. (4.9a,b)) to observed data (BASF, unpublished).
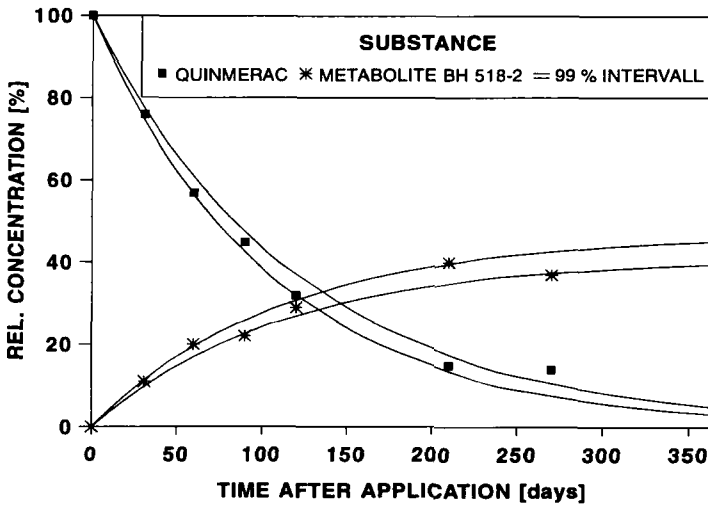


**Fig. 4.3:** 99% confidence intervals of predicted time courses of Quinmerac and its metabolite BH 518-2.

Statistical criteria like confidence limits, mean square errors and correlation coefficients alone do not suffice to judge the goodness of a fit. In addition to statistical measures the fit has always to be judged by eye. This is supported by the analysis of the residuals. Figure 4.4 a shows the time course of the residuals, which do not exhibit a systematic trend. Furthermore, the statistical distribution of all residuals is analyzed by a normal probability plot as given in Fig. 4.4 b. The plot reveals only minor deviations from a normal distribution.
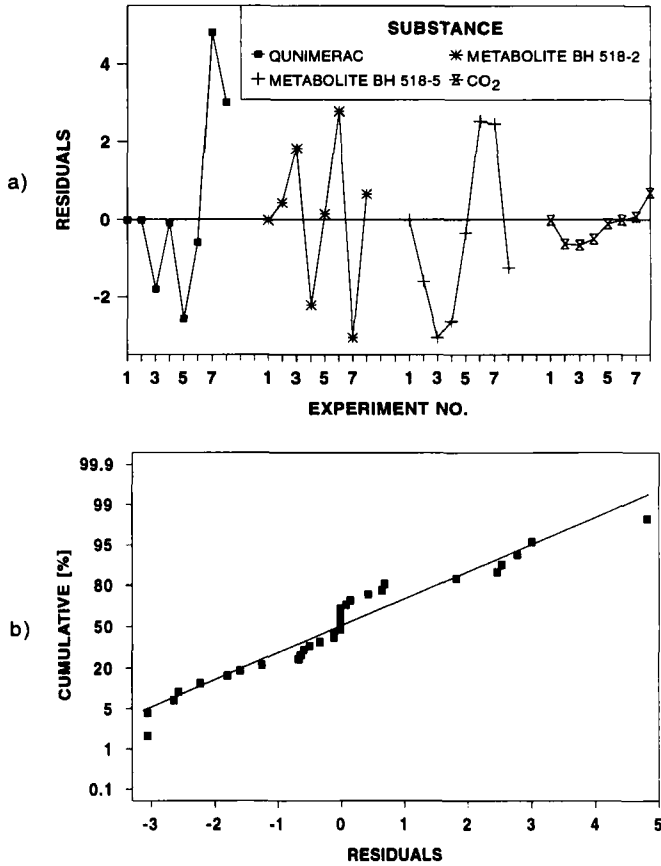
**Fig. 4.4:** Analysis of residuals of the Quinmerac example: a) time course of the residuals and b) analysis of the statistical distribution of the residuals by a normal probability plot.

## 4.2.2   Strong Sorption and Degradation

The binding of organic chemicals to soil was treated in the foregoing chapter in some detail. Apart from fast reversible sorption-desorption processes chemicals may be bound strongly to the soil matrix. The strong binding is a slow process compared to sorption and desorption. The following simple model is valid for the situation that only one binding site exists and that the binding is irreversible. For linear kinetics the model equations are

$$\frac{d\theta c}{dt} = -\theta\left(k_l + k_b\right)c \tag{4.11a}$$

$$\frac{d\rho S}{dt} = \theta k_b c \tag{4.11b}$$

From the solution of these equations with the initial values $c(t=0) = c_0$ and $S(t=0) = 0$ the total concentration $c_{tot}$ is obtained as (cf. chapter 3)

$$c_{tot}(t) = \theta c + \rho S = \theta c_0 e^{-(k_l + k_b)t} + \frac{\theta k_b c_0}{k_l + k_b}\left[1 - e^{-(k_l + k_b)t}\right]$$

$$= \frac{\theta c_0}{k_l + k_b}\left[k_b + k_l e^{-(k_l + k_b)t}\right]$$

(4.12)

## Example 4.3: Binding and Degradation of Atrazine

The kinetics of Alachlor, Atrazine and Metolachlor can be described well by this model (Richter et al., 1992a). As an example, kinetic data of Atrazine are analyzed here. Experiments were performed with initial concentrations differing by a factor of ten (2 and 20 µg/ml). There are only four measurements in each series. The data base is rather poor and it is questionable, whether a sound statistical analysis is still possible. In a first step, each data set is analyzed separately. Comparisons of the estimates (cf. Tab. 4.3) and of the resulting trajectories (cf. Figs. 4.5 a,b) do not reveal significant differences. Therefore, it may be assumed that the model is valid for both concentration ranges. To improve the estimates by increasing the degrees of freedom, parameters are estimated from both experiments simultaneously.

**Tab. 4.3:** Comparison of results achieved by analysis of single experiments and by simultaneous analysis of both experiments (standard deviations in brackets). The underlying model is given by Eq. (4.12).

| | Singular Fit | | Simultaneous Fit |
|---|---|---|---|
| Parameter | Initial Concentration 2 µ/g | Initial Concentration 20 µg/g | |
| $k_l$ | 0.030 (0.005) | 0.036 (0.0006) | 0.037 (0.0008) |
| $k_b$ | 0.008 (0.005) | 0.021 (0.0008) | 0.021 (0.0010) |
| r | 0.857 | 0.879 | 0.873 |

Thus it is possible to get reasonable parameter estimates and good fits even if only few data are available by combining data from several experiments. (Assuming the model is correct and measurement errors are small.)
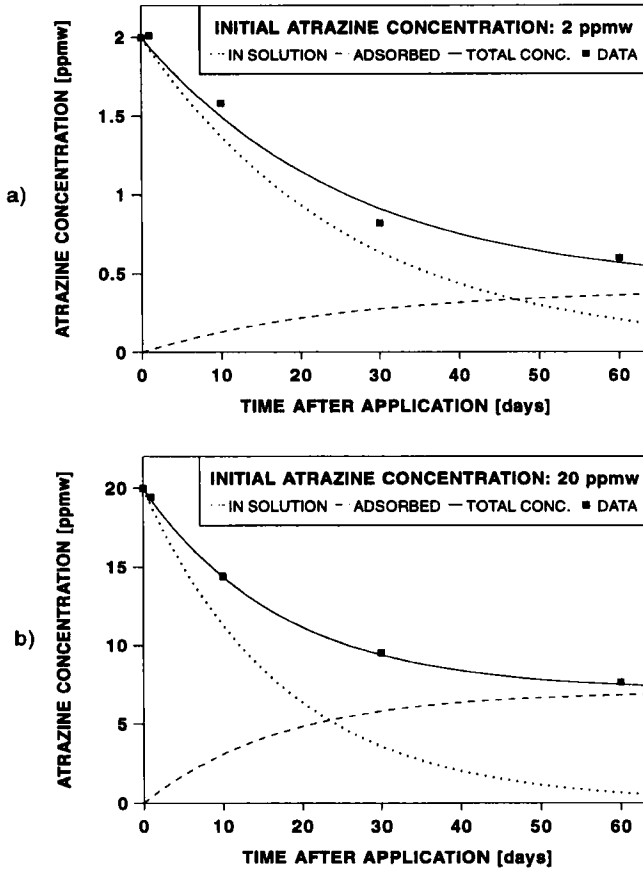
**Fig. 4.5:** Degradation of Atrazine in a Vertic Eutrochrept soil and simulated time courses of Atrazine concentration in soil solution and soil matrix. The data (Richter et al., 1992a) are fitted to the model for the total concentration (Eq. (4.12)): a) initial concentration 2 ppmw Atrazine and b) initial concentration 20 ppmw Atrazine.

## Temperature and Humidity Dependence of Kinetic Parameters

In section 3.4 the temperature and humidity dependence of degradation kinetics was considered in detail. This section is concerned with the technical problem of parameter estimation. The analysis of temperature and humidity dependence of a reaction necessitates the performance of series of experimental runs under different temperatures and humidities. There are in principal two methods for parameter estimation.

i) Two stage procedure

In the first stage, the rate of decay is estimated from each experiment separately. In the next step, these values are used as independent variables of a nonlinear regression problem for the temperature (humidity) model.

ii) Simultaneous estimation

The data of all experimental runs are used to estimate the parameters of the temperature (humidity) model. The setup of the residual sum of squares is given by Eq. (4.7). For the case of an Arrhenius law this equation is specified by

$$L\left(k_0, E_A\right) = \sum_{i=1}^{n} \sum_{j=1}^{l} \left[ y_{0j} \exp\left( -k_0 t_i e^{-\frac{E_A}{RT_j}} \right) - y_{ij} \right]^2 \tag{4.13}$$

Here, the index $i$ refers to data within one experimental run and the index $j$ refers to the experimental run. The parameters to be estimated are the activation energy $E_A$ and the reference reaction rate $k_0$. $y_{0j}$ denotes the initial concentration of the $j^{th}$ experimental run.

**Example 4.4: Temperature Dependence of Isoproturon Degradation**

The degradation of Isoproturon (cf. Pestemer, 1992) was measured under three constant temperatures. The fit to an Arrhenius law (cf. Fig. 4.6) reveals systematic deviations between data and predicted values. At low temperature, the estimated reaction rate is too fast and most data points lie above the predicted curve. This corroborates the assumption that the Arrhenius law is not appropriate for degradation reactions mediated by microorganisms. Although the fit shows that the applied model is not correct, the correlation coefficient (coefficient of determination) for this fit amounts to $R^2 = 0.96$. This underlines the warning that one statistical criterion alone is not sufficient to judge the goodness of a model.

If a biological temperature response function is used the problem arises that the number of different temperatures in the experiment is too small to allow the estimation of all parameters of the response curve. The model is overparameterized with respect to the experimental design. This is a situation frequently met in practice. Consider for instance the O'Neill temperature response function (cf. section 3.4.1.1).

$$k(T) = k_{max} \left[ \frac{T_{max} - T}{T_{max} - T_{opt}} \right]^a e^{\frac{a(T - T_{opt})}{T_{max} - T_{opt}}} \tag{4.14}$$

This function contains the four parameters $k_{max}$, $a$, $T_{max}$ and $T_{opt}$. The last two parameters have a simple biological meaning and it is easy to choose reasonable optimum and maximum temperatures. In this example $T_{max}$ was set to 50°C and $T_{opt}$ to 35°C. The remaining free parameters $k_{max}$ and $a$ were estimated.

Figure 4.7 shows the resulting fit. Comparison with Fig. 4.6 clearly demonstrates the superiority of the biological temperature function over the Arrhenius function.
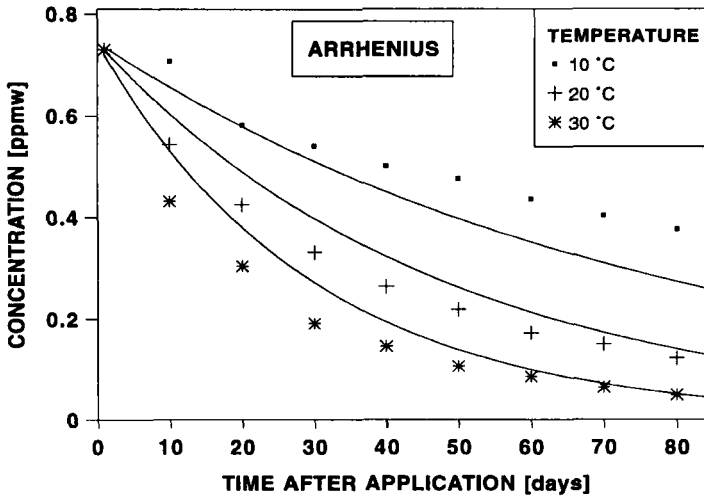
**Fig. 4.6:** Degradation of Isoproturon at three different temperatures. The fit is obtained by use of the Arrhenius temperature law. Reaction rates are overestimated at low temperatures and underestimated at high temperatures (data courtesy of Pestemer, 1992).
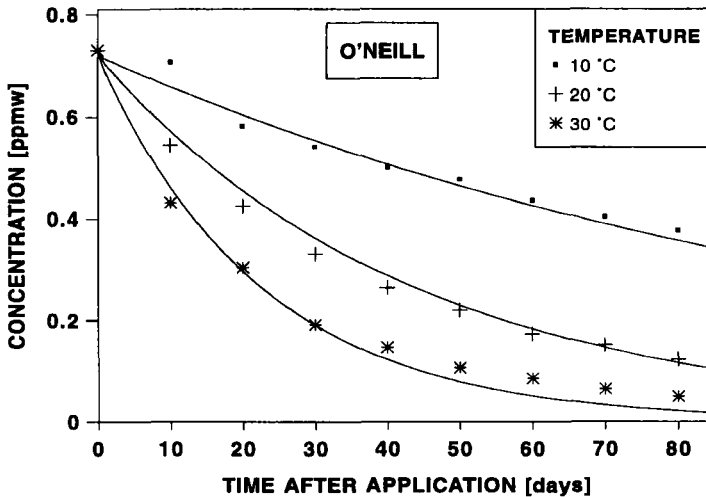


**Fig. 4.7:** By use of the biologically motivated temperature law of O'Neill it is possible to describe the degradation at all three temperatures fairly well. The fit was obtained by using the same data set as in Fig. 4.6 (Pestemer, 1992).

Table 4.4 summarizes the results of both fits. Note that $R^2$ has augmented to 0.99 for the biological temperature function, which does not seem much compared to the value of 0.96 achieved with the Arrhenius approach. However, systematic deviations are obviously removed.

**Tab. 4.4:** Parameters of the Arrhenius and O'Neill temperature response function estimated from Isoproturon degradation data (Pestemer, 1992) at different temperatures (example 4.4), standard deviations in brackets.

| Arrhenius-Function | | O'Neill-Function | |
|---|---|---|---|
| **Parameter** | **Estimate** | **Parameter** | **Estimate** |
| $k_0$ | 1835.9 (3088.3) | $k_{opt}$ | 0.078 (0.002) |
| | | $T_{max}$ | 50.00 (fixed) |
| $E_A$ | 26400.8 (5489.4) | $T_{opt}$ | 35.00 (fixed) |
| | | $a$ | 2.039 (0.002) |
| $R^2$ | 0.960 | $R^2$ | 0.991 |

## Example 4.5: Temperature and Humidity Dependence of the Degradation of Quinmerac and Chlorotoluron

For the combined influence of temperature and humidity on the degradation rate a product approach was chosen

$$k(T,\theta) = k(T)\,k(\theta) \tag{4.15a}$$

where $k(T)$ is given by Eq. (4.14) and the humidity response by

$$k(\theta) = \left(\frac{\theta}{\theta_{crit}}\right)^b e^{\;1 - \left(\frac{\theta}{\theta_{crit}}\right)^b} \tag{4.15b}$$

A plot of this function is shown in section 3.4 (Fig. 3.58). As in the previous example, the model is slightly overparameterized in view of the data available. The parameter $T_{max}$ was fixed to 50°C, all other parameters were allowed to vary. Figures 4.8 a,b show model curves and data for the parameter values given in Tab. 4.5.

**Tab. 4.5:** Parameters of the combined temperature and humidity response function (Eqs. (4.14) and (4.15)) estimated from degradation data of Quinmerac (Nörtersheuser, 1993) and Chlorotoluron (Pestemer, unpublished) (example 4.5), standard deviation in brackets.

| **Parameter** | **Quinmerac** | **Chlorotoluron** |
|---|---|---|
| $k_{opt}$ | 0.018 (0.001) | 0.021 (0.002) |
| $T_{max}$ | 50.00 (fixed) | 50.00 (fixed) |
| $T_{opt}$ | 26.01 (0.594) | 28.55 (2.495) |
| $a$ | 9.715 (1.435) | 4.501 (2.063) |
| $\theta_{crit}$ | 0.626 (0.021) | 0.690 (0.074) |
| $b$ | 2.207 (0.145) | 1.514 (0.233) |
| $R^2$ | 0.923 | 0.926 |
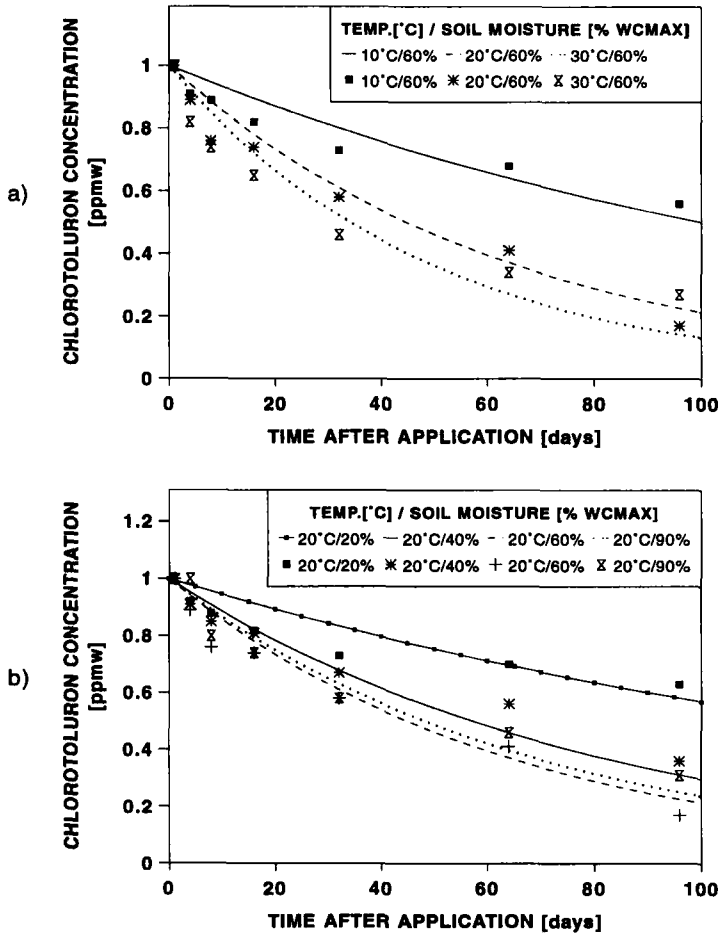
**Fig. 4.8:** Dependence of degradation rate of Chlorotoluron (Pestemer, unpublished) on temperature [°C] and moisture of soil [% of max. water capacity]. The fit is based on a combination of the O'Neill Function and the moisture dependence formulated by Eq. (4.15b): a) different temperatures and constant soil moisture of 60 % of maximum water capacity, b) different soil moistures and constant temperature of 20°C. Note that the whole data field as shown in both figures is described by only one model.


## 4.3   Models in Form of Ordinary Differential Equations

As was shown in chapter 3, most nonlinear kinetic models lead to initial value problems, which are not amenable to analytical solutions. Therefore, one is faced with the parameter identification problem for regression functions, which are only implicitly defined as solutions of nonlinear initial value problems and are not available as explicit functions.

A straightforward procedure is a combination of nonlinear regression algorithms with algorithms for the numerical solution of initial value problems. This method has been applied since about two decades (cf. Bard, 1974). It is implemented into the statistical program

package BMDP (Ralston et al., 1984) and is thus available for routine tasks. To enable the reader to handle this program, a detailed example is given including BMDP instructions and FORTRAN program where the differential equations are defined.

However, from the point of view of scientific computing and of numerical mathematics, this so-called initial value method, suffers from major drawbacks concerning the range of convergence of initial parameter sets and speed of calculation. Therefore, a numerical advanced method based on a boundary value approach will also be described, although it is not available as a program package as yet.
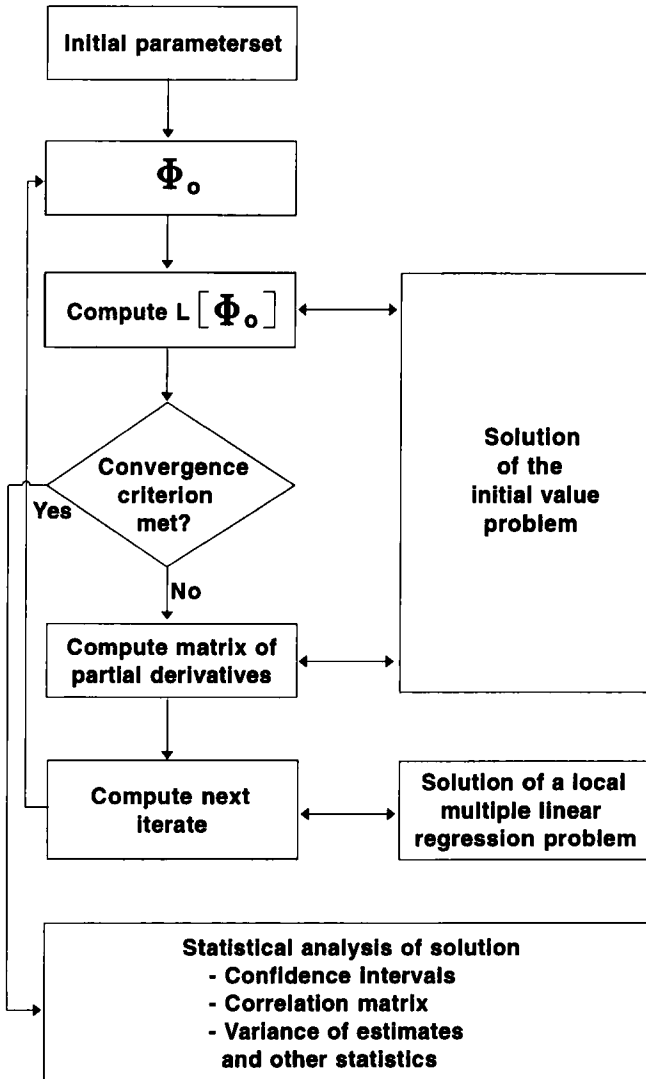


**Fig. 4.9:** Flow chart of the initial value procedure. At each step of the iteration, the differential equations are solved numerically. Implementation is achieved by linking a differential equation solver with a standard routine for derivative free nonlinear regression.

### 4.3.1   Initial Value Method

A flow chart of this method is given in Fig. 4.9. As can be seen from this chart, a subroutine for the numerical solution of initial value problems is embedded in an iteration procedure for the solution of least squares problems. The latter are usually derived from a gradient procedure such as the Gauss-Newton or Levenberg-Marquard scheme. Since these iteration schemes need the derivates of the regression function with respect to parameters, these partial derivates have to be computed along with each iteration step.

This can be achieved by numerical integration of the sensitivity equations along with the solution of the differential equations. This approach is described by Bard (1974), a practical application is given by Haffner et al. (1981). Although this procedure is quite attractive from a mathematical point of view, the major disadvantage of this method is that the number of differential equations is augmented by the product of number of parameters times the number of model equations. Apart from errors in the setup frequently numerical instabilities are met in the course of the iteration due to the increased number of equations, which are, in general, nonlinear.

So called "derivative free" regression methods as implemented in various statistical program packages evaluate the derivatives by a finite difference approximation. Such a procedure is used in the BMDP subprogram PAR 'Derivative free nonlinear regression'.

The algorithm in BMDP (Ralston et al., 1984) is based on a sequence of local multiple linear regression problems. Numerical integration of the differential equations is performed by a Runge-Kutta-Fehlberg routine, which is a $5^{th}$ order method with variable step size control.


### Example 4.6: Degradation of 2-4 D by Microorganisms

The underlying experiments were carried out by Li-Tse Ou (1985). The data obtained in these experiments are an excellent basis for parameter estimation in degradation models with explicit microbial population dynamics. 10 mg/kg $^{14}$C-labeled 2,4-D was applied to a Cecil and a Webster soil respectively. 2,4-D concentration, bound residues, microbial biomass and labeled $CO_2$ were measured simultaneously. Microbial biomass was estimated by the most probable number method.

In a first trial, the model given in chapter 3 (Eqs. (3.107) and (3.108)) was analyzed. However, correlation coefficients very close to one between parameter estimates, for example between the parameters of the Michaelis-Menten law $K_M$ and $V_{max}$, indicated that this model is overparameterized with respect to the data structure, i.e. the model contains superfluous parameters. As a consequence, a simplified version was used assuming first order reactions instead of Michaelis-Menten kinetics and no density dependent mortality rate. This reduction in the number of parameters removed the degeneracies encountered in the original estimation problem. A further equation is added for the bound residues. The model equations are:

$$\frac{dc}{dt} = -k_e cm - k_b c \qquad\qquad (4.16a)$$

$$\frac{dm}{dt} = \gamma k_e cm - dm \tag{4.16b}$$

$$\frac{dS}{dt} = k_b c \tag{4.16c}$$

The model is specified by the four parameters $k_e$, $\gamma$, $d$ and $k_b$. To illustrate the easy handling of the BMDP program, BMDP control instructions and the FORTRAN program, where the differential equations are supplied by the user, are listed in Tabs. 4.6 a,b. BMDP instructions are organized in paragraphs (beginning with /) and sentences. In the input and variable paragraphs the number of variables, the format and variable names are defined. In the regression paragraph the dependent variable is chosen. The data are organized in sequence, so only one dependent variable (KONZ) is needed. The variable KOMP determines the component (concentration of 2,4-D, microbial biomass, bound residues and $CO_2$). In the parameter paragraph initial values and constraints are specified.

**Tab. 4.6:** Setup of a BMDP program to solve a regression problem in ordinary differential equations. a) The BMDP instructions are the same as in explicit problems. The user has to supply a FORTRAN subroutine (Tab. 4.6b) where the differential equations are defined. The program pertains to example 4.6.

**Tab. 4.6 a:** BDMP instructions

```
/PROB TITLE IS "HERBICIDE DEGRADATION EXAMPLE 4.6".
/INPUT VARIABLES ARE 3.
FORMAT IS FREE.
/VARIABLE NAMES ARE ZEIT,KONZ,KOMP.
/REGRES DEPENDENT IS KONZ.
PARAMETERS ARE 4.
ITER=200.
/PARAM INITIAL ARE 0.012,20.9,0.125,0.026.
MIN=0,0,0,0.
MAX=1,30,1,1.
NAMES ARE AK,GAMMA,D,AKB.
/PLOT VARIABLE IS ZEIT.
RESIDUALS.
PROBIT.
/END.
0    10.000   1
3     8.500   1
        :
0     0.004   2
3     7.000   2
        :
        :
```

**Tab. 4.6 b:** FORTRAN subroutine which contains the model equations

```
00001          SUBROUTINE DIFFEQ(F,P,X,N,KASE,NVAR,NPAR,IPASS,XLOSS)
00002          IMPLICIT REAL*8 (A-H,O-Z)
00003          COMMON/DECON/Z(10),DZ(10),T,NEQN,IGO,IT,NEW
00004          DIMENSION X(NVAR),P(NPAR)
00005          AK=P(1)
00006          GAMMA=P(2)
00007          D=P(3)
00008          AKB=P(4)
00009          GOTO (199,200,300),IGO
00010 100      Continue
00011          IT=1
00012          MXCNT=100000
00013          NEQN=3
00014          Z(1)=10
00015          Z(2)=0.004
00016          Z(3)=0
00017
00018          RETURN
00019 200      CONTINUE
00020          V=AK*Z(1)
00021          DZ(1)=-V*Z(2)-AKB*Z(1)
00022          DZ(2)= V*Z(2)*GAMMA-D*Z(2)
00023          DZ(3)= AKB*Z(1)
00024
00025          RETURN
00026 300      CONTINUE
00027          F=Z(1)
00028          IF (X(3).EQ.2) F=Z(2)
00029          IF (X(3).EQ.3) F=Z(3)
```

In the FORTRAN subroutine the differential equations are supplied in the IGO = 200 part of the subroutine. The arrays P and X contain the current parameter values and the data respectively. DZ is the array for the differential equations, Z for the state variables. In the IGO = 100 part of the program initial values are specified, which may also be defined as parameters to be estimated. In this example initial values are kept fixed. F denotes the value of the regression function which is needed for the computation of the sum of squares. F is defined in the IGO = 300 part of the program. The current value of X(3) determines the component to be chosen as regression function. Table 4.7 summarizes the results of a BMDP run obtained for the data of Li-Tse Ou (1985) from two experiments performed in two different soils.

Figure 4.10 a shows the behavior in the loamy soil Webster. Under the conditions in this soil, microbial activity is markedly decreased compared to the sandy soil Cecil (cf. Fig. 4.10 b), although maximum population densities differ only slightly. Note that the amount of bound residues is higher under optimal microbial conditions.

**Tab. 4.7:** Results of the BMDP program presented in Tab. 4.6 obtained for degradation data of 2,4-D in two soils (Cecil and Webster; data from Li-Tse Ou, 1985), standard deviation in brackets. The underlying model is given by Eqs. (4.16a-d). Note that the efficiency factor gamma is estimated > 1. This simply reflects the different dimensions of biomass and 2,4-D concentration (cf. Figs. 4.10 a,b).

| Parameter | Cecil (loamy sand) | Webster (loam) |
|-----------|--------------------|----------------| 
| $k_e$ | 0.021 (0.004) | 0.008 (0.001) |
| $\gamma$ | 7.652 (1.660) | 7.913 (1.703) |
| $d$ | 0.182 (0.037) | 0.170 (0.020) |
| $k_b$ | 0.023 (0.005) | 0.003 (0.001) |
| $m_0$ | 0.004 (fixed) | 0.009 (fixed) |
| $c_0$ | 10.00 (fixed) | 10.00 (fixed) |
| $R^2$ | 0.95 | 0.98 |
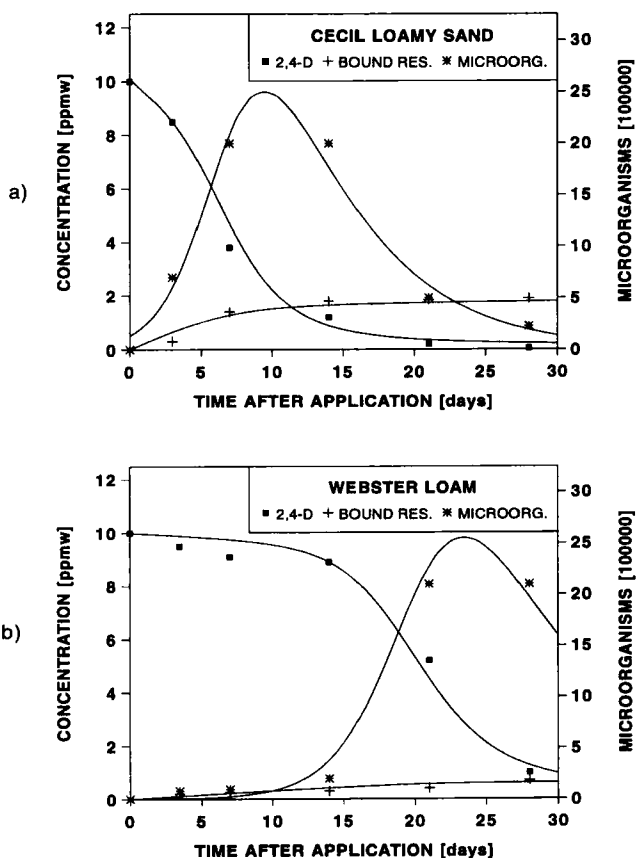


**Fig. 4.10:** Degradation of 2,4-D and microbial growth in two soils, a) Cecil loamy sand and b) Webster loam (data from Li-Tse Ou, 1985).

**Example 4.7: Estimation of Enzyme Kinetic Parameters from a Series of Experiments**

Nonlinearity arising from Michaelis-Menten kinetics is difficult to analyze from single experiments. Unless the initial concentrations are high above saturation, pseudo zero order kinetics cannot be distinguished from first order kinetics due to measurement errors. The assessment of Michaelis-Menten kinetics necessitates a series of experiments with varying initial concentrations. As an example degradation curves of Bentazone for three different initial concentrations are analyzed. Table 4.8 shows the results of the analysis of single experiments assuming first order kinetics.

**Tab. 4.8:** Results of single fits of a simple first order degradation model to degradation data of Bentazone at different initial concentrations (data from BASF, unpublished). Note that the half-lives ($DC_{50}$-values) vary considerably with initial concentrations.

| Initial Concentration [ppmw] | $k_e$[1/d] | $DC_{50}$ [d] | $R^2$ |
|---|---|---|---|
| 2 | 0.062 (0.020) | 11.18 | > 0.99 |
| 5 | 0.037 (0.007) | 18.73 | > 0.99 |
| 10 | 0.020 (0.005) | 34.66 | > 0.99 |

For each initial concentration the fit to a first order model is very close with $R^2$-values greater than 0.99. However, the rate constants and half-lives differ considerably indicating deviations from first order kinetics. It is evident, that predictions based on a first order model are not reliable if half-lives are in the range from 11 to 35 days. However, single analysis with a Michaelis-Menten model fails because of high correlations between the parameters. In order to estimate the parameters $V_{max}$ and $K_M$ of the Michaelis-Menten kinetic law, all experimental data have to be analyzed simultaneously. From the statistical point of view one has to solve a **multi-experiment regression problem**. According to Eq. (4.17) the sum of squares is constructed from all experiments.

$$L\left(V_{\max}, K_M\right) = \sum_{i=1}^{a} \sum_{j=1}^{n} \left[c_i(t_j) - c_{ij}\right]^2 \qquad (4.17)$$

where $c_i(t_j)$ is the solution of the initial value problem

$$\frac{dc_i}{dt} = - \frac{V_{\max} c_i}{c_i + K_M} \qquad for \quad i = 1,2,3 \qquad (4.18)$$

at time $t_j$ with initial concentration $c_i(t=0) = c_{i0}$. This regression problem was solved by use of the statistical program package BMDP, subprogram PAR (Nonlinear Derivative Free Regression). The multi-experiment problem was programmed in a straightforward manner by formulating a system of repeated identical differential equations differing only with respect to their initial values. Table 4.9 shows the results of the regression analysis. The parameters $V_{max}$ and $K_M$ become estimable. The correlation between parameter estimates is still high,

but the regression problem remains well posed from the numerical point of view and convergence is achieved. As shown in Fig. 4.11 the data of the three experimental runs are fairly well described by the nonlinear model.

**Tab. 4.9:** Simultaneous fit of three degradation curves of Bentazone obtained for three different initial concentrations to a Michaelis-Menten degradation model (example 4.7), standard deviations in brackets.

| Parameter | Estimate (std. dev.) |
|---|---|
| $V_{max}$ | 0.197 (0.04) |
| $K_M$ | 4.463 (2.02) |
| $R^2$ | 0.96 |
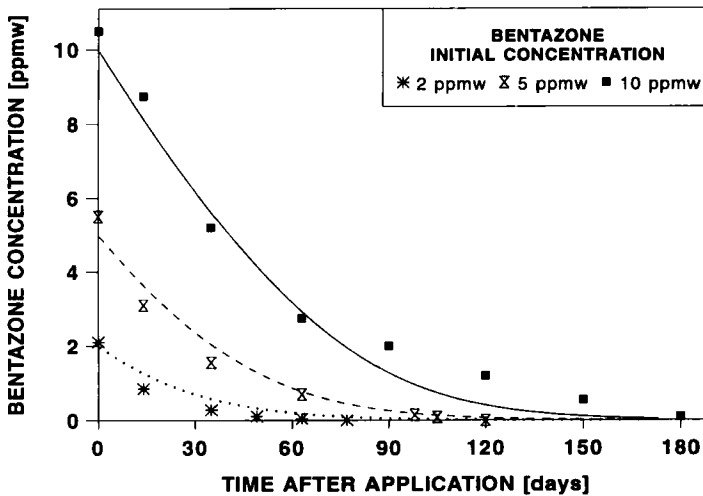


**Fig. 4.11:** Degradation of Bentazone at different initial concentrations fitted to the Michaelis-Menten kinetic law (data from BASF, unpublished).

## 4.3.2  Boundary Value Method

Although the initial value approach is intuitively appealing, it suffers from two major drawbacks which become apparent in numerical practice.

a) It frequently occurs that the differential equations become unsolvable for parameter values attained in the course of an iteration procedure, although the solution of the regression problem may exist. According to the authors' experience this is likely to happen in models containing growth terms. Often, the region of attraction of this procedure is quite small and appropriate initial values have to be searched by time consuming trial and error guesses.

b) The prior information available on the trajectories in form of the data or in form of knowledge is not used.

The boundary value approach, which was developed by Bock (1993 and 1987), uses the full information. In a first step, a suitable mesh $\tau_1 < \tau_2 < ... < \tau_m$ is chosen, which is a subset of the data points. The basic idea is, to avoid integration over the whole interval $[\tau_1, \tau_m]$. Therefore, $m - 1$ independent initial value problems are solved, one for each interval $[\tau_i, \tau_{i+1}]$.

For component $y_i$ the successive initial value problems are

$$\frac{dy_i}{dt} = f_i(\vec{y}, t, \Phi), \qquad y_i(\tau_j) = s_j, \qquad t \in \left[\tau_{ij}, t_{j+1}\right]$$

(4.19)

For each variable of the differential equation system $m$ initial values $(s_1, ..., s_m)$ are introduced as additional parameters (the index $i$ is dropped for ease of presentation). Natural initial values for the $s_j$ are the data. At this point, the prior information in form of the data enters the procedure. It is even possible, to "invent" plausible data points, if the density of the data is not sufficient or if data in one component of the system are totally lacking. Of course, these invented data are omitted in the construction of the performance criterion. By this trick, the trajectories remain close to the data even if only poor estimates of the initial values are available. By choosing a sufficiently small mesh size, it is always possible to avoid singularities. However, the trajectory thus obtained is discontinuous at the nodes. Therefore, constraints have to be added to ensure continuity of the solution.

$$x(\tau_{j+1}, s_j, \Phi) - s_{j+1} = 0$$

(4.20)

The optimization problem (Eq. (4.2)) is thus augmented by the number of the additional parameters $s_j$ and by the continuity constraints. In the algorithm PARFIT developed by Bock (1987) this problem is solved by a generalized Gauss-Newton method.

**Example 4.8: Degradation of 2,4-D by Microorganisms (continued)**

To illustrate the method, example 4.6 is reanalyzed by this procedure. Figures 4.12 a-c show a sequence of trajectories generated in the course of the iteration. The rationale behind the boundary value method becomes quite clear by this sequence: the first figure shows the solution obtained for the starting values: the trajectories of each interval start from a data point. In the course of the iteration, the discontinuities at the nodes are gradually smoothed as the initial values $s_j$ move from their initial values, which are the data. By this mode of convergence the residual sum of squares or similar measures of the goodness of the fit are zero at the beginning of the iteration and increase during the iteration procedure. This is just contrary to the behavior of the classical iteration schemes. Parameter estimates obtained by both methods are compared in Tab. 4.10. In both cases the convergence criterion was met. Whereas parameter estimates are quite similar, the standard deviations of the estimates differ. It is important to note that the initial value method did only converge, if the initial values $c_0$ and $m_0$ were kept fix. The boundary value method converged even for this case.
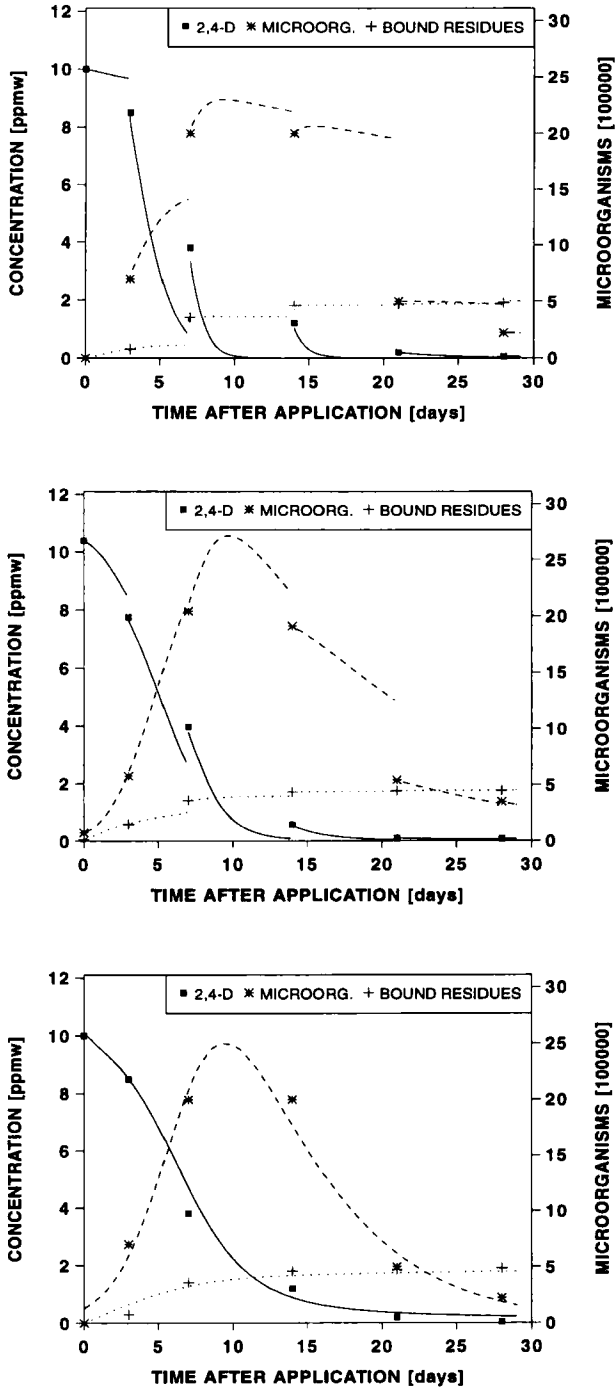
**Fig. 4.12:** Sequence of trajectories generated during the iteration of the boundary value method: a) starting trajectories, b) trajectories after the third iteration and c) final solution.

**Tab. 4.10:** Comparison between the initial value method and the boundary value method for the identification problem given in example 4.6 (Cecil loamy sand; data from Li-Tse Ou, 1985), standard deviations in brackets. A better fit was obtained by estimating also the initial values $c_0$ and $m_0$, which was not possible in the initial value method.

| Parameter | Initial Value Method (BMDP) | Boundary Value Method (PARFIT) | |
|:---:|:---:|:---:|:---:|
| $k_e$ | 0.021 (0.004) | 0.009 (0.001) | 0.024 (0.002) |
| $\gamma$ | 7.652 (1.660) | 7.808 (1.200) | 6.694 (1.250) |
| $d$ | 0.182 (0.037) | 0.186 (0.027) | 0.159 (0.031) |
| $k_b$ | 0.023 (0.005) | 0.028 (0.005) | 0.029 (0.005) |
| $m_0$ | 0.004 (fixed) | 1.328 (0.390) | 0.004 (fixed) |
| $c_0$ | 10.000 (fixed) | 9.854 (1.389) | 10.000 (fixed) |
| $R^2$ | 0.95 | 0.99 | 0.95 |
| RSQ | 55.78 | 13.52 | 57.34 |
| MSQ | 2.79 | 0.68 | 2.87 |

**Concluding Remarks**

The examples have shown that a thorough statistical analysis is feasible for nonlinear kinetic models even if the differential equations are not amenable to analytical solutions. Parameter estimation in nonlinear ordinary differential equations can be performed by use of a widely spread statistical program package. It is therefore obsolete describing reactions of fractal order simply for facilitating parameter estimation. There is no doubt, that such functions can be fitted to kinetic data. The use of such models for predictive purposes, however, is rather questionable.

Nowadays, there are many tools available for parameter identification in systems of ordinary differential equations. Only recently, the software system EASY-FIT (Schittkowski, 1996) was released. EASY-FIT is a multipurpose system to identify parameters in explicit functions, dynamic systems of equations, Laplace transformations, systems of ordinary differential equations, differential algebraic equations or systems of partial differential equations. The code is based on advanced mathematical techniques.

Another valuable tool is the software system MODEL MAKER (SB Technology, 1994). This system not only allows to develop simulation models quickly under Windows with much graphical support but offers also the opportunity of parameter identification and of performing sensitivity analyses of parameters in a systematic way.

# 4.4    Sparse Data Analysis

Additional notations:

$c_{ij}(t)$    : concentration measurement in the $j_{th}$ soil at time $t_i$ [M/L$^3$]

$f$    : known, even nonlinear, regression function

$\beta_j$    : regression parameters

$m_0$    : initial microbial activity [1]

$K_{max}$    : maximum microbial activity [1]

$\theta$    : vector of population parameters

$\sigma^2_\varepsilon$    : residual error variance  [M/L$^3$]

$\varepsilon_{ij}$    : random vector of error [M/L$^3$]

$\eta_j$    : individual random perturbation from $\theta$ with mean zero and variance $\sigma^2$

$X_j$    : vector of covariables (e.g. soil properties as pH-value, $C_{org}$-content of soil, temperature)

$\sigma^2_{Kmax}, \sigma^2_{m0}, \sigma^2_r$    : variances of $K_{max}$, $m_0$ and $r$, resp. [1], resp. [1/T]

$r(\theta_{Kmax}, \theta_{m0}, \theta_r)$    : growth rate [1/T]


In recent years techniques capable of analyzing sparse data have been developed, particularly for population based kinetic evaluation of phase III clinical studies. Such studies normally include a great number of patients, with a varying number of drug concentration measurements at different time points. With population based pharmacokinetics, factors which contribute to interindividual variability in pharmacokinetics can be identified, even in sparse data situations, e.g. in situations where only one or two blood concentration measurements per subject are available. These methods are meanwhile established in pharmaceutical research and realized in several statistical program packages e.g. NONMEM (Beal and Sheiner, 1982) or P-PHARM, version 1.3 (Simed, 1994).

The theory and implementation of these methods has been described elsewhere (Dempster et al., 1977; Beal and Sheiner, 1982; Beal, 1984; Sheiner, 1984; Colburn and Olson, 1988; Sanathanan, 1991; Aarons, 1993; Gomeni et al., 1994; Bressolle et al., 1996) and will not be considered here. We will only focus on the great benefits these new methods have for evaluation of kinetics and dynamics of pesticides and pesticide monitoring.

Distribution of kinetic model parameters and their dependencies on environmental conditions, e.g. soil characteristics are traditionally analyzed according to the so-called 'Two Stage Procedure'. That means that firstly, an appropriate kinetic model is fitted to the observed time courses of each soil separately, followed by a second stage in which the distribution of the fitted parameters is analyzed. This procedure requires intensive experimentation. Often time courses of pesticides are observed only for a limited number of soils, mostly standard soils.

With sparse data analysis techniques, it is possible to characterize the disposition of a pesticide in a soil e.g. with a kinetic model which may contain many parameters, in situations where only very few measurements (e.g. 1 or 2 samples per soil) are available for analysis and where parameter estimation with standard procedures fails.

Sparse data analysis techniques have great impact for pesticide monitoring and pesticide adjustment. With this new method pesticide kinetics and dependencies of kinetic parameters on environmental conditions can be evaluated with less experimental effort.

Population based analysis is particular appropriate for parameter estimation problems involving a lot of different soils, with a varying number of sampling points. For ease of presentation however, this method is applied to the 2,4-D concentration data in Melfort, Oxbow and Meota soil, shown in Fig. 1.4.

The $i^{th}$ concentration measurement in the $j^{th}$ soil, $c_{ij}$, at time $t_i$ is given by

$$c_{ij}(t) = f(\beta_j, t_{ij}) + \varepsilon_{ij} \tag{4.21}$$

where $f$ is a known, even nonlinear, function with regression parameters $\beta_j$ random vector of error $\varepsilon_{ij}$. Assuming that the degradation of the substance is proportional to the activity of microorganisms

$$\frac{dc}{dt} = -m(t)c \tag{4.22}$$

and describing the activity with the nonlinear differential equation of logistic growth (cf. chapter 2)

$$\frac{dm}{dt} = rm\left(1 - \frac{m}{K_{max}}\right) \tag{4.23}$$

yield the analytic solutions

$$c(t) = c_0 e^{-\int_0^t m(\tau)d\tau} \tag{4.24}$$

$$m(t) = \frac{m_0 K_{max}}{m_0 - \left(m_0 - K_{max}\right)e^{-rt}} \tag{4.25}$$

$$f = c_{0,j}\, e^{\left(-K_{max_j}t\right)}\left[\frac{K_{max_j}}{m_{0_j} - \left(m_{0_j} - K_{max_j}\right)e^{-r_j t}}\right]^{\frac{K_{max_j}}{r_j}} \tag{4.26}$$

The parameters $\beta_j$ account for the interindividual variability of soils and are assumed to arise from some multivariate probability distribution with mean $\theta$.

$$\beta_j = q(\theta, X_j, \eta_j) \tag{4.23}$$

The $\varepsilon_{ij}$-values are independent, identically distributed statistical errors with mean zero and and variance $\sigma^2$, and represent all uncertainty, e.g. caused by intra-individual time variation in the model parameters, model misspecification, analytical error in concentration measurement, or error in reported sampling time.

In the programs P-Pharm or NONMEM, cited above, the distribution of the random effects and the residual error variance can be modeled in different ways. The distribution of parameters within the population for example, can e.g. be assumed as lognormal and residual error variance as heteroscedastic (increase of error variance in proportion to the measured concentration). This details however will not be considered here. In our introductory example, the distribution of the random effects is assumed as normal and the residual error variance as homoscedastic.

Estimation of individual and population parameters is performed using the EM-type algorithm (Dempster, 1977), implemented in P-Pharm, version 1.3. This is an iterative two-step process suitable for computing the maximum likelihood estimates in complicated problems of missing and incomplete data.

In the **first step**, the expectation step (E-step), the individual parameters for each individual are estimated (Bayesian estimate) given the current population parameters and the individual data.

In the **second step**, the maximization step (M-step), the population parameters are estimated by maximum likelihood given the current estimates (E-step) of the individual parameters. The steps E and M are iterated up to the convergence of the algorithm (Bressolle et al., 1996).
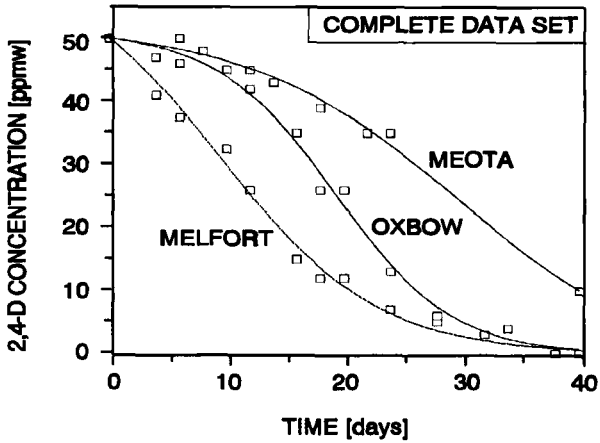
**Results**

In a first approach the kinetic model given above, is fitted simultaneously to all concentration measurements of the three soils. Sparse data analysis is based on the premise that population parameters can be modeled as random variables, with estimates of the kinetic parameters for any individual soil as a realization of the random variable distribution.

In our example, initial parameter values have to be given for the 7 population parameters: mean values for model parameter $K_{max}$, $m_0$, and $r(\theta_{Kmax}, \theta_{m0}, \theta_r)$, the variances ($\sigma^2_{Kmax}$, $\sigma^2_{m0}$, $\sigma^2_r$) and the residual error variance ($\sigma^2_\varepsilon$), which are shown in Tab. 4.11.

The results of parameter estimation are shown in Fig. 4.13 and Tabs. 4.12 a,b. As surrogate parameter for exposition of soils with 2,4-D, the time period needed for halving the initial concentration ($DC_{50}$-value) is calculated.

**Tab. 4.11:** Initial population parameter estimates.

| Parameter | Mean($\theta$) | Variance($\sigma^2$) | Coefficient of Variation [%] |
|---|---|---|---|
| $K_{max}$ [1/h] | 1.0 | 0.33 | 57.7 |
| $m_0$  [1/h] | 1.0 | 0.33 | 57.7 |
| $r$   [1/h] | 1.0 | 0.33 | 57.7 |
| $\sigma^2_\varepsilon$ | 1.0 | | |



**Fig. 4.13 :** Resulting fit with the complete data set.

**Tab. 4.12:** a) Final population with complete data set.

| Parameter | Mean($\theta$) | Variance($\sigma^2$) | Coefficient of Variation [%] |
|---|---|---|---|
| $K_{max}$ [1/h] | 0.183 | 0.0026 | 27.7 |
| $m_0$   [1/h] | 0.013 | 0.0004 | 93.7 |
| $r$   [1/h] | 0.147 | 0.0017 | 28.4 |
| $\sigma^2_\varepsilon$ | 2.345 | | |

**Tab. 4.12:** b) Individual parameter estimates with complete data set.

| Soil | $K_{max}$ [1/h] | $m_0$ [1/h] | $r$ [1/h] | $DC_{50}$ [h] |
|---|---|---|---|---|
| Melfort | 0.149 | 0.0293 | 0.148 | 12.2 |
| Oxbow | 0.220 | 0.0047 | 0.189 | 19.5 |
| Meota | 0.181 | 0.0043 | 0.104 | 30.0 |

These values were compared to the ones estimated using only 4 observations per soil. The start values of model parameters were the same as shown in Tab. 4.11. Due to practical considerations, the concentration measurement 0, 12, 24 and 40 hours after application were used for parameter estimation (Fig. 4.14, Tabs. 4.13 a,b).
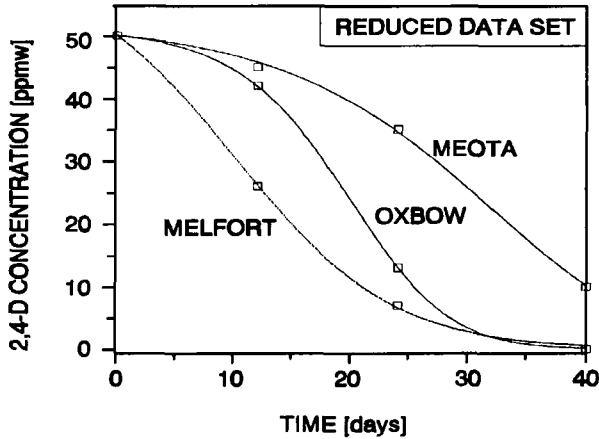


**Fig. 4.14:** Resulting fit with the reduced data set.

**Tab. 4.13:** a) Final population with reduced data set.

| Parameter | Mean($\theta$) | Variance($\sigma^2$) | Coefficient of Variation [%] |
|---|---|---|---|
| $K_{max}$ [1/h] | 0.176 | 0.00322 | 32.4 |
| $m_0$ [1/h] | 0.007 | 0.00003 | 82.7 |
| $r$ [1/h] | 0.199 | 0.00537 | 36.8 |
| $\sigma^2_\varepsilon$ | 0.554 | | |

**Tab. 4.13:** b) individual parameter estimates with reduced data set.

| Soil | $K_{max}$ [1/h] | $m_0$ [1/h] | $r$ [1/h] | $DC_{50}$ [h] |
|---|---|---|---|---|
| Melfort | 0.129 | 0.0148 | 0.269 | 12.7 |
| Oxbow | 0.218 | 0.0035 | 0.214 | 19.3 |
| Meota | 0.182 | 0.0033 | 0.114 | 30.6 |

Differences of the fitting results for both the complete and reduced data sets are very small. The use of prior knowledge provide a means for reducing experimental effort for quantifying exposition of soils with a given pesticide.

Given the population parameters, the time course of a pesticide in a given soil can even be modeled with one additional sampling, as shown in Figs. 4.15 and 4.16.

REL. FREQUENCY
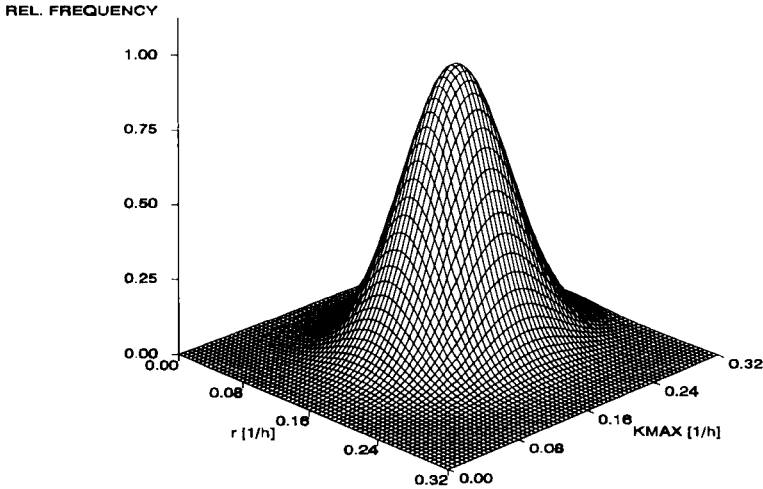


**Fig. 4.15:** Estimated distribution of model parameters $k_{max}$ and $r$ within the underlying population, follows a bivariate normal distribution (distribution parameters shown in Tab. 4.12).
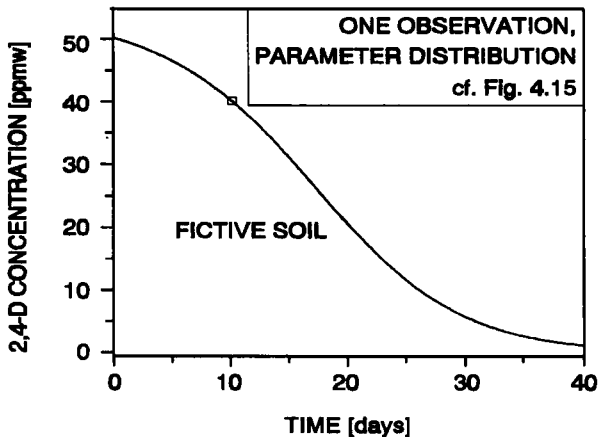


**Fig. 4.16:** Simulation of 2,4-D time course in a fictive soil with population parameter distribution, shown in Fig. 4.15 and one observation ($DC_{50} = 17.6$ h).

In the example given above, we give a short overview about the possibilities of sparse data analysis techniques. Pesticide concentrations obtained at random (but known) intervals after application can be used to model kinetic parameters, even of models with a greater number of parameters. This method allows the inclusion of pesticide measurements made at different times both within and across soils and also permits varying numbers of sampling points per soil. With those approaches covariables influencing the fate of pesticides in soils can be determined on basis of a great number of soils with a limited number of samplings, which have a great impact on a better dose adjustment and pesticide monitoring.

When prior knowledge of the mean and the dispersion of the kinetic parameters of the population (i.e. population of soils to which the selected soil belongs) is available, and treatment goals exists (e.g. assuring a minimum effective pesticide concentration over a distinct period of time), treatment strategies can be developed on basis of covariates and population parameters. With two or three additional samplings over the treatment period, the validity of the underlying model assumptions can be proofed. Following this procedure, the model basis for further simulations increases step by step, and additional sampling becomes superfluous step by step. One additional advantage is, that distribution of model parameters can be observed in the target population, so that factors, that control treatment variability may be discovered with a greater chance than in experiments with standard soils.

# 5 Transport and Reactions in the Soil

## 5.1 Water Movement

Notations

$\vec{q}$ : volumetric water flux density [L/T]

$S$ : $= S(\psi, x, y, z, t) =$ source and sink term [L$^3$/L$^3$/T]

$\psi_m$ : soil matric potential [hPa], resp. [(ML/T$^2$)/L$^2$]

$|\psi_m|$ : soil suction [hPa], resp. [(ML/T$^2$)/L$^2$]

$\psi_h$ : hydraulic potential [hPa], resp. [(ML/T$^2$)/L$^2$]

$\psi_z$ : gravitational potential [M/LT$^2$]

$\theta$ : water content [L$^3$/L$^3$]

$\theta_s$ : saturated water content [L$^3$/L$^3$]

$\theta_r$ : residual water content [L$^3$/L$^3$]

$\Theta$ : $= (\theta - \theta_r)/(\theta_s - \theta_r) =$ normalized water content [1]

$\phi$ : porosity [L$^3$/L$^3$]

$\rho$ : bulk density [M/L$^3$]

$K_r$ : normalized hydraulic conductivity [1]

$K_s$ : saturated hydraulic conductivity [L/T]

$K(\theta)$ : $= K_r K_s =$ hydraulic conductivity [L/T]

$C(\psi)$ : water capacity [cm$^3$/cm$^3$/hPa] resp. [L$^3$/L$^3$/((ML/T$^2$)/L$^2$)]

### 5.1.1 The Classical Approach: Richards' Equation

A transport equation for water is derived by applying the general principle outlined in section 2.2. The basic equation is the mass conservation equation

$$\frac{\partial \theta}{\partial t} = - \nabla \cdot \vec{q} + S \qquad (5.1)$$

which states that the rate of change of the water content per unit volume equals the net gain of fluid per unit volume plus sinks or sources within this unit. This equation has to be completed by a functional relationship between the flow vector $\vec{q}$ and the water content $\theta$. Darcy's law relates the water flow to the gradient of a potential, the hydraulic potential $\psi_h$, which in turn depends on the water content $\theta$.

The hydraulic potential is the sum of the gravitational potential, the matric potential and the pressure potential.

$$\psi_h = \psi_z + \psi_m + \psi_p \qquad (5.2)$$

The gravitational potential is simply expressed by the vertical distance from a reference elevation. The matric potential is due to the adsorptive forces of the soil matrix. It depends on the water content of the soil. The pressure potential is related to the weight of the water

column above the point under consideration. The latter potential is only important in saturated soils. For details concerning measurements confer any textbook on soil physics, e.g. Hanks and Ashcroft (1980). The water flow is then related to the water potential by

$$\vec{q} = -K(\theta)\nabla\psi_h \tag{5.3}$$

For a homogeneous, isotropic medium $K$ is a scalar, the hydraulic conductivity. In an anisotropic medium $K$ is a tensor, the conductivity tensor. In this case, Eq. (5.3) becomes

$$\vec{q} = - \begin{pmatrix} K_{xx} & K_{xy} & K_{xz} \\ K_{yx} & K_{yy} & K_{yz} \\ K_{zx} & K_{zy} & K_{zz} \end{pmatrix} \begin{pmatrix} \dfrac{\partial\psi_h}{\partial x} \\ \dfrac{\partial\psi_h}{\partial y} \\ \dfrac{\partial\psi_h}{\partial z} \end{pmatrix} \tag{5.4}$$

Note that $K$ is a function of the water content $\theta$. This relation is referred to as the conductivity curve. Combination of the equation of conservation of mass with Darcy's law yields

$$\frac{\partial\theta}{\partial t} = \nabla\cdot(K\nabla\psi_h) + S \tag{5.5}$$

If the soil is homogeneous and isotropic this equation takes the form

$$\frac{\partial\theta}{\partial t} = K\frac{\partial^2\psi_h}{\partial x^2} + K\frac{\partial^2\psi_h}{\partial y^2} + K\frac{\partial^2\psi_h}{\partial z^2} + S = K\Delta\psi_h + S \tag{5.6}$$

Equation (5.6) still contains both state variables, $\theta$ and $\psi_h$. The pressure potential $\psi_p$ is negligible in the unsaturated case, and the gravitational potential is given by $\psi_z = z$. Note that the sign of $z$ is negative below the surface, if the surface is chosen as reference level. If $\theta$ is given as a function of $\psi_m$, Eq. (5.6) can be written either in $\theta$ or in $\psi$. The functional relationship between $\theta$ and $\psi_m$ is referred to as water retention curve. (For ease of presentation the subscript $m$ of $\psi$ will be dropped in the following. Unless otherwise stated, $\psi$ has the meaning of the matric potential). Equation (5.6) is written in $\psi$ by elimination of $\theta$ by

$$\frac{\partial\theta}{\partial t} = \frac{\partial\theta}{\partial\psi}\frac{\partial\psi}{\partial t} = C(\psi)\frac{\partial\psi}{\partial t} \tag{5.7}$$

The function $C(\psi)$ is referred to as capacity function. The resulting partial differential equation for $\psi$

$$C(\psi)\frac{\partial\psi}{\partial t} = \frac{\partial}{\partial x}\left(K\frac{\partial\psi}{\partial x}\right) + \frac{\partial}{\partial y}\left(K\frac{\partial\psi}{\partial y}\right) + \frac{\partial}{\partial z}\left(K\frac{\partial}{\partial z}(\psi - z)\right) + S \tag{5.8}$$

is valid for both saturated and unsaturated conditions. In a similar way Eq. (5.6) can be written in the variable $\theta$. Replacing the partial derivatives of $\psi$ with respect to the spatial coordinates by

$$\frac{\partial\psi}{\partial x_i} = \frac{\partial\psi}{\partial\theta}\frac{\partial\theta}{\partial x_i} = \frac{1}{C(\psi)}\frac{\partial\theta}{\partial x_i} \qquad with \quad x_1 = x, \quad x_2 = y \quad and \quad x_3 = z \tag{5.9}$$

and introducing

$$D(\theta) = \frac{K(\theta)}{C(\theta)} \tag{5.10}$$

leads to

$$\frac{\partial\theta}{\partial t} = \frac{\partial}{\partial x}\left(D\frac{\partial\theta}{\partial x}\right) + \frac{\partial}{\partial y}\left(D\frac{\partial\theta}{\partial y}\right) + \frac{\partial}{\partial z}\left(D\frac{\partial\theta}{\partial z} - K\right) + S \tag{5.11}$$

Equation (5.11) is only valid for unsaturated conditions, because $C(\psi)$ becomes zero if the soil is saturated. Equations (5.8) and (5.11) have to be specified by the retention and conductivity curves. It is quite usual, to introduce normalized hydraulic conductivities and water contents. The conductivity function is written in the form $K = K_s K_r$, where $K_s$ denotes the saturated conductivity, which is a parameter, and $K_r$ describes the functional relationship. $K_r$ is referred to as normalized hydraulic conductivity. The normalized water content is defined by

$$\Theta = \frac{\theta - \theta_r}{\theta_s - \theta_r}$$

Several parameterizations of empirical relationships are in use. The parameterizations of Brooks and Corey (1964) and Burdine (1953) are given by

$$\Theta = \begin{cases} \left(\dfrac{\psi_b}{\psi}\right)^\lambda & for \quad \psi \leq \psi_b \\ 1 & for \quad \psi > \psi_b \end{cases} \tag{5.12}$$

$$K_r = \Theta^{3+2/\lambda} \tag{5.13}$$

in which $\psi_b$ denotes the bubbling pressure and $\lambda$ the pore size distribution index. The retention and conductivity curves according to van Genuchten (1980) and Mualem (1976), which are in wide use, are more flexible than the above functions, i.e. they can be applied to

a larger number of soil types.

$$
\Theta = \begin{cases} \dfrac{1}{\left(1 + (\alpha|\psi|)^n\right)^m} & \text{for} \quad \psi \leq 0 \\[4ex] 1 & \text{for} \quad \psi > 0 \end{cases} \tag{5.14}
$$

where $m = 1-1/n$ and $\alpha$ and $n$ are fitting parameters. The conductivity curves are parameterized as a function of the water content

$$
K_r = \Theta^{1/2}\left(1 - (1 - \Theta^{1/m})^m\right)^2 \tag{5.15}
$$

or as a function of the matric potential.

$$
K_r = \frac{\left(1 - (\alpha|\psi|)^{n-1}\left(1 + (\alpha|\psi|)^n\right)^{-m}\right)^2}{\left(1 + (\alpha|\psi|)^n\right)^{m/2}} \tag{5.16}
$$

Figures 5.1 and 5.2 show some retention and conductivity curves in the van Genuchten parameterization.

**Boundary conditions**

At the lower boundary, either continuously measured soil suction data, the measured depth of the groundwater table (both Dirichlet boundary conditions) or the water flux in a certain depth (Neumann boundary condition) has to be provided. When lysimeters are simulated a mixture of both boundary conditions has to be chosen. At the upper boundary either the net rainfall rate (precipitation - interception) or the evaporation rate has to be provided (Neumann boundary condition). For calculating the infiltration rate at the soil surface, the following cases have to be distinguished:

$$
q_{infil} = \begin{cases} r - f & \text{for} \quad \psi_n < dzmitt_{n+1}/2 \\[3ex] K(\Theta)\left(\dfrac{\psi_n - \psi_{n-1}}{dz_n} + 1\right) & \text{for} \quad \psi_n = dzmitt_{n+1}/2 \end{cases} \tag{5.17}
$$

According to this equation the infiltration rate equals the rainfall $r$ minus the interception $f$ until saturation occurs at the soil surface. Assuming a constant gradient of unity the soil suction at the middle of the upper computational layer $n$ equals half the depth of this layer at this time of ponding (cf. Fig. 5.3). In this case the boundary condition changes from a prescribed water flux (Neumann boundary condition) to a constant soil suction in the upper layer $\psi_n = dzmitt_{n+1}/2$ (Dirichlet boundary condition). In the latter case the infiltration rate and the runoff can be calculated from the solution of the Richards' equation. The Dirichlet boundary condition will not change until the net rainfall $r - f$ drops below the infiltration rate.
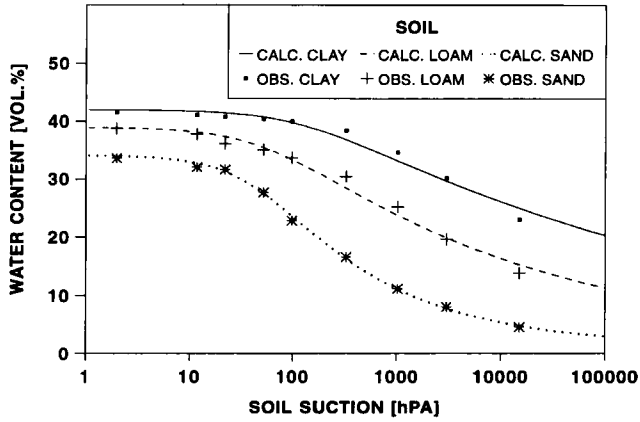
**Fig. 5.1:** Retention curves in the van Genuchten parameterization for different soils in different depths (clayey soil, 15 cm; loamy soil, 120 cm; sandy soil, 25 cm) fitted to observed water contents.
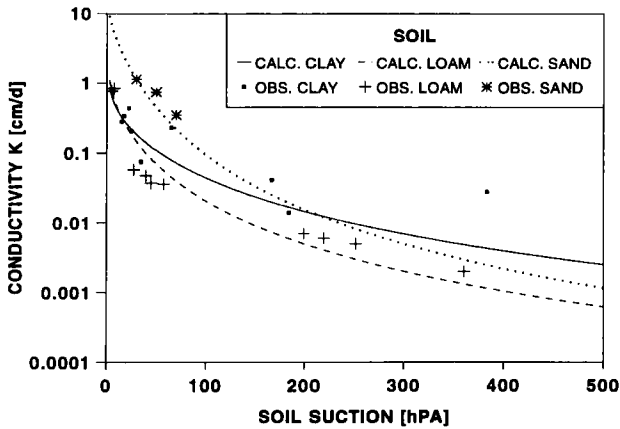


**Fig. 5.2:** Conductivity curves in the van Genuchten parameterization for different soils in different depths (clayey soil, 15 cm; loamy soil, 120 cm; sandy soil, 25 cm) fitted to observed conductivities.
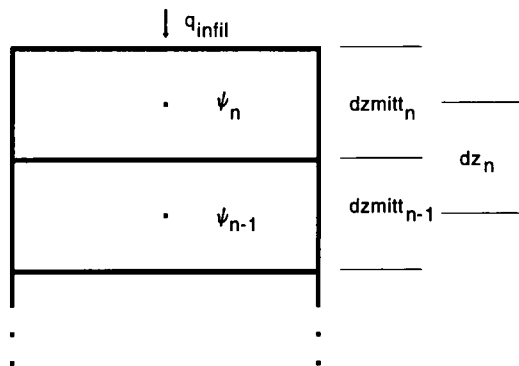


**Fig. 5.3:** Discretization of soil column for calculating the upper boundary condition.

### 5.1.2   Two-Region Models

In the model given before it is assumed that the porous media can be described by a macroscopic approach assuming uni-modal pore-size distribution (cf. Eqs. (5.12) to (5.16)). Often microscopic structures like fractures, fissures, aggregate pores and macropores influence the water fluxes significantly resulting in transport behavior not explainable by the classical one-domain approach (preferential flow). These micro-structures are reflected in the retention and conductivity curve close to saturation. Even if macropores are neglected the measured retention and conductivity curve often show two or more peaks of the pore-size distribution. These peaks are ignored when the van Genuchten or Brooks and Corey relationship is applied.

Models for water transport in structured porous media are often described by a two-domain approach. While most of the models concentrate on matric and macropore flow (German and Beven, 1985; Jarvis, 1991) only few approaches assume two (or more) capillary flow domains (Othmer et al., 1991; Diekkrüger, 1992; Gerke and van Genuchten, 1993).

**Water Transport in Soils with two Capillary Domains**

If the measured retention and conductivity data show significant deviation from a uni-modal pore-size distribution it is necessary to modify the standard approach for retention and conductivity curves as given in Eqs. (5.12) to (5.16). Assuming that the measurements on the macroscopic scale are representative for the capillary pore-system then the resulting conductivity and retention curves can be described as a superposition of two (or more) uni-modal curves (Othmer et al., 1991):

$$\theta_T(\psi) = \sum_{i=1}^{j} \theta_i(\psi) \tag{5.18}$$

$$\theta_T(\psi) = \sum_{i=1}^{j} \left[ \theta_{r_i} + \frac{(\theta_{s_i} - \theta_{r_i})}{\left(1 + (\alpha_i |\psi|)^{n_i}\right)^{m_i}} \right] \tag{5.19}$$

$$K_T(\psi) = \sum_{i=1}^{j} K_{s_i} \frac{\left(1 - (\alpha_i |\psi|)^{n_i - 1}\left(1 + (\alpha_i |\psi|)^{n_i}\right)^{-m_i}\right)^2}{\left(1 + (\alpha_i |\psi|)^{n_i}\right)^{m_i / 2}} \tag{5.20}$$

In this approach for each uni-modal pore-size distribution one conductivity curve has been derived using the approach of Mualem (1976). In opposite to this approach Durner (1992) applied Mualem's model to Eq. (5.18) using numerical integration which is time consuming compared to the analytical method. Durner's approach results in one instead of two (or more) conductivity curves. In order to apply his approach in simulation models it is necessary to store the results of this integration in a conductivity-soil suction table.

In order to decide if one or more distinct flow domains exist in the soil further information concerning aggregate distribution, fissures and fractures have to be provided. If it can be assumed that only one flow domain exists the derived multi-modal retention and conductivity curves can be applied directly in Eq. (5.8) (Diekkrüger, 1992; Durner, 1992). In this case the model is not able to calculate preferential flow because the basic assumptions on the flow behavior as included in the Richards' equation are still valid.

If the soil structure implies that two (or more) capillary flow domains exist then it is straightforward to compute the Darcy-type water flow by Richards' equation for each domain $i$ separately and linking the domains using a first-order water transfer term $S_w$ (cf. Fig. 5.4):

$$\frac{\partial \theta_i}{\partial t} = \frac{\partial}{\partial z}\left[K(\psi_i)\frac{\partial(\psi_i - z)}{\partial z}\right] - S_w \qquad (5.21)$$
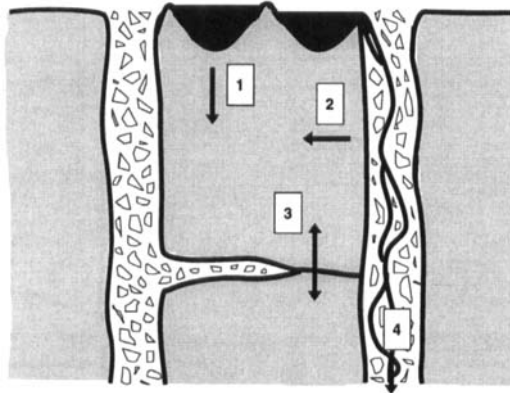


**Fig. 5.4:** Water flux in a soil with two flow-domains (Diekkrüger, 1992). There have to be considered: 1) the infiltration into soil aggregates, 2) the lateral infiltration into the aggregates, 3) vertical water fluxes within the aggregates and 4) infiltration and percolation between the aggregates.

It has to be noted that each flow domain is characterized by one soil suction which allows instationary simulation of water flow and non-equilibrium soil suction in all domains. The transfer term between the domains is usually derived from Darcy's law as lateral flow proportional to the gradient of soil suction between different domains (here given for a two-domain problem):

$$S_w = K_x\frac{\psi_1 - \psi_2}{\Delta x} \qquad (5.22)$$

The distance between both pore-systems $\Delta x$ is given as the sum of the characteristic half widths of both pore-systems (Othmer et al., 1991; Diekkrüger, 1992) or as the half width of the matrix pore-system (Gerke and van Genuchten, 1993). While Othmer et al. (1991) proposed that the conductivity used for calculating the lateral exchange ($K_x$) is best

represented by the minimum of the unsaturated conductivities of both pore-systems, Diekkrüger (1992) calculated the water fluxes using the geometric mean of both unsaturated conductivities. In opposite to these approaches Gerke and van Genuchten (1993) suggest to calculate the water fluxes using the relative hydraulic conductivity of the soil matrix and a significantly lower saturated hydraulic conductivity (in their sensitivity analysis the authors chose a value of 1 % of the conductivity of the soil matrix).

Water flux into the second pore-system occurs when the infiltration capacity of the soil matrix is exceeded. In this case the soil at the surface is saturated and runoff at the microscopic scale occurs. Calculating the infiltration rate $q_{infil}$ into the soil matrix (subscript 1) according to Eq. (5.17) the upper boundary condition (layer $n$) for two pore-systems can be described as

$$I_1 = r - f \qquad\qquad \psi_{1,n} < dzmitt_n/2$$

$$I_2 = 0$$

$$\text{(5.23)}$$

$$I_1 = q_{infil} \qquad\qquad \psi_{1,n} \geq dzmitt_{n+1}/2$$

$$I_2 = r - f - q_{infil}$$

In solute transport models the two-domain approach is well accepted although often for simplicity only water transport in one (mobile) domain is considered. The presented two-domain approach for water transport of Diekkrüger (1992) and Othmer et al. (1991) was used by Gerke and van Genuchten (1993) as the basis of their model. Except small changes of the water transfer term the main improvement was to complete the approach by a solute transport model for two mobile domains. For a comprehensive discussion of various model approaches concerning water and solute transport in structured soils we refer to the paper of Gerke and van Genuchten (1993) and for model application to Othmer et al. (1991) and Diekkrüger (1992).

**Water Transport in Soils with Macropores**

If macropores exist the water flow can not be described by the capillary two-domain concept.

As given before the one-dimensional water flow in the soil matrix

$$\frac{\partial \theta_{mi}}{\partial t} = \frac{\partial}{\partial z}\left(K_{mi}(\psi_{mi})\left(\frac{\partial \psi_{mi}}{\partial z}\right)\right) - S_W \qquad\qquad \text{(5.24)}$$

is coupled to the water flow in the macropore system

$$\frac{\partial \theta_{ma}}{\partial t} = \frac{\partial}{\partial z}(q_{ma}) + S_w \qquad\qquad \text{(5.25)}$$

by the exchange term $S_w$ (Eq. (5.22)).

Assuming film flow in the macropores $\Delta x$ of Eq. (5.22) is given as the half width of the matrix pore system.

According to German and Beven (1985) the gravity flow of water in the macropores can be described by the following relationship between water flux $q_{ma}$ and the macropore moisture content $\theta_{ma}$

$$q_{ma} = K_{s,ma}\left(\frac{\theta_{ma}}{\theta_{s,ma}}\right)^a \tag{5.26}$$

in which a is an empirical constant and $\theta_{s,ma}$ the macropore volume. The upper boundary condition of this model is the same as given in Eq. (5.23). Only few models consider that $\theta_{s,ma}$ is not a constant but may vary with soil structural changes due to swelling and shrinking (Jarvis, 1991; Bronswijk, 1992).
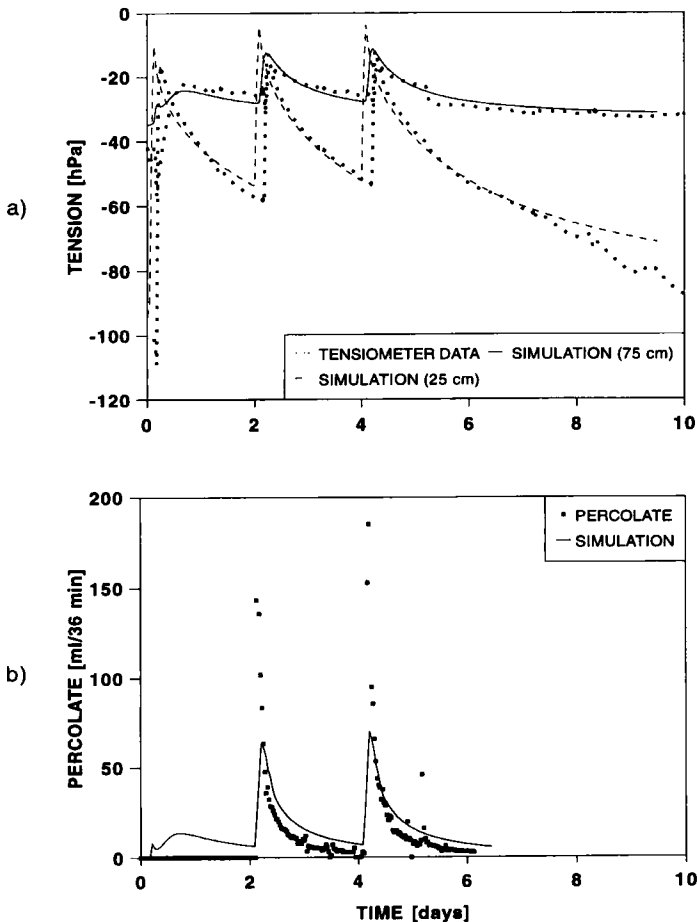


**Fig. 5.5:** Simulations and measurements of a) soil suctions (in depths of 25 and 75 cm) and b) percolating water for three irrigations.

Figures 5.5 a,b and 5.6 a,b show the results of a lysimeter study carried out by Stange et al. (1996). They extracted six undisturbed soil columns with a diameter of 30 cm and a height of 85 cm from a pit. The soil was loam with a silt content of about 80 %. In order to distinguish between soil matrix and macropore effects one of the soil columns was destroyed and repacked. Before the experiment the soil columns were saturated up to field capacity. In addition to the soil columns small soil samples were taken for analyzing the retention and the hydraulic conductivity.

All soil columns were irrigated three times with an intensity of 25 mm/h for one hour. Between subsequent irrigation periods the soil was covered to avoid evaporation. Each experiment lasted about ten days. The soil suction was measured in two different depths (25 and 75 cm) and the percolating water was measured every 36 minutes (cf. Fig. 5.5 a,b).

The tracer bromide was applied with the irrigation water. One hour before the first irrigation took place the two pesticides were applied. The pesticide Methabenzthiazuron (MBT) is strongly sorbing with a $K_d$-value of about 9.4 ml/g, Chlorotoluron (CT) is weakly sorbing with a $K_d$-value of about 2.2 ml/g. Figure 5.6 a shows the simulated and the measured bromide concentration in the disturbed soil column.
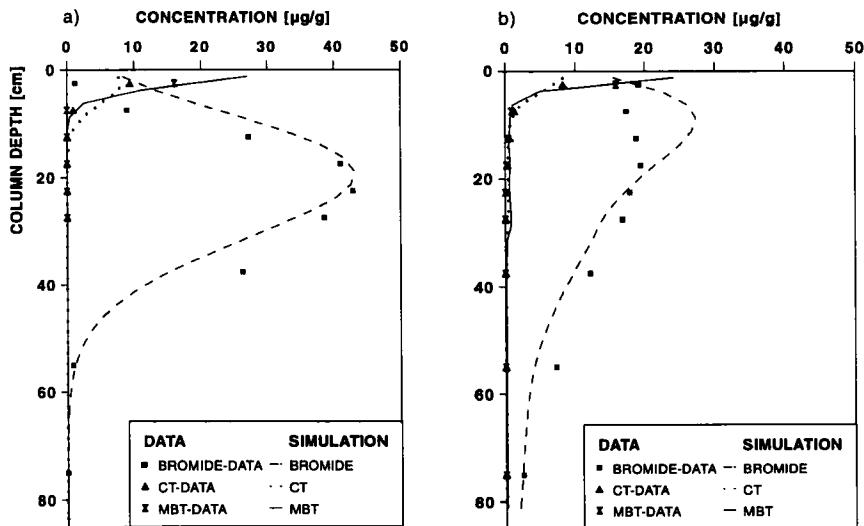


**Fig. 5.6:** Simulated and measured Bromide, Chlorotoluron (CT) and Methabenzthiazuron (MBT) concentrations 10 days after application a) in the disturbed and b) in an undisturbed soil column. Note that the pesticides are found in greater depth in the undisturbed column due to the bypass flow.

It demonstrates that the transport behavior can be described using the classical convection-dispersion equation. The profiles of bromide and pesticides are totally different in the undisturbed soil columns as it is shown in Fig. 5.6 b. Due to the bypass flow in the

macropores bromide as well as pesticides can be found in greater depths and in the percolating water (cf. Fig. 5.5 b). This was simulated by the model SIMULAT (Diekkrüger et al., 1996) in which the approaches discussed before are integrated. It has to be noticed that although many parameters were measured the parameters of the macropore model had to be calibrated. Nevertheless, a sensitivity analysis showed that the simulation results are mainly influenced by the choice of the boundary condition. The simulated profiles of solute concentration are only weakly influenced by the parameter of the macropore model.

## 5.2 Applications of the Convection Dispersion Equation

Notations

$c_t$        : total concentration $[M/L^3]$
$c$          : liquid phase concentration $[M/L^3]$
$g$          : gaseous phase concentration $[M/L^3]$
$S$          : solid phase concentration $[M/L^3]$
$\theta$     : volumetric water content $[L^3/L^3]$
$\vec{J}$    : flux density $[M/L^2/T]$
$\vec{q}$    : volumetric water flux density $[L/T]$
$Q$          : source and sink term $[M/L^3/T]$
$D_d$        : coefficient of molecular diffusion $[L^2/T]$
$D_m$        : coefficient of mechanical dispersion $[L^2/T]$
$D_h$        : coefficient of hydrodynamic dispersion $[L^2/T]$
$\alpha_L$   : longitudinal dispersivity $[L]$
$\alpha_T$   : transversal dispersivity $[L]$
$K_H$        : Henry constant $[1]$
$v_E$        : effective solute convection velocity $[L/T]$
$D_E$        : effective diffusion coefficient in soil $[L^2/T]$
$D_{air}$    : diffusion coefficient in air $[L^2/T]$
$D_g$        : diffusion coefficient in the gaseous phase of the soil $[L^2/T]$
$\kappa^g$   : transport coefficient across the soil-air boundary layer $[L^2/T]$
$d$          : thickness of the soil-air boundary layer $[L]$
$\phi$       : porosity $[L^3/L^3]$
$\rho$       : bulk density $[M/L^3]$
$\varepsilon$ : volumetric air content $[L^3/L^3]$

### 5.2.1 Derivation of the Convection Dispersion Equation

The starting point for the derivation of a transport equation for a chemical is the equation of mass conservation for the total concentration

$$\frac{\partial}{\partial t}(c_t) = -\nabla \cdot \vec{J}_t + Q \qquad (5.27)$$

with

$$c_t = \theta c + \rho S + \varepsilon g \qquad (5.28)$$

The mass balance equation has to be completed by an expression for the total flux $\vec{J}_t$. The total flux is composed of the following components:

i) Molecular diffusion in the liquid phase

The classical approach of diffusion theory is to relate a flux to a gradient, here the gradient of the concentration.

$$\vec{J}_D = - D_d \nabla c \qquad (5.29)$$

The negative sign determines the direction of the flux (from higher to lower concentration). The above relation only holds in an isotropic homogeneous medium. In general, $D_d$ is a tensor with space dependent components. In this section, only the case that $D_d$ is a scalar is treated. In the liquid phase of a porous medium, the coefficient of molecular diffusion depends in a nonlinear way upon the water content $\theta$. This is due to the fact that the microscale pathways in a porous medium are twisted. This effect is taken into account by an empirical tortuosity factor $\tau(\theta)$:

$$D_d(\theta) = \tau(\theta) D_0 \qquad (5.30)$$

where $D_0$ denotes the coefficient of molecular diffusion in water. Kemper and van Schaik (1968) proposed the empirical relationship

$$\tau(\theta) = a e^{b\theta} \qquad (5.31)$$

where $a$ and $b$ are positive constants. Millington and Quirk (1961) relate the tortuosity factor to the porosity $\phi$ in the following way:

$$\tau(\theta) = \frac{\theta^{10/3}}{\phi^2} \qquad (5.32)$$

ii) Molecular diffusion in the gaseous phase

$$\vec{J}_g = - D_g \nabla g \qquad (5.33)$$

Here, also the approach of Millington and Quirk (1961) is frequently used.

$$D_g = \frac{\varepsilon^{10/3}}{\phi^2} D_{air} \qquad (5.34)$$

iii) Convection

If there is water movement, the substance is in addition transported by convection giving rise to the flux

$$\vec{J}_c = \vec{q} c \qquad (5.35)$$

iv) Dispersion

The movement of the solute along with the water is associated with a further spread arising from the random motion of the water through the porous medium. I.e. streamlines are not straight lines but deviate in a random manner from the mean direction due to the random geometries of the pore space. This effect is called mechanical dispersion and is treated in analogy to molecular diffusion:

$$\vec{J}_m = - \theta D_m \nabla c \qquad (5.36)$$

In general, $D_m$ is a tensor. In the one dimensional case the following approach (cf. Ogata, 1970) is frequently used

$$D_m(q) = \alpha_L \frac{|q|}{\theta} \qquad (5.37)$$

assuming that $D_m$ increases linearly with pore water velocity. Since the diffusive and dispersive fluxes are both proportional to the gradient of $c$, they are combined to a single flux

$$\vec{J}_h = - \theta D_h \nabla c \qquad (5.38)$$

with

$$D_h(\theta, q) = \frac{D_d}{\theta} + D_m \qquad (5.39)$$

The coefficient (tensor resp.) $D_h(\theta, q)$ is referred to as the coefficient (tensor resp.) of hydrodynamic dispersion. Combining the mass conservation equation (Eq. (5.27)) with the fluxes yields the convection dispersion equation (CDE)

$$\frac{\partial}{\partial t}(\theta c + \rho S + \varepsilon g) = \nabla \cdot \left[ \theta D_h \nabla c + D_g \nabla g - \vec{q} c \right] + Q \qquad (5.40)$$

The term $Q$ summarizes all sources and sinks of the substance, i.e. all processes creating and consuming the substance.

### 5.2.2 Analytical Solutions in the One-Dimensional Case

Under steady state water flow conditions the one-dimensional version of the partial differential equation (Eq. (5.40)) is amenable to analytical solutions for a lot of boundary and initial conditions. A convenient method for solution is the Laplace transform technique, which was employed in chapter 3 for the solution of ordinary differential equations. In the

Laplace domain, ordinary differential equations are transformed to algebraic equations. In the case of partial differential equations the Laplace transform leads to ordinary differential equations in the Laplace domain. These are solved by use of the Laplace transformed initial and boundary conditions and transformed back into the time domain.

Let us consider now the following simple diffusion boundary value problem, which is a special case of the convection dispersion equation for $q = 0$ and $Q = 0$.

$$\frac{\partial c}{\partial t} = D \frac{\partial^2 c}{\partial x^2} \tag{5.41}$$

with boundary condition

$$c(x=0,t) = c_0 \qquad for \ t > 0$$

and initial condition

$$c(x,t=0) = 0 \qquad for \ x > 0$$

Laplace transform (cf. chapter 3) of the differential equation yields

$$L\left[\frac{\partial c}{\partial t}\right] = \int_0^\infty e^{-st} \frac{\partial c}{\partial t} dt = -c(0) + s\bar{c} \tag{5.42}$$

By interchanging the integral and differentiation operation one obtains

$$L\left[\frac{\partial^2}{\partial x^2} c(x,t)\right] = \frac{\partial^2}{\partial x^2} \int_0^\infty e^{-st} c(x,t) dt = \frac{d^2}{dx^2} \bar{c} \tag{5.43}$$

Taking into account that $c(x,t=0) = 0$ the resulting ordinary differential equation in the Laplace domain is derived as

$$D \frac{d^2}{dx^2} \bar{c} - s\bar{c} = 0 \tag{5.44}$$

Laplace transform of the boundary condition yields

$$L[c_0] = \int_0^\infty c_0 e^{-st} dt = \frac{c_0}{s} \tag{5.45}$$

The above ordinary differential equation is linear and second order. By trying the ansatz $e^{\lambda x}$ the general solution is found to be

$$\bar{c}(x) = A e^{-\lambda x} + B e^{\lambda x} \qquad with \quad \lambda = \sqrt{\frac{s}{D}} \tag{5.46}$$

Since the second term of the general solution increases exponentially with $x$, this term does not represent a physically meaningful solution and has to be omitted (setting $B = 0$) . The constant $A$ is determined by the Laplace transform of the boundary condition:

$$\bar{c}(x) = \frac{c_0 e^{\lambda x}}{s} \tag{5.47}$$

From the table of inverse Laplace transforms (cf. appendix A.1) one finally obtains the solution in the time domain as

$$c(x,t) = L^{-1}[\bar{c}] = C_0 \, erfc\left[\frac{x}{\sqrt{4Dt}}\right] \tag{5.48}$$

with $erfc(z) = 1 - erf(z)$, where $erf(z)$ denotes the errorfunction and $erfc(z)$ the errorfunction complement.

This function is defined by the integral (cf. section 2.2)

$$erf(z) = \frac{2}{\sqrt{\pi}} \int_0^z e^{-\xi^2} d\xi \tag{5.49}$$

Figure 5.7 shows a plot of Eq. (5.48) as a function of $x$ at several time points.
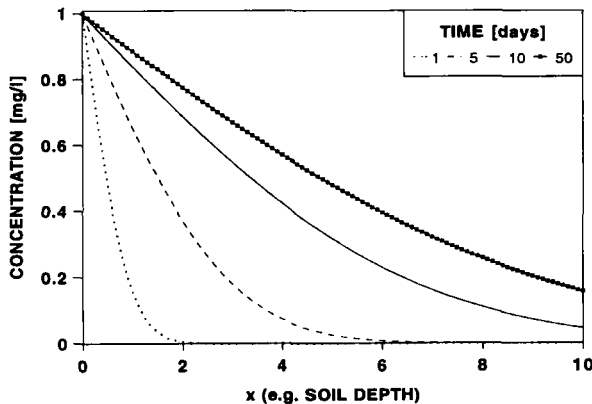


**Fig. 5.7:** Plot of Eq. (5.48) as a function of $x$ at the time points 1, 5, 10 and 50 days.

Let us now consider the same boundary value problem for $q > 0$:

$$\frac{\partial c}{\partial t} = D \frac{\partial^2 c}{\partial x^2} - v \frac{\partial c}{\partial x} \qquad with \quad v = \frac{q}{\theta} \tag{5.50}$$

with

$$c(x=0,t) = c_0 \qquad for \ t > 0$$

and initial condition

$$c(x,t=0) = 0 \qquad for \ x > 0$$

Following the procedure of the previous example the Laplace transform of Eq. (5.50) is obtained as

$$\frac{d^2 \bar{c}}{x^2} - \frac{v}{D} \frac{d\bar{c}}{dx} - \frac{s\bar{c}}{D} = 0 \tag{5.51}$$

The solution of this ordinary differential equation is

$$\bar{c}(x) = A e^{\lambda_1 x} + B e^{\lambda_2 x} \tag{5.52}$$

with

$$\lambda_{1/2} = \frac{v}{2D} \pm \sqrt{\frac{v^2}{4D^2} + \frac{s}{D}}$$

Since the positive root leads to a positive value of $\lambda$, the second term of Eq. (5.52) grows exponentially with increasing $x$ in contradiction to physical evidence. Therefore, only the negative root is taken and $B$ is set equal to zero. The remaining integration constant $A$ is determined via the Laplace transform of the initial condition

$$L[c_0] = \frac{c_0}{s} \tag{5.53}$$

yielding

$$\bar{c}(x) = \frac{c_0}{s} e^{\frac{v}{2D}x} \exp\left(-\sqrt{\frac{v^2}{4D^2} + \frac{s}{D}}x\right) \tag{5.54}$$

In the table of Laplace transforms in appendix A.1 one finds the inverse Laplace transform

$$L^{-1}\left[\frac{e^{-qx}}{s-\alpha}\right] \qquad with \quad q = \sqrt{\frac{s}{D}} \qquad (5.55)$$

which is, after a change of variables, appropriate for the solution of the above problem. Employing the transformation

$$\frac{z}{D} = \frac{v^2}{4D^2} + \frac{s}{D} \qquad with \qquad s = z - \alpha \quad and \quad \alpha = \frac{v^2}{4D} \qquad (5.56)$$

one obtains

$$\bar{c}(z) = \frac{c_0}{z-\alpha} e^{\frac{v}{2D}} \exp\left(-\sqrt{\frac{z}{D}}\, x\right) \qquad (5.57)$$

Remember that the inverse Laplace transform is the integral over the Gaussian plane

$$f(t) = \frac{1}{2\pi} \int\limits_{\sigma-i\infty}^{\sigma+i\infty} F(s) e^{st} ds$$

Therefore the substitution $s = z - \alpha$ transforms $e^{st}$ to $e^{zt} e^{-\alpha t}$. Application of the Laplace transform (Eq. (5.55) to Eq. (5.57)) yields

$$L^{-1}[\bar{c}(x)] = \frac{c_0}{2}\left[erfc\left(\frac{x-vt}{\sqrt{4Dt}}\right) + e^{\frac{v}{D}x} erfc\left(\frac{x+vt}{\sqrt{4Dt}}\right)\right] \qquad (5.58)$$

These two examples may suffice to get a feeling for classical analytical methods, which are "laborious but straightforward " (Lindstrom et al., 1967). Van Genuchten and Alves (1982) have published a collection of analytical solutions of the convection dispersion equation for various initial and boundary conditions.

## 5.2.3 Linear Sorption and First Order Degradation

Sorption and degradation is incorporated into Eq. (5.40) by simply adding two reaction terms on the right hand side. If degradation proceeds only in the liquid phase, the reaction rate has to be multiplied by the water content $\theta$. If degradation takes place at equal rates in both phases e.g. for radioactive decay, this factor is set equal to one. As usual, $S$ denotes the solid phase concentration. Assuming linear kinetics one obtains

$$\frac{\partial \theta c}{\partial t} + \frac{\partial \rho S}{\partial t} = \frac{\partial}{\partial x}\left[\theta D \frac{\partial}{\partial x} c\right] - \frac{\partial}{\partial x} q c - \theta k c \tag{5.59}$$

Under equilibrium conditions, $S = K_d\, c$, Eq. (5.59) is simplified to

$$R \frac{\partial c}{\partial t} = \frac{\partial}{\partial x}\left[D \frac{\partial}{\partial x} c\right] - \frac{\partial}{\partial x} v c - k c \tag{5.60}$$

with retardation factor (cf. chapter 3)

$$R = 1 + \frac{\rho}{\theta} K_d$$

Note that the linear decay term does not change the form of the basic convection dispersion equation. This is seen by the following argument. After division by $R$ the decay term becomes $-k/R\ c$. The equation is now multiplied by the factor $e^{(k/R)t}$. This is equivalent to the "trick" of the integrating factor previously applied to the solution of ordinary differential equations (cf. sections 2.1 and 3.1.2). After rearranging one obtains

$$e^{\frac{k}{R}t} \frac{\partial c}{\partial t} + \frac{k}{R} c e^{\frac{k}{R}t} = D^* \frac{\partial^2}{\partial x^2}\left(c e^{\frac{k}{R}t}\right) - \frac{\partial}{\partial x}\left(v^* c e^{\frac{k}{R}t}\right) \tag{5.61}$$

$$with \quad D^* = \frac{D}{R} \quad and \quad v^* = \frac{v}{R}$$

The left hand side of this equation may be written as

$$e^{\frac{k}{R}t} \frac{\partial c}{\partial t} + \frac{k}{R} c e^{\frac{k}{R}t} = \frac{\partial}{\partial t}\left(c e^{\frac{k}{R}t}\right)$$

Introducing now the variable $c^* = c\ e^{(k/R)t}$ one easily sees that the resulting partial differential equation in $c^*$ is identical to

$$\frac{\partial c^*}{\partial t} = D^* \frac{\partial^2 c^*}{\partial x^2} - v^* \frac{\partial c^*}{\partial x} \tag{5.62}$$

This is an important result: **the basic CDE is invariant with respect to linear equilibrium sorption and linear degradation.**

The following initial and boundary value problem describes a typical column outflow experiment.

$$
\left(- D \frac{\partial c}{\partial x} + v c \right)_{x=0} = \begin{cases} v c_0 & 0 < t \le t_0 \\ 0 & t > t_0 \end{cases} \tag{5.63a}
$$

$$
c(x,t) = 0 \qquad \textit{for } t = 0
$$

The analytical solution of this boundary value problem is (cf. van Genuchten and Alves, 1982)

$$
c(x,t) = \begin{cases} A(x,t) & 0 < t \le t_0 \\ A(x,t) - A(x,t - t_0) & t > t_0 \end{cases} \tag{5.63b}
$$

with

$$
A(x,t) = \frac{v}{v + U} e^{\frac{(v - U)x}{2D}} \, erfc\left[\frac{Rx - Ut}{2\sqrt{DRt}}\right]
$$

$$
+ \frac{v}{v - U} e^{\frac{(v + U)x}{2D}} \, erfc\left[\frac{Rx + Ut}{2\sqrt{DRt}}\right]
$$

$$
+ \frac{v^2}{2kD} e^{v\frac{x}{D} - k\frac{t}{R}} \, erfc\left[\frac{Rx + vt}{2\sqrt{DRt}}\right]
$$

$$
U = \sqrt{v^2 + 4kD}
$$

Figure 5.8 shows time courses of concentrations obtained by this equation for several combinations of the retardation factor $R$ and decay constant $k$. Note that the retardation causes longer half-lives of the substance due to the assumption that degradation only proceeds in the solute phase.

Thus far $c$ is always referred to as the volume averaged **resident concentration**. For the simulation of outflow experiments, e.g. the determination of a solute breakthrough curve from effluent measurements, **flux-averaged concentrations** have to be defined. These are the ratio of the solute and water fluxes. Flux averaged concentrations and resident concentrations are related via

$$
c_{flux} = c_{resident} - \frac{D}{v} \frac{\partial c_{resident}}{\partial x} \tag{5.64}
$$
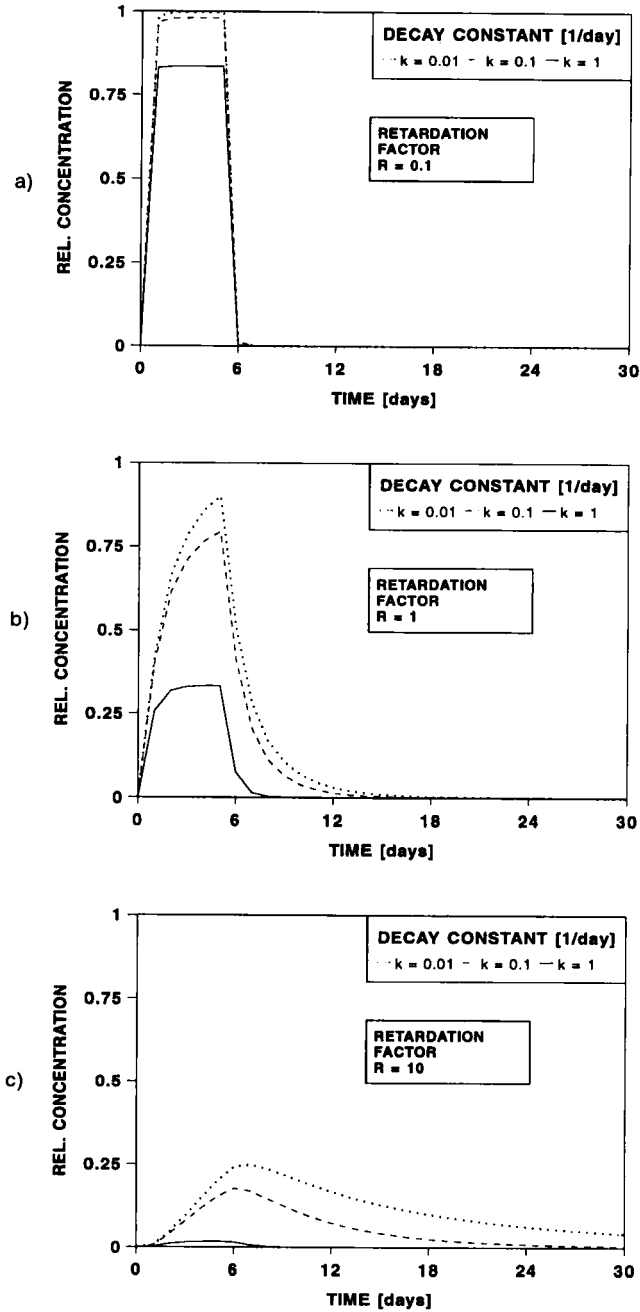
**Fig. 5.8:** Time courses of concentrations for a typical column outflow experiment. Shown are plots of the analytical solution referring to van Genuchten and Alves (1982) for combinations of the retardation factors a) $R = 0.01$, b) $R = 0.1$ and c) $R = 1$ and decay constants $k = 0.01$ $d^{-1}$, $0.1$ $d^{-1}$ and $1$ $d^{-1}$ in a soil depth of 1 cm.

## 5.2.4   Volatilization

Following the approach of Jury et al. (1983) volatilization is included into the model in a straightforward way by specifying boundary conditions at the soil surface. The model development is based on the general transport equation Eq. (5.40) in one-dimensional form as given by

$$\frac{\partial}{\partial t}(\theta c + \rho S + \varepsilon g) = \frac{\partial}{\partial z}\left[\theta D(\theta, q)\frac{\partial c}{\partial z} - qc + D_g \frac{\partial g}{\partial z}\right] \tag{5.65}$$

Assuming linear kinetic laws and equilibrium conditions the above mass balance equation can be written in only one variable. With

$$S = K_d c$$

$$g = K_H c$$

the total concentration $c_t$ is expressed as

$$c_t = R_s S = R_l c = R_g g \tag{5.66}$$

where

$$R_s = \rho + \frac{\theta}{K_d} + \varepsilon\frac{K_H}{K_d}$$

$$R_l = \rho K_d + \theta + \varepsilon K_H$$

$$R_g = \rho\frac{K_d}{K_H} + \frac{\theta}{K_H} + \varepsilon$$

Employing these relations, Eq. (5.65) may be written in terms of only one variable. It is convenient to formulate the equation in terms of the total concentration and then to derive the remaining concentrations via the equilibrium relations. Thus, Eq. (5.65) is written as

$$\frac{\partial c_t}{\partial t} = \frac{\partial}{\partial z}\left[D_E\frac{\partial c_t}{\partial z} - v_E c_t\right] - kc_t \tag{5.67}$$

in terms of the total concentration, where

$$D_E = \frac{K_H D_g + D_h}{R} \quad and \quad v_E = \frac{q}{R_l}$$

In this model the rate of decay is assumed to be identical in each phase.

Jury et al. (1983) solved the above equation for the following situation:

i)       The pesticide is uniformly incorporated to a depth $L$.
ii)      The soil column is homogeneous.
iii)     There exists a stagnant air boundary layer at the surface controlling the rate of volatilization.
iv)      The water flux is constant.

The initial conditions for this situation are

$$c_t(z,0) = \begin{cases} c_0 & 0 < z \le L \\ 0 & z > L \end{cases}$$

At the upper boundary, diffusion controlled volatilization occurs. Employing Fick's law of diffusion for transport across the stagnant boundary layer of thickness $d$, the diffusive flux is given by

$$J_V = -\kappa\big[g(0,t) - g(d,t)\big] \tag{5.68}$$

The diffusion coefficient for diffusion across the surface layer, $\kappa$, is related to the diffusion coefficient in air by

$$\kappa = \frac{D_{air}}{d} \tag{5.69}$$

The concentration at the upper surface of the boundary layer, $g(d,t)$, is assumed to be zero. Therefore, the flux boundary condition at $z = 0$ becomes

$$-D_E\frac{\partial c_t}{\partial z} + v_E c_t = -\kappa_E c_t \tag{5.70}$$

with

$$\kappa_E = \frac{\kappa}{R_g}$$

Note that loss by volatilization at the surface is equivalent to a first order decay process. As usual, the lower boundary condition is taken to be

$$\lim_{z \to \infty} c_t(z,t) = 0$$

The analytic solution of this boundary value problem is given by Jury et al. (1983) as

$$c_t(z,t) = \frac{c_0}{2} e^{-kt} \left\{ erfc\left(\frac{z - L - v_E t}{\sqrt{4 D_E t}}\right) - erfc\left(\frac{z - v_E t}{\sqrt{4 D_E t}}\right) \right.$$

$$+ \left(1 + \frac{v_E}{\kappa_E}\right) e^{\frac{v_E z}{D_E}} \left[ erfc\left(\frac{z + L + v_E t}{\sqrt{4 D_E t}}\right) - erfc\left(\frac{z + v_E t}{\sqrt{4 D_E t}}\right) \right]$$

$$+ \left(2 + \frac{v_E}{\kappa_E}\right) e^{\frac{\kappa_E (\kappa_E + v_E)t + (\kappa_E + v_E)z}{D_E}} \left[ erfc\left(\frac{z + (2\kappa_E + v_E)t}{\sqrt{4 D_E t}}\right) \right.$$

$$\left. \left. - e^{\frac{\kappa_E L}{D_E}} erfc\left(\frac{z + L + (2\kappa_E + v_E)t}{\sqrt{4 D_E t}}\right) \right] \right\} \qquad (5.71)$$

Thickness $d$ of the boundary layer determines the volatilization flux at the surface. According to Jury et al. (1983), $d$ may be related to the evaporation flux $E$ by

$$E = D_{WV} \frac{\rho_{WV}(0) - \rho_{WV}(d)}{\rho_{WL} d} \qquad (5.72)$$

The following assumptions are made:

i)  Water vapor is saturated at the surface: $\rho_{WV}(0) = \rho_S$.
ii) Evaporation occurs only during the day.

With $\rho_{WV}(d) = \rho_S R_H$ the thickness $d$ of the boundary layer is given as

$$d = \frac{1}{2} \frac{D_V^{air} \rho_S (1 - R_H)}{\rho_L E} \qquad (5.73)$$

where the factor 1/2 reflects assumption (ii). As shown in Figs. 5.9 a,b volatilization fluxes are strongly influenced by upward water flow. The figures also reveal the influence of physico-chemical properties of the chemicals on volatilization. Here, the behavior of 2,4-D and Lindane is compared for various evaporation rates. The adsorption affinity of Lindane is much higher than the affinity of 2,4-D. Therefore, 2,4-D is more mobile, whereas Lindane remains localized near the soil surface. This is demonstrated in Figs. 5.10 a,b, which show depth profiles obtained 30 days after application. From this it becomes plausible, that volatilization is the major loss pathway of Lindane and degradation is the major loss pathway of 2,4-D. The parameters of these calculations, which are taken from the paper of Jury et al. (1983), are given in Tab. 5.1.
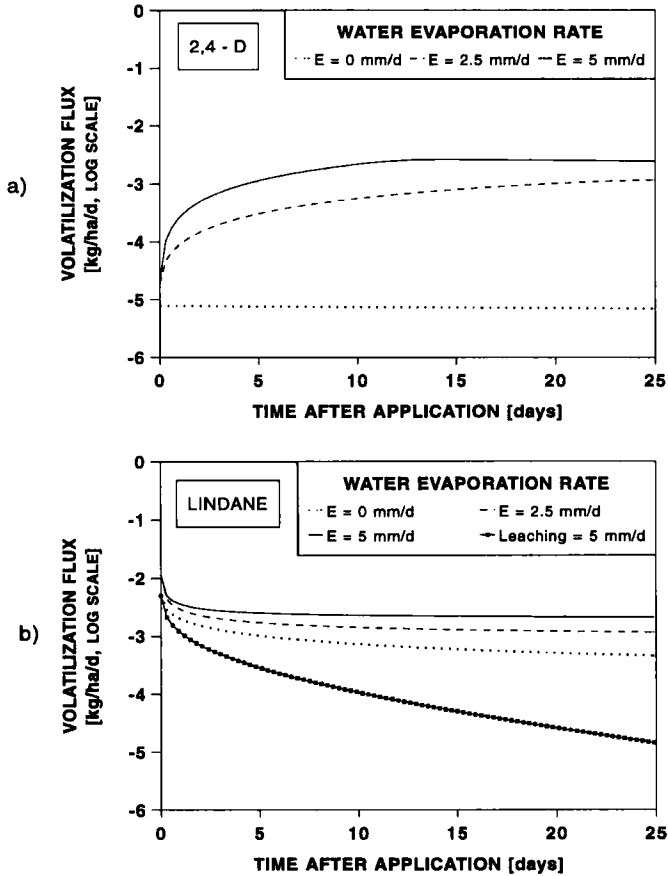
**Fig. 5.9:** Volatilization fluxes of a) 2,4-D and b) Lindane for various evaporation rates in semilogarithmical plots.

**Tab. 5.1:** Physical-chemical properties of Lindane and 2,4-D at 25°C.

| Property | Lindane | 2,4-D |
|---|---|---|
| Saturated vapor density, $C_G°$ [g/m$^3$] | $10^{-3}$ | $5 * 10^{-6}$ |
| Solubility, $C_L°$ [g/m$^3$] | 7.5 | 900 |
| Organic carbon partition coefficient, $K_{OC}$ [m$^3$/kg] | 1.3 +/- 16% | $2 * 10^{-2}$ +/- 7% |
| Degradation coefficient, μ [1/d] | $2.67 * 10^{-3}$ | $4.62 * 10^{-2}$ |
| Henry's constant, $K_H$ [1] | $1.33 * 10^{-4}$ | $5.5 * 10^{-9}$ |
| Half-life, $T_{1/2}$ [d] | 260 | 15 |
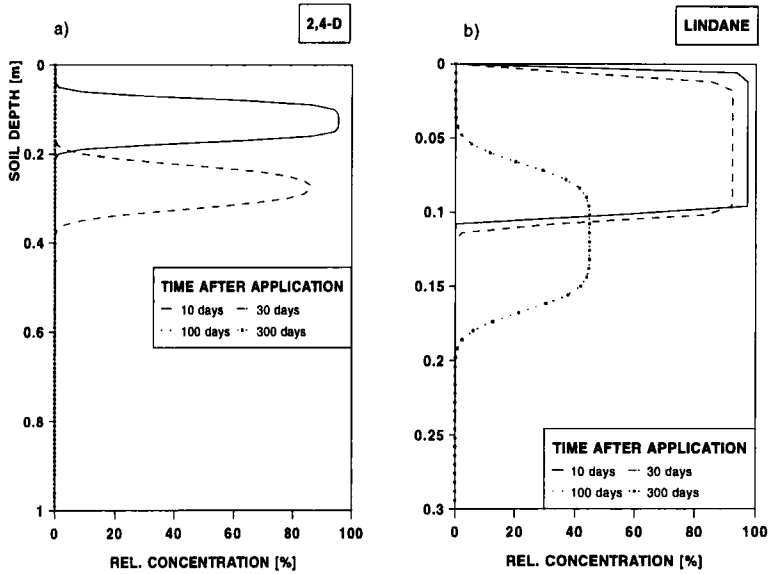
**Fig. 5.10:** Depth profiles of a) 2,4-D and b) Lindane obtained 10, 30, 100 and 300 days after application. Lindane remains near the soil surface. Therefore the maximal soil depths differ in both profiles.

## 5.2.5 Kinetic Adsorption

In the following, the kinetic equations derived in chapter 3 (cf. Eqs. (3.15 a,b)) are coupled to the transport equation. Neglecting the transport in the gaseous phase, one obtains in the non-equilibrium case a partial differential equation for the mobile liquid phase concentration and an ordinary differential equation for the solid phase concentration, which is immobile. Degradation may occur in the liquid phase and in the solid phase with rates $k_l$ and $k_S$ respectively.

$$\frac{\partial}{\partial t}(\theta c) = \frac{\partial}{\partial z}\left[\theta D(\theta,q)\frac{\partial c}{\partial z} - qc\right] - \alpha\left(K_d c - S\right) - \theta k_l c \tag{5.74}$$

$$\frac{\partial S}{\partial t} = \alpha\left(K_d c - S\right) - k_S S \tag{5.75}$$

For the case of two site adsorption with $S_1$ (equilibirum) and $S_2$ (kinetic) binding sites (cf. chapter 3, Eqs. (3.42 - 3.45) and Fig. 3.10) one obtains the equations

$$\frac{\partial c}{\partial t}(\theta + f\rho K_d) =$$
$$\frac{\partial}{\partial z}\left[\theta D(\theta,q)\frac{\partial c}{\partial z} - qc\right] - \theta k_l c - f\rho K_d k_{S1} c - \alpha\rho\left[(1 - f)K_d c - S_2\right] \tag{5.76}$$

$$\frac{\partial S_2}{\partial t} = \alpha\big[(1 - f)K_d c - S_2\big] - k_{S2} S_2 \tag{5.77}$$

Degradation takes place in the liquid phase ($k_l$) and in both solid phases ($k_{S1}$, $k_{S2}$). Total adsorption is then given as $S = S_1 + S_2$.

Van Genuchten and Wagenet (1989) give analytical solutions for an initially solute free soil column under a pulse input:

$$\left(- D\frac{\partial c}{\partial x} + vc\right)_{x=0} = \begin{cases} vc_0 & 0 < t \le t_0 \\ 0 & t > t_0 \end{cases} \tag{5.78}$$

$$c(z,t) = S_1(0,t) = S_2(0,t) = 0 \qquad \text{for } t = 0$$

It is convenient to write the equations in the mathematically most simple form for ease of representation and to facilitate the mathematical derivations. The "relatively straightforward but extremely lengthy" (van Genuchten and Wagenet, 1989) details of the derivation shall not be repeated here. The solutions are obtained by the Laplace transformation technique.

All distances are normalized with respect to a characteristic length $L$, which may be thought of as the depth of the soil profile under study. The equations are then written in dimensionless form as

$$\beta R\frac{\partial c_1}{\partial \tau} = \frac{1}{P}\frac{\partial^2 c_1}{\partial z^2} - \frac{\partial c_1}{\partial z} - \omega(c_1 - c_2) - \xi c_1 \tag{5.79}$$

$$(1 - \beta)R\frac{\partial c_2}{\partial \tau} = \omega(c_1 - c_2) - \eta c_2 \tag{5.80}$$

with

$$\tau = \frac{vt}{L}, \qquad\qquad z = \frac{x}{L}, \qquad\qquad P = \frac{vL}{D},$$

$$\beta = \frac{\theta + f\rho K_d}{\theta + \rho K_d} = \frac{R_m}{R}, \qquad R = 1 + \frac{\rho K_d}{\theta}, \qquad R_m = 1 + \frac{f\rho K_d}{\theta},$$

$$\omega = \frac{\alpha}{v}(1 - \beta)RL, \qquad c_1 = \frac{c}{c_0}, \qquad c_2 = \frac{S_2}{(1 - f)K_d c_0},$$

$$\xi = \frac{L}{q}\left(\theta k_l + f\rho K_d k_{S1}\right) \quad and \quad \eta = \frac{L}{q}(1 - f)\rho K_d k_{S2}$$

The solution of the above boundary value problem as given by van Genuchten and Wagenet (1989) is

$$c_1(z,\tau) = \begin{cases} c_a(z,\tau) & 0 < \tau \le \tau_0 \\ c_a(z,\tau) - c_a(z,\tau - \tau_0) & \tau > \tau_0 \end{cases} \tag{5.81}$$

$$c_2(z,\tau) = \begin{cases} c_b(z,\tau) & 0 < \tau \le \tau_0 \\ c_b(z,\tau) - c_b(z,\tau - \tau_0) & \tau > \tau_0 \end{cases} \tag{5.82}$$

where

$$c_a(z,\tau) = \int_o^\tau g(z,\zeta)\, J(a,b)\, d\zeta$$

and

$$c_b = \frac{\omega}{\omega + \eta} \int_o^\tau g(z,\zeta)\left[1 - J(a,b)\right] d\zeta$$

with

$$\tau_0 = \frac{v\, t_0}{L}$$

$J(a,b)$ is defined by the following integral

$$J(a,b) = 1 - e^{-b} \int_o^a e^{-\lambda} I_0\left[2\sqrt{b\lambda}\right] d\lambda \tag{5.83}$$

where $I_0$ denotes the modified Bessel function of order zero. The parameters $a$ and $b$ are given by

$$a = \frac{\omega^2 \tau}{(\omega + \eta)\beta R}$$

$$b = \frac{(\omega + \eta)(\tau - \zeta)}{(1 - \beta)R}$$

$g(z,\varsigma)$ is obtained from the analytical solution of the equation

$$\beta R \frac{\partial G}{\partial \tau} = \frac{1}{P} \frac{\partial^2 G}{\partial z^2} - \frac{\partial G}{\partial z} - \left(\xi + \frac{\omega \eta}{\omega + \eta}\right)G \qquad (5.84)$$

subject to the initial and boundary conditions given above as

$$g(z,\tau) = \frac{\partial G(z,\tau)}{\partial \tau}$$

For the case of volume-averaged resident concentrations the solution is obtained as

$$g(z,\tau) = \exp\left[-\left(\frac{\xi}{\beta R} + \frac{\omega \eta}{(\omega + \eta)\beta R}\right)\tau\right] \cdot$$

$$\left[\sqrt{\frac{P}{\pi \beta R}} \exp\left(-\frac{P(\beta R z - \tau)^2}{4\beta R \tau}\right) - \frac{P}{2\beta R} e^{Pz} erfc\left(\sqrt{\frac{P}{4\beta R \tau}}(\beta R z + \tau)\right)\right] \qquad (5.85a)$$

For flux averaged concentrations (cf. Eq. (5.64)), the expression for $g(z,\tau)$ becomes

$$g(z,\tau) = \exp\left[-\left(\frac{\xi}{\beta R} + \frac{\omega \eta}{(\omega + \eta)\beta R}\right)\tau\right]\frac{z}{\tau}\frac{P\beta R}{4\pi \tau} \exp\left[-\frac{P(\beta R z - \tau)^2}{4\beta R \tau}\right] \qquad (5.85b)$$

### 5.2.6   Two-Region Transport Model

Additional notations

$c_m$    : concentration in mobile phase [M/L$^3$]
$c_{im}$   : concentration in immobile phase [M/L$^3$]
$\theta_m$    : water content of mobile phase [L$^3$/L$^3$]
$\theta_{im}$   : water content of immobile phase [L$^3$/L$^3$]
$k_m$    : mobile phase degradation rate [1/T]
$k_{im}$   : immobile phase degradation rate [1/T]

In section 5.1.2 two-region models for water transport were derived partitioning the soil into regions of different mobility. The following model, which goes back to van Genuchten and Wagenet (1989), partitions the soil into mobile and totally immobile regions. If one assumes that diffusion of a solute between these regions occurs, the resulting equations are equivalent to those derived for kinetic adsorption.

Figure 5.11 illustrates the concept of the underlying two-region soil system.
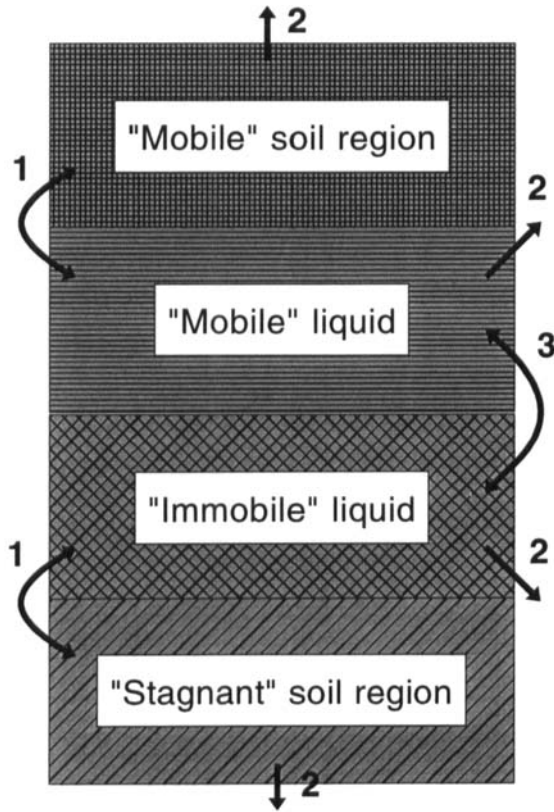


**Fig. 5.11:** Concept of the two-region soil system (van Genuchten and Wagenet, 1989); with: 1 = sorption, 2 = degradation, and 3 = solute exchange between mobile and immobile liquid regions.

The underlying assumptions are:

i)      Convective-dispersive transport occurs only in mobile liquid regions.
ii)     Exchange of a solute between mobile and immobile regions takes place by simple diffusion in analogy to a reversible linear first order reaction. This presumes that mobile and immobile regions are intermingled at a small scale.
iii)    Degradation rates are different in mobile and immobile regions due to $O_2$-availability or distribution of microbial activities.

Omitting sorption the transport equation for the mobile phase is given by

$$\frac{\partial(\theta_m c_m)}{\partial t} = \frac{\partial}{\partial z}\left[\theta_m D \frac{\partial}{\partial z}c_m - qc_m\right] - \alpha(c_m - c_{im}) - \theta_m k_m c_m \qquad (5.86)$$

For the stagnant region no convection or diffusion occurs. The mass balance equation can be simplified to

$$\frac{\partial \theta_{im} c_{im}}{\partial t} = \alpha(c_m - c_{im}) - \theta_{im} k_{im} c_{im} \tag{5.87}$$

These equations are identical in structure with the kinetic adsorption model described by Eqs. (5.74) and (5.75). Van Genuchten and Wagenet (1989) complete these equations by introducing sorption in the inter- and intra-aggregate regions. Written in dimensionless form they prove to be identical in structure with Eqs. (5.79) and (5.80).

## 5.2.7   Three-Dimensional Form of the Convection Dispersion Equation

The application range of the one-dimensional form of the convection dispersion equation is limited to substrates with only slight spatial heterogeneities. Lateral flow becomes important if the soil contains random three-dimensional structures giving rise to random parameter fields. In chapter 7 some examples will be given.

In a general three-dimensional situation the coefficient of hydrodynamic dispersion $D_m$ becomes a tensor. The anisotropy is due to the flow field of the water. This tensor has the general form (Bear, 1979):

$$D_{ij} = a_{ijkm} \frac{v_k v_m}{|\vec{v}|} f(Pe, \delta) \tag{5.88}$$

$f$ is a correction factor, which depends on the peclet number $Pe$ and on the pore geometry.

$$Pe = Peclet \ number = \frac{L\vec{v}}{D_d}$$

with $L$ being some characteristic length of the pores and $D_d$ being the coefficient of molecular diffusion of the solute in the considered liquid phase. In most application $f$ is set equal to 1. The coefficient $a_{ijkm}$ is element of a fourth rank tensor, the dispersivity tensor. In the isotropic case it reduces to

$$a_{ijkm} = \alpha_T \delta_{ij} \delta_{km} + \frac{\alpha_L - \alpha_T}{2} \left( \delta_{ik} \delta_{jm} + \delta_{im} \delta_{jk} \right) \tag{5.89}$$

where $\delta_{ij}$ denotes the Kronecker symbol and $\alpha_L$ and $\alpha_T$ are the longitudinal and transversal dispersivity. The elements of the tensor of hydrodynamic dispersion are thus given by

$$D_{ij} = \alpha_T |\vec{v}| \delta_{ij} + \left( \alpha_L - \alpha_T \right) \frac{v_i v_j}{|\vec{v}|} \tag{5.90}$$

In cartesian coordinates the above equation yields

$$D_{xx} = \frac{\alpha_T\left(v_y^2 + v_z^2\right) + \alpha_L v_x^2}{\vec{v}}$$

$$D_{xy} = D_{yx} = \frac{\left(\alpha_L - \alpha_T\right) v_x v_y}{\vec{v}}$$

$$D_{yy} = \frac{\alpha_T\left(v_x^2 + v_z^2\right) + \alpha_L v_y^2}{\vec{v}} \tag{5.91}$$

$$D_{xz} = D_{zx} = \frac{\left(\alpha_L - \alpha_T\right) v_x v_z}{\vec{v}}$$

$$D_{zz} = \frac{\alpha_T\left(v_x^2 + v_y^2\right) + \alpha_L v_z^2}{\vec{v}}$$

$$D_{yz} = D_{zy} = \frac{\left(\alpha_L - \alpha_T\right) v_y v_z}{\vec{v}}$$

At every point in space the components of the velocity field determine the elements of the dispersivity tensor.

## 5.3  Coupling of Nonlinear Kinetics and Transport

The art of obtaining analytical solutions of initial boundary value problems involving the convection dispersion equation coupled to sorption and degradation is confined to linear kinetic laws. Nonlinearities have two effects:

1. In all practically relevant cases no analytical solutions can be obtained.
2. Nonlinear kinetics may drastically change the transport behavior.

### 5.3.1  Nonlinear Sorption

Sorption may influence both transport behavior and degradation. This was shown in the preceding chapters (cf. sections 3.1 and 5.2.3). In the linear equilibrium case the effect of sorption is summarized in one parameter, the retardation factor $R$. This factor decreases the diffusion constant and the convective flux term. If first order degradation occurs only in the

liquid phase retardation reduces the rate constant without changing the linear character of the reaction. In the following, a CDE with a first order degradation term is coupled with nonlinear sorption omitting transport in the gaseous phase.

$$\frac{\partial}{\partial t}(\theta c + \rho S) = Lc - \theta kc \qquad \text{with}$$

$$Lc := \frac{\partial}{\partial z}\left[\theta D(\theta, q)\frac{\partial c}{\partial z} - qc\right]$$

(5.92)

For Langmuir binding the kinetic equation for $S$ is given by Eq. (3.86)

$$\frac{\partial S}{\partial t} = k_1(\beta - S)c - k_{-1}S \qquad (5.93)$$

Rao and Yessup (1989) relate the deviation of $S$ from its equilibrium value to the rate of change of $S$.

$$\frac{\partial S}{\partial t} = \alpha\left(\frac{\beta c}{c + K} - S\right) \qquad (5.94)$$

Both expressions become identical in the equilibrium case (cf. section 3.2.2.2).

For Freundlich binding a similar formulation is used by Rao and Yessup (1989).

$$\frac{\partial S}{\partial t} = \alpha(K_F c^{\kappa} - k_{-1}S) \qquad (5.95)$$

For small values of $c$ both functions are similar in shape for $n < 1$. At high concentrations, the Langmuir binding is bounded by a finite capacity $\beta$, which is not the case for Freundlich binding. Under equilibrium conditions the retardation factors (cf. section 3.2.2.1) are derived as

$$R_{Langmuir} = 1 + \frac{\rho}{\theta}\frac{\beta K}{(c + K)^2}$$

and

$$R_{Freundlich} = 1 + \frac{\rho}{\theta}K_F n c^{n-1}$$

For both binding laws the respective retardation factor decreases monotonically with increasing $c$. Note that Freundlich's approach becomes unrealistic for $c \to 0$ if $n < 1$.

The decreasing of retardation with concentration has drastic effects both on degradation and transport for substances with a small binding capacity. This is demonstrated in the following

simulations. Figure 5.12 a-c show three depth profiles of a substance obtained from initial *concentration values differing in order of magnitude. To allow comparison, the profiles are* all normalized with respect to initial concentration $c_0$.
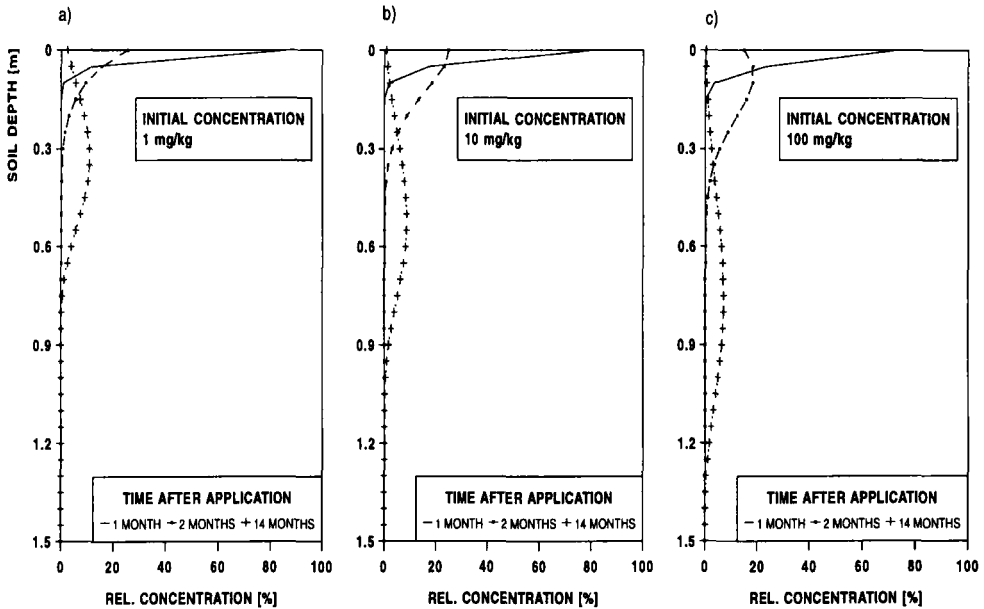


**Fig. 5.12:** Three depth profiles of a substance underlying Freundlich's adsorption. The initial concentrations differ in order of magnitude: a) initial concentration of 1 mg/kg, b) 10 mg/kg and c) 100 mg/kg. The profiles are normalized with respect to the initial concentration $c_0$.

## 5.3.2 Coupling Transport and Microbial Population Dynamics

Kinetic processes are formulated as ordinary differential equations, whereas transport processes are modeled by a set of partial differential equations. Under the assumption that the movement and transport of microorganisms is negligible compared to the movement of the substance, it is straightforward to extend the kinetic and population dynamic equations by a spatial component. Consider for instance the case that a herbicide is the primary carbon source of a microbial population. The state variables of Eq. (3.107) and (3.108)[1] are formally written as function of time and depth coordinate $z$:

---

[1] Notations are slightly changed, because $\alpha$ and $\beta$ are already used for binding.

$$m := m(t,z) \quad and \quad c := c(t,z)$$

and the differential equation (3.108) is completed by a transport part.

$$\frac{\partial c}{\partial t} = Lc - \frac{1}{\gamma} \frac{\mu c}{c + K_M} m(z,t) \tag{5.96}$$

$$\frac{\partial m}{\partial t} = \frac{\mu c}{c + K_M} m - \sigma m(1 + \alpha m) \tag{5.97}$$

For each differential soil layer $[z, z + dz]$ the ordinary differential equations have to be integrated along with the partial differential equations. Spatial variation of kinetic parameters can be taken into account by assigning a parameter set to each layer.

The combination of transport processes and populations dynamic models generates complex spatio-temporal patterns as is demonstrated by the following examples. The kinetic models of these examples are derived from experimental data. The parameters of the water retention curve refer to well defined soil types, e.g. loamy sand, and are derived from own data. However, the parameters related to leaching are only plausible guesses because of lack of appropriate data.

The above model equations are applied to 2,4-D. To allow for the long lag times observed, the first term of Eq. (5.97), the substrate response function, is multiplied by the substrate inhibition factor

$$f_I = \frac{1}{1 + \left(\dfrac{c}{K_I}\right)^\nu} \tag{5.98}$$

(cf. section 3.2.4.2). Figure 5.13 a,b show the fit of the solutions of the above equations for $L = 0$ (no transport, only kinetics) for a series of initial concentrations to data of 2,4-D obtained by Hurle (1982). For ease of presentation, data (cf. Fig. 5.13 a) and simulated time courses (cf. Fig. 5.13 b) are plotted separately. The model was fitted to the data of all experimental runs simultaneously by the boundary value method described in chapter 4.

The kinetic parameters thus obtained were then used in a simulation involving also nonstationary water transport. The parameters of the water retention curve refer to a loamy sand ($\theta_s=0.45$, $\theta_r=0.0$, $K_s=100$ cm/d, $\alpha=0.016$, $n=1.4$; cf. McVoy et al., 1995). Precipitation data were taken from an investigation site near Braunschweig in the year 1989 (cf. Fig. 5.14).
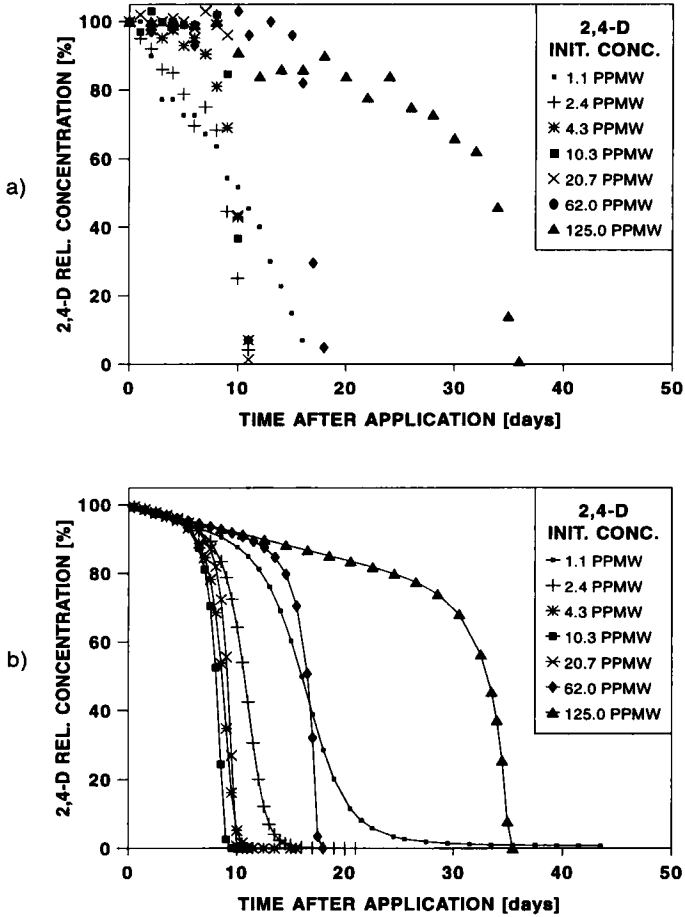
**Fig. 5.13:** a) Experimental data (Hurle, 1982) and b) simulated time courses of 2,4-D (Eqs. (5.96)-(5.98) with $L = 0$, i.e. no transport, only kinetics) for different initial concentrations.
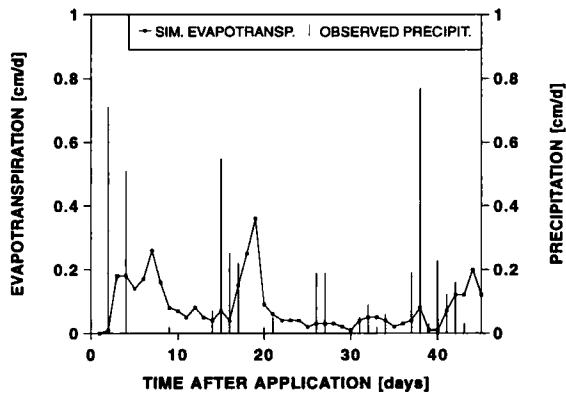


**Fig. 5.14:** Time course of measured precipitation and simulated evapotranspiration in the year 1989 at an investigation site near Braunschweig, used for simulation of herbicide transport in Figs. 5.13 a,b.
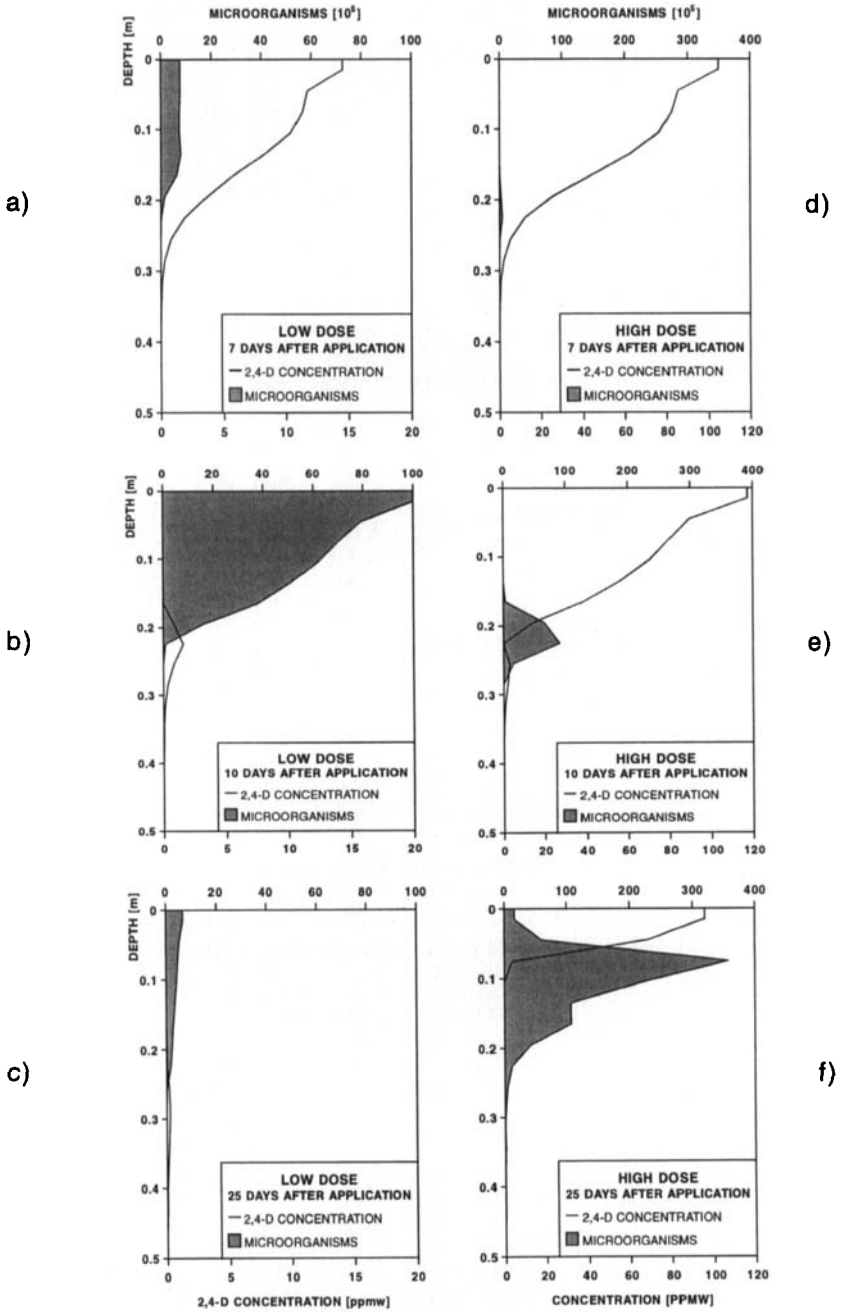
**Fig. 5.15:** Development in time of microbial activity and concentration profiles following the application of a-c) a "low" dose beyond and d-f) a "high" dose above the inhibition threshold of 2,4-D. a,d) 7, b,e) 10 and c,f) 25 days after application.

The spatio-temporal patterns generated by the application of low and high amounts of the pesticide were investigated. By "low" we mean a concentration below the inhibition threshold yielding pseudo first order kinetics. Figures 5.15 a-c show the development in time of the microbial activity profile and the concentration profile. Microbial activity builds up first in the upper layers and follows the movement of the pesticide. The time courses of concentration and activity in a depth of 10 cm are given in Fig. 5.16 a. The time lag is due to building up of the population.

This simple pattern is drastically changed, if a high dose is applied. Figures 5.15 d-f show the development of activity and concentration profiles: in the upper layers, concentrations are above the inhibition threshold suppressing the onset of microbial activity. In deeper layers, where concentrations are low due to diffusion and dispersion, microbial activity builds up first and decreases again. Only after a long lag phase, a zone of activity develops in the upper layer, too. This is also shown in the time courses of concentration and activity in a depth of 10 cm (cf. Fig. 5.16 b). Irregularities in the time course of concentrations are due to precipitation and evapotranspiration (cf. Fig. 5.14).
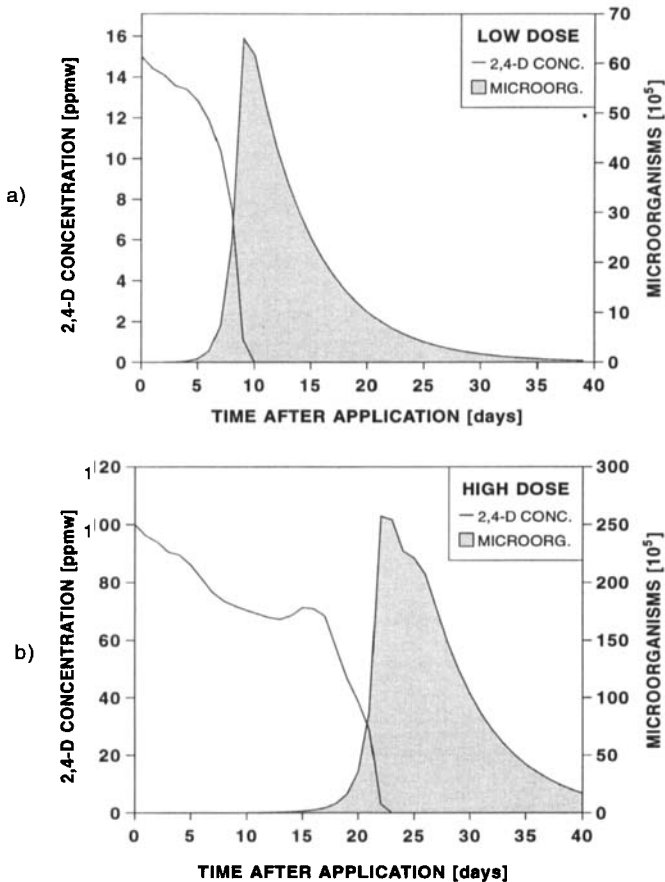


**Fig. 5.16:** Time courses of microbial activity and concentration in a depth of 10 cm following the application of a) a "low" and b) a "high" dose of 2,4-D.

The same model was applied to 1,3-D data (Vink et al., 1993). Figures 5.17 a,b show a fit of observed time courses of 1,3-D to the kinetic part of the model Eqs. (5.96) and (5.97). These laboratory experiments were carried out for four different initial concentrations (0.03, 0.3, 5 and 15 mg/kg). At the low initial concentrations the kinetic is apparent first order although in a log-plot deviation from the expected exponential decay can be detected. At high concentrations the nonlinearity of the system becomes obvious (cf. section 3.2.4). Both behaviors, apparent first order and nonlinear, can be described by one set of equations. Because microbial activity was not measured it is not possible to determine the microbial mortality rates.
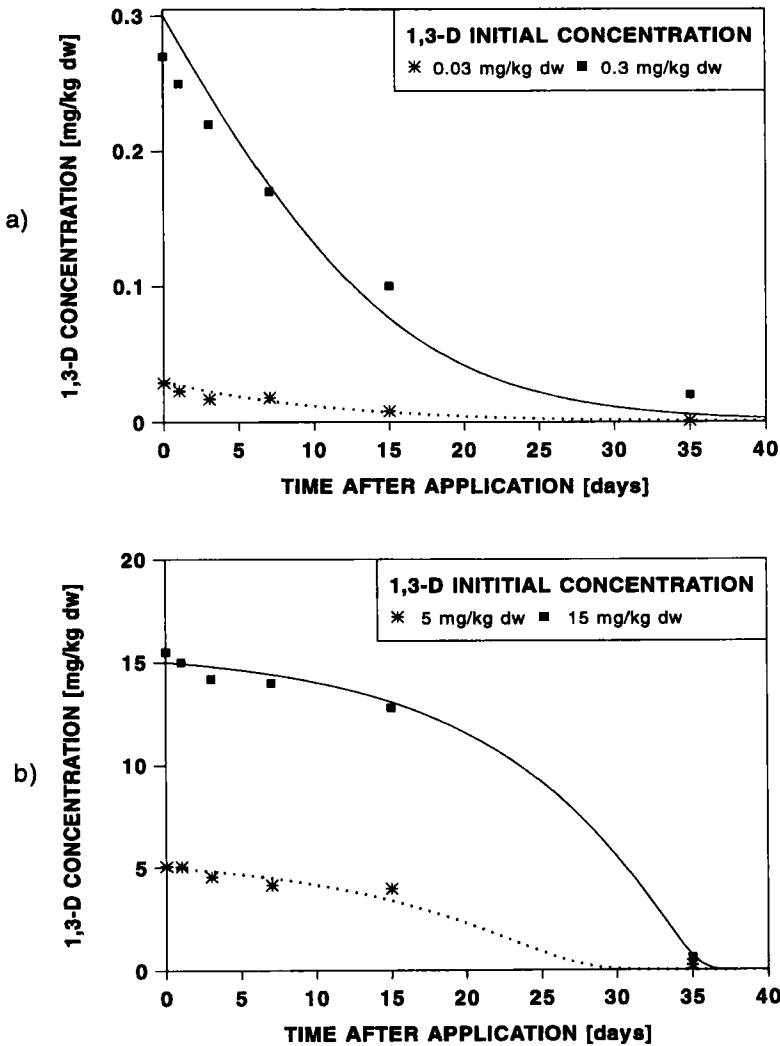


**Fig. 5.17:** Fit of observed time courses of 1,3-D concentration to the kinetic part of the model Eqs. (5.96) and (5.97) at 5°C and different initial concentrations. Note the different kinetic behavior at a) low and b) high concentrations.

The parameters were used to simulate transport and degradation of 1,3-D under field conditions (Vink et al., 1993). On the 14th of September 1990, 1,3-D was injected into the soil and the residues were monitored in different depths for a period of 40 days. Transport parameters were derived from measurements of water retention and hydraulic conductivity data. Figures 5.18 a,b show the time course of concentration and microbial densities for the depths of 10 and 30 cm. Figures 5.19 a-c show a comparison of modeled and measured concentration profiles together with the simulated microbial densities.

As explained before the microbial mortality rate could not be estimated from the laboratory experiments. Therefore, the simulated microbial activity does not decrease after reaching the maximum level. Considering that all parameters for this simulation of the field data were derived from laboratory experiments and that they were used in this simulation without further calibration the agreement between observed and forecasted values is not too bad.
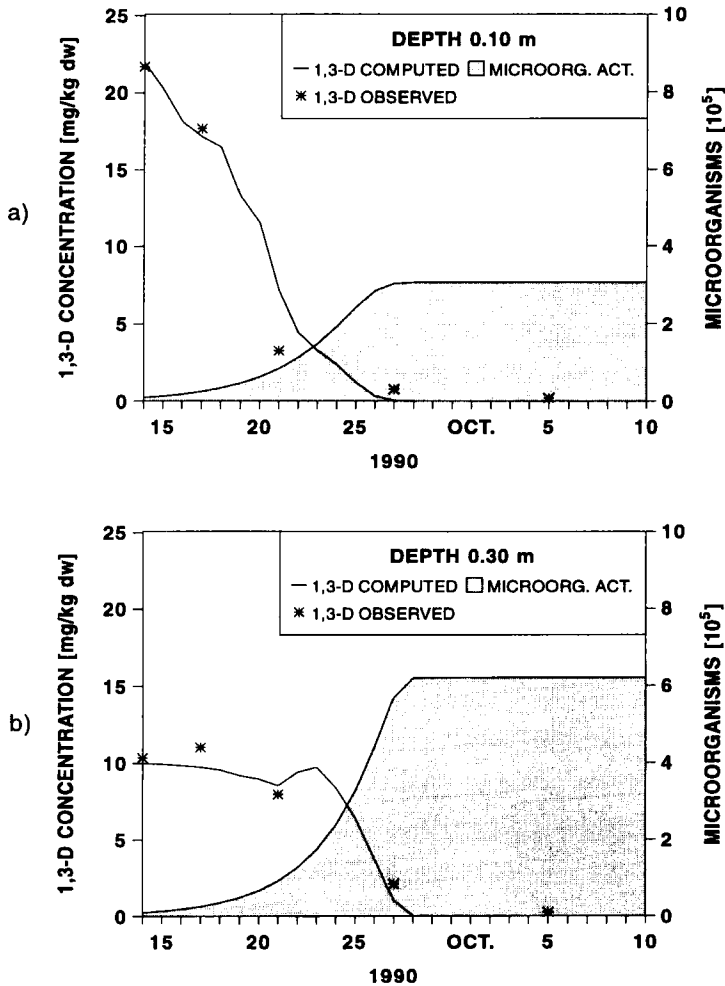


**Fig. 5.18:** Simulated time courses of 1,3-D concentrations and microbial activity at depths of a) 10 cm and b) 30 cm. Additionally, observed 1,3-D concentrations are shown.
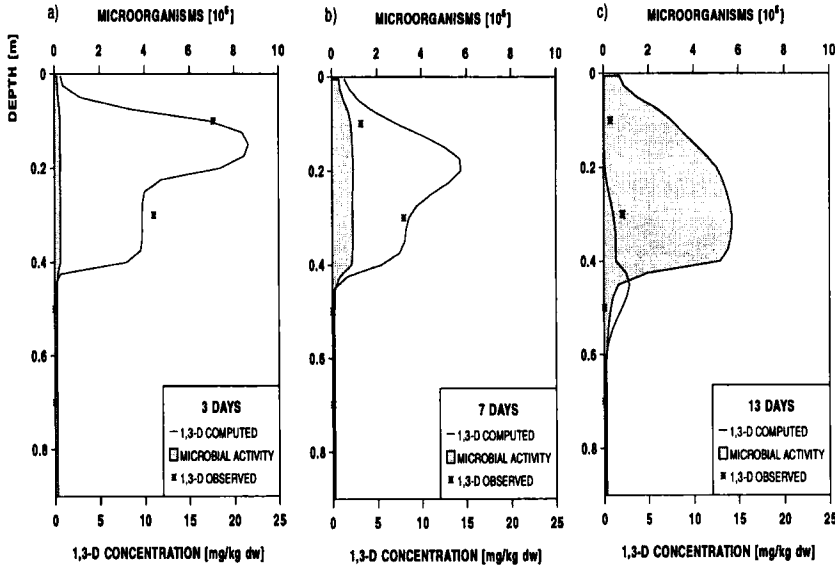
**Fig. 5.19:** Simulated and observed concentration profiles of 1,3-D and of microbial activity a) 3, b) 7 and c) 13 days after application (Vink et al., 1993).

### 5.3.3   Soil Aggregate Model

Notations

$c(r,t)$   : concentration of substrate [M/L$^3$]

$\bar{c}(t)$   : substrate consumed up to time $t$ [M/L$^3$]

$\bar{\bar{c}}(t)$   : total residual concentration in the aggregate at time $t$ [M/L$^3$]

$m(r,t)$   : microbial density [M/L$^3$]

$M(t)$   : total biomass within an aggregate [M/L$^3$]

$D$   : coefficient of molecular diffusion [L$^2$/T]

$\mu$   : maximum growth rate [1/T]

$d$   : microbial decay rate [1/T]

$\sigma$   : maintenance coefficient [M/M/T]

$\gamma$   : yield coefficient [1]

$K_M$   : Michaelis-Menten constant [M/L$^3$]

$J_I$   : intrinsic substrate release rate [M/L$^3$]

$F_{layer}$   : volume of the surface layer [L$^3$]

$F_{sphere}$ : volume of the aggregate [L$^3$]

$R$   : aggregate radius [L]

The models considered so far do not explicitly take into account soil structure. They consider the soil as represented by the parameters of water and matter transport such as the water conductivity or the coefficient of dispersion. The spatial variability of model parameters can

be regarded as realizations of a spatial random process. In a later chapter, it will be shown how to generate realizations from the underlying spatial stochastic process and to solve the transport equation over the random parameter field. In this section, we take a closer look to the soil structure. A structured soil consists of a distribution of aggregates differing in shape and size. Following the theory of Nietfeld et al. (1992), microbial growth and biodegradation mainly take place within an aggregate, a so called microhabitat. For computational ease, the case of spherical microhabitats is analyzed. The model concept, which is depicted in Fig. 5.20, involves a homogeneous spherical aggregate surrounded by a thin layer of substrate. As initial condition it is assumed that a minimal substrate concentration is homogeneously distributed within the aggregate maintaining a low level of microbial density.
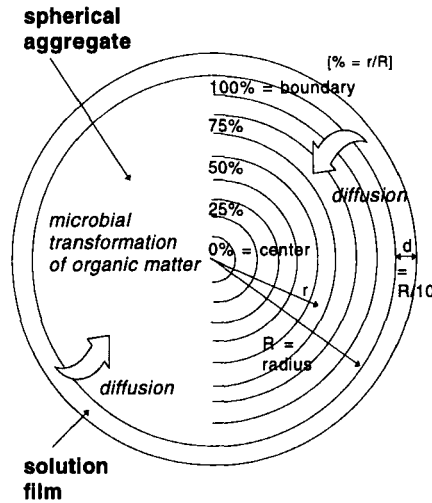


**Fig. 5.20:** Model concept referring to Nietfeld et al. (1992), additionally showing the subdivision of the aggregate into layers for computational use.

The basic mass balance equation for the substrate within an aggregate is given by

$$\frac{\partial c}{\partial t} = J_D + J_M + J_I \tag{5.99}$$

This equation couples the spread of the substrate due to diffusion (first term of the r.h.s) with the consumption by the growing microbial population (second term). It is necessary to introduce an intrinsic substrate release rate $J_I$ in order to maintain a low stationary microbial density. Because of the spherical symmetry the model is written in spherical coordinates. For isotropic aggregates only the radial component needs to be considered.

For the diffusion term one obtains

$$J_D = D\left(\frac{\partial^2 c}{\partial r^2} + \frac{2}{r}\frac{\partial c}{\partial r}\right) \tag{5.100}$$

The total consumption rate of the microorganisms is given by

$$J_M = - \frac{1}{\gamma} \frac{\mu c}{c + K_M} m \tag{5.101}$$

Microbial population dynamics is modeled by Eq. (5.97) omitting the density dependent part of the mortality rate.

$$\frac{\partial m}{\partial t} = \left[ \frac{\mu c}{c + K_M} - d \right] m$$

In the approach of Nietfeld et al. (1992), the second term in the bracket is interpreted as the rate of substrate utilization for maintenance respiration. In this case

$$d = \sigma \gamma$$

The intrinsic substrate release rate $J_I$ compensates for the maintenance respiration necessary to maintain the initial density $m_0$.

$$J_I = \sigma m_o \tag{5.102}$$

With all terms specified, Eq. (5.99) now reads

$$\frac{\partial c}{\partial t} = D \left( \frac{\partial^2 c}{\partial r^2} + \frac{2}{r} \frac{\partial c}{\partial r} \right) - \frac{1}{\gamma} \frac{\mu c}{c + K_M} m + \sigma m_0 \tag{5.103}$$

The boundary condition at the surface of the aggregate is derived from the mass balance equation: at each time $t$ the total amount of substrate which was initially present in the surface layer and within the aggregate partitions into the substrate present in the surface layer, the amount of substrate consumed by the microorganisms and into the remaining substrate within the aggregate.

$$F_{layer} c_0 + F_{sphere} c_{min} = F_{layer} c(R,t) + F_{sphere} \left[ \bar{c} + \tilde{c} \right] \tag{5.104}$$

The concentration necessary to maintain the initial population density, $m_0$, is given as the stationary solution of Eq. (5.97) neglecting the density dependent part of the mortality rate ($\beta \doteq 0$).

$$c_{min} = \frac{\gamma \sigma K_M}{\mu - \sigma \gamma} \tag{5.105}$$

The substrate consumed up to time $t$ is obtained by the integral

$$\tilde{c}(t) = \frac{3}{R^3} \int_0^R \int_0^t \left[ \frac{1}{\gamma} \frac{\mu c}{c + K_M} - J_I \right] r^2 dr d\tau \tag{5.106}$$

and the total amount of residual substrate within the aggregate is obtained by integration over

the sphere

$$\bar{c}(t) = \frac{3}{R^3} \int_0^R c(r,t) r^2 dr \tag{5.107}$$

The total biomass within the sphere is obtained in an analogous manner

$$M = \frac{3}{R^3} \int_0^R m(r,t) r^2 dr \tag{5.108}$$

Nietfeld et al. (1992) solved the above equations for the following initial and boundary conditions. The initial densities within the aggregate are assumed as homogeneous. The initial substrate density on the surface layer, $c_0$, is assumed to be greater than $c_{min}$. In the center of the aggregate, by symmetry reasons

$$\frac{\partial c}{\partial r}\Big|_{r=0} = 0$$
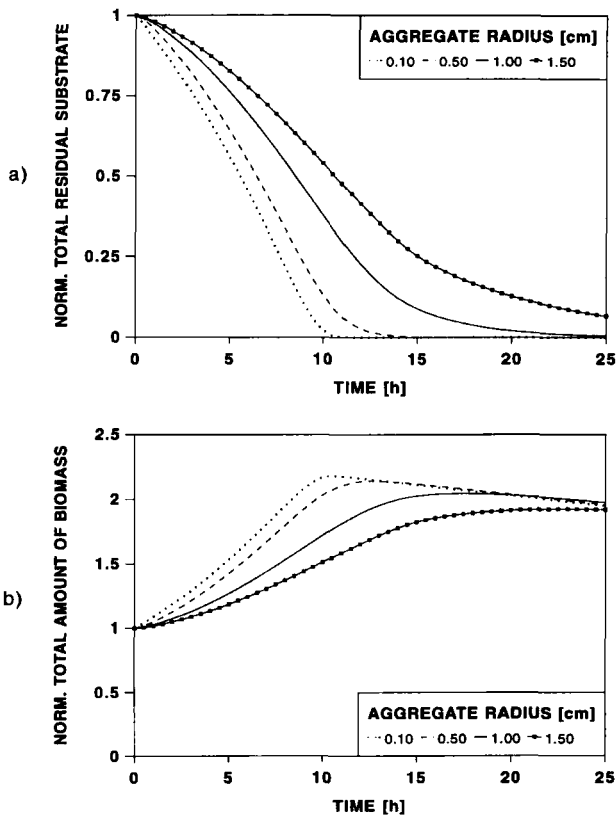


Fig. 5.21: a) Normalized total amount of residual substrate and b) normalized total amount of biomass in aggregates with radii $R = 0.1$ cm, $R = 0.5$ cm, $R = 1.0$ cm and $R = 1.5$ cm.

An important result of the simulations is the dependence of the kinetics on the geometry, i.e. the size of the aggregates. Figure 5.21 a,b show series of biomass growth curves and total concentration degradation curves for different aggregate radii. Since the substrate supply of the microorganisms within an aggregate is diffusion limited, degradation proceeds fastest in small aggregates. A closer view inside the aggregates indicates an effect of the aggregate size on the distribution of substrate and biomass as well. Figures 5.22 a,b and 5.23 a,b show the development in time of substrate concentration and total microbial density in distinct layers of aggregates ($R = 0.1$ cm and $R = 0.5$ cm).
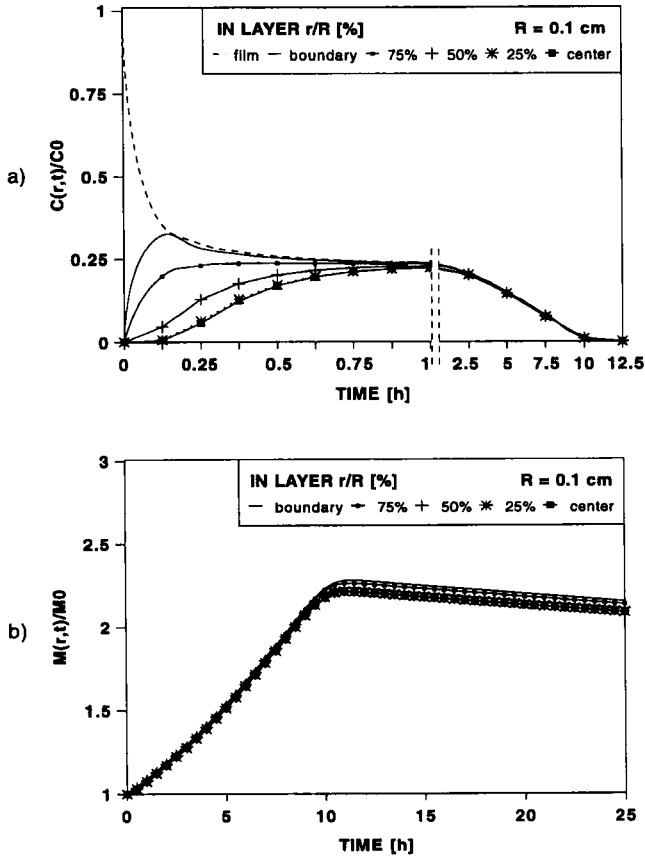


**Fig. 5.22:** a) Relative substrate concentration $c(r,t)$ and b) relative microbial density $m(r,t)$ in distinct layers of an aggregate with radius $R = 0.1$ cm.

Comparison of the kinetics obtained in small ($R < 0.2$ cm) and bigger aggregates leads to the following conclusions:

i) A fast balancing of substrate concentration takes place in the small aggregates (cf. Fig. 5.22 a). This ensures nearly identical microbial growth in all layers (cf. Fig. 5.22 b). The diffusion is fast in comparison to the process of substrate consumption. Consequently the diffusional limitation has no effect on the substrate supply.

ii) Microbial consumption in the outer parts of the larger aggregates is faster than the subsequent delivery of substrate by diffusion. Hence gradients of microbial density and substrate concentrations are built up inside of the larger aggregates ($R > 0.2$ cm) (cf. Fig. 5.23 a). Within aggregates of large size biomass growth is accelerated in the outer parts (cf. layers "boundary" and "75%" in Fig. 5.23 b). In contrast the biomass growth is hardly noticed in the inner regions (cf. layers "center" and "25%" in Fig. 5.23 b). The larger the size of the aggregate, the greater is this effect and the more important is the gradient.
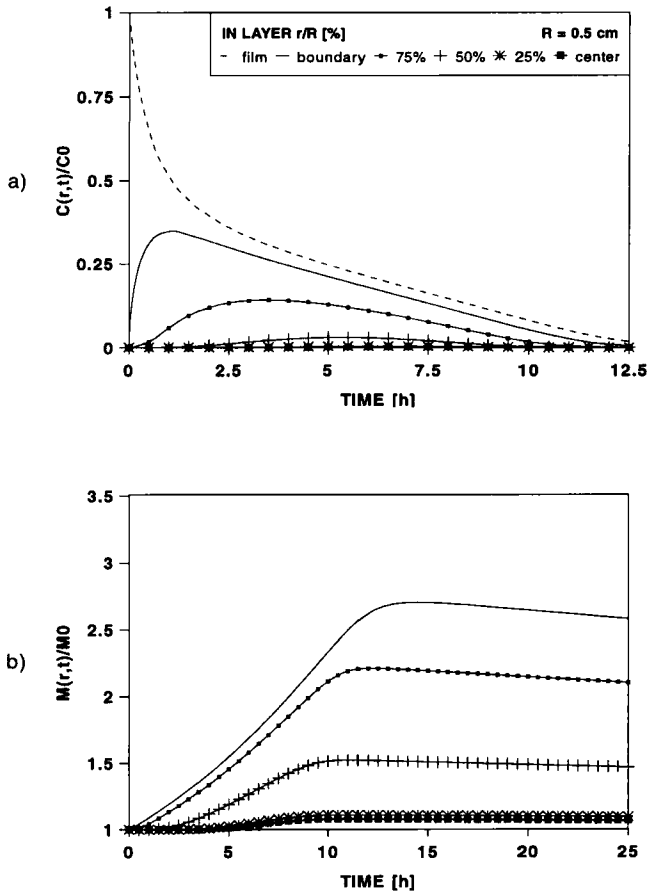


**Fig. 5.23:** a) Relative substrate concentration $c(r,t)$ and b) relative microbial density $m(r,t)$ in distinct layers of an aggregate with radius $R = 0.5$ cm.

Figures 5.24 a-c allow a different look at these geometric effects. They show the development in time of microbial density profiles of aggregates with radii $R = 0.1$ cm, $R = 0.5$ cm and $R = 1.0$ cm. In the case of large aggregates with radii $R > 1.0$ cm the transformation of substrate is limited to the outer spheres. Omitting the intrinsic substrate supply (term $J_I$ in Eq. (5.99)) the biomass decreases in the central regions of these aggregates (cf. Fig. 5.24 c).
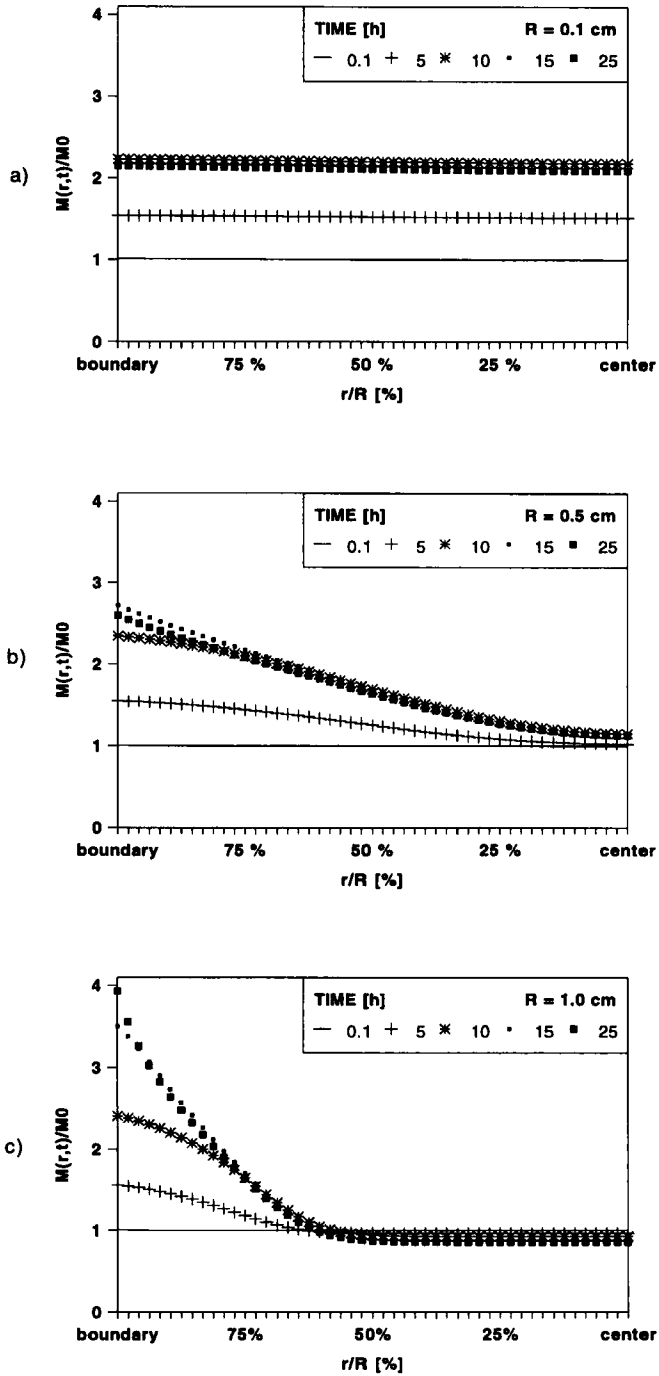
**Fig. 5.24:** Development in time of microbial density profiles. The aggregate radii are: a) $R = 0.1$ cm, b) $R = 0.5$ cm and c) $R = 1.0$ cm.

The corresponding concentration profiles are shown in Fig. 5.25 a-c. Simulations with larger microbial growth rates or lower effective diffusion coefficients lead to results which are similar to those obtained by using larger aggregate sizes.
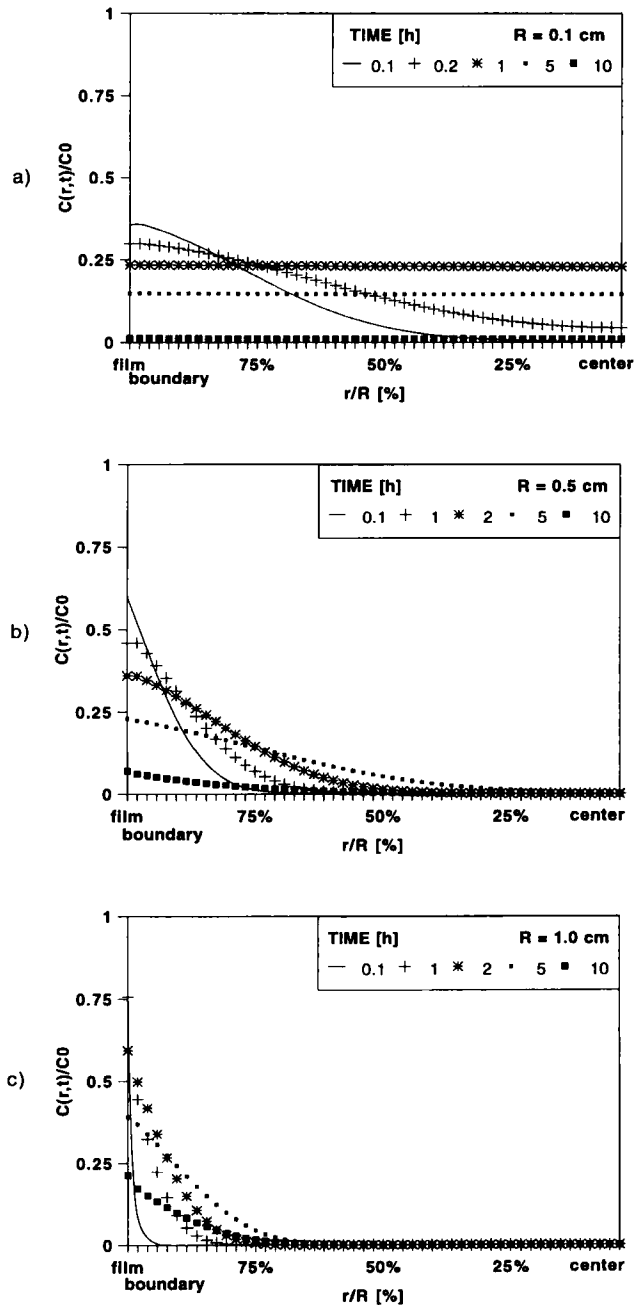


**Fig. 5.25:** Development in time of substrate concentration profiles in aggregates with radii: a) $R = 0.1$ cm, b) $R = 0.5$ cm and c) $R = 1.0$ cm.

**Statistical distribution of aggregate sizes:**

In a study of Schröder et al. (1996) the model of Nietfeld et al. (1992) was applied to an ensemble of aggregate sizes, that characterize natural soils. This procedure allows to find a representative aggregate size. It can be used in simulations that do not consider the effects induced by the geometry.

First the distribution of aggregate sizes has to be discretized to obtain a set of aggregates.

A "graphical" Monte-Carlo-Simulation was adapted: a random processor for uniformly distributed pseudo-random numbers generates $(x,y)$-coordinates, standardized to the maximum relative frequency and the boundaries of the distribution. The $x$-coordinate of each point lying inside the area of the distribution is accepted into the desired set of aggregate radii. Since each class of the distribution covers exactly that part of the whole "simulation area" corresponding to its relative frequency, the random variables thus generated are distributed according to the underlying density function (histogram). Figure 5.26 should help to clarify this procedure. It shows a distribution of aggregate sizes for a vertic cambisol (Pelosol) and the generated cluster of points.
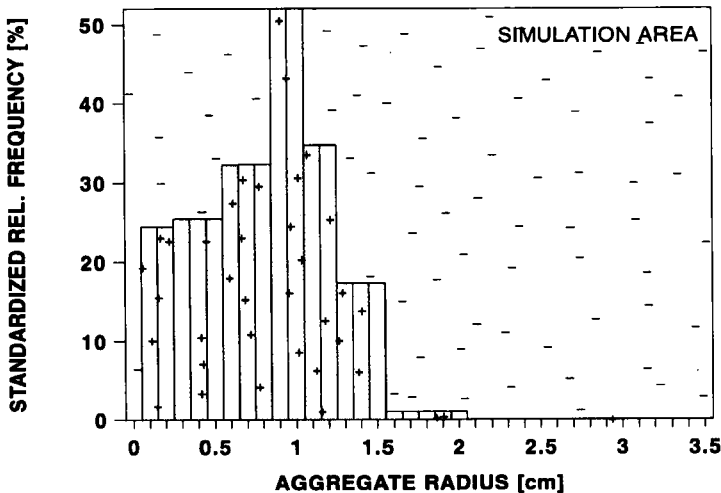


**Fig. 5.26:** Distribution of aggregate sizes for a vertic cambisol (Pelosol) (Albers and Hartmann, 1991) and the overlaid cluster of points generated by Monte-Carlo-Simulation. The $x$-coordinates of those points characterized by "+" are accepted in the data set, those of points characterized by "-" are not accepted.

The set of radii thus generated in turn generates a population of microbial growth curves and substrate depletion curves. Figure 5.27 a,b show as an example an ensemble of 10 000 aggregates. To represent the ensemble of curves, an effective radius has to be identified. The curve resulting from this parameter should be in a yet to be defined way closest to the mean of all curves. The problem to obtain so called effective parameters is treated in section 7.4.
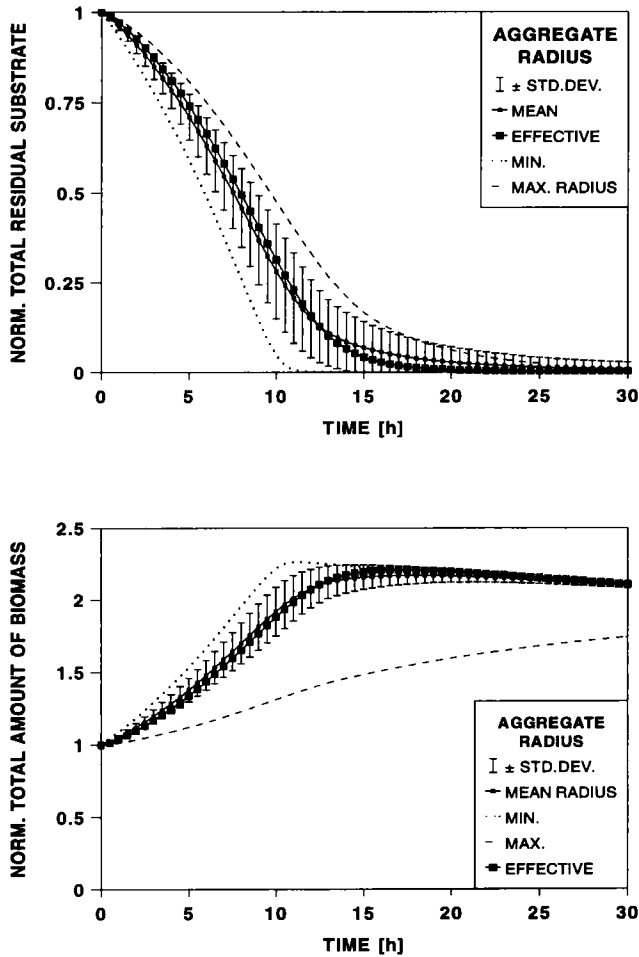
**Fig. 5.27:** Simulation result for a distribution of 10 000 aggregate sizes. Shown are mean and standard deviation of all curves as well as the curves referring to minimal, maximal and mean radius of the ensemble. The curves refer a) to the normalized total amounts of substrate and b) the normalized total amounts of biomass.

The analysis of a large number of realizations of Monte-Carlo-Simulation shows that the mean radius is quite suitable as representative radius.

## 5.3.4  Metabolites

Biodegradation of organic compounds leads to reaction products with modified physico-chemical properties. Frequently, degradation products have lower $K_d$-values than the parent substance. Most degradation experiments are confined to measurements of the parent substance. Because of analytical difficulties only few studies (Bahadir and Kreuzig, 1994)

also consider the kinetics and sorption properties of metabolites. However, metabolites cannot be neglected in the assessment of the environmental impact of a chemical. As an example a system with a parent substance and one metabolite is considered.

$$\frac{\partial}{\partial t}(\theta c_1 + \rho S_1) = L_1 c_1 - \theta k_1 c_1 \tag{5.109}$$

$$\frac{\partial}{\partial t}(\theta c_2 + \rho S_2) = L_2 c_2 - f \theta k_1 c_1 - \theta k_2 c_2 \tag{5.110}$$

with

$$L_i c_i := \frac{\partial}{\partial z}\left[\theta D_i(\theta,q)\frac{\partial c_i}{\partial z} - q c_i\right]$$

$f$ denotes that fraction of the parent substance, which goes into the metabolite $c_2$. As an example, Fenpropimorph (FPM) and its metabolite Fenpropimorphic acid (FPMA) is considered. Because of the higher polarity of the metabolite, $K_d$-values of the parent substance and metabolite differ considerably. Bahadir (1993) measured values of 128.5 ml/g for FPM and 1.6 ml/g for FPMA in a loamy soil and 50.5 ml/g and 0.4 ml/g in a sandy soil. Figures 5.28 a,b show the development in time of simulated depth profiles of FPM and FPMA respectively.
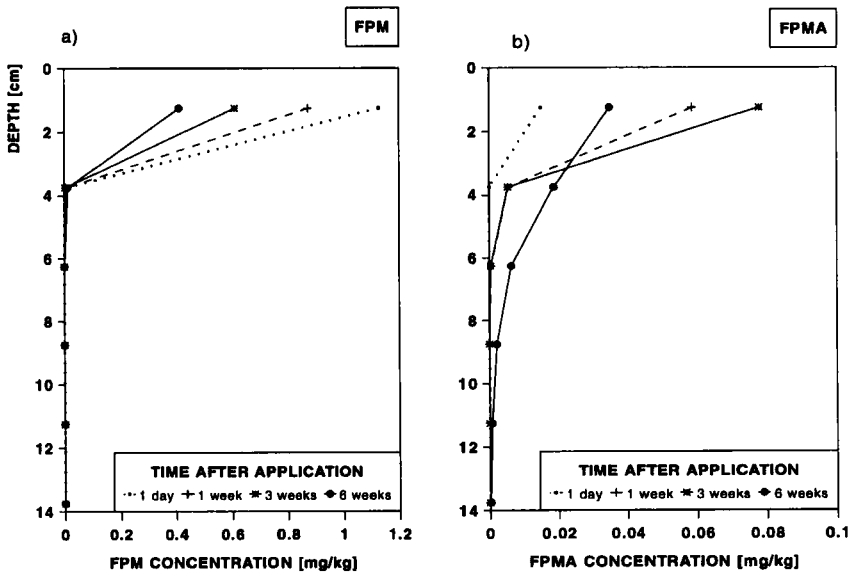


**Fig. 5.28:** Depth profiles of a) FPM and b) its metabolite FPMA 1 day, resp. 1, 3 and 6 weeks after application of FPM.

# 5.4   Soil Temperature Fields

## 5.4.1   The Heat Conduction Equation

Notations:

$\vec{q}_h$    : heat flux [W/m$^2$]
$\vec{q}_d$    : heat flux due to diffusion [W/m$^2$]
$\vec{q}_c$    : heat flux due to convection [W/m$^2$]
$\vec{q}_w$    : water flux [m/s]
$\lambda$    : thermal conductivity [W/m/K]
$T$    : temperature [°C]
$z$    : depth [m]
$c_w$    : specific heat capacity of water [J/g/K]
$c_h$    : volumetric heat capacity [J/m$^3$/K]
$c_s$    : heat capacity of solids [J/m$^3$/K]
$c_w$    : heat capacity of water [J/m$^3$/K]
$c_a$    : heat capacity of air [J/m$^3$/K]
$c_o$    : heat capacity of organic material [J/m$^3$/K]
$\phi_s$    : volume fraction of solids $= \phi_d + \phi_m$ [m$^3$/m$^3$]
$\phi_d$    : volume fraction of quartz [m$^3$/m$^3$]
$\phi_m$    : volume fraction of other minerals [m$^3$/m$^3$]
$\theta$    : water content [m$^3$/m$^3$]
$\phi_a$    : volume fraction of air [m$^3$/m$^3$]
$\phi_o$    : volume fraction of organic material [m$^3$/m$^3$]
$T_m$    : mean daily temperature [°C]
$T_a$    : amplitude of the mean daily temperature [°C]
$\omega$    : $(2\,\pi)$ / (time period) [1/d]
$T_{mean}$  : mean annual temperature [°C]
$T_{ampl}$  : max. amplitude at the lower boundary [°C]
$t_0$    : time at which $T = T_{mean}$ [d]

The heat conduction equation is derived in a similar manner as the convection dispersion equation. Starting point is the continuity equation for heat flow

$$c_h \frac{\partial T}{\partial t} + \nabla \cdot \vec{q}_h = 0 \tag{5.111}$$

stating that the rate of temperature change in a control volume equals the net gain of heat per unit volume plus sinks or sources within this volume. In direct analogy with Fick's law of diffusion the heat flow is related to the temperature gradient by

$$\vec{q}_h = -\lambda \nabla T \tag{5.112}$$

If there is in addition a flow of water in the soil, heat is also transported by conduction

$$\vec{q}_c = c_w \vec{q}_w T \tag{5.113}$$

Combining the continuity equation for heat with the flow equations yields the heat conduction equation

$$c_h \frac{\partial T}{\partial t} = \nabla \cdot \left( \lambda \nabla T - c_w \vec{q}_w T \right) \tag{5.114}$$

Note that this equation is only valid if frost and thaw of ice are neglected.

**Boundary Conditions**

**Upper boundary**

At the upper boundary the soil surface temperature depends on the air temperature and the radiative and latent heat transfer. The surface temperature equals the air temperature when the radiative and latent heat transfer can be neglected.

In cases where the heat transfer can not be neglected the radiative heat transfer can be calculated considering global radiation, longwave sky irradiance, the surface albedo and the air temperature. The latent heat flux can be computed by evaporation models like the Penman-Monteith equation (Monteith, 1976).

**Lower boundary**

At the lower boundary the annual fluctuation of temperature with time can be described by a sinusoidal cycle

$$T(t) = T_{mean} + T_{ampl} \sin\left( \frac{2\pi(t - t_0)}{365.25} \right) \tag{5.115}$$

This assumes that the daily variation of soil temperature at the lower boundary can be neglected in the chosen depth. Analytic solutions of the one-dimensional version of Eq. (5.111) can be obtained for simplified boundary conditions and constant soil properties. Assuming that the thermal conductivity and the volumetric heat capacity are constant with depth and the upper boundary condition is given by

$$T(0,t) = T_m + T_a \sin(\omega t) \tag{5.116}$$

then the boundary value problem has the analytical solution

$$T(z,t) = T_m + T_a e^{(-z/z_d)} \sin\left( \omega - z/z_d \right) \tag{5.117}$$

$$z_d = \sqrt{\frac{2\lambda}{\omega c_h}}$$

Figures 5.29 a-c show the time courses of daily temperatures at different depths computed by the numerical solution of Eq. (5.114) during a vegetation period. The soil properties necessary for the simulation model were not calibrated but estimated using approach of McInnes (1981) which will be discussed below. Because this simulation is a forecast and no calibration was performed the results are satisfactory.
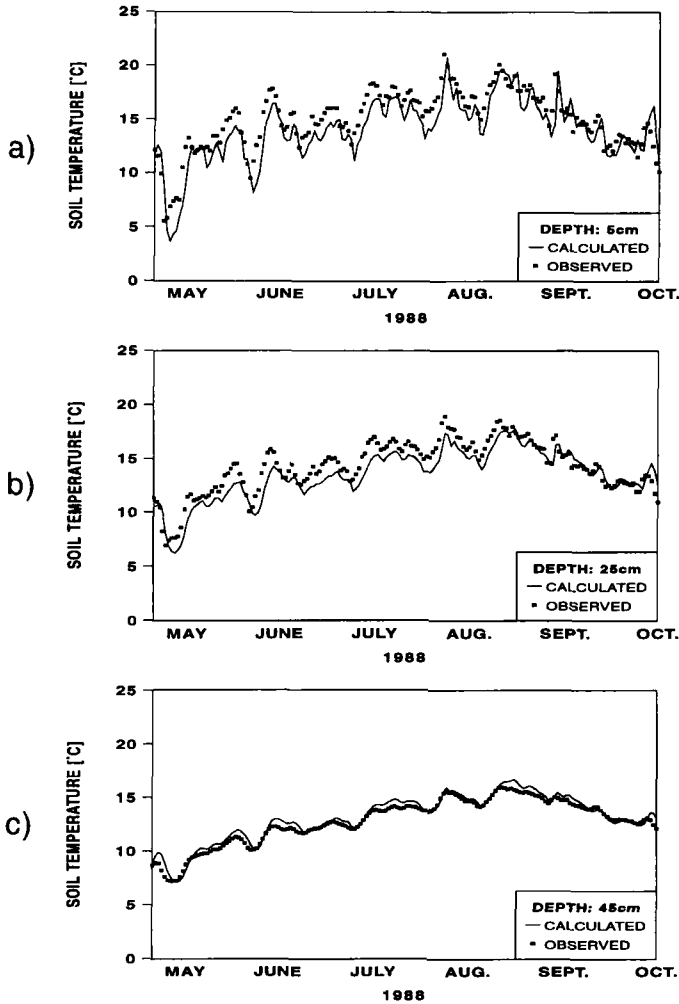


**Fig. 5.29:** Fig. 5.29: Comparison of simulated and measured daily temperatures for the depths of a) 5 cm, b) 25 cm and c) 50 cm obtained by the numerical solution of Eq. (5.114).

## Soil properties

The parameter of the heat flow model depend on soil constituents and water content. The volumetric heat capacity of the soils is the sum of all soil constitutents

$$c_h = c_s \phi_s + c_w \theta + c_a \phi_a + c_o \phi_o \tag{5.118}$$

Typical values for heat capacity and for thermal conductivity are given in Tab. 5.2 for different soil constituents. Ignoring the contribution of the soil air and assuming similar properties for mineral and organic material Eq. (5.118) reduces to:

$$c_h = c_s \left(1 - \theta_s\right) + c_w \theta \tag{5.119}$$

The non-linear relationship between the thermal conductivity and water content can be described by the empirical approach of McInnes (1981):

$$\lambda = A + B\theta - (A - D)e^{-(C\theta)^E} \tag{5.120}$$

in which

$$A = \frac{0.57 + 1.73\phi_d + 0.93\phi_m}{1 - 0.74\phi_d - 0.49\phi_m} - 2.8\phi_s (1 - \phi_s)$$

$$B = 2.8 \phi_s \theta$$

$$C = 1 + 2.6\sqrt{m_c}$$

$$D = 0.03 + 0.7\phi_s^2$$

$$E = 4.0$$

and $m_c$ denotes the clay fraction.

For mineral soils with a particle density ($\rho$) of 2.65 g/cm$^3$ the following simplification holds

$$B = 1.06\rho\theta$$

$$D = 0.03 + 0.1\rho^2$$

If the quartz fraction can be neglected the parameter $A$ reduces to

$$A = 0.65 - 0.78\rho + 0.60\rho^2$$

**Tab. 5.2:** Thermal properties of soil materials (Campbell, 1985).

|  | **Density** <br> $[Mg/m^3]$ | **Specific Heat** <br> $[J/g/K]$ | **Thermal Conductivity** <br> $[W/m/K]$ | **Volumetric Specific Heat** <br> $[MJ/m^3/K]$ |
|---|---|---|---|---|
| **Quartz** | 2.66 | 0.80 | 8.80 | 2.13 |
| **Clay minerals** | 2.65 | 0.90 | 2.92 | 2.39 |
| **Organic matter** | 1.30 | 1.92 | 0.25 | 2.50 |
| **Water** | 1.00 | 4.18 | 0.57 | 4.18 |
| **Air (20°C)** | 0.0012 | 1.01 | 0.025 | 0.0012 |
| **Ice** | 0.92 | 1.88 | 2.18 | 1.73 |

## 5.4.2   Influence of the Temperature Field on Degradation and Transport

Temperature influences degradation and transport in several ways. In the first place, it directly affects degradation rates as described in detail in section 3.4. In addition, the parameters of the water transport equation are temperature dependent. This effect is neglected here. However, the effect on degradation rates indirectly influences the leaching behavior. Assuming, that the microbial activity is related to the $C_{org}$-profile of the soil, degradation decreases with depth. That part of the substance, which will have surpassed the reactive zone will undergo only chemical transformation and will eventually reach the groundwater. Thus the amount of substance reaching the aquifer is influenced by the temperature regime in the upper soil. This effect is simuated by the following scenarios: a herbicide is applied under two different temperature regimes (cf. Fig. 5.30 a) all other factors held constant. In Fig. 5.30 b the breakthrough curves under the active soil horizon are shown. Since the area under the breakthrough curve is a measure of the total amount of substance it is evident from these figures that under lower temperatures more subtance is transported to the groundwater.

It should be kept in mind, however, that this is only a scenario invented to demonstrate the effect. In a real situation, other processes such as volatilazation losses at the surface have also to be considered.
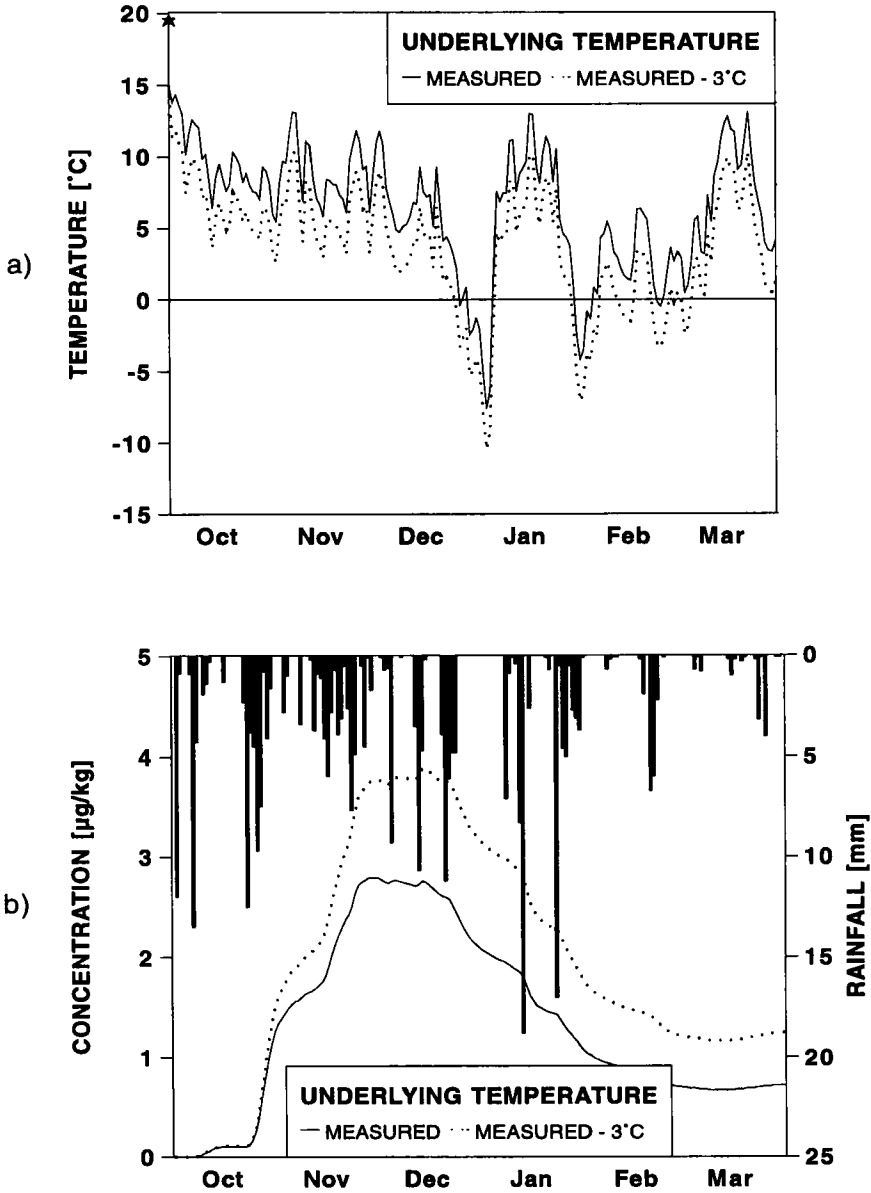
**Fig. 5.30:** a) Time courses of temperatures used for simulating the effect of temperature on degradation and leaching. Simulation were carried out by using measured daily temperatures and temperatures 3°C lower than measured. b) Simulated breakthrough curves below the plowing layer. Because the area under the breakthrough curve is a measure of the total amount of substance it is evident that under lower temperatures more substance is transported to the groundwater.

# 6 Parameters for Water Transport Models

As mentioned earlier water transport models based on Richards' equation need parameters of the retention curve and the saturated hydraulic conductivity of each soil horizon. Different methods for deriving these parameters are available:

a)    Measurement of soil hydraulic properties

Several methods for measuring hydraulic parameters of the unsaturated zone in a laboratory and under field conditions have been developed (Campbell, 1974; Klute, 1986). These methods can be divided into steady state and unsteady state (dynamic) methods. However, they include restrictions, which make their application expensive and time consuming. Therefore these methods are applicable only for single investigation sites. Furthermore, due to the boundary conditions the laboratory methods are only partly transferable to field conditions.

b)    Estimating soil hydraulic properties from basic soil data

This method provides an easy to use method to derive parameters necessary for simulation models from available soil information stored in a soil map. This method is explained in detail below.

c)    Calibration of soil hydraulic properties using field measurements

Often calibration of water transport model based on Richards' equation is performed using a trial and error method to determine the hydraulic parameters. By this method the parameters are varied until the simulated and the measured time courses agree. Because the trial and error method is subjective, no statistical measure can be given concerning the quality of the estimates. Performing automatic parameter estimation leads to the question how to solve the inverse problem. This will be discussed in section 6.2.

## 6.1    Pedotransfer Functions for Water Retention Curves and Saturated Hydraulic Conductivities

An alternative method for estimating soil properties is necessary especially if large catchments are simulated from which only basic soil data like soil texture and bulk density are available. This method is referred to as pedotransfer function technique (PTF) (Bouma and van Lanen, 1987).

PTFs are algorithms (mostly regression functions) which compute saturated hydraulic conductivities and retention data or parameters of the retention curve according to van Genuchten (1980) or Brooks and Corey (1964) relation from particle size distribution, organic carbon content and pore volume (cf. section 5.1):

$$
\begin{pmatrix} T_1 \\ T_2 \\ \cdot \\ \cdot \\ \cdot \\ T_n \end{pmatrix}
\quad
\begin{array}{c} \textit{pedotransfer} \\ \Rightarrow \\ \textit{function} \end{array}
\quad
\begin{pmatrix} \phi_1 \\ \phi_2 \\ \cdot \\ \cdot \\ \cdot \\ \phi_m \end{pmatrix}
\quad
\begin{array}{c} \textit{water transport} \\ \Rightarrow \\ \textit{model} \end{array}
\quad
\begin{pmatrix} \theta(t) \\ \psi(t) \\ q(t) \end{pmatrix}
$$

$$
\begin{array}{ccc}
\textit{basic soil} & & \\
\textit{properties} & \textit{model parameters} & \textit{simulation results} \\
\textit{(e.g. texture)} & \textit{(e.g. } \theta(\psi) \textit{ curves)} &
\end{array}
$$
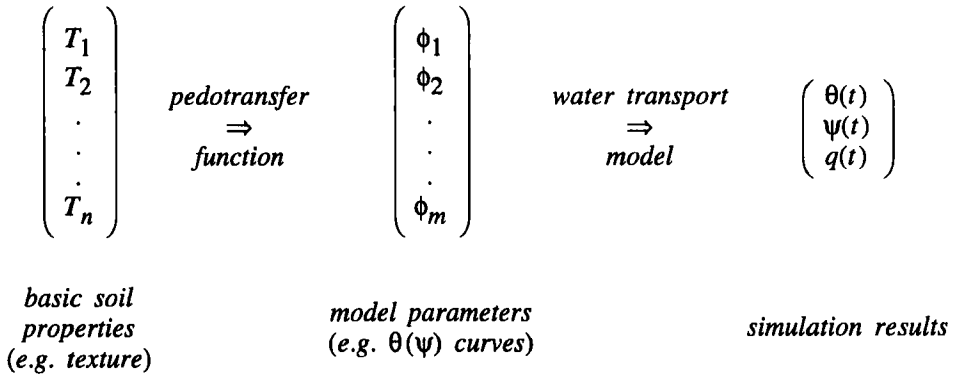
According to Tietje and Tapkenhinrichs (1993) three different methods are available:

a)     Point regression method

The water content at certain matrix potentials is computed in this method by means of (generally multiple linear) regression analysis (e.g. Husz, 1967; Gupta and Larson, 1979; Rawls and Brakensiek, 1982; Puckett et al., 1985). The main disadvantage of this method is that for simulation models a curve fitting must be performed after estimating retention data. Some of the PTFs do not provide enough data to fit parameters of a closed form equation from the retention data (e.g. Husz, 1967).

b)     Physical model method

This method consists of three steps: 1) calculation of the pore-size distribution from the particle size distribution, 2) predicting water content from pore-size distribution considering mass conservation and 3) calculating matrix potential from pore-size distribution by means of capillarity equation. The transformation between particle size and pore size may be linear (Haverkamp and Parlange, 1986), non-linear (Arya and Paris, 1981) or fractal (Tyler and Wheatcraft, 1989).

c)     Functional parameter regression method

Parameters of closed form equations for the relation between $\psi$ and $\theta$ are estimated using regression techniques (e.g. Cosby et al., 1984; Rawls and Brakensiek, 1985; Vereecken et al., 1989).

The quality of 13 different pedotransfer functions were analyzed by Tietje and Tapkenhinrichs (1993). They compared measured with estimated soil hydraulic properties for more than 1000 soil samples from Northern Germany. The authors differentiated between PTFs which compute water content at distinct matrix potentials, methods based on physical principles and PTFs which estimate parameters of a retention function.

PTFs which compute the parameters of retention and conductivity curves are directly applicable in simulation models. If a PTF only computes single retention data a following

curve fitting has to provide the parameters necessary for the simulation models. This presumes that a sufficient amount of retention data were estimated which is not true in all cases. Furthermore some of the PTFs only compute retention curves and not saturated conductivities. In this case not all parameters necessary for modelling are available.

In order to recommend a PTF for simulation purposes it is important to know on which data set the PTF was established and calibrated. If possible it would be most satisfactory to find a PTF applicable to all texture classes. Although it can be assumed that the prediction of a PTF would be more accurate if information on soil genesis is included (Wagenet, 1990) only slight dependence of the performance on soil type was reported by Tietje and Tapkenhinrichs (1993).

In their comparison Tietje and Tapkenhinrichs found the PTF of Vereecken et al. (1989) to be the best applicable for all soils even for high organic matter contents. Nevertheless, analyzing the mean differences and the root of the mean squared differences computed by Tietje and Tapkenhinrichs it can be found that some of the PTFs show a bias in the computed retention curve. This is illustrated in Fig. 6.1 in which measured retention data of a loamy soil and the estimated retention curve according to Rawls and Brakensiek (1985) is compared. This figure shows that the shape of the retention curve is described correctly which means that the water capacity (Eq. 5.7) of the estimated curve is similar to the water capacity of the data. Although the absolute differences in water content are unimportant for calculating the water fluxes it may lead to a systematic bias in calculating the leaching of solutes due to the effect the water content has on the pore water velocity and the degradation process.
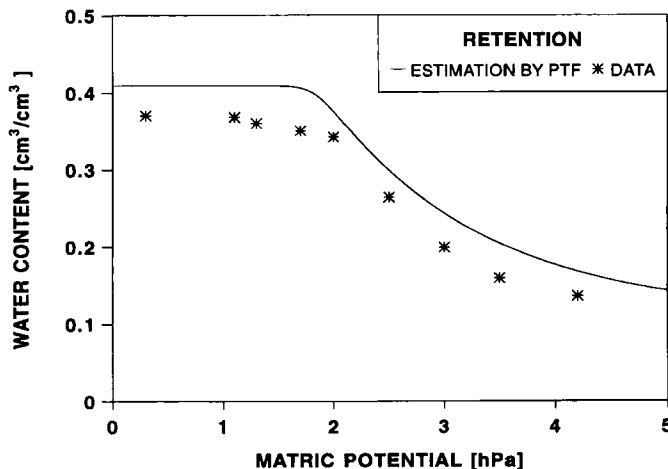


**Fig. 6.1:** Measured retention data and retention curve estimated by the pedotransfer function of Rawls and Brakensiek (1985). The PTF of Rawls and Brakensiek is known to underestimate the water content.

Because it is difficult to forecast the effects of the differences between measured and predicted conductivity and retention data on the water fluxes it is necessary to evaluate the applicability of PTFs in simulation models. Diekkrüger (1992) used those PTFs for simulating water fluxes which in the study of Tietje and Tapkenhinrichs yielded acceptable

results. He compared the simulation results for a three years period of time using PTFs with the simulation results obtained by using calibrated parameters. The calibration was performed by minimizing the differences between simulated and measured time courses of soil suction and water content. Because some of the PTFs work well only under certain conditions (e.g. only for sandy soil) it was decided to use simulations from a clayey soil, a loamy and a sandy soil in this comparison.

From the 13 PTFs analyzed by Tietje and Tapkenhinrichs (1993), Diekkrüger (1992) recommended only two for the application in simulation models: Vereecken et al. (1989) and Rawls and Brakensiek (1985). Vereecken et al. (1989) estimate the parameters of the van Genuchten (1980) approach for the retention curve, the parameters of the Gardner (1958) approach for the unsaturated hydraulic conductivity and the saturated hydraulic conductivity. The disadvantage of this approach is that Vereecken et al. fixed $m$ to 1 in Eq. (5.14) which may lead to values for $n < 1$. In this case Eq. (5.14) becomes singular for $\psi \rightarrow 0$. This causes problems in simulating the transition from the unsaturated to the saturated situation. Rawls and Brakensiek estimate the parameters of the Brooks and Corey (1964) relation and the saturated hydraulic conductivity. In a former study the PTF of Rawls and Brakensiek was already applied successfully to the simulation of water fluxes on different sites in Northern Germany using the simulation model OPUS (Diekkrüger et al., 1991). The disadvantage of this PTF is that the water content is underestimated permanently (about 0.05 cm$^3$/cm$^3$), especially for clayey and loamy soils and soils with high organic carbon content.

## 6.2    Inverse Problems in Partial Differential Equations

Several methods have been developed for the identification of the hydraulic parameters under laboratory conditions by solving the inverse problem. These methods require measured data such as water flux, water content or soil suction. Many authors are using water flux data from soil columns (one-step outflow experiments), where the boundary conditions are clearly fixed (Hornung, 1983; Parker et. al., 1985 a,b; Passiora, 1976; Valiantzas and Kerkides, 1990; Zachmann et. al., 1981 a,b). Others are using water contents and soil suction data measured in time and space (Dane and Hruska, 1983; Kool and Parker, 1988; Milly, 1987). All methods have shown that the identification of hydraulic parameters of the Richards' equation is feasible although the problem is frequently ill posed. Ill posedness is a mathematical technical term meaning that the solution of the mathematical problem is not unique. Nevertheless, it is not shown whether the optimization procedure is applicable to field conditions.

In the following a method for estimating hydraulic parameters from field measurements is introduced. This method is tested using measured water contents and soil suction data from a five year period from an investigation site (loamy soil) in northern Germany. We investigated whether these measurements offer enough information for calibrating the hydraulic parameters by solving the inverse problem. Furthermore, we studied whether the estimated parameter vectors are reliable in comparison with water retention curves and conductivity curves obtained by laboratory methods and estimated using a pedotransfer function (Rawls and Brakensiek, 1985).

## The Estimation Problem

Given are

i)     a dynamical model in form of a partial differential equation with parameter vector
       $\Phi = (\phi_1, \ldots, \phi_p)$ and with initial and boundary conditions,

ii)    time courses of measured state variables, e.g. water content and/or soil suction in one
       or several depth layers,

iii)   a performance criterion which measures the deviations between model predictions and
       observations and

iv)    an error structure.

The mathematical problem then is to find a parameter vector $\Phi$ which minimizes the
performance criterion chosen.

## Performance Criteria

The choice of the performance criterion has a large influence on the convergence of the
optimization procedure. The most widely used criterion is the weighted sum of squared
deviations between predicted and observed values.

$$L\left(\Phi|y_{11},\ldots,y_{kn}\right) = \sum_{i=1}^{k} \sum_{j=1}^{n} w_{ij}\left[y_{ij} - \hat{y}_{ij}(\Phi)\right]^2 \tag{6.1}$$

with weighting factors $w_{ij}$. The $y_{ij}$ denote measurements taken at time $t_j$ in depth layer $i$ and
$\hat{y}_{ij}$ denote the solution of the boundary value problem.

In water transport models time lags of several days between observed and simulated time
courses of the soil suction frequently occur and are acceptable. In this case the application
of the least squares criterion results in large residual sum of squares and in a bad
performance of the optimization procedure. Convergence is frequently not achieved at all or
the procedure converges to a "wrong" minimum yielding parameter values which cause the
trajectories to run through the mean values of the data.

It is therefore necessary to employ alternative measures of deviations between model
predictions and measurements (cf. Fig. 6.2). One possibility is to use the euclidean distance
between the simulated curve and the measurements:

$$L\left(\Phi|y_{11},\ldots,y_{kn}\right) = \sum_{i=1}^{k} F_i \tag{6.2}$$

for any depth $i$ $F$ is given by

$$F = \left((y_j - \hat{y}(\Phi))^2 + (t_j - \hat{t}(\Phi))^2\right)^{1/2} \tag{6.3}$$

where $\hat{t}$ and $\hat{y}$ are the coordinates of the point with minimum distance from the data point $y(t)$. The disadvantage is that in cases where large amplitudes at a small temporal scale are measured this method may try to minimize the wrong deviations, e.g. to minimize the deviation between an increase in measurements and a decrease in simulation results.

The third criterion is the difference of the areas under the simulated and measured time curves where the time course of measured data is approximated by a polygon:

$$L\left(\Phi|y_{11},...,y_{kn}\right) = \sum_{i=1}^{k} \left[ \frac{1}{t_1 - t_0} \int_{t_0}^{t_1} |\bar{y}_i(t) - \hat{y}_i(\Phi,t)|\, dt \right] \tag{6.4}$$

in which $\bar{y}(t)$ denotes the polygon of the measurements in depth layer $i$.
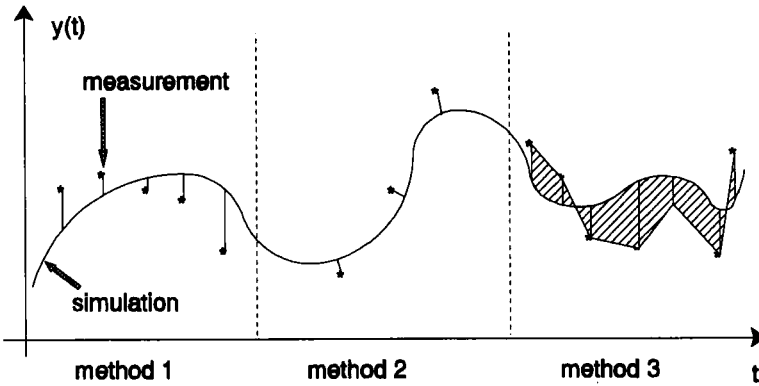


**Fig. 6.2:** Comparison of different optimization criteria. Criterion 1: deviation between simulation and measurement at time $t$. Criterion 2: deviation between simulation and any measurement in a given time span. Criterion 3: area between simulation and measurements.

In a study of Arning et al. (1996) it was shown that this criterion gives the best results when time lags occur.

The identification problem is thus to find a parameter vector $\Phi$ such that

$$L\left(\hat{\Phi}|y_{11},...,y_{kl}\right) = \min_{\Phi \in U} \left[ L\left(\Phi|y_{11},...,y_{kl}\right) \right] \tag{6.5}$$

where $U$ denotes the admissible parameter space and $\Phi = (K_s,\ \theta_s,\ \theta_r,\ \alpha,\ n)$. If data sets of water content $\theta$ and matrix potential $\psi$ are used simultaneously for the estimation, the total deviation is calculated as a weighted sum of both performance criteria:

$$L_{total} = L_\psi + g L_\theta \tag{6.6}$$

where $g$ denotes a weighting factor. The weighting factor is necessary to compensate for different orders of magnitude between water content and soil suction.

In order to reduce the programming effort it is necessary to combine commercial statistical software with simulation models. In the example discussed below we used:

- the Deterministic Site Model (DESIM, Diekkrüger et al., 1982), which solves Richards' equation numerically using the van Genuchten/Mualem parameterization (1980), cf. section 5.1.
- the model AMBETI (Braden, 1995), which solves the upper boundary condition (evaporation and interception) and the transpiration using the Penman-Monteith equation (Penman, 1948; Monteith, 1965). AMBETI is connected to DESIM by the sink/source term of Eq. (5.1).
- the subroutine AR of the statistic software BMDP (Dixon, 1981) for solving the least square problem by using a derivate-free algorithm (Ralston and Jennrich, 1978). This statistical software was already used for estimating parameters in ordinary differential equation (cf. chapter 4).

The models DESIM and AMBETI are interconnected in such a way that both models run simultaneously and exchange their results. Most statistical program packages provide capabilities for the solution of non-linear regression problems. The program package BMDP offers an interface for a user-written FORTRAN subroutine for derivate free non-linear regression problems. The algorithm is based on the Gauss-Newton scheme.

By means of this interface, the water transport model (DESIM and AMBETI) is linked to the BMDP routine AR. From the deviation between simulation results and measurements BMDP calculates a new parameter vector which is afterwards used in the next simulation. This iterative scheme stops when a given number of iterations is reached, the performance criterion is less than a given value, or the performance criterion does not change anymore.

## 6.3   Worked Examples

In a study Arning et al. (1995) investigated whether it is possible to estimate all five parameters of the van Genuchten/Mualem functions (Eqs. (5.14) - (5.15)) from field measurements. In a first step the authors used "error-free" measurements of a non-layered soil generated by means of a simulation model. The range of these measurements were limited to the range of the field measurement devices (e.g. 1000 hPa for soil suction). They showed that a unique solution can only be obtained when the "measurements" are exact. If a normal distributed error superimposes the "measurements" no unique solution can be gained. This is due to the fact that the hydraulic relationship is significantly influenced by the saturated soil properties. Because saturation rarely occurs under field conditions the estimated van Genuchten parameterization is reliable in the range of measurements (e.g. 100 - 1000 hPa) but not for wet or dry conditions. This is shown in Figs. 6.3 a,b where the deviation of the estimated functions derived from erroneous measurements is compared with the soil properties used to generate the "measurements". For the measurement range the curves compare well but especially for wet conditions great differences occur. In order to obtain a unique solution it is necessary either that the range of measurements covers the whole range from saturation to the permanent wilting point or that soil properties at saturation or for dry conditions are determined by other methods.
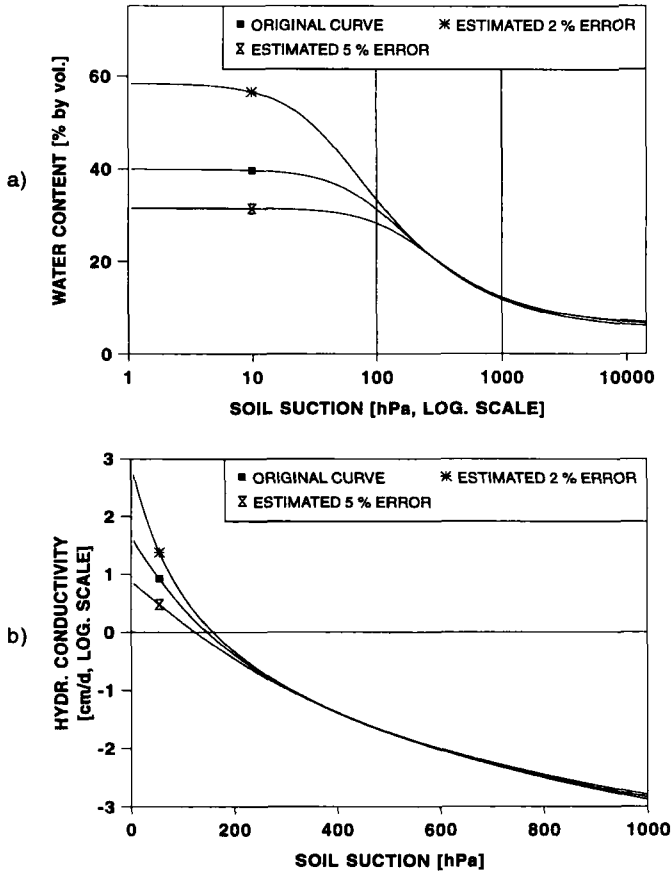
**Fig. 6.3:** Comparison of a) the retention curve and b) the conductivity curve used for generating "field measurements" with retention curves obtained by solving the inverse problem. The field measurements are superimposed by an error of 2 and 5 %. For the parameter estimation the range of measurements is constrained from 100 to 1000 hPa. Note that for the range of measurements the estimated curves are reliable but not for wet conditions.

In a second step the authors studied whether continuous field measurements contain enough information to determine hydraulic properties for a layered soil profile. They used measurements of soil suction and water content from two different sites with loamy and sandy soils  consisting of five and four horizons respectively. This means that up to 25 parameters have to be estimated simultaneously from the field measurements.

A further objective of the investigation of Arning et al. (1995) was the study of the influence of different measurement periods on the estimates. The qualities of the estimated sets of parameters were verified by comparing long-term simulations of about five years with field measurements. For all calibration periods it was possible to find a set of parameters which computes an acceptable agreement with the measurements. This is illustrated for one example in Figs. 6.4 a-d.
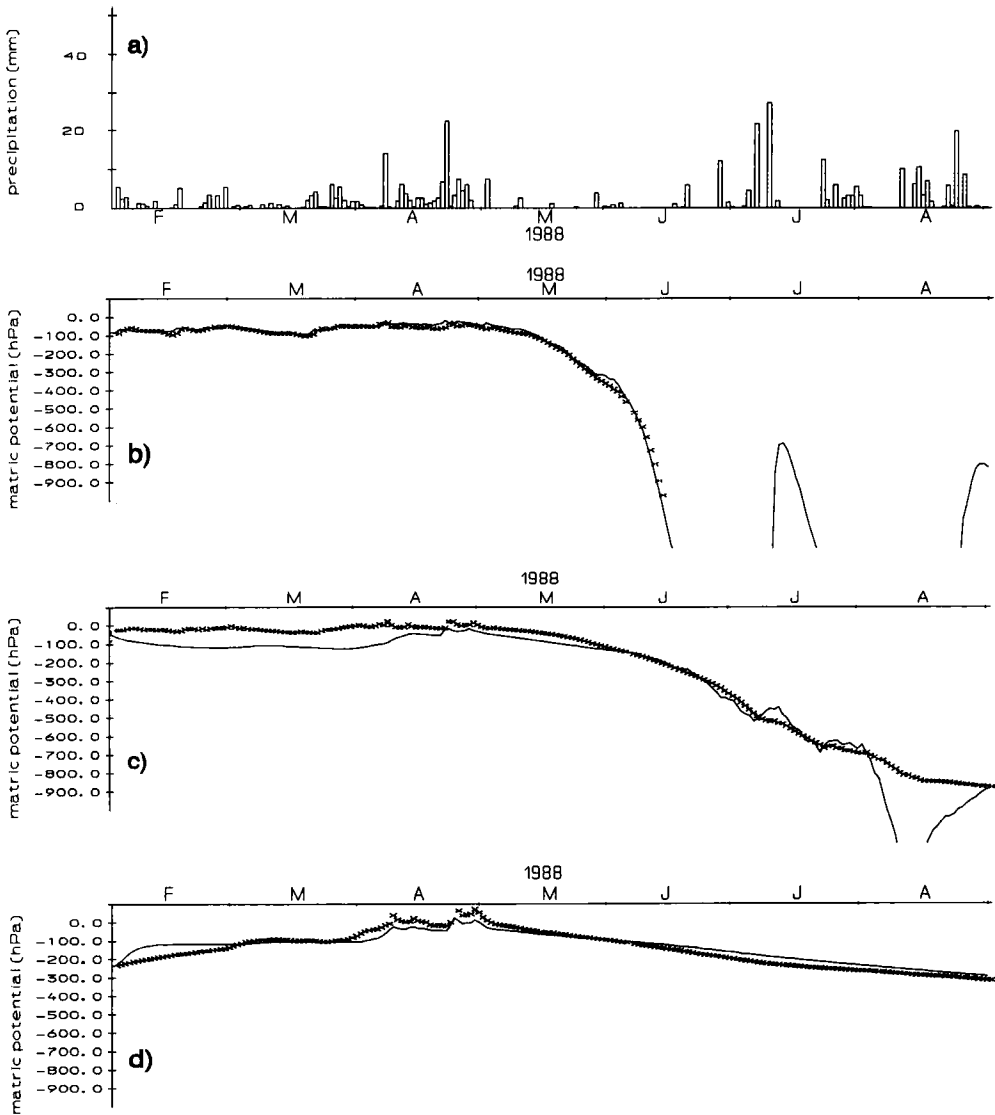
**Fig. 6.4:** a) Precipitation data and b-d) simulated and measured soil suction for the calibration period 2/1988 - 8/1988 for the depths of b) 40 cm, c) 100 cm and d) 210 cm.

When the estimated set of parameters is applied to a long-term forecast often reliable simulation results are obtained (cf. Figs. 6.5 a-e and Figs. 6.6 a-e) for the upper and lower part of the soil profile. In the root zone a large range of soil suction and water content was measured while in the lower part of the profile only wet condition due to a perched water table occur during the whole period. Because the temporal variability of the state variables is low below the root zone the estimates for this layer exhibit high standard deviations.
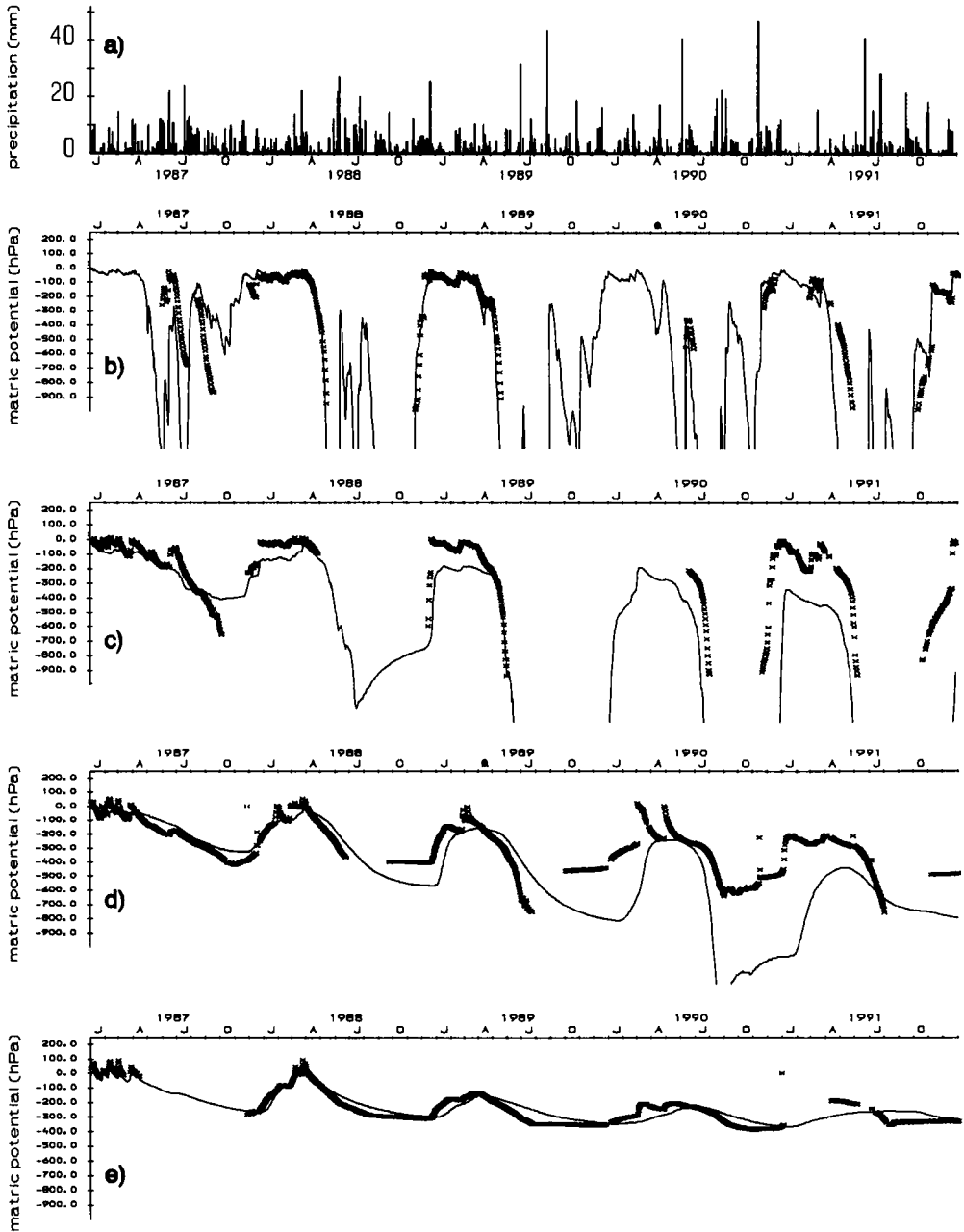
**Fig. 6.5:** a) Precipitation data and b-e) simulated and measured soil suction for a five years period of time for the depths b) 40 cm, c) 80 cm, d) 150 cm and e) 240 cm. The parameters were estimated by solving the inverse problem employing criterion 3.
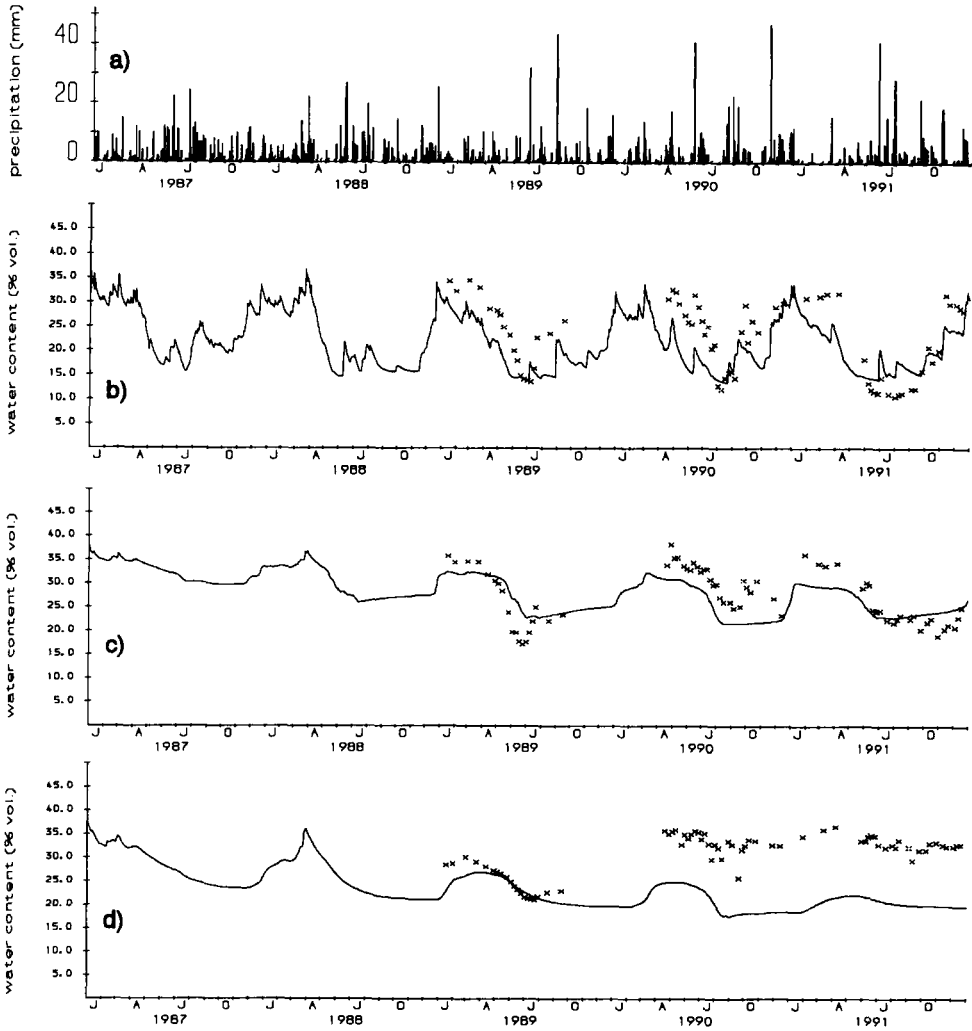
**Fig. 6.6:** a) Precipitation data and b-d) simulated and measured soil suction for a five years period of time for the depths b) 40 cm, c) 80 cm and d) 150 cm. The parameters were estimated by solving the inverse problem employing criterion 3.

This demonstrates that it is indispensable to estimate the saturated properties of the soil in a different way. As described in section 6.1 pedotransfer functions offer the possibility to estimate the soil hydraulic properties from soil texture. This would help to fix the wet part of the conductivity and retention curves in order to obtain a unique solution.

The performance of different sets of parameters can be evaluated by comparing the water balances. This is shown in Tab. 6.1 where groundwater recharge and evapotranspiration are given for a simulation period of five years. The hydraulic properties were measured in the laboratory, estimated using the pedotransfer function of Rawls and Brakensiek (1985) and

estimated by solving the inverse problem for two different calibration periods. The differences between these simulations are small. It has to be noted that the evapotranspiration exerts the largest influence on the model outcomes. In this study the authors assumed that the evapotranspiration model is calibrated correctly because the most important parameters were determined in lysimeter studies. However, it is difficult to measure the temporal and spatial variable root length. Therefore the computed evapotranspiration may also be uncertain.

Nevertheless, considering the spatial and temporal variability of soil properties and boundary conditions the results of the study of Arning et al. (1995) are promising because they showed that plausible estimates of hydraulic properties are feasible. Assuming a further improvement of the measurement devices inverse modelling may be an appropriate method for determining model parameters.

**Tab. 6.1:** Simulated water balances [mm] for the period 1/1987 - 12/1991 using parameters measured in the laboratory, derived from a pedotransfer function and by solving the inverse problem for two different periods.

| [mm] | Lab | PTF | Inverse Problem P2 2/1988 - 9/1988 | Inverse Problem P5 12/1990-6/1991 |
|---|---|---|---|---|
| Groundwater Recharge | 579 | 538 | 605 | 510 |
| Evapo-transpiration | 2343 | 2397 | 2498 | 2519 |
| Evaporation | 927 | 1066 | 1080 | 1060 |
| Transpiration | 1416 | 1331 | 1418 | 1459 |

# 7    Regionalization

## 7.1    Transport Processes in Random Environments

The models developed in the preceding chapters were derived under the assumption of homogeneous environments. As was pointed out before, model development has to start from simple situations, to which elementary physical and chemical laws or basic biological models can be applied. The resulting models are deterministic at scales larger than elementary volumes. Adequate mathematical structures are ordinary and partial differential equations. For applications, initial value and boundary value problems have to be solved. The advantage of this approach is that one is able to study the behavior of the system at a more general level by mathematical means. It is desirable to start from classes of problems, which are amenable to analytical solutions describing simple experimental situations. Analyses of this kind, together with laboratory experiments, are important to test the validity of the underlying physical, chemical and biological mechanisms.

However, physical properties and chemical composition of real soils are inhomogeneous. Frequently, this inhomogeneity is not simply a noise, which can be dealt with by averaging, it is essential for the transport properties of a given soil. Let us consider water flow through a medium exhibiting a large range of water conductivities. If the conductivities are spatially correlated, then it is highly probable that interconnected regions of low and high conductivities occur giving rise to a random flow pattern with zones of preferential flow (cf. section 7.3.2, Fig. 7.14).

Should one abandon therefore the deterministic approaches? We are faced with the dilemma, that deterministic models function well at the laboratory level under homogeneous conditions and that homogeneous conditions do not prevail in the field. A possible way out of this dilemma is the incorporation of the statistical variation of soil parameters into deterministic process models.

This demands the development of stochastic models of spatial variability. To this end, soil parameters are conceived as the realization of a random spatial field. If it is possible to identify the rules of this random process, one is able to generate patterns according to these rules. The rules assign a value of the parameter e.g. water conductivity to each point in space. The patterns thus obtained are possible realizations of the underlying random process. In a subsequent step, the deterministic transport equations are solved for a given realization. The solutions of the transport equations are then, via the random parameter field, realizations of a random process.

Each stochastic simulation creates a pattern, which is **not exactly identical** to any existing pattern - the probability to obtain an identical pattern is even zero for continuous processes -, **but which is similar** to existing patterns. Furthermore, by generating a large number of realizations, one is able to study the properties of the statistical distribution of model trajectories.

At larger scales, the parameters have to be aggregated into so called **effective parameters** representing a subunit of land in a yet to be defined way. Here we are confronted with the problem of scaling. The notions scaling, upscaling and downscaling are used in different ways in the literature. Frequently scaling is used in the sense of regionalization. Norman (1993) distinguishes between "Integration" and "Scaling". Integration is understood as an "orderly process of bringing component parts together as a whole" whereas "Scaling implies an intuitive leap that provides a quantitative connection between distant phenomena - a short cut." King (1991) defines "scaling up" as "the translation or extrapolation of ecological information from small local scales to larger landscapes and regional scales". Norman's definition is very ambitious because it demands a new theoretical concept. In addition it supposes that new phenomena will emerge at larger scales. This is not necessarily the case.

Furthermore, scaling is confounded with statistical problems caused by spatial heterogeneity and by missing information. In conclusion one can state that there does not exist a general theory which allows to derive rules for scaling for the particular problem under study.

In the following we will approach this problems from different angles trying to elucidate different aspects of scaling.

## 7.2    The Concept of Random Soil Columns

### 7.2.1    Introduction of Variability into Deterministic Models

In this section we shall introduce a simple method to combine variability with deterministic models. The underlying concept bases on the notion of an **ensemble of uncorrelated soil columns** each with a different set of soil parameters. This implies that lateral flow can be neglected. Model parameters are sampled from statistical distributions yielding a distribution of model trajectories. This method was already introduced in section 3.2.3 for distribution of the decay parameter $k$. In technical terms, this method transforms a density function (from which the parameter is sampled) of a parameter into a density function of a concentration (or water content) via a deterministic model. This technique is mostly applied to one-dimensional transport models. Note that this method is completely lacking any spatial aspect.

Let us consider as an example the analytical solution of the CDE Eq. (5.63b) for the boundary conditions as given in Eq. (5.63a). Model parameters are the retardation factor $R$, the coefficient of hydrodynamic dispersion $D$, which is proportional to the pore water velocity, and the rate constant $k$ for first order decay. Assume that the parameter set for each soil column is a realization of the joint statistical distribution of these parameters. Then the expectation of the concentration profile at any time $t$ is given by

$$E[c(x,t)] = \int\limits_{R=0}^{\infty} \int\limits_{D=0}^{\infty} \int\limits_{k=0}^{\infty} c(x,t,R,D,k) f(R,D,k) \, dR \, dD \, dk \qquad (7.1)$$

with $c(x, t, R, D, k)$ given by Eq. (5.63b). Since $c$ depends in a nonlinear way on the parameters

$$E[c(x,t,R,D,k)] \neq c(x,t,E[R,D,k]) \qquad (7.2)$$

i.e. the expectation of $c(x, t, R, D, k)$ cannot be obtained by simply inserting the expectations of the parameters into the formula for $c$.

The calculation of the expectation Eq. (7.1) requires the knowledge of the joint distribution function of the parameters $R$, $D$ and $k$. For single parameters, such as the $K_d$-value, skewed density functions were established which can be modeled by lognormal or gamma distributions. However, the assessment of the type of a distribution function requires large sample sizes. Often, only the first and second moment of the distribution (mean and variance) are known. Therefore, it is of practical importance to investigate, whether the shape of the expectation curve is similar to the shape obtained by inserting the mean parameter values into the original function. In section 3.2.3 it was shown for a simple first order decay model and a gamma distributed k-value, that the mathematical form of the expectation curve differs from the mono-exponential decay curve.

Let us consider as an example the case that only the parameter $D$ is random with all other parameters held fixed. Certainly the type of distribution function chosen will have an influence on the expectation curve. The above integral (Eq. 7.1) will be evaluated for the uniform, the normal, the lognormal and the gamma density function (for a brief description of some frequently used distribution functions cf. appendix A.2). For a gamma density Eq. (7.1) takes the form

$$E[c(x,t)] = \int_{D=0}^{\infty} c(x,t,D\,|\,R,k)\frac{\lambda}{\Gamma(r)}(\lambda D)^{r-1}\, e^{-\lambda D}\, dD \qquad (7.3)$$

The notation $c(x,t,D\,|\,R,k)$ reads "for $R$ and $k$ fixed". The parameters of the gamma-distribution are related to the expectation and variance by

$$E[D] = \frac{r}{\lambda} \quad and \quad V[D] = \frac{r}{\lambda^2}$$

If one wants to investigate the influence of the form of the distribution function on the expected profile, one has to ensure that the first two moments of the distribution functions are identical. For given expectation $\mu$ and variance $\sigma^2$ the parameters of the gamma distribution are

$$r = \frac{\mu^2}{\sigma^2} \quad and \quad \lambda = \frac{\mu}{\sigma^2}$$

The parameters of the uniform and lognormal distribution are adjusted accordingly. In the case of the lognormal distribution a nonlinear equation system has to be solved.

Figure 7.1 shows a plot of the density functions of these distributions. In the case of the normal distribution, a truncated version has to be used, since the parameter $D$ can take only

positive values.

$$f_{trunc}(D) = N \exp\left(-\frac{(D - \mu_D)^2}{2\sigma_D^2}\right) \qquad 0 \leq D < \infty \tag{7.4}$$

with normalization factor

$$N = \int_0^\infty \exp\left(-\frac{(D - \mu_D)^2}{2\sigma_D^2}\right) dD$$
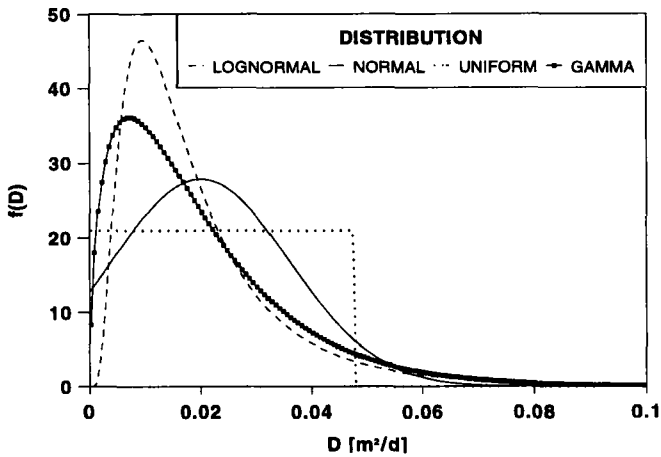


**Fig. 7.1:** Uniform, normal, lognormal and gamma density functions (cf. appendix A.2) for the parameter $D$. Because $D$ can take only positive values, the normal distribution is truncated at $D = 0$.

The subsequent plots (Figs. 7.2 a-d) show the time courses of the expected concentration (Eq. (7.1)) together with the curve obtained by the mean parameter curve. Surprisingly, the shapes of the expectation profile are very similar, although the underlying density functions are rather different in shape.

Obviously, the variance of the distribution is more important than its form. Figure 7.3 shows a series of expectation curves obtained for increasing variance.

Although these results cannot be generalized, they show us to which degree the ensemble curve is represented by the "mean parameter" curve. In practice transport models are applied to real soils and not to a single soil column. Usually only few measurements are available. Frequently only the soil type is known and model parameters are derived from pedotransfer functions or simply by rules relating soil types to likely parameter values. The question is then how well the fieldplot under study is represented by this single parameter value. In the above example the answer for the parameter $D$ is that the expectation may be used as a representative parameter and that the expectation curve is robust against the shape of the density function. The decisive parameter is the variance of the distribution.
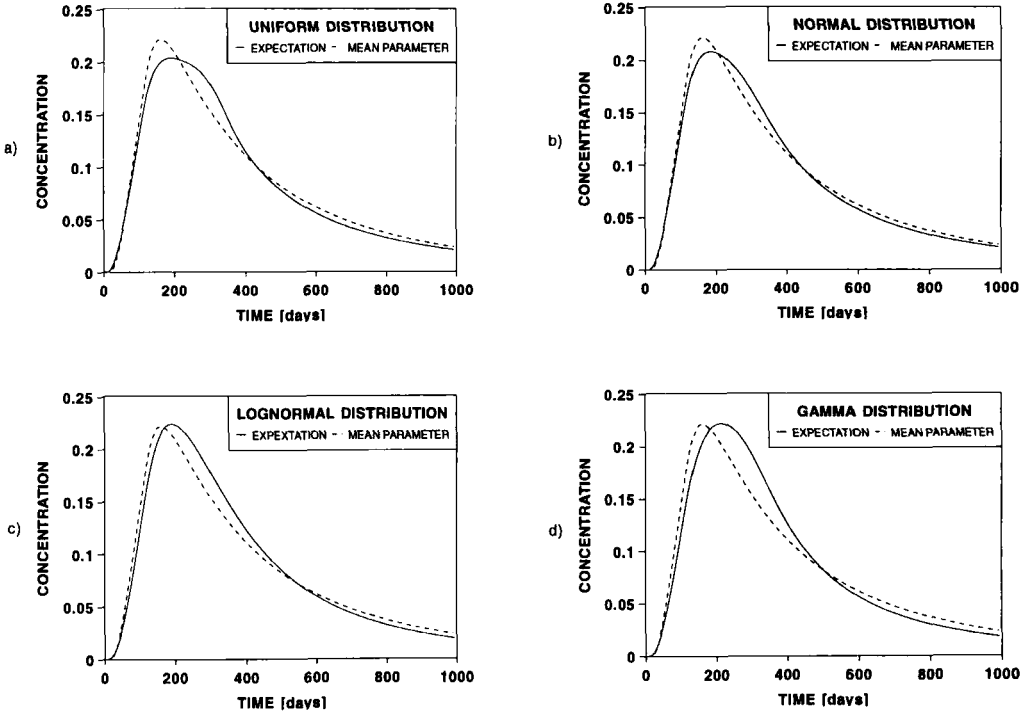
**Fig. 7.2:** Expectation of time courses of concentrations at a given depth obtained for different distributions of the parameter $D$. For comparison, the curve obtained by inserting the mean value of the parameter $D$ into the model equations is also shown. The underlying distributions are a) uniform distribution b) truncated normal distribution c) lognormal distribution d) gamma distribution.
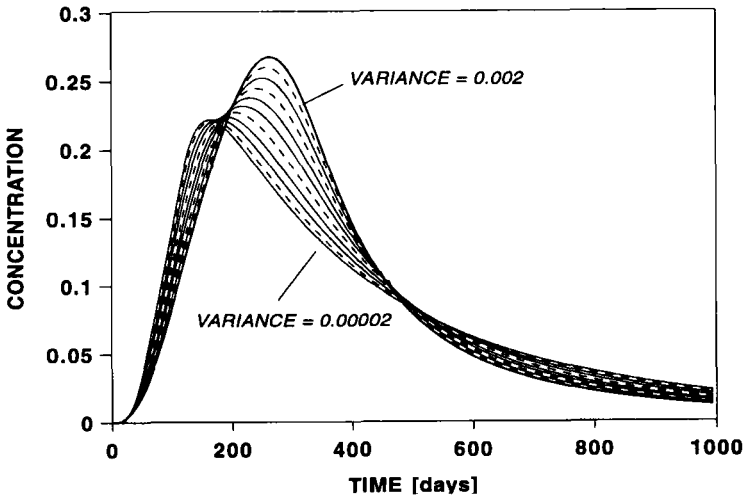


**Fig. 7.3:** Influence of the variance of the distribution of the parameter $D$ (lognormal distribution) on the expectation of the time courses of concentrations.

The next problem concerns the computation of the variance of the concentration. By taking $E[D] + \sigma_D$ and $E[D] - \sigma_D$ as limiting parameters a first impression of the variability can be obtained. However, these concentration curves are not the true variances of the concentration $c$. Since $c$ depends on the random parameter $D$ it is itself a random variable with density function $f^c(c)$. In order to evaluate the formula for the variance of $c$

$$V[c] = \int_0^{c_{max}} (c - E[c])^2 f^c(c)\,dc \tag{7.5}$$

one has to derive the density function $f^c(c)$ from the probability density function $f^\phi(\phi)$ of the parameter $\phi$. Let $\phi$ be a continuous random variable with probability density function $f^\phi(\phi)$ and $g(\phi)$ a one-to-one mapping with continuous differentiable inverse function $\phi = g^{-1}(c)$. By application of a standard theorem from calculus on the change of variable in a definite integral the probability density function of $c = g(\phi)$ is given by

$$f^c(c) = |\frac{d}{dc}g^{-1}(c)|\, f^\phi(g^{-1}(c)) \tag{7.6}$$

Let us consider as an easy example a first order degradation model with random kinetic parameter $\phi$. With

$$c = g(\phi) = c_0 e^{-\phi t} \quad and \quad g^{-1}(c) = -\frac{1}{t}\ln\frac{c}{c_0}$$

Eq. (7.6) becomes

$$f^c(c) = |-\frac{1}{tc}|\, f^\phi\left(-\frac{1}{t}\ln\frac{c}{c_0}\right) \tag{7.7}$$

For a Gamma density (Eq. (3.94)) one obtains

$$f^c(c) = \frac{1}{tc}\frac{\lambda}{\Gamma(r)}\left(\frac{\lambda}{t}\ln\frac{c_0}{c}\right)^{r-1}\left(\frac{c}{c_0}\right)^{\frac{\lambda}{t}} \qquad 0 < c \le c_0 \tag{7.8}$$

This density function is shown in Fig. 7.4 for some values of $t$. Figure 7.5 shows the time courses of $E[c(t)]$ and $E[c(t)] \pm (V[c(t)])^{1/2}$. It is instructive to compare these curves with those obtained by inserting $E[\phi]$, $E[\phi] - \sigma_\phi$ and $E[\phi] + \sigma_\phi$ into the original model (Fig. 7.6).
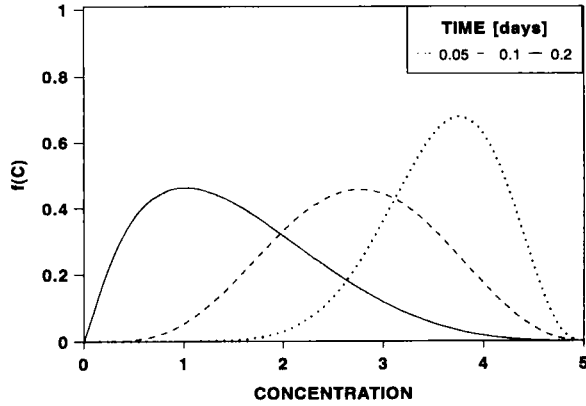
**Fig. 7.4:** Density function of concentration $c$ at three different times.
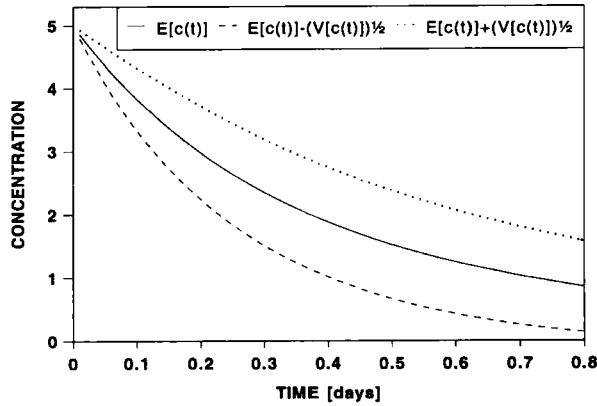


**Fig. 7.5:** Plot of the expectation of concentration $E[c(t)]$ and $E[c(t)] \pm (V[c(t)])^{1/2}$ (upper and lower curves) as a function of time.
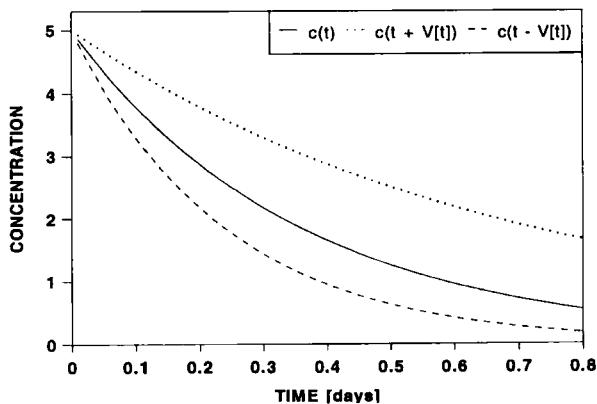


**Fig. 7.6:** These curves are obtained by inserting the expectation of the parameter, $E[\phi]$, $E[\phi] + \sigma_\phi$ and $E[\phi] - \sigma_\phi$ into a mono-exponential decay model.

The results of this analysis can be summarized as follows:

1. The expectation curve markedly differs from the mean parameter curve. This leads to a systematic underestimation of concentrations. Relative differences increase with time.

2. Standard deviations obtained from the transformed density function are smaller than those obtained from inserting the mean and standard deviation of the parameter into the model.

### 7.2.2   The Latin Hypercube Method

The examples of the foregoing section have shown that the computation of higher sample moments (variance) by direct integration demands the transformation of the density function. An analytical expression of the transformed density function can be obtained in only few cases. In most practical applications, the boundary value problems are not even amenable to analytical solutions.

**Problem statement:**

Given:   i)   a deterministic dynamical model in form of a boundary value problem with parameter vector $\Phi$

ii)   the density function of the parameter vector $\Phi$, $f(\Phi)$

The mathematical problem is to find estimators for the moments of the distribution of the state variables determining the dynamical model. The state variables, which are a function of time and of space, are the analytical or numerical solution of a boundary value problem.

An intuitive appealing method is to generate a random sample of the parameter vector and to derive estimators from the sampling statistics of the model output. This approach is referred to as Monte Carlo method. In many practical situations the number of replications is limited by the running time of the numerical code. Therefore sampling techniques have been developed, which are more efficient than simple random sampling (McKay et al., 1979). These are stratified random sampling and Latin hypercube sampling. Let $S$ denote the sampling space of the parameter vector $\Phi$. Stratified sampling is performed by partitioning $S$ into disjoint subsets and to obtain random samples from each subset. Latin hypercube sampling is an extension of stratified sampling. Assuming that the components of $\Phi$ are uncorrelated, the technical procedure is as follows:

i) The range of each component of the random vector $\Phi$, $\Phi_i$, is partitioned into n intervals. The intervals are spaced such that the probability that $\Phi_i$ falls into any interval is $1/n$. The intervals can easily be constructed by means of the distribution function of $\Phi_i$ (cf. Fig. 7.7). Let $k$ denote the number of components of $\Phi$. The sample space is thus partitioned into $n^k$ cells.
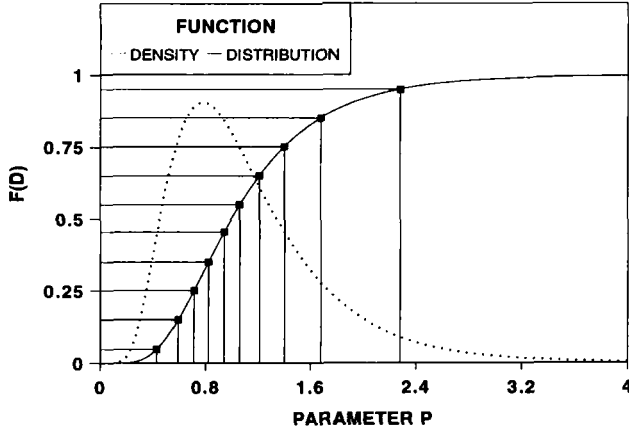
**Fig. 7.7:** Generation of realizations of random variables by means of its distribution function.

ii) Select n cells such that all intervals are represented for each component. This is achieved by the so called latin hypercube sampling method. The rationale behind this method is explained by a two dimensional example with n = 5. The sample space is thus partitioned into 25 cells. Suppose now that a sample of size n = 5 is to be obtained. A sampling scheme with the above properties can be constructed in the following way.

Let the rows and columns of a 5 x 5 square represent the partitions of component $\Phi_1$ and $\Phi_2$ respectively. The restriction that each interval must be represented in the sample is equivalent to the condition that each row and each column is sampled once. Let $a$, $b$, $c$, $d$, $e$ denote the cells of the first column of the square. Then subsequent columns are constructed by permutation. Figure 7.8 shows a possible arrangement. Feasible random samples are obtained by selecting all cells with the same label. It is easily seen from Fig. 7.8 that these cells occur once in each row and in each column. Such an arrangement is called a Latin square. The number of possible arrangements increases with the size of the square. For n = 3, there exist only 12 possible Latin squares, whereas for n = 5 the number of possible arrangements amounts to 161 280. So it is always possible, to choose a Latin square at random.
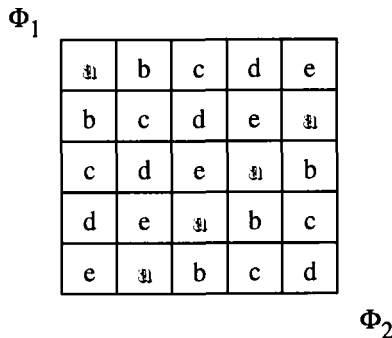


**Fig. 7.8:** Latin square arrangement for a two-dimensional sampling problem.

This method ensures that each component of the random vector $\Phi$ has all partitions of its sample space represented and that the components are properly matched. Extension to more than two dimensions leads to Latin hypercubes.

In the above example all components could be easily matched (n = 25 replications). In practice, the typical number of parameters is in the order of 5 to 10. Consider the case of 5 parameters with 10 intervals for each parameter. Typical computation times for water transport models in the unsaturated zone including crop growth and evaporation over a vegetation period are in the order of 1 min on an IBM-3090 computer. If for one replication all $10^5$ partitions of the parameter space are simulated this would amount to about 70 days computing time. It is obvious that the computer time is prohibitively large and that only a limited number of partitions can be used.

Frequently, parameters are correlated. In the case of a multivariate normal distribution, i.e.

$$\vec{x} \sim N(\vec{\mu}, \Sigma)$$

correlated random variables are generated as follows:

In the first step n realizations $y_1, \ldots, y_n$ of a standard normal distribution are generated. In the second step, these are transformed to the vector

$$X = L\ \vec{y} + \mu$$

where $L$ denotes the Cholesky decomposition of the variance covariance matrix $\Sigma$, i.e.

$$L\ L^t = \Sigma$$

The Latin hypercube sampling method has several advantages over random sampling and stratified random sampling, which was shown by McKay et al. (1979), who proved the following **theorem**:

Let denote $y(\phi_1, \ldots, \phi_p)$ the state variable (solution of a boundary value problem) as a function of the parameters $\phi_1, \ldots, \phi_p$. Let the parameters be a p-variate random variable with known probability density function. Let $T_L$, $T_R$ and $T_S$ denote the estimators of the mean of $Y$ obtained by Latin hypercube, random sampling and stratified random sampling respectively.

Then:

i) all three estimators are unbiased,
ii) if $y(\phi_1, \ldots, \phi_p)$ is monotonic in each of its arguments then $V[T_L] \leq V[T_S] \leq V[T_R]$.

Let us resume as example the convection-dispersion-equation. In the foregoing simulations, only the parameter $D$ was taken as random. Since the coefficient of dispersion is linearly related to pore water velocity $v$, $D = \alpha\ v$ (cf. Eq. (5.37)), its randomness may be due to either the randomness of the coefficient $\alpha$ or the randomness of pore water velocity. In the

example at the beginning of this section it was (tacitly) assumed that $v$ is constant. However, the pore water velocity is related to soil properties (hydraulic conductivity), which are random. In the following simulations, both parameters, $v$ and $\alpha$, are taken as lognormally distributed.

Figure 7.9 shows mean breakthrough curves obtained by mean parameters, random sampling, and Latin hypercube sampling respectively.
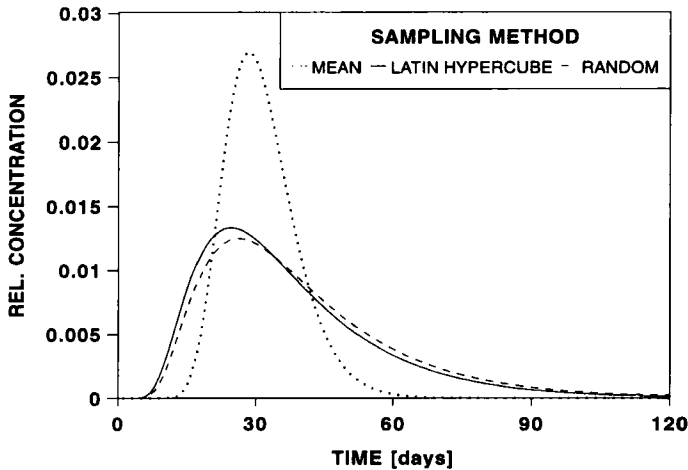


**Fig. 7.9:** Comparison of results obtained by mean parameters, Latin hypercube and random (Monte Carlo; 625 random numbers) sampling. Partitioning the distribution function into 25 intervals and performing Latin hypercube sampling (25 simulations) leads to identical results than performing all (25 x 25) simulations.

# 7.3    Microscale Variation of Spatial Structure

## 7.3.1    Random Spatial Processes

As was already stressed the concept of uncorrelated soil columns is based on the assumption that lateral flow can be neglected. This assumption is valid, if the soil properties are homogeneous within a soil column. If the soil consists of different layers, this assumption is made for each layer. Each soil column is described by a one-dimensional transport model. But what if microscale variation creates heterogeneous soil structure within a layer? Parameter fields can be modeled as realizations of spatially correlated random processes (cf. section 2.3). Consider for instance the hydraulic conductivity. If this parameter is the realization of a second order stationary stochastic process with a gaussian shape variogram then a realization creates connected zones of different conductivities. If the correlation length is in the order of magnitude of the column under study then it is most likely that connected regions of high conductivity will emerge. In these regions water flow and hence transport are facilitated. Obviously one-dimensional models are not capable of simulating these effects. How can one handle this kind of heterogeneity? A possible procedure involves the following steps:

1. Identification of the spatial random process and its parameters, e.g. the correlation length.
2. Generation of realizations of the process.
3. Three dimensional simulation of water and matter transport over realizations of the random parameter field.
4. Assessment of the statistical properties from a large number of realizations.

Let us assume that the basic stochastic process is given by

$$\phi(\vec{x}) = \mu + \omega(\vec{x}) + \varepsilon \tag{7.9}$$

where $\mu$ denotes the general mean, $\omega$ a second order stationary process and $\varepsilon$ a white noise (uncorrelated random variable). Stationarity ensures that

$$E[\phi(\vec{x})] = \frac{1}{|G|} \int_G \phi(\vec{x}) d^3 x = \mu \tag{7.10}$$

The properties of the second order process are determined by the form of the variogram. In order to solve deterministic transport processes over a random field it is necessary that the random field is differentiable. This is ensured, if the slope of the variogram in the origin is zero as is the case for the Gaussian model.

$$\gamma(\vec{h}) = \sigma^2 \left( 1 - e^{-\left| \frac{\vec{h}}{a} \right|^2} \right) \tag{7.11}$$

The parameter $a$ characterizes the correlation length. Figure 7.10 shows a plot of a Gaussian variogram function. Figures 7.11 a-c show realizations of a random field for two different correlation lengths obtained by the turning bands method (cf. section 2.3; Journel and Huijbregts, 1989).
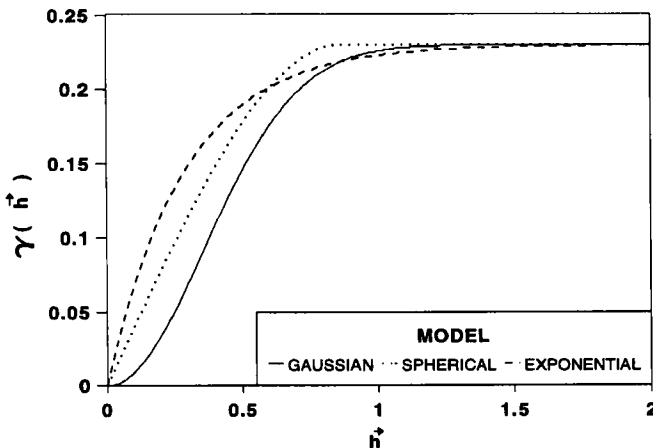


**Fig. 7.10:** Gaussian, spherical and exponential variogram functions.

GAUSSIAN MODEL



SPHERICAL MODEL
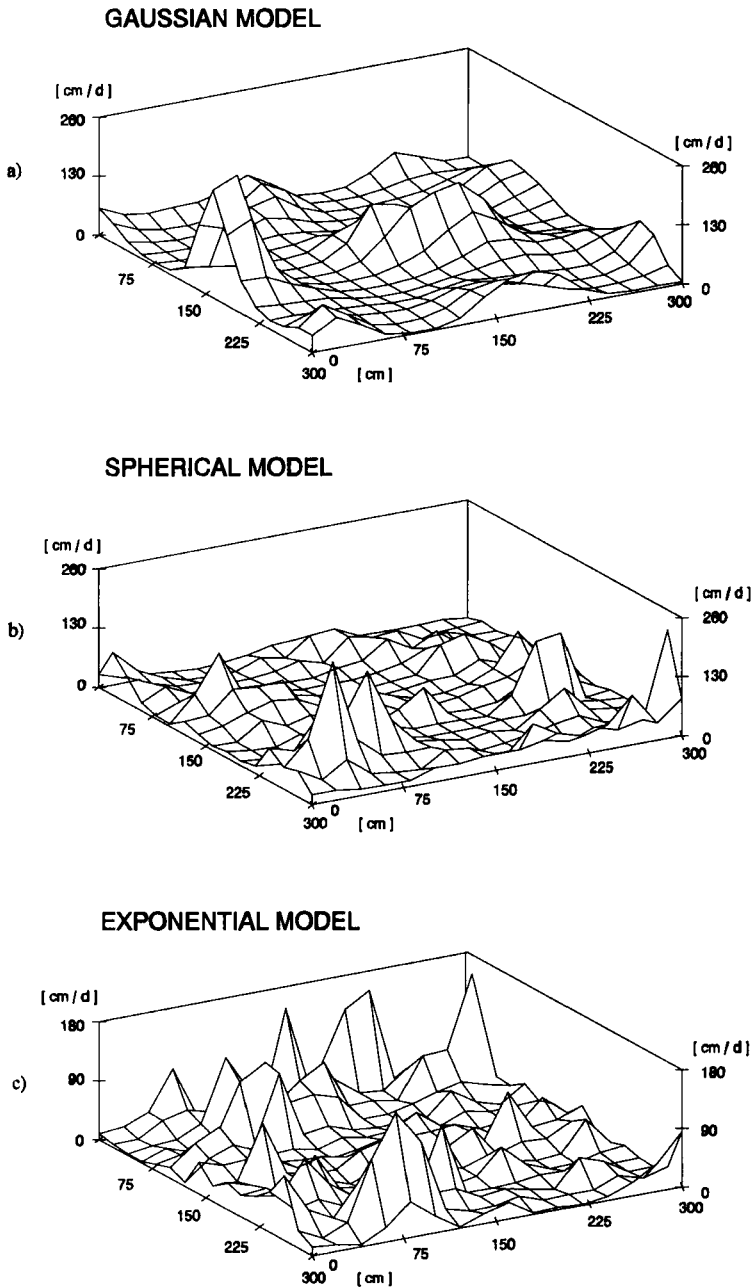


EXPONENTIAL MODEL



**Fig. 7.11:** Realization of a spatial random field of hydraulic conductivity $K_s$ with three underlying variogram models: a) gaussian model, b) spherical model and c) exponential model. The realizations are generated by the turning bands method (Journel and Huijbregts, 1989). The parameters are chosen such that all variograms have the same sill and the same range (range = 87 cm, $Var$ ($lg(K_s)$) = 0.23, $E[K_s]$ = 20.97 cm d$^{-1}$).

The surfaces generated by the process are smooth and it is clear by intuition that these surfaces are differentiable. For variograms with a nonzero derivative in the origin rather coarse surfaces are generated, which are not differentiable. Richards' equation (Eq. (5.5)) for water transport is no more valid, if the water conductivity is not a differentiable function of the space coordinates. Therefore only those random processes are admitted which yield L2-continuous (differentiable) surfaces.

## 7.3.2   Transport Processes over Realizations of Random Fields

Additional notations:

$\alpha_{ijkl}$  : elements of dispersivity tensor [1], resp. [L]
$L$     : characteristic length [L]
$K_{ij}$  : elements of conductivity tensor [1], resp. [L/T]
$k_{ij}$  : elements of permeability tensor [1], resp. [L$^2$]
$v$     : kinematic viscosity [L$^2$/T]
$B$     : conductance of a medium channel [L/T]
$T_{ij}$  : elements of tortuosity tensor [1], resp. [L$^2$]
$BT_{ij}$ : oriented conductance of a channel [L/T]

Under unsaturated conditions, the variability of water conductivity and retention curves have to be taken into account. The parameterization of van Genuchten (1980) and Mualem (1976) (cf. section 5.1, Eqs. (5.14) and (5.15)) depends on the five parameters $K_s$, $\alpha$, $n$, $\theta_r$ and $\theta_s$.

The water transport equation in the $\psi$ formulation (Eq. (5.8)) depends on the capacity function $C(\psi)$, which is the derivative of the retention function with respect to $\psi$. For the van Genuchten parameterization one obtains

$$C(\psi) = \frac{\partial \theta}{\partial \psi} = \theta_w \frac{(n - 1)\alpha |\alpha\psi|^{n - 1}}{(1 + |\alpha\psi|^n)^{1 - 1/n}} \qquad (7.12)$$

where $\theta_w = \theta_s - \theta_r$. Therefore the water transport depends only on the four parameters $K_s$, $\alpha$, $n$ and $\theta_w$, which are written in vector form as

$$\vec{Z}(\vec{x}) = \begin{pmatrix} \alpha \\ K_s \\ n \\ \theta_w \end{pmatrix}$$

$\vec{Z}$ is the realization of a vector random field. In the stationary case the parameters reduce to $K_s$, $\alpha$ and $n$.

In the following example, which is taken from a paper of Tietje and Richter (1993), it is assumed that all parameters are lognormally distributed and that they are uncorrelated. Figure

7.12 shows the realization of the spatial parameter field of the parameter $K_s$, Fig. 7.13 shows the resultant flow field.
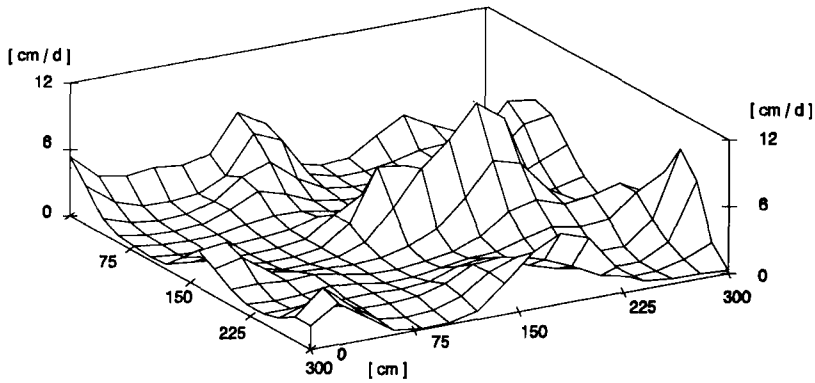


**Fig. 7.12:** Realization of a random spatial $K_s$-field.
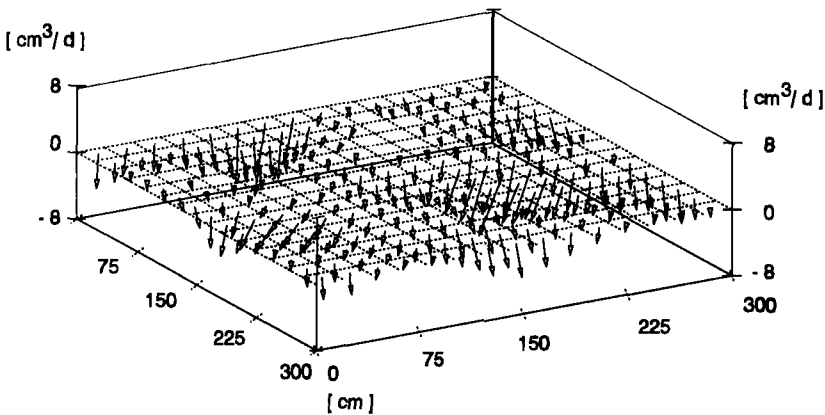


**Fig. 7.13:** Flow field over this realization of a random spatial $K_s$-field.

The three-dimensional transport of a substance depends on the dispersivity tensor (Eq. (5.90)). In a random soil, one has to generate a random tensor field. The components of the dispersion tensor depend on the components of the velocity field of the water and, in isotropic soils, on the longitudinal and transversal dispersivity coefficients $\alpha_L$ and $\alpha_T$. To complicate matters, these coefficients are correlated to parameters of the water transport. In the following simulation, it is assumed that these coefficients are inversely proportional to the square of the hydraulic conductivity.

$$\alpha_L \propto \frac{1}{K^2} \tag{7.13}$$

Thus regions of high conductivity are assumed to exhibit low dispersivity. The heuristic argument goes as follows. Both, the tensor of hydraulic conductivity and the dispersivity tensor are related to the permeability tensor as was shown by Bear (1969):

$$K_{ij} = \frac{k_{ij}\, g}{v} \tag{7.14}$$

Both the elements of the permeability tensor and the elements of the dispersion tensor are related to the elements of a tensor $BT_{ij}$. This tensor reflects the microscopic configuration of the medium. $B$ denotes the conductance of an elementary medium channel and $T_{ij}$ denotes the medium's tortuosity. According to Bear and Verruijt (1987) the elements of the permeability tensor are related to the mean values of $BT_{ij}$

$$k_{ij} = n E[BT_{ij}] \tag{7.15}$$

and the elements of the dispersivity tensor are related to the variance of $BT_{ij}$

$$\alpha_{ijkm} = \frac{E\left[\left(BT_{il} - E[BT_{il}]\right)\left(BT_{jp} - E[BT_{jp}]\right)\right]}{E[BT_{lk}]\, E[BT_{pm}]} \tag{7.16}$$

From this equation, the above postulated inverse relationship between the conductivity and dispersivity coefficients becomes plausible. In isotropic soils, the dispersion tensor simplifies to the form given by Eq. (5.90), which depends on the two parameters $\alpha_L$ and $\alpha_T$.

From the point of view of the stochastic process, the transport model acts as transformation of the random parameter field into a spatio-temporal random concentration field $c(x,t)$

$$\begin{pmatrix} \phi_1 \\ \phi_2 \\ ... \\ \phi_r \end{pmatrix} \underset{MODEL}{\Rightarrow} \quad c(\vec{x},t) \tag{7.17}$$

In the study of Stock (1995) stationary flow and water content fields were generated by solving the water transport equation over a random field of $K_s$-values. In addition a random field of the dispersivity coefficients was generated under the above assumption of a inverse proportional relationship between these coefficients and $K_s$. Figure 7.14 shows the realization of inversely correlated $K_s$- and $\alpha_L$-fields.
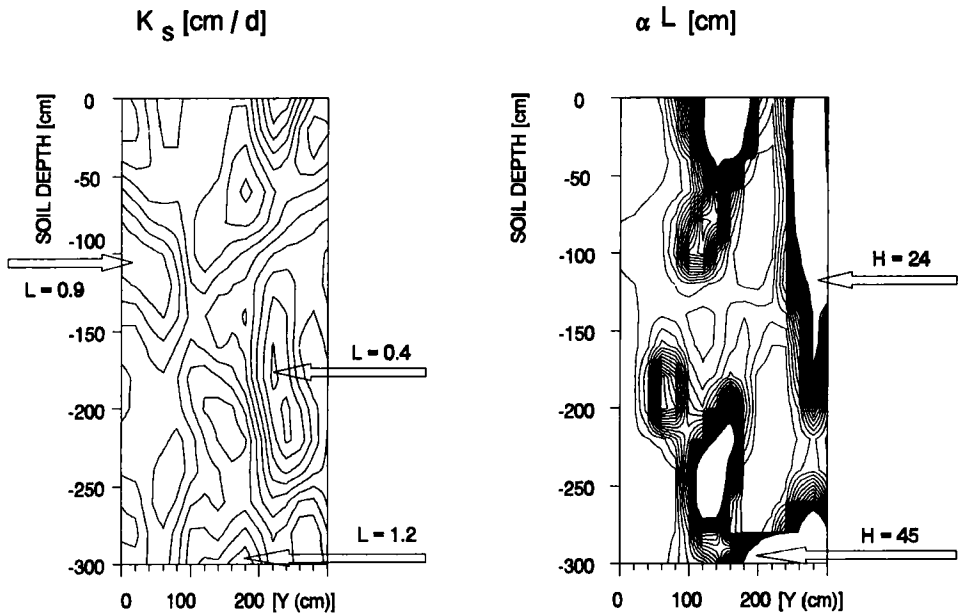
**Fig. 7.14:** Realization of inversely correlated $K_s$- and $\alpha_L$-fields. $L$ and $H$ mark the location where the lowest and highest values occur.

Figures 7.15 a-c show the development in time of a vertical cross section of the concentration field for a tracer for the following initial and boundary conditions:

$$c(x,y,z,t = 0) = 0 \qquad (x,y,z) \in G$$

$$c(x,y,z,t = 0) = c_0 \qquad \text{if } z = 0, \text{ i.e. on the surface}$$

Each figure also shows the mean concentration profile and the profile obtained from a hypothetical bore hole in the center of the region.

For degradable substances a decrease of the degradation rate with depth has to be taken into account. This effect is due to the decreasing organic matter content, which is closely related to the degradation capacity and to the decreasing oxygen content of the soil (not included in the model). Figures 7.15 a-c show the development in time of a vertical cross section of the concentration field generated by the above initial conditions for a linear decreasing rate constant. The spatial heterogeneity has a large influence on the amount of the substance passing the reactive zone. Figures 7.16 a-c show the fate of a fast degradable substance, which nearly completely disappears during its passage through the reactive zone. In case of a slow degradable substance a significant amount of the applied substance will pass the reactive zone (cf. Figs. 7.17 a-c).
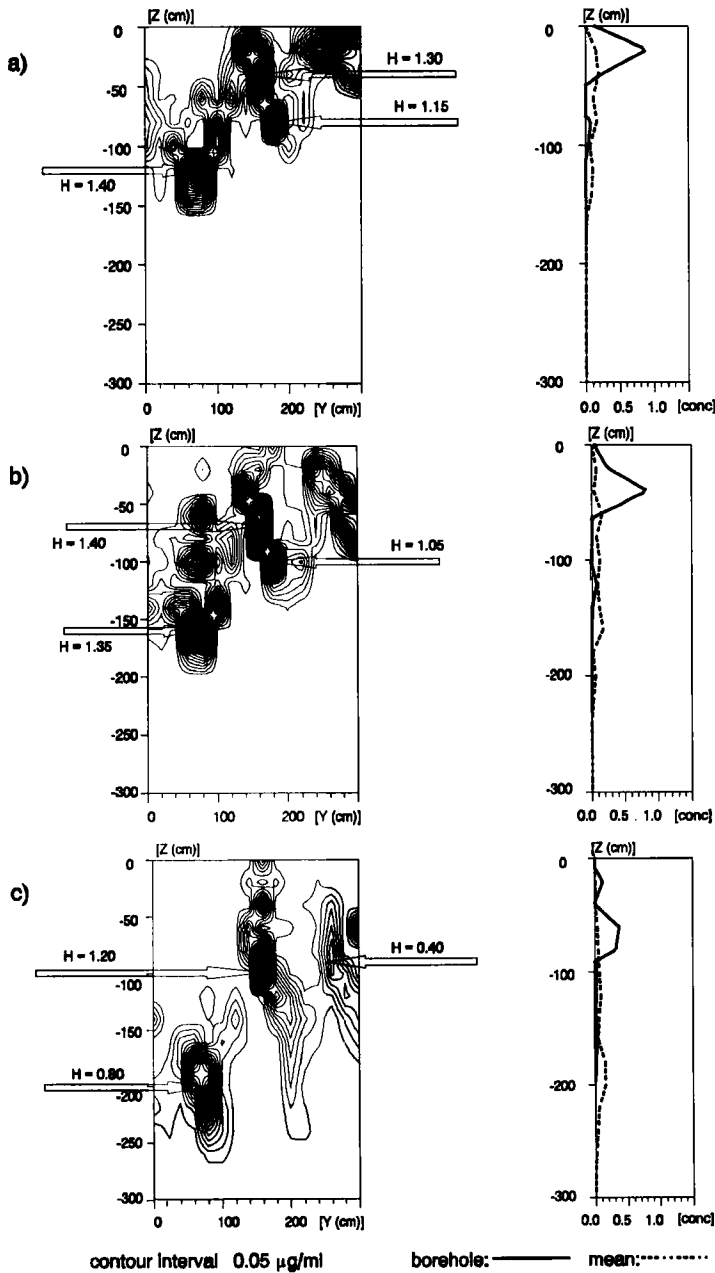
**Fig. 7.15:** Development in time of a cross section of a concentration field of a tracer in a soil with a high degree of heterogeneity. On the right side of the figures the mean concentration profiles and the concentration profiles obtained from a fictitious borehole in the middle of the cross section are shown: a) 5 days, b) 10 days and c) 20 days after simulation start. *H* marks the location where the highest values occur.
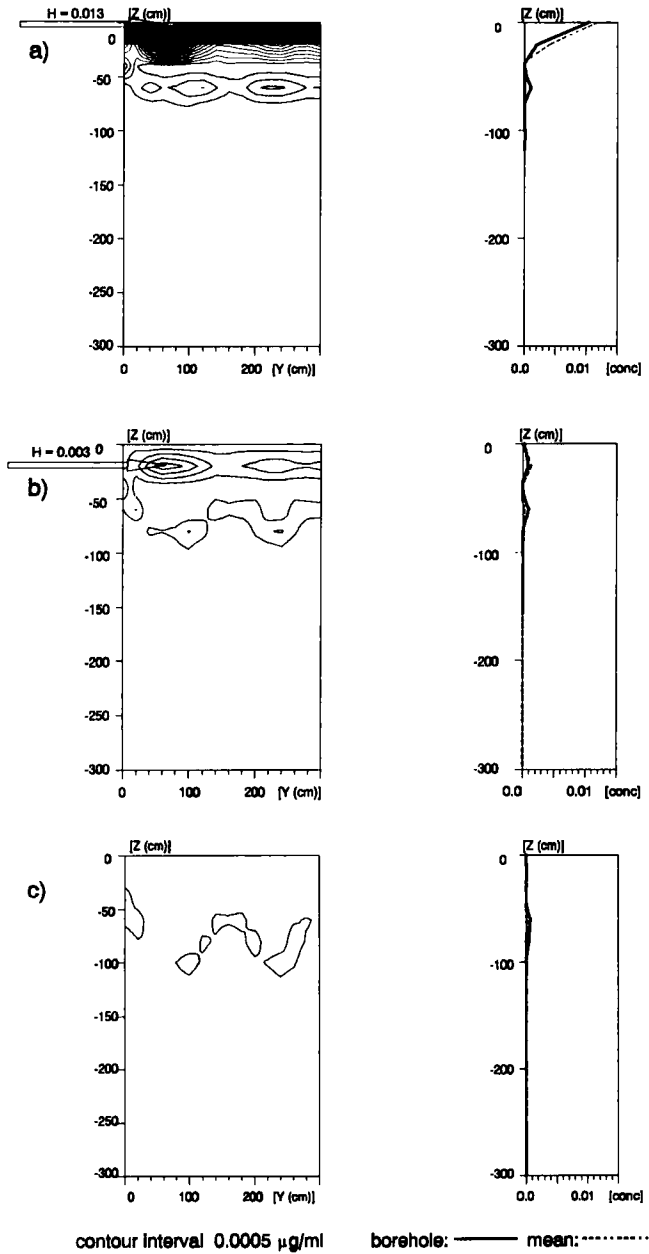
**Fig. 7.16:** Development in time of a cross section of a concentration field of a fast degradable substance in a soil with a low degree of heterogeneity. On the right side the mean depth profiles and the profiles obtained by a fictitious borehole in the middle of the cross section: a) 5 days, b) 10 days and c) 20 days after simulation start. $H$ marks the location where the highest values occur.
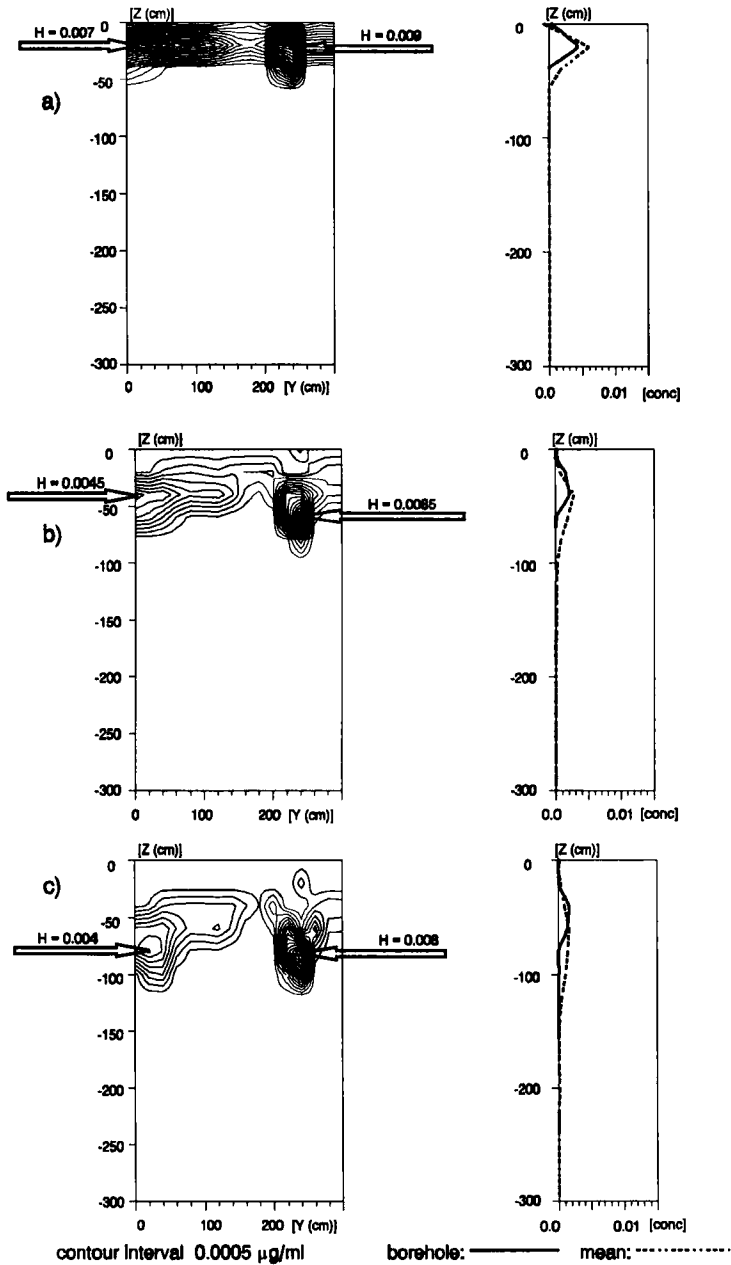
**Fig. 7.17:** Development in time of a cross section of a concentration field of a slowly degradable substance in a soil with a low degree of heterogeneity. On the right side the mean depth profiles and the profiles obtained by a fictitious borehole in the middle of the cross section: a) 5 days, b) 10 days and c) 20 days after simulation start. $H$ marks the location where the highest values occur.

# 7.4   Effective Parameters

## 7.4.1   Performance Criteria

As we have seen the translation of transport and kinetic models from the laboratory scale to the field and to the catchment scale demands new concepts. One has to abandon the deterministic view valid at the laboratory level for homogeneous soil columns. The question is then: is it still possible to make reasonable predictions at larger scales on the basis of local process models? Mathematically, the problem is posed in the following way:

**Given:** a process model valid on a local scale

**Problems:**

1.    Find a parameter set, which summarizes small scale spatial heterogeneity.
2.    Derive a model, which describes the same process on a larger scale taking explicitly into account lower scale spatial heterogeneity.

The second problem is very demanding from the mathematical point of view. Several approaches have been proposed such as stochastic partial differential equations. The whole subject is still in rapid development. In this book we shall dwell on the mathematically less ambitious problem of finding effective parameters.

The concept of effective parameters means to apply the original deterministic model to a defined region - plot or field - with an appropriate set of parameters. These are called effective parameters or sometimes referred to as representative parameters. They can be defined only with respect to a given performance index. An obvious criterion is a measure of distance between the expectation of the concentration field and the value obtained by using an effective parameter:

$$L(\phi) = \| E[c(x,t,\phi)] - c(x,t,\phi) \| \tag{7.18}$$

where $\| \ \|$ denotes a suitable measure of distance. Then it is straightforward to define an effective parameter $\phi_{eff}$ by

$$L(\phi_{eff}) = \min_{\phi \in U} \{L(\phi)\} \tag{7.19}$$

This definition is only of theoretical importance, since all the necessary information is already given by the knowledge of the probability density function of the parameters. However, the performance criterion allows the comparison between several definitions of effective parameters. A convenient measure of distance is the integral

$$L(\phi) = \int\limits_{G} \int\limits_{t=0}^{T} (E[c(x,t,\phi)]) - c(x,t,\phi))^2 d^3x \, dt \tag{7.20}$$

Let us apply now this criterion to the analytic solution of the convection dispersion equation used in the example treated in section 7.2.1. Figure 7.18 shows the dependence of this criterion on the effective parameter $D_{eff}$ for a lognormal distribution of $D$. Figure 7.19 shows the breakthrough curve obtained by the value of $D$ which minimizes the criterion in comparison to the expectation and mean parameter curve.
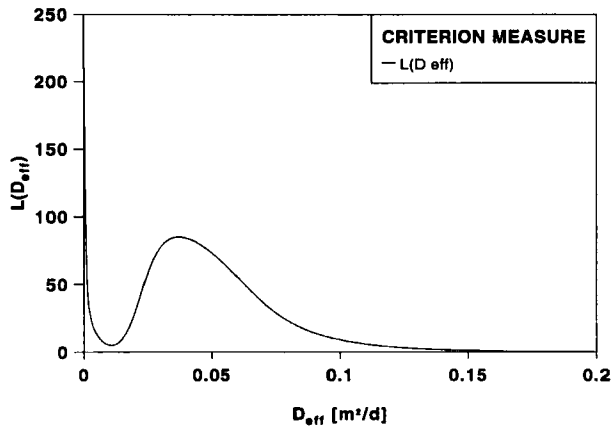


**Fig. 7.18:** Dependence of the performance criterion on the effective parameter $D_{eff}$ for a lognormal distribution of $D$.
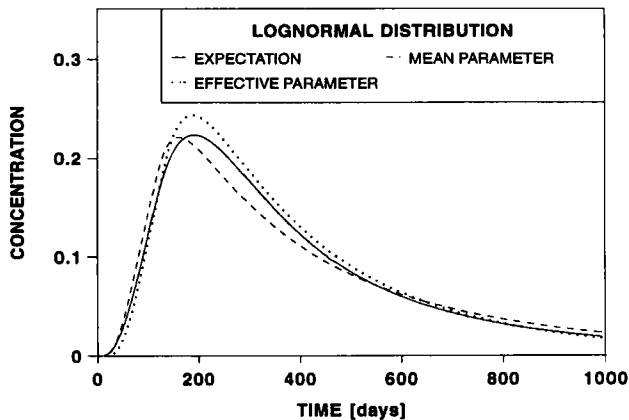


**Fig. 7.19:** Effective parameter curve, mean parameter curve, expectation.

In practice, one has to derive effective parameters by the information available from the probability density function (estimated by the histogram). We will tentatively define effective parameters by the mean value of $D$, by the mode of the density function and by the median. The integral (Eq. (7.20)) is computed for the integration intervals [0,100] cm and [0,30] days.

The best performance is achieved by the median if the underlying distribution is skewed. (For the normal density median and expectation are identical).

For the assessment of environmental impacts, one is interested in mean properties of concentration and flow fields over large regions. The following mean properties are most important for practical applications:

1.  The amount of pesticide resident in the upper layer down to the plow horizon.

$$c_p(t) = \frac{1}{|G|} \int_G c(\vec{x},t) d^3x \tag{7.21}$$

2.  The flow of pesticide across the reactive soil layers into the ground water. The activity of a soil layer (with respect to pesticide degradation) is assumed to be proportional to its $C_{org}$-content.

$$J_u = \int_{\partial G_u} q(x,y,z_u) c(x,y,z_u) dx dy \tag{7.22}$$

These two properties are important criteria to judge the performance of effective parameters.

### 7.4.2 Guidelines for the Use of Effective Parameters

The foregoing analysis has shown that it is not recommendable to characterize transport by only one parameter, the effective parameter, alone without considering measures of uncertainty. Even in homogeneous soils such as loess soil parameters are statistically distributed. Figure 7.20 shows the density function of the $K_s$-value derived from data of a sandy soil.
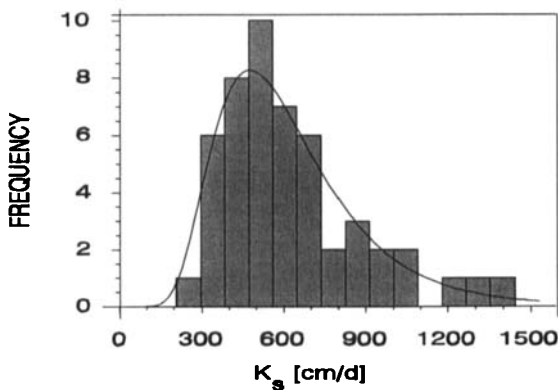


**Fig. 7.20:** Histogram of $K_s$-value in a sandy soil (data from Wierenga et al., 1989).

The following guidelines should be regarded only as tentative. They reflect the authors experience with spatial variability in quaternary soils of Northern Germany.

Two aspects have to be distinguished. The first concerns randomness due to the underlying spatial random field. The second concerns missing information.

## Random soil columns

This concept is based on the assumption, that lateral flow can be neglected. This implies that the correlation lengths of the underlying spatial fields are large so that microscale patterns only weakly influence the flow field. We consider first the case that the density function is known (this demands that the sample size is very large allowing to identify the distribution law). The recommended procedure is then straightforward.

1.    Calculate mean profiles either by direct integration or by the Latin Hypercube method!
2.    Construct percentile bands for the profiles at chosen locations or time points. This can either be done by density transformation techniques as demonstrated in section 7.2.1 or by the Latin Hypercube method. The latter method has a larger range of applicability than the former, which demands a density transformation!
3.    Take any parameter set, which results in a profile within a prescribed percentile band as representative parameter set!

However, in practice, sample sizes are frequently very small and the type of density function cannot be identified, or the data do not match any classical model such as a normal or lognormal density. In this case Latin Hypercube methods still apply. Calculations are performed based on the empirical distribution function.

In large scale applications, model parameters have to be derived from the information contained in soil survey maps. The derivation of model parameters from this kind of information can be achieved by use of pedotransfer functions (cf. chapter 6).

## Soils with large microscale variation

In these soils microscale variation creates heterogeneous patterns within the spatial dimension of a soil horizon. Only three-dimensional models are capable of simulating water and matter flow in such environments. One has to recall that an effective parameter is meant to replace an inhomogeneous block of soil by an equivalent homogeneous one. It is obvious that this approach yields only crude approximations in a block of soil with complicated spatial patterns, especially if degradation is involved. Hence in this situation effective parameters are only of limited value. Instead, we propose a new concept which is based on the notion of a **representative parameter field**.

1.    Generate realizations of the random process!
2.    For each realization compute the value of an appropriate criterion measure, e.g. the amount of pesticide crossing a soil layer!
3.    Construct the histogram of the criterion measure!
4.    Take any realization belonging to the modal value of the histogram as representative parameter field!

# 7.5    Macroscale Variation

## 7.5.1    The Implementation of Simulation Models into Geographical Information Systems

Pesticides are applied in large quantities at regional scales. The assessment of environmental fate and environmental impact has therefore to take into account the macroscale variation of soil types in connection with land use patterns and application habits of the farmers and meteorological data. The necessary link between spatial information and pesticide environmental fate models can best be achieved in the frame of a geographical information system (GIS). GIS efficiently store, manipulate, retrieve, analyze, and display geo-referenced spatial and nonspatial data (Burrough, 1986). In general, two types of data are stored in GIS: geographic definitions of earth surface features (objects) and attributes or qualities related to these objects. There are two different modes of storage.

1. In the **vector representation** the boundary of any object is described as a point, a line or a polygon. Attributes are stored by using a database management software program. Data files are linked by an identifier number given to each feature in a map. Vector systems are efficient in database management and storage, because only boundaries of features are stored. This offers the advantage of a correct description of map features.

2. **Raster systems** combine objects and attributes in unified data files. The land surface is subdivided into a fine mesh of grid cells. For each cell, a representative feature attribute is stored as code value. Although raster systems have some advantages over vector based systems concerning the simplicity of the data structure, the distortion of the object boundaries at high resolutions is a major drawback.

Environmental modeling with GIS is an active area of research (Goodchild et al., 1993). It implies the coupling or even integration of models into a GIS. This demands that the models have a reference to spatial features both via initial and boundary conditions and via model parameters. There are two problems involved. The first one is a technical problem and concerns the level of model integration into a GIS. The second one concerns the link between earth surface features stored in the GIS and the model parameters. Consider the case of water transport in the unsaturated zone (cf. chapter 5). The model parameters required are the shape parameters of the water retention curve and the hydraulic conductivity. These parameters are not available from soil survey maps. They have to be derived from basic soil survey data (texture) by means of pedotransfer functions (cf. chapter 6).

The simplest way to couple a GIS with a model is the ad-hoc integration (Tim and Jolly, 1994). This means, that process models and GIS are developed separately each with its own operating system. Interaction is solely mediated by file exchange. The GIS provides initial and boundary conditions and the features for each elementary unit of space relevant for the process under study. This may be a hydrological unit or an ecotope, which results from the intersection of the soil survey map with the landuse map. In a first step, the qualitative information provided by the GIS have to be transformed to model parameters via pedotransfer functions. In the one dimensional case simulations are run for each dataset separately. Simulation results are then stored on files, which can be further processed by the

# 3-DIMENSIONAL VIEW



# 2-DIMENSIONAL VIEW



# LANDUSE



# SOIL MAP



# CATCHMENTS AND RIVERS



# FINITE ELEMENT MESH



# GEOSTATISTICAL DATA

**GIS ARC/INFO**

**RDBMS ORACLE**

**Pedotransfer Functions**

**Numerical Models, e.g.:**

$$R_i \frac{\partial x_i}{\partial t} = \nabla D \nabla x_i + \sum_j Q_j$$
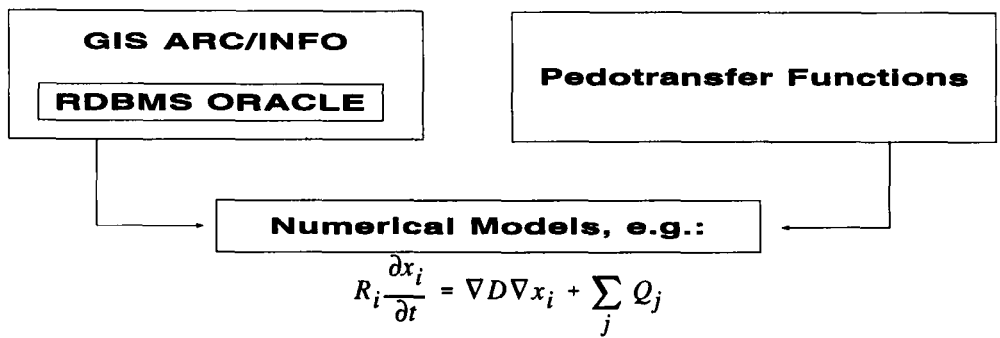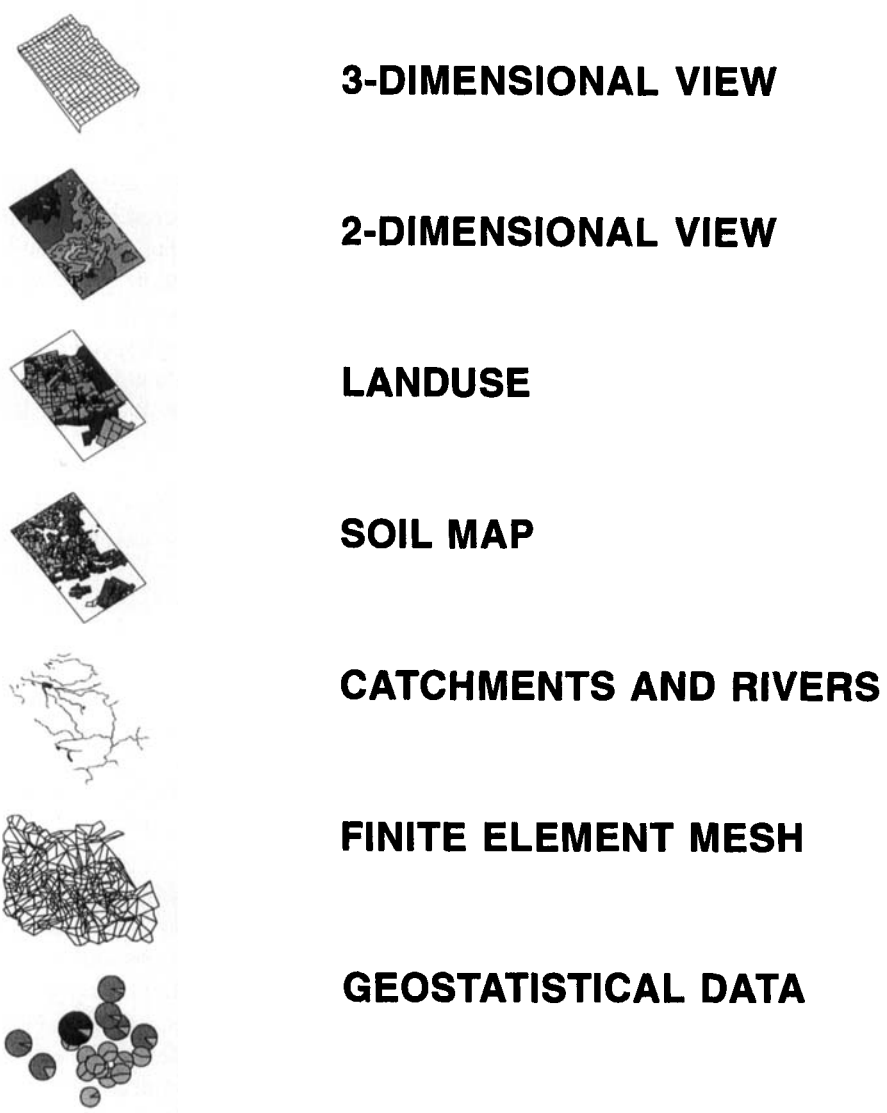
**Fig. 7.21:** General layout of GIS-model integration.

GIS for graphical display (cf. Fig. 7.21). However, such a system is difficult to handle and
is time consuming, because two different software products are involved.

Therefore, a form of integration is to be preferred, where model and GIS are linked by a
common user interface. This can be easily done in ARC/INFO by programming a user
interface with the GIS ARC/INFO programming language AML (Arc Macro Language). This
interface allows easy access to the simulation models and the GIS, even for users without
much knowledge of the code.

## 7.5.2 Case Study

In the following study (Lücke et al., 1995) the herbicide model FLOWCONC (Walker, 1987)
was implemented into the GIS ARC/INFO. The objective of this study is the assessment of
the recropping risk of winter wheat following sugar beet in a crop rotation. Typically, the
herbicide Ethofumesate is applied to sugar beet cultures in spring, and the question is if
residues 150 days after application are likely to cause crop damage in a catchment with
different soil types.

Figure 7.22 shows the layout of the coupling of FLOWCONC, pedotransfer functions and
ARC/INFO. The storage of the attribute data was realized using the ORACLE Data Base
Management System (RDBMS). The GIS ARC/INFO offers a direct link to the data base.
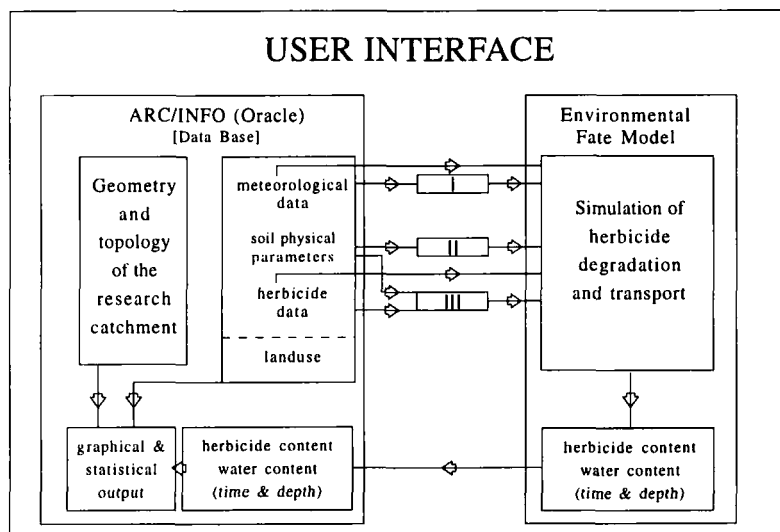


**Fig. 7.22:** Scheme for the coupling of the GIS ARC/INFO with a pesticide simulation model.
*I* indicates calculation of potential evaporation according to Haude (1955). *II* indicates a pedotransfer
function for calculation of water content at field capacity and at -200 kPa according to Rawls and
Brakensiek (1985). *III* indicates selection of adsorption/degradation parameters.

**Simulation Model**

The simulation model FLOWCONC (Walker, 1987) was used to predict the herbicide persistence in soils. In this model herbicide degradation is described by first order kinetics dependent on soil temperature and moisture content. The temperature dependence is described by the Arrhenius function (cf. Eq. (3.157)) and the humidity dependence by an empirical function (Eq. (3.162)). The joint effect of both variables on the degradation rate is modeled by the product of both functions (cf. Eq. (3.162)). FLOWCONC refers to the half-life written in the following form, which is equivalent to Eq. (3.164).

$$t_{1/2} = A\,\Theta^{-B}\exp\left[-\frac{\Delta E}{R}\frac{T-T_0}{TT_0}\right] \tag{7.23}$$

with the notations

$\Delta E$    : activation energy [kJ/mol]
$R$       : gas constant [kJ/(mol K)]
$T$       : temperature [K]
$T_0$     : standard temperature (in this study: 20 °C)
$A$       : half-life at $T_0$ [K] and at $\theta = 1$ %
$B$       : moisture slope at $T_0$
$\Theta$       : water content [% by weight]

The parameters $A$, $B$, and $\Delta E$ used in this model are determined in laboratory incubation assays according to Walker (1974) at different temperatures and soil moisture contents. Adsorption is described by a linear equilibrium approach. The distribution coefficient $K_d$ is determined in laboratory measurements as described by Pestemer and Auspurg (1987). Since adsorption may increase with time (cf. section 3.1), the $K_d$-value is allowed to increase during the simulation (Walker, 1987). The calculation of transport and water flux is based on a cascade model, where water exceeding field capacity moves downwards. The model requires maximum and minimum air temperature, rainfall data and the potential evaporation on a daily base to predict the moisture content and soil temperature of each layer. Further input data required by the model are soil moisture content at field capacity and at pressure head of -200 kPa, bulk density, initial water content, and herbicide degradation parameters and distribution coefficients for the adsorption of the herbicide in soils.

**Integration GIS-Model**

The implementation of the herbicide model into GIS ARC/INFO was realized by programming a user interface with the ARC/INFO programming language AML (Arc Macro Language). In the GIS, geometrical and topological data of the Eisenbach research catchment are stored (cf. Fig. 7.23). Overlaying land use patterns and soil type distribution yields 789 small homogeneous areas (ecotopes) which are used for the simulations. Each ecotope is characterized by a parameter set for the degradation/leaching model. The AML is used to generate a control file for the herbicide model. It controls the selection of correct model parameters from the data base and the transfer of the results to the RDBMS. After simulation, ARC/INFO is used to visualize the results.
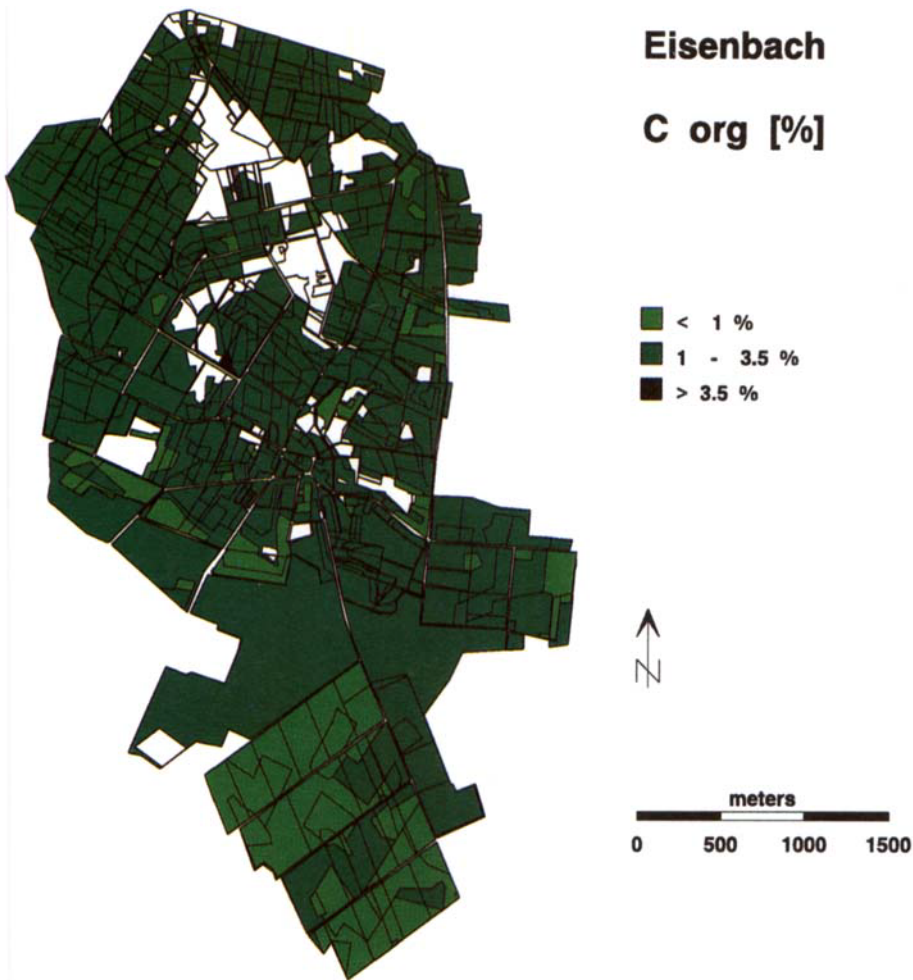
**Fig. 7.23:** Soil map of the Eisenbach research catchment. Here: $C_{org}$- content.

**The Catchment**

The Eisenbach catchment is located in the north German Pleistocene sand plain about 80 km north of the city of Braunschweig, encompasses about 16 km$^2$ and ranges between 60 and 130 m above sea level. The catchment consists mainly of sandy soil with clay and loam lenses and is surrounded in the east, south and west by moraines. The geology and geomorphology are dominated by glacial sands and gravel deposited during the Saale (Illinoian) ice age. The main crops grown in this area are rye, barley, sugar-beet, and potatoes (McVoy, 1995).

**Soil Properties**

A first soil survey ("Reichsbodenschätzung") was carried out in Germany starting in the thirties to provide fair taxation for arable land. For this purpose, grid samples were taken with 50 meters distance between the bore holes, each 1 meter deep. Samples with the same properties were grouped to homogeneous areas, each described by one representative data set. The measurements were made over the agricultural regions of Germany and have recently been repeated for Lower Saxony. The data set is available in digital form.

**Tab. 7.1:** Translation of stored string classification to input data for the model. Field capacity is calculated using the pedotransfer function of Rawls and Brakensiek (1985).

| String classes | | Translated input data [%] | | | | | |
|---|---|---|---|---|---|---|---|
| Texture[1] | Organic carbon content | Sand | Clay | Silt | Organic carbon content | Porosity | Water content at field capacity |
| mSfs | h1 | 92.5 | 2.5 | 5.0 | 0.29 | 36 | 15.0 |
| mSfs | h1 | 92.5 | 2.5 | 5.0 | 0.29 | 40 | 13.9 |
| mSfs | h3 | 92.5 | 2.5 | 5.0 | 3.49 | 46 | 16.8 |
| mSfs | h4 | 92.5 | 2.5 | 5.0 | 6.69 | 54 | 19.6 |
| mS | h2 | 92.5 | 2.5 | 5.0 | 1.74 | 42 | 15.5 |
| mS | h2 | 92.5 | 2.5 | 5.0 | 1.74 | 41 | 15.2 |
| mSfs | h1 | 92.5 | 2.5 | 5.0 | 0.29 | 41 | 15.2 |
| Sl2 | h1 | 78.5 | 6.5 | 15.0 | 0.29 | 50 | 21.0 |
| Sl2 | h4 | 78.5 | 6.5 | 15.0 | 6.69 | 65 | 25.6 |
| Sl2 | h3 | 78.5 | 6.5 | 15.0 | 3.49 | 54 | 22.4 |
| Sl2 | h2 | 78.5 | 6.5 | 15.0 | 1.74 | 51 | 21.3 |
| Su2 | h2 | 80.0 | 2.5 | 17.5 | 1.74 | 49 | 20.9 |
| Su2 | h3 | 80.0 | 2.5 | 17.5 | 3.49 | 53 | 22.4 |
| f3Sanl3 | h2 | 66.5 | 10.0 | 23.5 | 1.74 | 41 | 21.0 |
| Sl3 | h3 | 66.5 | 10.0 | 23.5 | 3.49 | 55 | 25.6 |
| Sl3 | h2 | 66.5 | 10.0 | 23.5 | 1.74 | 52 | 24.5 |
| Sl3 | h1 | 66.5 | 10.0 | 23.5 | 0.29 | 51 | 24.2 |
| Su3 | h2 | 63.5 | 4.0 | 32.5 | 1.74 | 51 | 25.9 |
| Su3 | h3 | 63.5 | 4.0 | 32.5 | 3.49 | 55 | 27.5 |
| Sl4 | h2 | 60.0 | 14.0 | 26.0 | 1.74 | 52 | 26.2 |
| Ul2 | h2 | 12.5 | 9.5 | 78.0 | 1.74 | 54 | 42.9 |

---

[1]   Refers to the German Guideline for Soil Characterisation "Bodenkundliche Kartieranleitung" (Anon., 1982) (e.g. Su = silty sand, Sl = loamy sand; the number indicates the variable fractions of sand clay and silt content).

The soil properties are grouped into different classes. For example the soil texture and organic carbon content is represented by string classification. The range for organic carbon content may be e.g. from 1 to 2 % (h2) or from 2 to 4 % (h3), according to the German Guideline for Soil Characterization "Bodenkundliche Kartieranleitung" (Anon., 1982). Table 7.1 shows the transfer of string classes to numerical input data. For the translation from string classes, the average clay/silt/sand or organic matter content of each class are used. Water content at field capacity and at soil suction of 2 bar are calculated using retention curves which are estimated by the pedotransfer function (PTF) of Rawls & Brakensiek (1985) (cf. section 6.1).

**Herbicide Properties**

Ethofumesate is a herbicide mainly applied to sugarbeet in spring. Degradation in soil is fastest under wet and warm conditions (Rahman, 1978) and is mainly caused by microorganisms (Schweizer, 1976). Their activity is mainly influenced by the organic carbon content of the soil (Schweizer, 1976).

Herbicide degradation characteristics were determined in laboratory assays at different soil moisture contents and temperatures according to Walker (1974). Degradation parameters are available for 5 and $K_d$-values for 11 different soils (Gottesbüren, 1991). They are stored in the ORACLE data base.

The possible damage to winter crop succeeding sugar beet was derived from a dose response curve for wheat established in hydroponic culture by Pestemer (1983) (cf. Fig. 7.24).
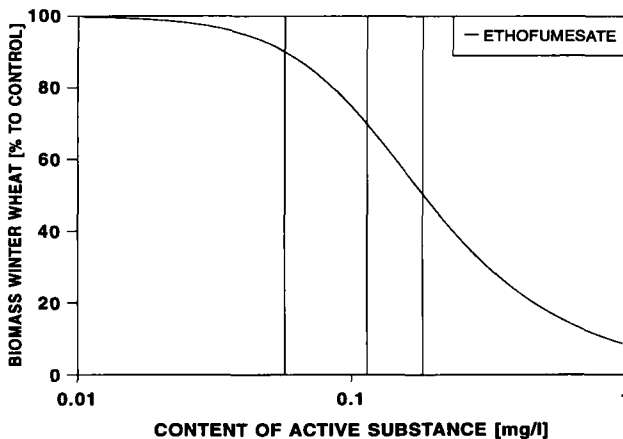


**Fig. 7.24:** Dose-response curve of Ethofumesate for winter wheat as established by Pestemer (1983).

If sample sizes are large, it is possible to derive pedotransfer functions estimating sorption and degradation parameters (cf. section 3.4.2). Due to the limited amount of information on degradation rates and sorption constants a pedotransfer function can not be developed for Ethofumesate. In addition, the organic matter content of the soils is available only in three classes in the soil maps. Therefore, pesticide sorption was not related to organic carbon using $K_{oc}$-values.

This lack of data is a situation commonly met in practice. There are data available, but not enough to establish exact relationships between soil data and model parameters. There is only one way out of this dilemma: one has to resort to more heuristic approaches. Anyway, the results of the last section of this chapter have drastically demonstrated that the randomness of soil properties renders the notion of exactness obsolete. The following method allows to derive model parameters from soil properties even from samples of small size. Each sample is presented as a point in the sample space. To each point belongs a model parameter, e.g. the half-life. For the parameter value of an arbitrary point in the sample space the value of its nearest neighbor is taken. Gottesbüren (1991) introduced the following distance function for the $K_d$-value of Ethofumesate, which weighs the influence of the soil properties.

$$D\left[(C,T,P),(C_m,T_m,P_m)\right] = w_1 |C - C_m| + w_2 |T - T_m| + w_3 |P - P_m| \qquad (7.24)$$

with the notations

$D$    : distance [cm]
$C$    : organic matter content [% by weight]
$T$    : clay content [% by weight]
$P$    : pH [1]
$w_i$   : weight coefficient of soil property $i$

The index $m$ denotes those soil properties, for which parameters are available. The coefficients for the distance function of the $K_d$-values are $w_1 = 0.8$, $w_2 = 0.1$ and $w_3 = 0.1$, for the degradation rates $w_1 = 0.3$, $w_2 = 0.6$ and $w_3 = 0.1$.

**Model Application Example**

Tramat 500 (50 % Ethofumesate) was assumed to be applied with a rate of 3 kg ha$^{-1}$ on May 1$^{st}$, 1988. Weather data used in the simulation (daily minimum and maximum temperatures and rainfall) were provided by a weather station located within the catchment. The mean annual temperature in the catchment is about 9°C, the mean annual rainfall about 700 mm. In addition to the natural rainfall, this catchment is irrigated with about 125 mm year$^{-1}$. In the growing season 1988 (May to September) the precipitation rate was 302 mm, the mean air temperature 15°C. Daily potential evaporation for this period was calculated by the empirical formula of Haude (1955) considering the actual and the saturated air humidity and the air temperature at the time 2 pm.

Due to different textures, organic matter contents and field capacities, 21 different ecotope classes were derived from the 789 sites. Some important characteristics of these classes are shown in Tab. 7.1. The degradation parameters selected from the data base were estimated from laboratory studies with similar soils. Of five available parameter sets, two were selected by the system according to soil properties. For soils with clay content of 6.5 % or higher, moisture parameters $A$ and $B$ were 1247 d and 1.28, respectively, and the activation energy was 49.8 kJ mol$^{-1}$. For the pure sandy soils, $A$ was 231 d, $B$ was 0.48, and $\Delta E$ was 54.1 kJ mol$^{-1}$. Adsorption coefficients ($K_d$-values) between 1.41 dm$^3$ kg$^{-1}$ for low organic matter soils and 2.93 dm$^3$ kg$^{-1}$ for higher organic matter contents were selected from the data base according to the corresponding soil properties.

The simulation was run for 150 days, a common duration for cropping of sugarbeet. Residue levels of Ethofumesate in the top 30 cm of the soil were given by the model. For the top 10 cm layer also plant available residues were calculated. The possible damage to a succeeding winter wheat crop at this date was assessed by comparing the available residues with dose-response values for wheat established in hydroponic culture according to the method of Pestemer (1983).

**Results**

After 150 days, the simulation resulted in total residues between 0.2 and 23.8 % of the initial concentration in soils, as shown in Fig. 7.25.



**Eisenbach**

**Herbicide content after 150 days in percent of initial concentration**

☐   < 10 %
☐   10 - 20 %
■   > 20 %
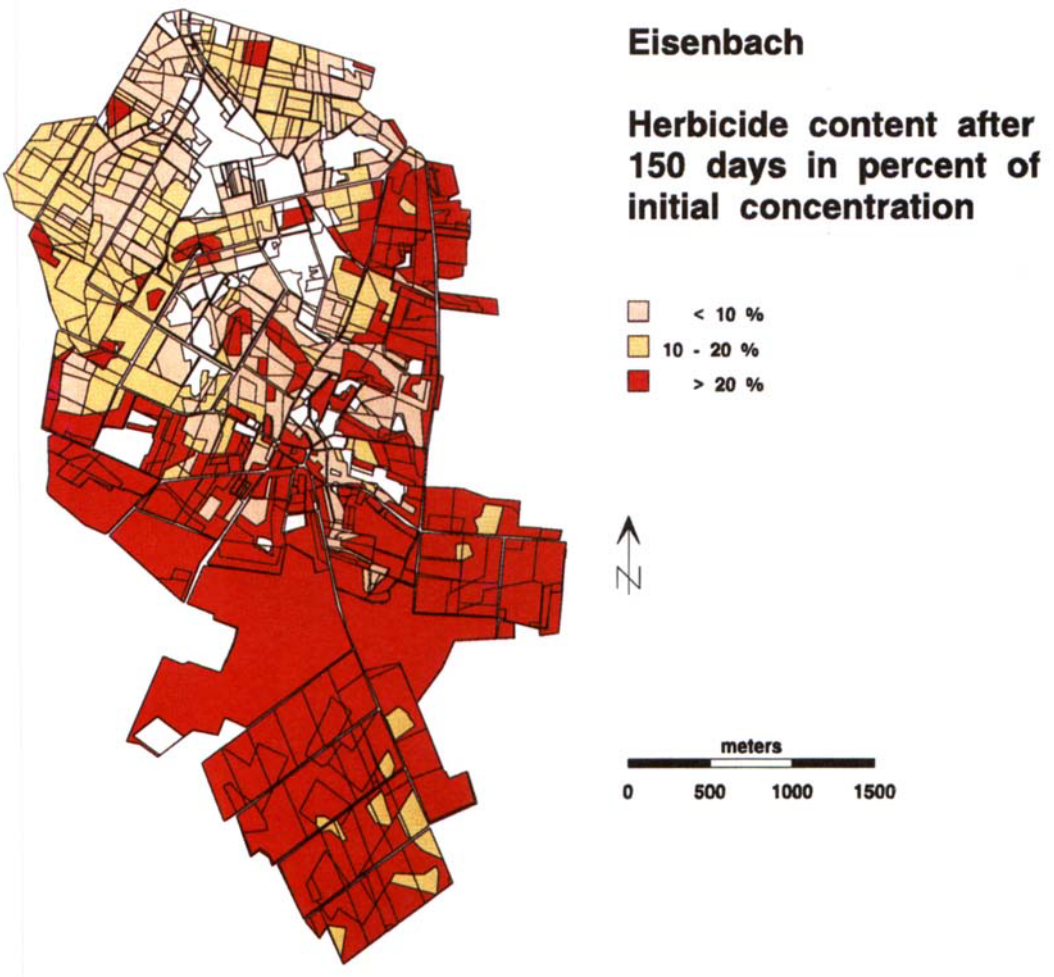
**Fig. 7.25:** Map of residues in % of initial dose 150 days after application.

The spatial distribution of residues over the catchment correlate well with the clay content. Higher residues are found mainly in the sandy regions in the south and east of the catchment, where a lower moisture content throughout the period of the simulation caused a slower degradation compared to the silty and loamy soils with higher field capacities in the center of the area.

For 17 % of the arable land (1.6 km$^2$), the total residues remaining in soil were below 10 % of initial dose. For 62 % (5.7 km$^2$), the residues were higher than 20 % of initial dose. These residue levels are in accordance with other field persistence trials (Schweizer, 1976; Copin et al., 1985). Gottesbüren et al. (1994) observed between 15 and 20 % of the dose on three different sites in three different years after about 5 months.

On the sandy soils, residue levels are higher than 14 % of initial dose after 150 days on all sites. On the other soils, residues were below 8 % of initial dose.

The field capacity is a sensitive parameter. Differences in residue levels in ecotopes with identical degradation parameter sets are mostly due to different field capacities and thus moisture contents (cf. Fig. 7.26).

As shown in Fig. 7.26 a strong relationship ($r$ = - 0.983) between water content at field capacity and residue level exists on the sandy soils. On the silty and loamy soils the correlation is less pronounced ($r$ = - 0.783).
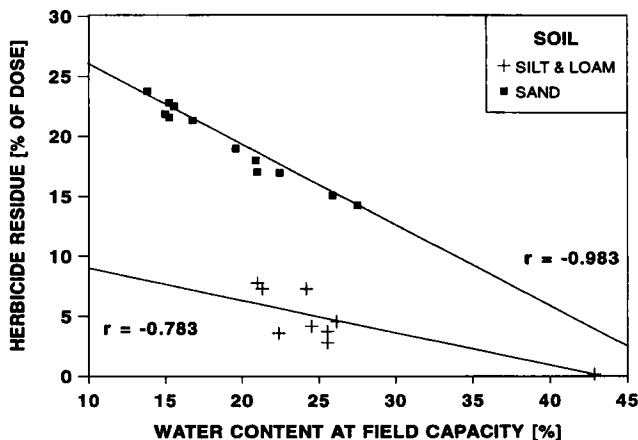


**Fig. 7.26:** Relationship between water content and residue levels.

Different field capacity and adsorption values in soils may lead to different leaching behavior of herbicides in the study area. Analyzing all simulations, no Ethofumesate was leached below 20 cm depth during this summer period, and below 10 cm only traces occurred. From all simulated findings below 10 cm (1324 out of 1850 sites), only in 58 sites or 6 % of the area (0.55 km$^2$) the residues were higher than 0.1 %, but in all cases they were below 1 % of the initial dose. These sites are all located in the sandy, low sorptive moraine area of the catchment, where the ground water level is below 10 m. Under these circumstances, even during a relatively wet summer season, the risk of ground water contamination is very low.

Similar leaching behavior, with no residues found below 10 cm depth in field trials during 6 months, was found by Copin et al. (1985). Rahman (1978) found most of the applied Ethofumesate remained in the top 5 cm of soil.

**Recropping Risk**

For the evaluation of recropping risk, only the top 10 cm of the soil are taken into account where the roots of germinating plants and the highest herbicide concentrations are located. The results of the comparison between available residues and the dose-response curve are shown in Fig. 7.27.
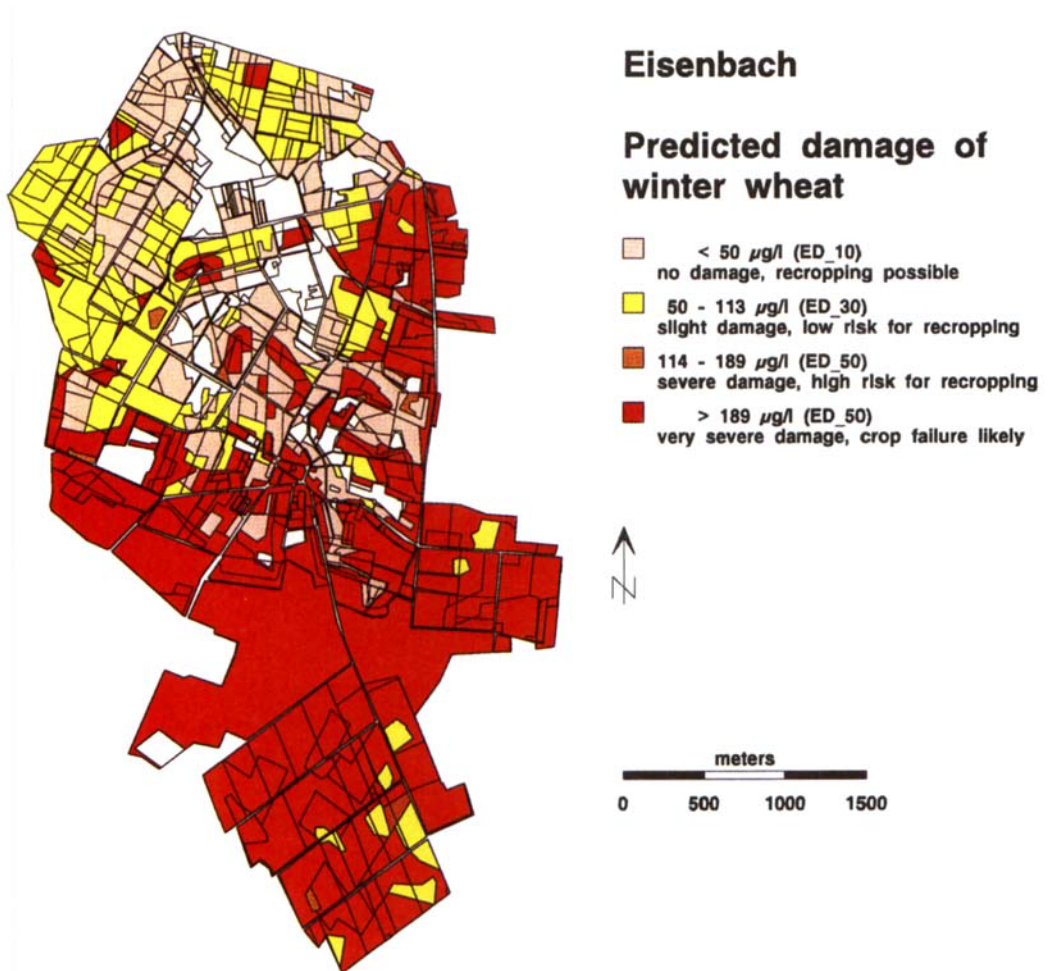


**Fig. 7.27:** Map of recropping risk.

For 17 % of the arable land (1.6 $km^2$), no damage was predicted. For 21 % of the area (1.9 $km^2$) the residue levels were between $ED_{10}$ (10 % growth reduction in hydroponic culture) and $ED_{30}$. In these cases, a slight crop damage may occur, but normal yields can still be expected. For 55 % of the area (5.1 $km^2$), available residues were higher than the $ED_{30}$, and for the remaining 7 % (0.6 $km^2$) higher than the $ED_{50}$. In both classes recropping with winter wheat cannot be recommended, because a great crop loss or even crop failure is likely. The sites of high risk were located mainly on the lighter soils in the eastern and southern parts of the catchment, where degradation was slower and availability to plants higher due to lower adsorption.

Ethofumesate applied to sugar-beet in late spring is known to cause problems in crop rotations with susceptible crops (e.g. Stryckers et al., 1978). If applied in late autumn to grassland at 1 kg $ha^{-1}$ its phytotoxic activity may persist up to 7 months depending on the climate (Rahman, 1978). Gottesbüren et al. (1994), however, did not find damage of winter wheat sown in autumn after spring application of 1.5 kg $ha^{-1}$ Ethofumesate, although slight or severe damage response was predicted for two sites. In general, the model tends to overestimate residues and therefore has an inherent safety margin for predictions of crop damage.

## 7.6   Fuzzy-Approaches

Notations

| | |
|---|---|
| $A_i$ | : input fuzzy sets |
| $n$ | : number of input fuzzy sets |
| $B_j$ | : output fuzzy sets |
| $n_r$ | : number of rules |
| $c_j$ | : certainty factor of $j^{th}$ rule |
| $p$ | : number of premises of a rule |

A totally new concept to cope with soil heterogeneity and uncertainty is based on fuzzy-logic. There are only few applications of fuzzy-logic in environmental fate modelling thus far (Ganoulis, 1994). The authors do not regard these approaches in contradiction to deterministic or stochastic process models. However, there are situations, where the information does not suffice to identify the process properly or to estimate parameters. In this case one has to resort to all sources of knowledge combining them into an expert system. It is assumed that the reader already has at least some notions of fuzzy-logic, which has gained broad attention these days in the field of control of technical systems. The following example of the application of fuzzy-logic to the prediction of the mode of decay and the $DC_{50}$-value only serves to illustrate the modelling philosophy. This short section is not thought of as an introduction to fuzzy-logic. For this purpose, the reader is referred to standard textbooks (e.g. Zimmermann, 1991; Yager and Zadeh, 1992; Zadeh, 1987).

**Fuzzy-Sets**

In ordinary set theory a set consists of well defined objects or elements. One can decide in a unique way whether an element belongs to the set or not. This can be expressed by its membership function. Let $M$ denote a set and $x$ an element out of a reference set $X$. Then the membership function is

$$\mu(x) = \begin{cases} 1 & \text{if } x \in M \\ \\ 0 & \text{if } x \notin M \end{cases} \tag{7.23}$$

The key concept of fuzzy theory is the introduction of membership functions, which can take on values in the interval [0,1], characterizing the degree by which an element belongs to a set. Let $A$ denote the set "$DC_{50}$-value of a substance" with the three elements "slow", "medium" and "fast". Let us define as reference set $X$ the time interval [0,100] days. Is a value of 30 days to be regarded as fast or as medium or as slow? Of course, this depends on the context. In the context of herbicide kinetics a $DC_{50}$-value of 1 day would surely be regarded as fast, and a $DC_{50}$-value of 100 days would surely be judged as slow. For a $DC_{50}$-value of 30 days it is not that easy to decide to which category it belongs. This uncertainty or vagueness is modeled by the membership function expressing for any given $DC_{50}$-value the degree by which it belongs to any of the three categories. Figure 7.28 shows plausible membership functions for this example.
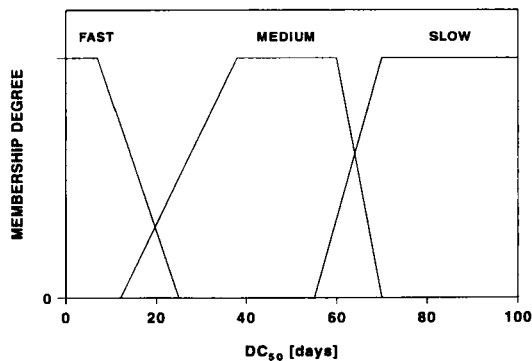


**Fig. 7.28:** Membership function for the fuzzy-set "low","medium" and "high" $DC_{50}$-value.

**Degradation of Bentazone**

As an example the decay of Bentazone dependent on soil properties is modeled by a fuzzy-expert system. Experimental data of a small sample size show that the kinetic behavior drastically changes with soil properties. In soils with high $C_{org}$-content mono-exponential decay is observed, whereas in soils with low $C_{org}$-content long lag-phases occur followed by either a slow or fast decay. All decay curves vary between these two extremes. One can classify the decay curves into the four types: fast mono-exponential decay, slow mono-exponential decay, short lagphase followed by fast decay, long lagphase followed by slow decay. For ease of presentation, these classes are noted as mono-fast, mono-slow, lag-fast and lag-slow. Figure 7.29 shows sample curves for the classes mono-fast, mono-slow and lag-fast.
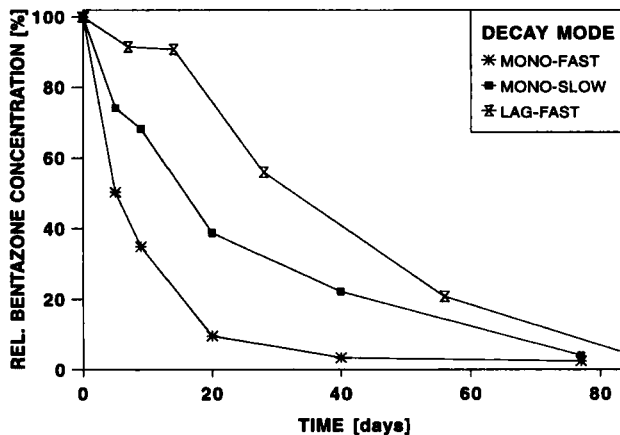
**Fig. 7.29:** Decay modes of Bentazone.

The decay mode and the degradation rate are further influenced by the pH-value of the soil. We want to construct now a fuzzy-expert system, which predicts both the decay mode and the $DC_{50}$-value. Information on both variables are important to judge the toxic effect of a herbicide, because the area under the concentration curve depends on the decay mode for otherwise identical $DC_{50}$-values. We introduce the three fuzzy variables $C_{org}$-*content, pH-value* and *kinetics*. The components of a fuzzy-variable are fuzzy-sets. The fuzzy-sets of the variables are

$$C_{org} = \left(low,\ medium,\ high,\ very\ high\right) \tag{7.24}$$

$$pH = \left(low,\ medium,\ high\right) \tag{7.25}$$

$$kinetics = \left(mono\text{-}fast, mono\text{-}slow, lag\text{-}fast, lag\text{-}slow\right) \tag{7.26}$$

The linguistic variables are defined over their reference sets {$C_{org}$-content}, {pH-value} and {$DC_{50}$-value}. The ranges of organic matter content are chosen according to the german guideline for soil survey (Anon., 1982). Figures 7.30 a-c show the membership functions of the fuzzy-set of each variable. In accordance with common practice, trapezoidal and triangular membership functions are chosen.

**Rule Base**

The fuzzy-expert system consists of a set of rules, which map input fuzzy-sets *A*, here {$C_{org}$-content} and {pH-value} into output fuzzy-sets *B*, here {$DC_{50}$-value}. The rules can be formulated by familiar "if ... then" statements, for example

**If ($C_{org}$ is low) and (*pH* is low) then (*kinetics* is lag-slow) with certainty 1.**

The certainty factor expresses our confidence in the validity of this rule. Table 7.2 contains all rules for the prediction of the kinetics. Since there are four fuzzy-sets for the $C_{org}$-content and three fuzzy-sets for the pH-value, there are a total of twelve different combinations.
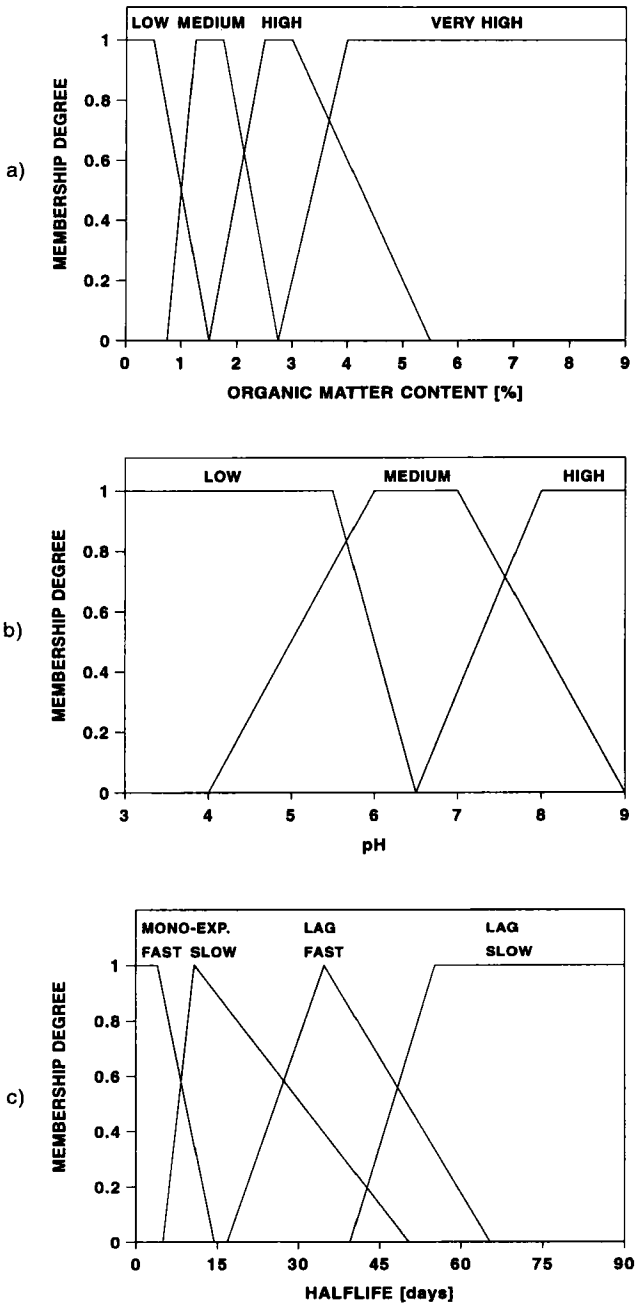
**Fig. 7.30:** Fuzzy-sets of a) $C_{org}$-content b) pH-value and c) kinetics.

**Tab. 7.2:** Rule base of the example fuzzy system.

| Rule No. | IF | $C_{org}$ is | OPERATOR | pH is | THEN | kinetics is | with CF |
|---|---|---|---|---|---|---|---|
| 1 | | very high | AND | medium | | mono-fast | 1 |
| 2 | | very high | AND | high | | mono-slow | 0.7 |
| 3 | | very high | AND | low | | mono-slow | 0.7 |
| 4 | | high | AND | high | | mono-slow | 0.8 |
| 5 | | high | AND | medium | | mono-slow | 1 |
| 6 | | high | AND | low | | lag-fast | 0.7 |
| 7 | | medium | AND | medium | | lag-fast | 1 |
| 8 | | medium | AND | high | | lag-slow | 0.7 |
| 9 | | medium | AND | low | | lag-slow | 0.8 |
| 10 | | low | AND | high | | lag-slow | 1 |
| 11 | | low | AND | medium | | lag-slow | 0.8 |
| 12 | | low | AND | low | | lag-slow | 1 |

The collection of rules together with the collection of logical operators constitute the so-called inference machine. It maps input fuzzy sets into output fuzzy sets.

**Inference Machine**

Figure 7.31 shows the layout of a general inference machine. An inference machine has $n$ input variables $X_1, \dots , X_n$ and one output variable $Y$. $A_{ij}$ denotes the element of the $i^{th}$ linguistic variable within rule $j$ and $B_j$ denotes the element of the output fuzzy-variable of rule $j$. With these notations the general form of a rule takes the form

$$IF \ X_1 = A_{1j} \ AND \ X_2 = A_{2j} \ AND \ ... \ AND \ X_n = A_{nj} \ THEN \ Y = B_j$$

$$j = 1, 2, \dots, n_r$$

An inference machine proceeds in four steps.

In the **first step**, the compatibility between the actual facts $(F_1, F_2, \dots , F_n)$ and the premises of each rule is computed via the membership functions. This is achieved by use of the so-called compatibility operator (*compOp*), which measures the distance between the actual fact and the premise of the rule. If the facts are real numbers, the compatibility measure is simply the value of the membership function of the fuzzy set of the premise in question.

$$\alpha_{ij} = compOp\left(A_{ij}, F_i\right) \qquad i = 1, \ldots, p$$

The compatibility measures $\alpha_{ij}$ can take on values in the interval $[0,1]$.

In the **next step** the compatibility measures of all premises of a rule are aggregated to one value $a_j$ by use of a so-called aggregation operator ($aggOp$).

$$a_j = aggOp\left(\alpha_{1j}, \alpha_{2j}, \ldots, \alpha_{pj}\right)$$

where $p$ denotes the number of premises of rule $j$. (A possible aggregation operator is the minimum operator.) To each rule a certainty factor $c_j$ is assigned, which expresses the degree to which the expert believes that the rule is valid. The compatibility measure is finally modified by the certainty factor applying the so-called certainty operator ($cerOp$).

$$a_j^* = cerOp\left(a_j, c_j\right)$$

Again, a reasonable operator is the minimum operator.

In the **third step**, the fuzzy-set $B_j$ pertaining to the $j^{\text{th}}$ rule is modified by its compatibility measure by use of the so-called inference operator ($infOp$).

$$B_j^* = infOp\left(a_j^*, B_j\right)$$

In the **final step**, all partial results are accumulated to a common fuzzy-output set via the so-called accumulation operator ($accOp$).

$$B_{total} = accOp\left(B_1^*, B_2^*, \ldots, B_{n_r}^*\right)$$
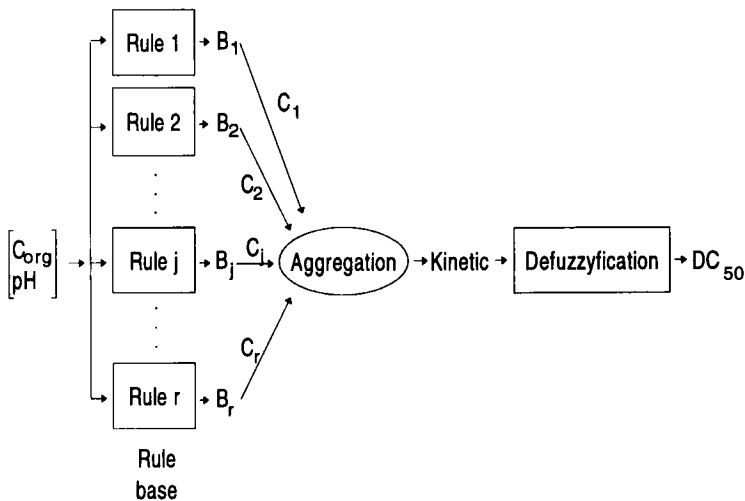


**Fig. 7.31:** Layout of an inference machine.

The **operators** *compOp*, *aggOp*, *infOp* are derived from a class of operators called t-Norm operators. The simplest operator of this class is the minimum operator. Let $\mu_A$ and $\mu_B$ denote the membership functions of two fuzzy-sets $A$ and $B$. Then the membership function of the fuzzy-set $C = A \cap B$ is defined as

$$\mu_C(x) := \min\left(\mu_A(x), \mu_B(x)\right)$$

The accumulation operator *accOp* pertains to the union of fuzzy-sets. A possible definition is the maximum operator. The membership function of the fuzzy-set $C = A \cup B$ is defined as

$$\mu_C(x) := \max\left(\mu_A(x), \mu_B(x)\right)$$

**Defuzzification**

The output of an inference machine is a fuzzy-set. Frequently, the user of an expert system is interested in a number. In our example not only the qualitative information on the decay mode is important but also the $DC_{50}$-value. To get the $DC_{50}$-value, one has to derive a number from the output fuzzy-set. This procedure is called defuzzification. A frequently used method is the computation of the center of gravity of the output fuzzy-set. Another possibility is to take the value where the maximum of the fuzzy-set occurs. If the output fuzzy-set has a plateau, one can take the right or left modal value or the midpoint value.

We will follow all these steps for a $C_{org}$-content of 1.5 % and a pH-value of 5 as input. From the fuzzy sets of the variable $C_{org}$ as shown in Fig. 7.30 a one sees that the above value belongs exclusively to the set "medium" with membership degree of 1 (cf. Fig. 7.32 a). The above pH-value belongs to the fuzzy set "low" with membership degree 1 and to the set "medium" with membership degree of 0.5 (cf. Fig. 7.32 b). The facts given above activate the two rules (cf. Tab. 7.2):

Rule 7 : IF ($C_{org}$ IS medium) AND (*pH* IS medium) THEN (*kinetics* IS lag-fast)
                                                                                    with $CF = 1$
and

Rule 9 : IF ($C_{org}$ IS medium) AND (*pH* IS low)     THEN (*kinetics* IS lag-slow)
                                                                                    with $CF = 0.8$.

For rule 7 the overall compatibility factor for both premises with the facts given is thus min {1,(min {0.5,1})} = 0.5. For rule 9 the decreased certainty of the rule has to be taken into account, so that the overall compatibility factor for both premises with the facts given is min {0.8,(min {1,1})} = 0.8. Figures 7.32 a-c show, how the output fuzzy sets are modified by the inference operation. The last step consists of forming the union of both output fuzzy sets (cf. Fig. 7.32 c). Defuzzyfication is achieved by computing the center of gravity of the accumulated output fuzzy set yielding a value of 62.7 days for the $DC_{50}$-value.
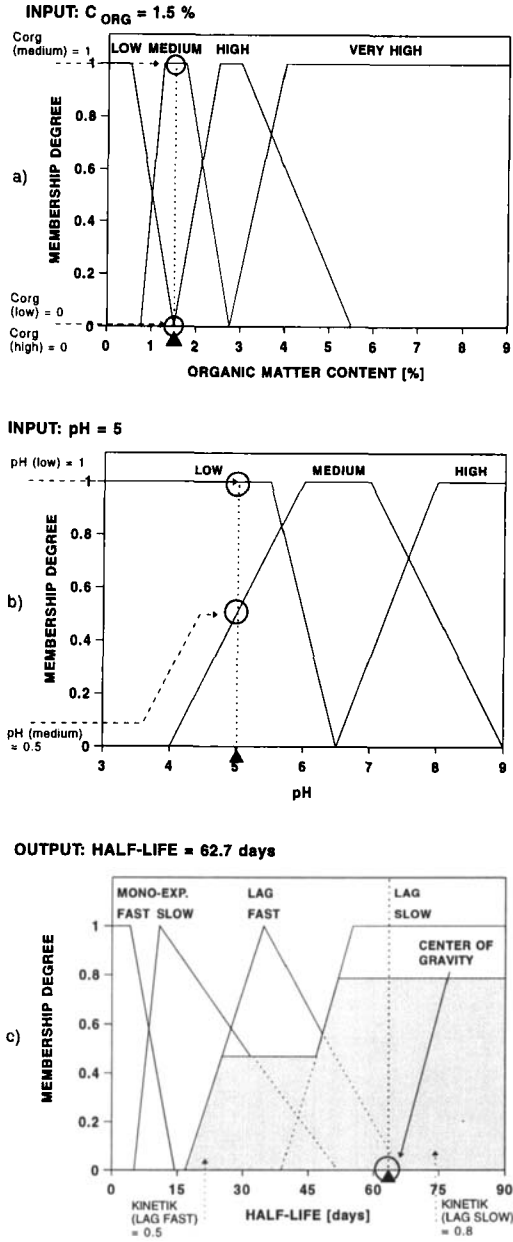
**Fig. 7.32:** Inference operation for an input of a $C_{org}$-content of 1.3 % and a pH-value of 4: a) input derived from the fuzzy set for the $C_{org}$-content, b) input derived from the fuzzy set for the pH-value and c) output fuzzy set and half-life derived by defuzzyfication by use of the center of gravity method.

## Performance of the Fuzzy-Expert System

The fuzzy-sets and the rule base are derived from a kinetic study involving 14 soils differing with respect to $C_{org}$-content, pH-value and other soil properties (von Götz, 1996). Only the

first two properties have an effect on the mode of the kinetics and on the $DC_{50}$-value. Inspection of the data shows that the mode of decay is closely related to the $C_{org}$-content. The pH-value modifies these relations slightly. pH-values below or above the neutral range cause an increase of the $DC_{50}$-value and possibly a shift of the decay mode from mono-exponential to the lag-phase type. This knowledge was used to set up the rule base as given in Tab. 7.2. Defuzzification was achieved by the center of gravity method. The expert system was then applied to the prediction of the $DC_{50}$-value in four other soils. Figure 7.33 b shows the comparison between data and the outcome of the expert system for the training sample and the validation sample. The corresponding input values are shown in Fig. 7.33 a.
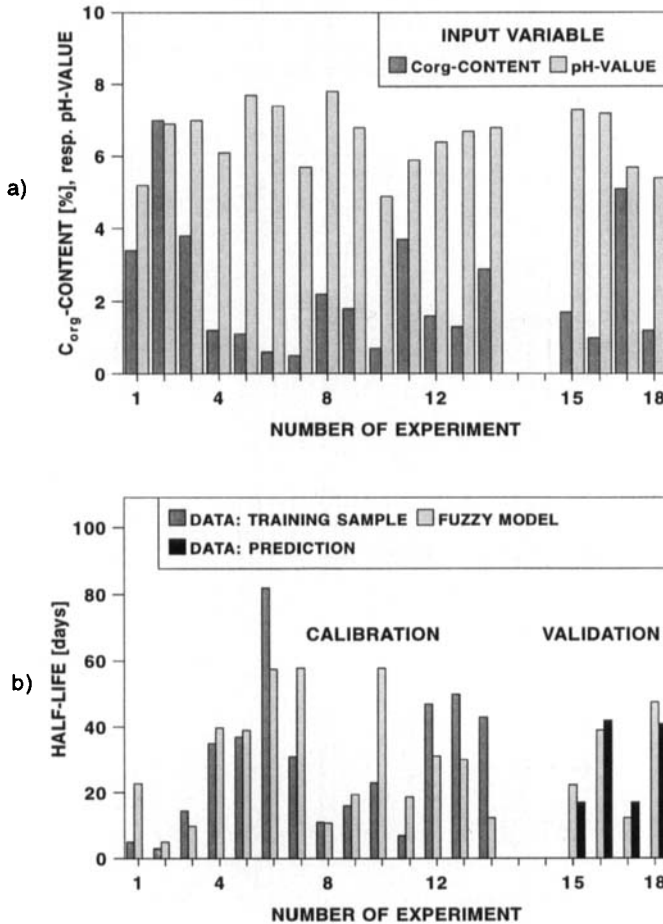


**Fig. 7.33:** Performance of the fuzzy-expert system. a) Input variables and b) resulting half-lives in comparison with the measured data. The left part of the graphic shows the data used for calibration of the expert system. This sample is denoted as training sample. In the right part of the graphic predicted values are compared to data, which are not part of the training sample.

Although the small sample size of this study does not allow to give a final statement on the performance of this expert system, the preliminary results are encouraging and show that fuzzy-expert system modelling is a possible means to cope with incomplete knowledge.

# A    Appendix

## A.1    Table of Laplace Transforms

Let $f(t)$ denote a function with domain $[0, \infty)$ and $s$ a complex variable with $\mathrm{Re}(s) > 0$. Then the Laplace transform of $f(t)$ is defined by

$$L[f(t)] := \int_0^\infty e^{-st} f(t)\, dt := F(s)$$

$$q = \sqrt{\frac{s}{D}}$$   $D$ and $x$ are always positive. $\alpha$ is unrestricted.

**Tab. A1:** Laplace Transforms (cf. Crank, 1975).

| $F(s) = L[s]$ | $f(t) = L^{-1}[F(s)]$ |
|:---:|:---:|
| $\dfrac{1}{s}$ | $1$ |
| $\dfrac{1}{s^{v+1}}$ $\quad$ with $\quad v > -1$ | $\dfrac{t^v}{\Gamma(v+1)}$ |
| $\dfrac{1}{s+\alpha}$ | $e^{-\alpha t}$ |
| $\dfrac{\omega}{s^2 + \omega^2}$ | $\sin(\omega t)$ |
| $\dfrac{s}{s^2 + \omega^2}$ | $\cos(\omega t)$ |
| $e^{-qx}$ | $\dfrac{x}{2\sqrt{(\pi D t^3)}} e^{\frac{-x^2}{4Dt}}$ |

| $\dfrac{e^{-qx}}{q}$ | $\left(\dfrac{D}{\pi t}\right)^{\frac{1}{2}} e^{\frac{-x^2}{4Dt}}$ |
|---|---|
| $\dfrac{e^{-qx}}{s}$ | $erfc \dfrac{x}{2\sqrt{Dt}}$ |
| $\dfrac{e^{-qx}}{sq}$ | $2\left(\dfrac{Dt}{\pi}\right)^{\frac{1}{2}} e^{\frac{-x^2}{4Dt}} - x\,erfc \dfrac{x}{2\sqrt{Dt}}$ |
| $\dfrac{e^{-qx}}{s^2}$ | $\left(t + \dfrac{x^2}{2D}\right) erfc \dfrac{x}{2\sqrt{Dt}} - x\left(\dfrac{t}{\pi D}\right)^{\frac{1}{2}} e^{-\frac{x^2}{4Dt}}$ |
| $sf(s)$ | $\dfrac{d}{dt} f(t)$ |

## A.2   Basic Distributions

In the following a brief list of some frequently used distribution functions will be given (cf. Richter and Söndgerath, 1990):

### 1. Uniform Distribution:

The density function is given by

$$f(x) = \begin{cases} \dfrac{1}{a - b} & x \in [a,b] \\ 0 & otherwise \end{cases} \qquad with \ -\infty < a,b < \infty$$

The expecation and variance of a uniformly distributed random variable are

$$E[X] = \frac{1}{2}(a - b)$$

$$V[X] = \frac{(a - b)^2}{12}$$

The uniform distribution could as well be defined over the open interval $(a,b)$ or over either of the halp-open-half-closeed intervals $(a,b]$ or $[a,b)$. All four of the possible densities have the same cumulative distribution function.

## 2. Normal Distribution:

The density function is given by

$$f(x) = \frac{1}{\sqrt{2\pi}\,\sigma} e^{-\frac{1}{2}\frac{(x-\mu)^2}{\sigma^2}} \qquad \textit{for} \quad -\infty < x < \infty$$

$$\textit{with} \; -\infty < \mu < \infty \quad \textit{and} \quad \sigma > 0$$

The expecation and variance are the parameters $\mu$ and $\sigma^2$:

$$E[X] = \mu \quad \textit{and} \quad V[X] = \sigma^2$$

A normal distribution with $\mu = 0$ and $\sigma^2 = 1$ is called a **standard normal distribution**.

## 3. Truncated Normal Distribution:

If $X$ is a normally distributed random varibale, then the density of $X$ truncated on the left at $a$ and on the right at $b$ is given by:

$$f(x) = \frac{\dfrac{1}{\sqrt{2\pi}\,\sigma} e^{\frac{-(x-\mu)^2}{2\sigma^2}}}{\dfrac{1}{\sqrt{2\pi}\,\sigma} \displaystyle\int_a^b e^{\frac{-(u-\mu)^2}{2\sigma^2}} du} \qquad \textit{for} \quad x \in [a,b]$$

which is the usual density function over the integral from the right to the left truncation.

## 4. Lognormal Distribution:

Let $X$ be a positive random variable, and let a new random variable $Y$ be defined as $Y = \ln X$. If $Y$ has a normal distribution, then $X$ is said to have a lognormal distribution. The lognormal density function is given by

$$f(x) = \frac{1}{x\sqrt{2\pi}\,\sigma}\, e^{-\frac{1}{2\sigma^2}(\ln x - \mu)^2} \qquad -\infty < \mu < \infty \quad and \quad \sigma > 0$$

The expectation and variance of a lognormally distributed random variable are:

$$E[X] = e^{\mu + \frac{1}{2}\sigma^2}$$

$$V[X] = e^{2\mu + 2\sigma^2} - e^{2\mu + \sigma^2}$$

and

$$E[\ln(X)] = \mu \quad and \quad V[\ln(X)] = \sigma^2$$

## 5. Gamma Distribution:

The gamma density function is given by

$$f(x) = \frac{\lambda}{\Gamma(r)}(\lambda x)^{r-1} e^{-\lambda x} \qquad for \quad r > 0 \quad and \quad \lambda > 0$$

with $\Gamma$ the **gamma function**.

This function is defined as follows:

$$\Gamma(x) = \int_0^\infty e^{-t} t^{x-1} dt \qquad for \quad x > 0$$

and it has the following properties:

$$\Gamma(1 + x) = x\Gamma(x) \quad and \quad \Gamma(x)\Gamma(1 - x) = \frac{\pi}{\sin(\pi x)}$$

$$\Gamma(x)\Gamma\left(x + \frac{1}{2}\right) = \frac{\sqrt{\pi}}{2^{2x-1}}\Gamma(2x)$$

$$and \quad for \quad x \in \mathbb{N}: \qquad \Gamma(x) = (x - 1)!$$

The expectation and variance of a gamma distributed random variable are:

$$E[X] = \frac{r}{\lambda}$$

$$V[X] = \frac{r}{\lambda^2}$$

## 6. Exponential Distribution:

If in the gamma density $r = 1$, the gamma density specializes to the **exponential density**, given by:

$$f(x) = \lambda e^{-\lambda x} \qquad for\ x \geq 0$$

with the following expectation and variance:

$$E[X] = \frac{1}{\lambda} \quad and \quad V[X] = \frac{1}{\lambda^2}$$

# References

Aarons, L. (1993): Sparse data analysis. European Journal of drug metabolism and pharmacokinetics. 18: 97-100.

Albers, B.P. & A. Hartmann (1991): Untersuchungen zur mikrobiellen Aktivität in Bodenaggregaten. Mitteilgn. Dtsch. Bodenkundl. Gesellsch. 66 I: 449-452.

Anderson, J. & K.H. Domsch (1980): Relationship between herbicide concentration and the rates of enzymatic degradation of $^{14}$C-Dillate and $^{14}$C-Triallate in soil. Institut für Bodenbiologie FAL. Springer Verlag New York.

Anonymous (1982): Bodenkundliche Kartieranleitung. Bundesanstalt für Geowissenschaften und Rohstoffe. Hannover.

Arning (1994): Lösung des Inversproblems von partiellen Differentialgleichungen beim Wassertransport im Boden. PhD Thesis. 137 p. University of Braunschweig, Germany.

Arya, L.M. & J.F. Paris (1981): A physico-empirical model to predict the soil moisture characteristic from particle-size distribution and bulk density data. Soil Sci. Soc. Am. J. 45: 1023-1030.

Auspurg, B. (1985): Kombinationseffekte von Pflanzenschutzmitteln im Boden. Berichte über Landwirtschaft. Paul Parey Hamburg. Sonderheft 198.

Bahadir, M. & R. Kreuzig (1993): Rückstandsuntersuchungen von Pflanzenschutzmittel-Wirkstoffen und korrespondierenden Metaboliten in Böden. Wasser-und Stoffdynamik in Agrar-Ökosystemen. TU Braunschweig. SFB 179 Finanzierungsantrag 1994-96: 297-319.

Bailey, G.W. & J.L. White (1964): Review of adsorption and desorption of organic pesticides by soil colloids with implications concerning pesticide bioactivity. J. of Agric. and Food Chem. 12: 324-332.

Bard, Y. (1974): Nonlinear parameter estimation. Academic Press N.Y.

Beal S.L. & L.B. Sheiner (1982): Estimating population kinetics. CRC Crit. Rev. Biomed. Eng. 8: 195-222.

Beal, S.L. (1984): 1. Population pharmacokinetic data and parameter estimation based on their first two statistical moments. Drug Metabolism Reviews. 15: 173-193.

Bear, J. (1969): Hydrodynamic dispersion. De Wiest, Roger, J.M. (Ed.): Flow through porous media. Academic Press. N.Y., London: 109-199.

Bear, J. (1979): Hydraulics of groundwater. McGraw-Hill series: Water Resources and Environmental Engeneering. McGraw-Hill Company: 569 pp.

Bear, J. & A. Verruijt (1987): Modeling groundwater flow and pollution. D. Reidel Publishing Company. Dordrecht-Boston-Lancaster-Tokyo: 414 pp.

Blackburn, J.W. (1989): Is there an "uncertainty principle" in microbial waste treatment? in M. Hantley (ed.) Biotreatment agricultural wastewater. CRC Press, Boca Raton, Fl.: 149-161.

Bock, H.G. (1983): Recent advances in parameter identification technique for O.D.E. systems. Progress in Scientific Computing 2. Birkhäuser, Boston.

Bock, H.G. (1987): Randwertprobleme zur Parameteridentifizierung in Systemen von nicht linearen DGLn. Bonner math. Schriften, Bonn.

Bouma, J. & J.A.J. van Lanen (1987): Transfer functions and threshold values: From soil characteristics to land qualities. K.J. Beck et al. (Eds.): Quantified land evaluation. Proc. Workshop ISSS and SSSA. Washington DC. Int. Inst. Aerospace Surv. Sci. Publ. No. 6:

106-110. Enschede, the Netherlands.

Bozler, G., Heinzel, G., Koss, F.W. & M. Wolf (1977): Modellentwicklung in der Pharmakokinetik. 1. Teil: Allgemeine Strategie. Arzneim.-Forsch. 4: 897-899.

Braden, H. (1995): The model AMBETI - a detailed description of a soil-plant-atmosphere model. Berichte des Deutschen Wetterdienstes No. 195. 117 p. Offenbach.

Brain, P. & R. Cousens (1989): An equation to describe dose responses where there is stimulation of growth at low doses. Weed Res. 29: 93-96.

Bressolle, F., Bologna, C., Edno, L., Bernard, J.C., Gomeni, R., Sany, J. & B. Combe (1996): A limited sampling method to estimate methotrexate pharmacokinetics in patient with rheumatoid arthritis using a Bayesian approach and the population data modeling program P-Pharm. Eur J Clin Pharmacol. 49: 285-292.

Bronswijk, J.J.B. (1992): A general approach to incorporate swelling and shrinkage processes in soil water transport simulation models. Modeling of Geo-Biosphere Processes, 1: 253-270.

Brooks, R.H. & A.T. Corey (1964): Hydraulic properties of porous media. Hydrology Paper. 3: 22-27.

Bunte, D. (1991): Abbau- und Sorptionsverhalten unterschiedlich persistenter Herbizide in Abhängigkeit von Flächenvariabilität und Alter der Rückstände. Dissertation. Universität Hannover.

Burdine, N.T. (1953): Relative permeability calculation from size distribution data. Trans. AIME 198: 71-78.

Burrough, P.A. (1986): Principles of geographical information systems for land resources assessment. Clarendon Press Oxford.

Campbell, G.S. (1974): A simple method for determining unsaturated conductivity from moisture retention data. Soil Sci. 117: 311-314.

Campbell, G.S. (1985): Soil physics with basic. Transport models for soil-plant systems. Dep. of Agronomy and Soils.Washington State University. Pullman WA 99163 USA.

Colburn, W.A. & S.C. Olson (1988): Classic and population pharmacokinetics. P.G. & F.L.S. Tse (Ed.): Pharmacokinetics. Marcel Dekker. New York.

Copin, A., Deleu, R., Salembier, J.F. & J.M. Belien (1985): Étude en conditions naturelles du transfert dans le sol de trois pesticides de solubilités différentes. Comportement et effets secondaires des pesticides dans le sol: 47-56.

Cosby, B.J., Hornberger, G.M., Clapp, R.B. & T.R. Ginn (1984): A statistical exploration of the relationship of soil moisture characteristics to the physical properties of soil. Water Resour. Res. 20: 682-690.

Crank, J. (1975): The mathematics of diffusion. (first edition 1956, second edition 1975, reprint 1976). Arrowsmith Bristol.

Dane, J.H. & S. Hruska (1983): In situ determination of soil hydraulic properties during drainage. In: Soil Sci. Soc. Am. J. 47: 619-624.

Dempster, A.P., Laird, N.M. & D.B. Rubin (1977): Maximum likelihood from incomplete data vial the EM algorithm. J. R. Stat. Soc. 39: 1-38.

Dieckmann, H., Stockmaier, M., Kreuzig, R. & M. Bahadir (1993): Rückstandsunter-suchungen von Pflanzenschutzmittel-Wirkstoffen und korrespondierenden Metaboliten in Böden. Wasser-und Stoffdynamik in Agrar-Ökosystemen. TU Braunschweig. SFB 179 Forschungsbericht 1991-93. 2: 601-616.

Diekkrüger, B., Nörtersheuser, P. & O. Richter (1995): Modeling pesticide dynamics of a loam site catchment using HERBSIM and SIMULAT. Ecological Modelling 81(1-3):

111-119.

Diekkrüger, B., Smith, R.E., Baumann, R. & D. Krug (1991): Validation of the model system OPUS. CATENA Supplement 19: 139-153.

Diekkrüger, B. (1992): Standort- und Gebietsmodelle zur Simulation der Wasserbewegung in Agrarökosystemen. Landschaftsökologie und Umweltforschung. 19: 169 pp.

Dixon, W. J. (1981): BMDP statistical software. Barkeley, Los Angeles. University of California Press: 725 pp.

Durner, W. (1992): Predicting the unsaturated hydraulic conductivity using multi-porosity water retention curves. Van Genuchten, M.T., Leij, F.J. & L.J. Lund (Eds.): Indirect methods for estimating the hydraulic properties of unsaturated soils, Riverside, California: 185-202 pp.

Felsot, H., Wei L. & J. Wilson (1982): Environmental chemodynamic studies with terbufos (counter) insecticide in soil under laboratory and field conditions. J. Environ. Sci. Heath. 17: 649-673.

Fournier, J.C., Codaccioni, P. & G. Soulas (1981): Soil adaption to 2,4-D degradation in relation to the application rates and the metabolic behaviour of the degradating microflora. Chemosphere. 10: 977-984.

Ganoulis, J.G. (1994): Engeneering risk analyses of water pollution-Probabilities and fuzzy sets. VCH-Verlag Weinheim.

Gardner, W.R. (1958): Some steady state solution of the unsaturated moisture flow equation with application to evaporation from a water table. Soil Sci. 85: 288-232.

Gerke, H. and M. Th. van Genuchten (1993): A dual porosity model for simulating the preferential movement of water and solutes in structured porous media. Water Resour. Res. 29.2: 305-319.

German, P. and K. Beven (1985): Kinematic wave approximation to infiltration into soils with sorbing macropores. Water Resour. Res. 21.7: 990-996.

Gomeni, R., Pineau, G. & F. Mentre (1994): Population kinetics and conditional assessment of the optimal dosage regimen using the PHARM software package. Anticancer Res. 14: 2321-2326.

Goodchild, M.F., Parks, B.O. & L.T. Steyaert (1993): Environmental Modeling with GIS (Eds.). 488 p. Oxford University Press.

Goring, C.A.I. & J.W. Hamaker (1972): Organic chemicals in the soil environment. Marcel Dekker Inc. New York.

Gottesbüren, B. (1991): Konzeption, Entwicklung und Validierung des wissensbasierten Herbizid-Beratungssystems HERBASYS. Dissertation. Unversität Hannover.

Gottesbüren, B., Beulke, S., Heiermann, M. & W. Pestemer (1994): Freilandversuche zur Validierung von Prognosemodellen des Expertensystems HERBASYS zur Nachbauproblematik nach Herbizideinsatz. Weed Research 34: 63-78.

Gupta, S.C. & W.E. Larson (1979): Estimating soil water characteristic from particle size distribution, organic matter percent and bulk density. Water Resour. Res. 15: 1633pp.

Gustavson, D.I. & L.R. Holden (1990): Nonlinear pesticide dissipation in soil: A new model based on spatial variability. Environ. Sci. Technol. 24: 1032-1038.

Haffner, D., Borchard, U., Richter, O. & M. Neugebauer (1981): Parameter estimation in Hodgkin-Huxley-Type equations for membrane action potentials in nerve and heart muscle. J. theor.Biol. 91: 321-345.

Hamaker, J.W. & J.M. Thompson (1972): Adsorption. Goring C.A.J. & J.W. Hamaker (Eds.): Organic chemicals in the soil environment. Vol.1. Marcel Dekker: 49-143.

Hanks, R.J. & G.L. Ashcroft (1980): Applied soil physics. Adcvanced series in agricultural sciences 8: 159 p. Springer Verlag.

Harris, C.I. & T.J. Sheets (1965): Influence of soil properties on adsorption and phytotoxicity of CIPC, Diuron and Simazine. Weeds 13: 215-219.

Harvey, R.G. (1982): Wild proso millet control in field and sweet corn. Proc. North. Cent. Weed Control Conference 37: 29-38.

Haude, W. (1955): Zur Bestimmung der Verdunstung auf möglichst einfache Weise. Mitteilungen des Deutschen Wetterdienstes 2: 1-23.

Haverkamp, R. & J.Y. Parlange (1986): Predicting the water retention curve from particle size distribution. 1. Sandy soils without organic matter. Soil Sci. 142: 325-339.

Hornung, U. (1983): Identification of nonlinear soil physical parameters from an input-output experiment. Deuflhard P. & E. Harrier (Eds.): Workshop on numerical treatment of inverse problems in differantial and integral equations. Birkhäuser. Boston, Mass.: 227-237.

Hurle, K. & V. Pfefferkorn (1972): Experiments on the rate of decomposition of DNOC in soils: the effect of pretreatments. Proc. 11th British Weed Control Conference: 806-810.

Hurle, K. (1973): Lag-Phase Studien mit DNOC und 2,4-D im Boden. Proceedings of the European Weed Research Council Symposium Herbicides-Soil: 151-162.

Hurle, K. & A. Walker (1980): Persistence and its prediction. Hance R.J. (Ed.): Interactions between herbicides and the soil. Academic Press. London, 1980.

Hurle, K. (1982): Untersuchungen zum Abbau von Herbiziden in Böden. Acta Phytomedica 8. Paul Parey. Berlin, Hamburg.

Husz, G. (1967): The determination of pF-curves from texture using multiple regressions. (in German). Z. Pflanzenernähr. Düng. Bodenkd. 116 (2): 23-29.

Jarvis, N. (1991): MACRO - A model of water movement and solute transport in macroporous soils. Reports and Dissertations 9: 58 pp. Department of Soil Sciences. Swedish University of Agriculture Sciences. Uppsala, Sweden.

Journel, A.B. & C.J. Huijbregts (1991): Mining geostatistics. Academic Press. New York.

Jury, W.A., Spencer, W.F. & W.J. Farmer (1983): Use of models for assessing relative volatility, mobility and persistence of pesticides and other trace organics in soil systems. Saxena J. (Ed.): Hazard Assessment of Chemicals. Vol.2, New York. Academic Press.

Kibler, E. (1979): Freiland - und Laboruntersuchungen zur Abbaukinetik von Chlortoluron und Simazin in Böden in Gegenwart anderer Pflanzenschutzmittel. Dissertation. Universität Hohenheim.

King, A.W. (1991): Translating models across scales in the landscape. Turner, M.G. & R.H. Gardner (Eds.): Quantitative methods in landscape ecology. The analysis and interpretation of landscape heterogeneity. Ecological Studies. Springer Verlag New York. Vol.82: 479-513.

Klute, A. (1986): Methods of soil analysis. Part 1: Physical an mineralogical methods. Agronomy 9 (1):1173 pp.

Kool, J.B. & J.C. Parker (1988): Analysis of the inverse problem for transient unsaturated flow. Water Resour. Res. 24 (6): 817-830.

Krige, D.G. (1951): A statistical approach to some basic mine valuation problems on the Witwatersrand. Journal of the chemical metallurgical and Mining Society of South Africa. 52: 119-139.

Kukowsky, H. & G. Brümmer (1987): Untersuchungen zur pH-abhängigen Adsorption ausgewählter Chemikalien durch die organische Substanz der Böden. Mitteilgn. Dtsch.

Bodenkundl. Gesellsch. 55: 375-380.

Kunc, F. & J. Rybarova (1983): Mineralization of carbon atoms of [14]C 2,4-D side chain and degradation ability of bacteria in soil. Soil Biol. Biochem. 15: 141-144.

Lindstrom, F.T., Haque, R., Freed, V.H. & L. Boersma (1967): Theory on the movement of some herbicides in soils. Environ. Sci. Technol. 1 (7): 561-565.

Lotka, A.J. (1925): Elements of physical biology. Williams & Wilkins (1956): Elements of mathematical ecology. Dover, New York.

Loux, M.M., Liebl, R.A. & F.W. Slife (1989): Availability and persistence of Imazaquin, Imazethapyr and Chlomazone in soil. Weed Sci. 37: 259-267.

Lücke, A., Günther, P., Diekkrüger, B., Pestemer, W. & O. Richter (1995): Implementation of a herbicide simulation model in a geographical information system with an example of a site specific application. Weed Res. 35: 333-342.

McCall, P.J., Vrona, S.A. & S.S. Kelley (1981): Fate of uniformly carbon-14 ring labeled 2,4,5,-Trichlorophenoxyacetic acid and 2,4-Dichlorophenoxyacetic acid. J. Agric. Food Chem. 29: 100-107.

McInnes, K.J. (1981): Thermal conductivities of soils from dryland wheat regions of Eastern Washington. M.S. Thesis. Whashington State University. Pullman.

McKay, M.D., Beckman, R.J. & W.J. Conover (1979): A comparison of three methods for selecting values of input variables in the analysis of output from a computer code. Technometrics. 2(21): 239-245.

McVoy, C.W., Kersebaum, K.C., Arning, M., Kleeberg, P., Othmer, H. & U. Schröder (1995): A data set from north Germany for the validation of agroecosystem models: documentation and evaluation. Ecol. Model. 81: 265-297.

Michaelis, L. and M. Menten (1913): Die Kinetik der Invertinwirkung. Biochem. Zeitschr. 49: 333

Millington, R.J. & J.P. Quirk (1961): Permeability of porous solids. Trans. Faraday Soc. 57: 1200-1207.

Milly, P.C.D. (1987): Estimation of Brooks-Corey parameters from water retention data. In Water Resourc. Res. 23(6): 1085-1089.

Moe, P.G. (1970): Kinetics of microbial decomposition of the herbicides IPC and CIPC. Environmental Science and Technology 4: 429-431.

Monteith, J.L. (1965): Evaporation and environment. Symp. Soc. Exp. Biol. 19: 205-224.

Monteith, J.L. (1976): Vegetation and the atmosphere, 2. Academic Press.

Mualem, Y. (1976): A new model for predicting the hydraulic conductivity of unsaturated porous media. Washington D.C. Water Resour. Res. 12: 513-522.

Müller-Wegener, U. (1982): Über die Adsorption umweltrelevanter Chemikalien in Böden. Erde. 41: 175-181.

Nash, R.G. (1981): Phytotoxic interaction studies - Techniques for evaluation and presentation of results. Weed Science. 29: 147-155.

Nietfeld, H., Priesack, E., & F. Beese (1992): A model of solute transport and microbial growth in aggregates. Modeling of Geo-Biosphere Processes. 1: 1-12.

Norman, J.M. (1993): Scaling processes between leaf and canopy levels. Ehleringer, J.R. & C.B. Field (Eds.): Scaling physiological processes-Leaf to globe. Academic Press N.Y.

Nörtersheuser, P. (1993): Aufbau von Modellen zur Beschreibung des Verhaltens von Pflanzenschutzmitteln im Boden und Anwendung am Beispiel des Herbizids Quinmerac. Landschaftsökologie und Umweltforschung, 20: 219 pp.

Obrigawitch, T., Martin, A.R. & F.W. Roeth (1983): Degradation of thiocarbamate herbicides

in soils exhibiting rapid EPTC breakdown. Weed Sci. 31: 187-192.

O'Neill, R.V. (1968): Population energetics of a milipede. Narceus Americanus (Beavois). Ecology. 49: 803-809.

O'Neill, R.V., Oldstein, R.A., Shugart, H.H. & J.B. Makin (1972): Terrestrial ecosystem energy model. Eastern deciduous forest biome memo report No. 72-19: 38 pp.

Othmer, H., Diekkrüger, B. & M. Kutilek (1991): Bimodal porosity and unsaturated hydraulic conductivity. Soil Sci. 152.3: 139-150.

Ou, L.T. (1984): 2,4 D degradation and 2,4 D degradating microorganismus in soils. Soil Sci. 137: 100-107.

Panikov, N.S., Blagodatsky, S.A., Blagodatskaya, J.V. & M.V. Glagolev (1992): Determination of microbial mineralization activity in soil by modified Wright and Hobbie method. Biol. Fertil. Soils. 14: 280-287.

Parker, L.W. & K.G. Doxtader (1982): Kinetics of microbial decomposition of 2,4-D in soil: Effects of temperature and moisture. J. Environ. Qual. 12: 553-557.

Parker, J.C. (1984): Analysis of solute transport in column tracer studies. Soil Sci. Soc. Am. J. 48 (4): 719-724.

Parker, J.C., Kool, J.B. & M.Th. van Genuchten (1985): Determining soil hydraulic properties from one - step outflow experiments by parameter estimation: 1. Theory and numerical studies. Soil Sci. Soc. Am. J. 49: 1348-1354.

Parker, J.C., Kool, J.B. & M.Th. van Genuchten (1985): Determining soil hydraulic properties from one - step outflow experiments by parameter estimation: 2. Experimental studies. Soil Sci. Soc. Am. J. 49: 1354-1359.

Passiora, J.B. (1976): Determing soil water Diffusivities from onestep outflow experiments. Austr. J. Soil Res. 15: 1-18.

Penman, H.L. (1948): Natural evaporation from open water, bare soil and grass. Proc. R. Soc. London. 193: 120-145.

Pestemer, W. (1983): Methodenvergleich zur Bestimmung der Pflanzenverfügbarkeit von Bodenherbiziden. Ber. Fachg. Herbologie Universität Hohenheim. 24: 85-96.

Pestemer, W. & B. Auspurg (1987): Prognose-Modell zur Erfassung des Rückstandsverhaltens von Metribuzin und Methabenzthiazuron im Boden und deren Auswirkungen auf Folgekulturen. Weed Res. 27: 275-286.

Pestemer, W. & G. Krasel (1992): Loss from pesticides from plant and soil by volotilization. Proceedings. BCPC Conference Pests and Diseases.

Poschenrieder, G. (1978): Untersuchungen über Interaktionen chemischer Pflanzenschutzmittel im Boden. Dissertation. Technische Universität München.

Puckett, W.E., Dane, J.H. & B.F. Hajek (1985): Physical and mineralogical data to determine soil hydraulic properties. Soil Sci. Soc. Am. J. 49: 831-836.

Rahman, A. (1978): Effect of climatic and edaphic factors on the persistence and movement of ethofumesate. Proceedings British Crop Protection Conference. Weeds: 557-563.

Rahman, A. & T.K. James (1983): Decreased activity of EPTC + R-25788 following repeated use in some New Zealand soils. Weed Sci. 31: 783-789.

Ralston, M. & R.I. Jennrich (1978): Derivate-free nonlinear regression. Proceedings of computer science and statistics: Tenth Anual Symposium on the Interface. Hogben, D. & D. Fife (Eds.) Washington D.C. Bureau of Standards: 312-322.

Ralston, M., Jennrich, R.I., Sampson, P. & F. Uno (1984): Fitting models defined by differential equations. BMDP Statistical Software Inc. Technical Report 70, Los Angeles, California.

Rao, P.S.C. & R.E. Jessup (1982): Development and verification of simulation models for describing pesticide dynamics in soils. Ecological Modelling. 16: 67-75.

Rauber, R. (1978): Möglichkeiten der Erarbeitung von Modellen zur Befallsprognose bei Unkräutern, dargelegt am Beispiel von Flughafer (*Avena fatua*) in Getreide. Dissertation. Universität Hohenheim.

Rawls, W.J., Brakensiek, D.L. & K.E. Saxton (1982): Estimation of soil water properties. Trans. ASAE 108: 1316-1320.

Rawls, W.J. & D.L. Brakensiek (1985): Prediction of soil water properties for hydrological modeling. Proceedings of the symposium watershed management in the eighties: 293-299, Denver.

Renner, K.A., Meggitt W.F. & R.A. Leavitt (1988): Influence of rate, method of application and tillage on Imazaquin persistence in soil. Weed Sci. 36: 90-95.

Repiquet, C. and J.C. Fournier (1977): Étude en laboratoire de la dégradation du 2,4-D et de l'isoproturon en présence d'autres produits de traitments. Comptes des journées détudes sur les herbicides Columa: 801-810.

Richter, O. & D. Söndgerath (1990): Parameter estimation in ecology - The link between data and models. VCH Weinheim.

Richter, O., Nörtersheuser, P. & W. Pestemer (1992): Nonlinear parameter estimation in pesticide degradation. The Science of the total Environment. 123/124: 435-450.

Richter, O., Nörtersheuser, P. & B. Diekkrüger (1992): Modeling reactions and movement of organic chemicals in soils by coupling of biological and physical processes. Modeling of Geo-Biosphere Processes. 1: 95-114.

Sanathanan, L.P. (1991): Random effects modeling in population: Kinetic/dynamic analysis. Drug Information Journal. 25: 307-318.

SB Technology (1994): Model Maker Version 2.0. 319 p. Cherwell Scientific Publishing.

Schittkowsky, K. (1995): Parameter estimation in dynamical systems with EAYSFIT, Version 1.0, User Guide. 172 p. University of Bayreuth

Schmider, F. (1990): Studien zum Verhalten von Quinmerac im Boden. BASF-Bericht: 2571.

Schröder, B. (1995): Simulation von mikrobiellem Wachstum in Bodenaggregaten (unpublished thesis, TU Braunschweig, Germany)

Schweizer, E. (1977): Persistance and movement of ethofumesale in soil. Weed Research. 16: 37-42.

Sheiner, L.B. (1984): The population approach to pharmacokinetic data analysis: Rationale and standard data analysis methods. Drug Metabolism Reviews. 15: 153-171.

SIMED (1994): P-Pharm. Version 1.3g. SIMED. Creteil. France.

Söndgerath, D. & W. Müller-Pietralla (1996): A model for the development of the cabbage root fly (*Delia radicum* L.) based on the extended Leslie model. Ecological Modelling, in press.

Stange, F., Nordmeyer, H. & B. Diekkrüger (1996): Herbicide leaching in soils with macropores. Journal of Environmental Science. In Preparation.

Stock, A. (1995): Untersuchungen der räumlichen Variabilität des Stofftransportes in der wasserungesättigten Bodenzone. Institut für Geographie und Geoökologie. Dissertation. TU Braunschweig.

Streibig, J.C. (1984): Measurement of phytotoxicity of commercial and unformulated soil-applied herbicides. Weed Res. 24: 327-331.

Streibig, J.C. (1988): Herbicide bioassay. Weed Res. 28: 479-484.

Stryckers J., Goodeers, H., Himme, M., Bulcke, R. & W. Verstraete (1978): Herbicide in

bieten: nawerking en inoloed op de boden microbiota. Mededelingen van de Fakuleit Landbouwwetenschappen. Grent. 43: 1141-1152.

Subba-Rao, R.V., Cromartie, T.H. & R.A. Gray (1987): Methodology in accelerated biodegradation of herbicides. Weed Technology. 1: 333-340.

Tietje, O. & O. Richter (1992): Stochastic modeling of the unsaturated water flow using auto-correlated spatial variable hydraulic parameters. Modeling of Geo-Biosphere Processes.

Tietje, O. & M. Tapkenhinrichs (1993) Evaluation of pedo-transfer functions. Soil Sci. Soc. Am. J.57: 1088-1095.

Tim, U.S. & R. Jolly (1994): Evaluating Agricultural Nonpoint-Source Pollution Using Integrated Geographic Information Systems and Hydrologic/Water Quality Model. J. Environ. Qual. 23: 25-35.

Timme, G., Frehse, H. & V. Laska (1986): Zur statistischen Interpretation und graphischen Darstellung des Abbauverhaltens von Pflanzenschutzmittelrückständen 2. Pflanzenschutznachrichten Bayer. 39: 188-204.

Tyler, S.W. & S.W. Wheatcraft (1989): Application of fractal mathematics to soil water retention estimation. Soil Sci. Soc. Am. J. 53: 987-996.

Valiantzas, J.D. & P.G. Kerkides (1990): A simple iterative method for the simultaneous determination of soil hydraulic properties from one step outflow data. Water Resour. Res. 26 (1): 143-152.

van Genuchten, M.Th. (1980): A closed-form equation for predicting the hydraulic conductivity of unsaturated soils.Madison. Soil Sci. Soc. Am. J. 44: 892-898.

van Genuchten, M.Th. (1981): Analytical solutions for chemical transport with simultaneous adsorption, zero-order production and first order decay. J. Hydrol. 49: 213-233.

van Genuchten, M.Th. & W.J. Alves (1982): Analytical solutions of the one-dimensional-convective-dispersive solute transport equation. U.S. Department of Agriculture. Agricultural Research Service. Washington D.C. Technical Bulletin Nr. 1661.

van Genuchten, M.Th. & R.J. Wagenet (1989): Two-site/two-region models for pesticide transport and degradation. Theoretical development and analytical solutions. Soil Sci. Soc. Am. J. 53: 1303-1310.

Vereecken, H., Maes, J. Feyen, J. & P. Darius (1989): Estimating the soil moisture retention characteristic from texture, bulk density and carbon content. Soil Sci. 148: 389-403.

Vink, J.P.M., Nörtersheuser, P., Richter, O., Diekkrüger, B. & K.P. Groen (1994): Modeling the microbial breakdown of pesticides in soil using a parameter estimation technique. Pestic. Sci. 40: 285-292.

Volterra, V. (1926): Fluctuations in the abundance of a species considered mathematically. Nature 188: 558-560.

von Götz, N. and O. Richter (1996): Vorhersage von Herbizidkinetiken durch ein Fuzzy-Expertensystem. Z. PflKrankh. PflSchutz, Sonderh. XV: 635-641.

Wagenbreth, D. & E. Kluge (1970): Der Einfluß von Fungiziden (Thiuram, Vapam) auf den Triazinabbau im Boden. Archiv für Pflanzenschutz. 7: 451-459.

Wagenet, J. (1990): Estimation and application of soil hydological properties for land evaluation and environmental protection. Trans. Int. Congr. Soil. Sci. Vol. 1: 49.

Walker, A. (1974): A simulation model for prediction of herbicide persistence. Journal of Environmental Quality 3: 396-401.

Walker, A. (1978): The degradation of methazole in soil, effects of soil type, soil temperature and soil moisture content. Pestic. Sci. 9: 326-332.

Walker, A. & R. Allen (1984): Influence of soil and environmental factors on pesticide persistence. Symposium on soils and crop protection chemicals. 27: 89-100.

Walker, A. (1987): Evaluation of a simulation model for prediction of herbicide movement and persistence in soil. Weed Res. 27: 143-152.

Walker, A. (1989): Adsorption and degradation of chlorsulfuron and metsulfuron-methyl in soils from different depths. Weed Res. 29: 281-287.

Walker, A. & S.J. Welch (1990): Enhanced biodegradation of dicarboxymide fungicides in soil. Racke, K.D. & J.R. Coats (Eds.): Enhanced biodegradation of pesticides in the environment. ACS Symposium Series.

Webb, W.L., Schroeder, H.J. and L.A. Norris (1975): Pesticide residue dynamics in a forrest ecosystem's compartment model. Simulation 24: 161-169.

Wierenga, P.J., Toorman, A.F., Hudson, D.B., Vinson, J., Nash, M. & R.G. Hills (1989): Soil physical properties at the Las Cruces trench site. U.S. Nuclear Regulatory Commission NUREG/CR-5441. 91pp.

Zachmann, D.W., Duchateau, P.C. & A. Klute (1981): The calibration of the Richards' flow equation for a draining column by parameter identification. Soil Sci. Soc. Am. J. 45: 1012-1015.

Zachmann, D.W., Duchateau P.C. & A. Klute (1981): Simultaneous approximation of water capacity and soil hydraulic conductivity by parameter identification. Soil Sci. 143 (3): 157-163.

Zimmermann, H.J. (1991): Fuzzy set theory - and its applications. 2nd rev. ed., Kluwer, Dordrecht.

# Subject Index